Type 1 Insulin-like Growth Factor Receptor Inhibition as Treatment for Urological Cancer

Submission for the degree of Doctor of Philosophy (DPhil)
Department of Medical Oncology

Dr. Meenali M. Chitnis

Christ Church College, Oxford

Hilary 2013

Table of Contents

LIST OF FIGURES

LIST OF TABLES

LIST OF ABBREVIATIONS

ALS	acid labile subunit
APLF	aprataxin and pink like factor
AR	androgen receptor
ATM	ataxia Telangiectasia Mutated
53BP1	p53 binding protein
Bad	B cell leukaemia 2 antagonist of cell death
BCA	Bicinchoninic Acid
BRCA1	breast cancer type 1 susceptibility protein
BRCA2	breast cancer type 2 susceptibility protein
BSA	bovine serum albumin
ccRCC	clear cell renal cell carcinoma
CDK	cyclin dependent kinase
CO-IP	co-immunoprecipitation
DHRS3	short chain dehydrogenase/reductase member 3
DNAPKCS	DNAPK catalytic subunit
DSS1	deleted in split hand/split foot protein 1
4EBP1	eukaryotic translation initiation factor 4E-binding protein 1
eGFP	enhanced green fluorescent protein
eIF4E	eukaryotic translation initiation factor 4E
Elk-1	erythroblastosis virus E26 oncogene homolog 1-like gene 1
eNOS	endothelial nitric oxide synthase
ERK	extracellular signal–regulated kinases
FKHRL1	forkhead homolog (rhabdomyosarcoma) like 1
GAPDH	glyceraldehyde-3-phosphate dehydrogenase
GSK3	glycogen synthase kinase-3 beta
Hdm2	Human double minute 2
HIF	hypoxia inducible factor
HR	homologous recombination
IGF-1	insulin-like growth factor 1

IGF-2	insulin-like growth factor 2
IGF-1R	type 1insulin-like growth factor receptor
IGFBP	insulin-like growth factor binding protein
IHC	immunohistochemistry
IL-2	interleukin-2
INF-α	interferon alpha
IR	insulin receptor
IRS-1	IR substrate 1
JNK	c-Jun NH2-terminal kinase
KAP-1	KRAB-associated protein1
KIF20A	kinesin family member 20A
LHRH	leuteinising hormone releasing hormone
MAPK	mitogen-activated protein kinase
MEK	MAP kinase/ERK kinase
MMP	matrix metalloproteinases
mTORC1	mammalian target of rapamycin complex 1
mTORC2	mammalian target of rapamycin complex 2
MVP	major vault protein
NHEJ	non-homologous end joining
NSCLC	non-small cell lung carcinoma
OF	oligofectamine
OM	Opti-MEM®
PALB2	partner and localizer of BRCA2
PDGF	platelet derived growth factor
PDK1	phosphoinositide-dependent kinase 1
PFGE	pulsed-field gel electrophoresis
PI	propidium iodide
PI3K	phosphatidylinositide-3-kinase
PIP2	phosphatidylinositol 4,5-biphosphate
PIP3	phosphatidylinositol 3,4,5-triphosphate
PSA	prostate specific antigen
PTEN	phosphastase and tensin homologue
qRT-PCR	real time quantitative polymerase chain reaction
RPA	replication protein A

S6K	p70 ribosomal protein S6 kinase 1
SH2	Src homology 2
Shc	Src homology and collagen domain protein
siRNA	short interfering RNA
SOS	son of sevenless
TBST	tris-buffered saline with 0.05% Tween-20
TCC	transitional cell carcinoma
TdT	terminal deoxyribonucleotidyltransferase
TKI	tyrosine kinase inhibitors
TMA	tissue microarray
TNF	tumour necrosis factor
TSC	tuberous sclerosis
VEGF	vascular endothelial growth factor
VHL	von Hippel-Lindau
WRN	Werner’s syndrome protein

ACKNOWLEDGEMENTS

I would like to thank my supervisors, Dr. Valentine Macaulay and Dr. Andrew Protheroe, and all members of the IGF Lab for their support, advice and guidance throughout my DPhil. I would happily do it all over again.

I would like to acknowledge Uro-oncology Database manager Neviana Kilbey, and statistician Cheng Han, both of the CRUK Department of Medical Oncology, Oxford Cancer Centre, for their help with the renal tumour array data analysis. I would also like to acknowledge the Cancer Research UK Paterson Institute Microarray Service, and Stephen Taylor, Head of Computational Biology Research Group, Weatherall Institute of Molecular Medicine, for microarray data analysis.

This thesis is dedicated to many:

My parents Ajayya and Neelima for inspiring me with the belief that anything is achievable with hard work, dedication and honesty, and for making me the person that I am today.

My husband Cheerag for his unwavering belief in me, his unending love, and without whose support I would never have been able to complete this Dhil.

My daughters Ayanna and Surina for bringing a smile to my face even on the most frustrating days.

My sister Aneesha for always providing sound advice, love and for just knowing me.

My friend Kunal, for a million reasons that just cannot all be listed here, but without whose company this experience would not have been the same, and in whom I hope to have a lifelong friend.

ABSTRACT

The type 1 insulin-like growth factor receptor (IGF-1R) is a receptor tyrosine kinase that mediates diverse cellular functions including growth, differentiation, migration and apoptosis protection. IGF-1R signalling has been implicated in tumorigenesis in a variety of cancers, and IGF-1R inhibitory drugs are currently undergoing clinical evaluation. Previous work in our laboratory has shown IGF-1R over-expression in urological cancers at both the mRNA and protein level, thus making it a potential therapeutic target. The first aim of this project was to develop a protocol for IGF-1R immunohistochemistry, investigate the expression and cellular distribution of the IGF-1R receptor in clear cell renal cell carcinomas (ccRCC), and assess correlation with clinical parameters. In tissue microarray analysis, IGF-1R was detected in ~90% of 195 ccRCCs, with signal in the plasma membrane, cytoplasm and also in the nucleus. The presence of nuclear IGF-1R in up to 50% of ccRCCs and its association with adverse prognosis was a novel finding, and suggests that nuclear IGF-1R may influence ccRCC biology. Further investigations will clarify its role in the nucleus and its potential as a prognostic biomarker. The second aim was to investigate effects of IGF-1R inhibition on radiosensitivity and DNA repair, following previous work in our laboratory showing that IGF-1R depletion enhances chemo- and radio-sensitivity, delays double strand break (DSB) resolution, and may play a role in the homologous recombination (HR) pathway of DNA DSB repair. However, the repair defect seen in these early experiments was larger than could be entirely explained by a defect in HR. The current project used a small molecule IGF-1R tyrosine kinase inhibitor AZ12253801 (AstraZeneca), which blocked IGF-1 induced IGF-1R activation and inhibited cell survival. AZ12253801 enhanced the radiosensitivity of prostate cancer

cells, which appeared to be independent of effects of IGF-1R inhibition on cell cycle distribution and apoptosis induction. IGF-1R inhibition delayed the resolution of γH2AX foci, supporting a potential role for the IGF-1R in DSB repair. This delay in focus resolution was apparent at early time-points (less than 4 hr), and was epistatic with DNA dependent protein kinase (DNAPK) inhibition in prostate cancer cells and DNAPK deficiency in glioblastoma cells. These results suggest a role for the IGF-1R in the non-homologous end-joining (NHEJ) pathway of DNA DSB repair. A cell-based reporter assay in HEK-293 cells confirmed that IGF-1R inhibition suppressed DSB repair by NHEJ, helping to explain the radiosensitization demonstrated upon IGF-1R inhibition. There was lack of support for a transcriptional effect, with no significant change observed in gene expression on microarray analysis. Although the mechanism of this effect remains unclear, the observed inhibition of NHEJ has implications for the use of IGF-1R inhibitors in combination with DNA damaging agents in cancer treatment.

1 Chapter I: Introduction

1.1 Urological cancers

Urological cancers of the prostate, kidney and bladder account for considerable morbidity and mortality. Prostatic adenocarcinoma is the most common cancer in men in the UK (2009), accounting for almost a quarter of newly diagnosed cases (http://info.cancerresearchuk.org/cancerstats). It is the second most common cause of cancer death in men in the UK (2010). Bladder cancer and kidney cancer are the 7th and 8th most common cancers in the UK respectively (2009, http://info.cancerresearchuk.org/cancerstats). These urological cancers present considerable therapeutic challenge. Treatment can be curative if diagnosed early, but metastatic cancer is incurable, and standard treatment options are limited both in the number of lines of treatment, and in the survival advantage they provide. The following section reviews the current standard treatment options for patients with metastatic urological cancers, and then focuses on the insulin-like growth factor (IGF) axis as a potential treatment target.

1.1.1 Prostate cancer

Androgens are the primary stimulus to the growth of prostate cancer and the initial management of advanced prostate cancer is by achieving castrate levels of testosterone, utilising either leuteinising hormone releasing hormone (LHRH) analogues or by means of surgical castration (Parmar et al 1987). When resistance to these agents emerges, combined androgen blockade can be achieved with the addition of androgen receptor (AR) antagonists such as bicalutimide, and a response can be

observed with a decline in levels of prostate specific antigen (PSA). Inevitably the majority of tumours become androgen insensitive in a median of 18-24 months from achieving castrate levels of testosterone (Petrylak et al 2004). Until recently, the survival in metastatic androgen insensitive disease was a median of 10-12 months, with palliative chemotherapies such as mitoxantrone offering no survival advantage (Petrylak et al 2004). In 2004, docetaxel was shown to confer a survival advantage in the treatment of advanced hormone refractory prostate cancer, although median survival was prolonged by only 2-3 months when compared with mitoxantrone (Berthold et al 2008, Petrylak et al 2004, Tannock et al 2004). Until recently, clinical management following docetaxel chemotherapy was mainly palliative in nature. Now new treatments have expanded the repertoire of drugs demonstrating a survival advantage in patients with advanced prostate cancer. In docetaxel pre-treated patients, the novel taxane cabazitaxel has shown an improved median overall survival of 2.4 months compared to patients treated with mitoxantrone (de Bono et al 2010). However, 82% of patients on cabazitaxel had neutropenia, suggesting that toxicities including myelosuppression might limit the use of this second line treatment in advanced disease.

Two new forms of endocrine therapy have also become available recently, and it has emerged that further suppression of androgen levels, even in previously 'androgen insensitive' cases, is not only possible but confers a significant survival advantage. Abiraterone acetate (Zytiga) is a CYP17 inhibitor which blocks the extra-gonadal biosynthesis of androgens. In a Phase III trial of abiraterone versus placebo in docetaxel pre-treated, androgen insensitive cancers, a median survival advantage of 3.9 months was seen with abiraterone (de Bono et al 2011). Secondary end points of PSA decrease, time to PSA progression and radiographic progression-free survival

(PFS) were all significantly improved in patients taking abiraterone (de Bono et al 2011). MDV3100 (enzalutamide) is a potent androgen receptor antagonist and inhibitor of AR nuclear translocation and DNA binding. This agent has also demonstrated a survival advantage of 4.8 months compared to placebo in a Phase III trial in docetaxel pre-treated patients (Scher et al 2012). The optimal sequencing of these agents in relation to chemotherapy is not entirely clear. However, despite these new developments, the survival of patients with advanced prostate cancer remains modest post docetaxel, and there is a need for further improvement in treatments.

1.1.2 Renal Cancer

Renal cancers are characteristically chemo- and radio-resistant (Lane and Kattan 2005, Sfoungaristos et al 2011). Prior to the emergence of targeted therapies, the standard of care was cytokine therapy with agents such as interferon alpha (INF-α) and interleukin-2 (IL-2). Toxicity was often marked and response rates were modest, with poor overall survival benefit (Ravaud and Dilhuydy 2005). Treatment options have improved through an understanding of the biology of the commonest form of renal cancer, clear cell renal cell carcinoma (ccRCC). Mutations in the von Hippel-Lindau (*VHL*) gene occur in up-to 75% of sporadic ccRCC tumours, leading to constitutive expression of hypoxia inducible factors (HIFs), which up-regulate pro-angiogenic factors including vascular endothelial growth factor (VEGF), and platelet derived growth factor (PDGF) (Maxwell et al 1999). These findings have led to the development of small molecule inhibitors targeting the HIF/VEGF/PDGF pathway (Maranchie et al 2002, Maxwell et al 1999, Shen and Kaelin 2013). Four multi-targeted tyrosine kinase inhibitors (TKIs) have been approved for use in advanced or metastatic ccRCC following evaluation in Phase III clinical trials. The first was sorafenib, which was approved in 2005 following positive results in the TARGET

trial (PFS 5.5 months for sorafenib and 2.8 months for placebo) (Escudier et al 2009). In 2006, first-line treatment of patients with the multi-kinase inhibitor sunitinib clearly demonstrated the superiority of sunitinib over INF-α, thus changing the standard of care in ccRCC. An improvement of 6 months in progression free survival, and a significant improvement in response rate (31% vs 6%) and quality of life was observed in the sunitinib-treated group, with a trend towards overall survival improvement (Motzer et al 2007). Pazopanib, a TKI targeting VEGF, PDGF and c-kit was also approved for use in advanced or metastatic ccRCC in the first line setting (Sternberg et al 2010). More recently axitinib, a selective second generation inhibitor of VEGF receptor 1, 2 and 3, has been licensed for second or third line treatment of ccRCC, following prior use of a TKI. In the first direct comparison of two TKIs, axitinib demonstrated superior PFS (median PFS improvement of 2 months) and objective response rate (19% vs 9%) in comparison with sorafenib in the second line setting (Rini et al 2011).

Inhibitors of the mammalian target of rapamycin (mTOR) have demonstrated superiority to INF-α in the first-line setting, with the phase III ARCC study demonstrating a median PFS advantage of 2.4 months and a median overall survival benefit of 3.6 months with temsirolimus (Hudes et al 2007), which is licensed for first line treatment of poor prognosis patients. Another mTOR inhibitor, everolimus, has shown an improvement in median PFS of 2.1 months compared with best supportive care in patients already treated with TKIs and cytokine therapy, thus establishing a place for this agent in the second line treatment of ccRCC (Motzer et al 2008).

Overall, however, as with prostate cancer therapy, the PFS benefit is modest, even with the arrival of multi-kinase inhibitors and mTOR inhibitors, highlighting the need for development of new and improved treatments in patients with metastatic RCC.

1.1.3 Urothelial cancer

Urothelial cancers are transitional cell carcinomas (TCCs) arising in the renal pelvis, ureter or bladder. There have been no major advances in the treatment of metastatic urothelial carcinoma for many years, and overall life expectancy still remains low at around 14 months (Richter and Sridhar 2012). First line chemotherapy utilises platinum agents in combination with gemcitabine, with response rates of around 50%, and a proven but modest survival advantage (von der Maase et al 2000). The combination regime of methotrexate, vinblastine, doxorubicin and cisplatin (M-VAC) has a similar survival advantage to gemcitabine and cisplatin, but is more toxic, hence is reserved for second line treatment in the advanced or metastatic setting (von der Maase et al 2000). Vinflunine and taxanes are also used in the second line setting, but response rates are poor, 8-10%, and toxicity with vinflunine limits its use clinically (Bellmunt et al 2009, Richter and Sridhar 2012). Targeted treatments are undergoing evaluation but have not as yet shown benefit nor established themselves in routine practice (Choueiri et al 2012, Dreicer 2012), the principal reason for this being the failure to identify activating or driver mutations within receptors or signalling pathways that would serve as therapeutic targets. Development of novel agents in urothelial cancer is thus lagging behind the recent developments seen in prostate and renal cancers.

This highlights an urgent need for better therapeutic options for patients with urological cancers, aiming to achieve significant improvement in patient survival and quality of life. From this need has emerged an interest in further exploring tumour related signalling pathways to discover novel therapeutic targets that may be relevant both in the metastatic setting, and to prevent or delay the development of metastatic

disease. The type 1 insulin-like growth factor receptor (IGF-1R) pathway is one potential target.

1.2 Components of the IGF-1R axis

The IGF-1R receptor axis comprises the IGF-1R, its principal ligands IGF-1 and IGF-2, insulin-like growth factor binding proteins 1-6 (IGFBP 1-6), IGFBP proteases and IGF-1R hybrid receptors formed with the insulin receptor (IR).

1.2.1 IGF-1 and IGF-2 ligands

The ligands of the IGF-1R are IGF-1 and IGF-2. The IGF-1R binds IGF-1 with the highest affinity, followed by IGF-2 with five-times lower efficiency. Insulin can also bind to the IGF-1R but at a five hundred to one thousand times lower affinity than IGF-1 (De Meyts et al 1994). IGF-1 is secreted from the liver in response to pituitary growth hormone (GH), and is also produced locally in tissues where it exerts autocrine or paracrine effects (Cohick and Clemmons 1993). IGF-2 is also produced in the liver and locally in tissues, but is not regulated by GH (Pollak et al 2004).

1.2.2 The IGF-1R receptor and receptor hybrids

The IGF-1R is almost ubiquitously expressed in normal tissues (Moschos and Mantzoros 2002). It is a heterotetrameric receptor tyrosine kinase, comprising two extracellular alpha subunits and two trans-membrane beta subunits linked by disulphide bonds (Ullrich et al 1986). The *IGF1R* gene is located on the long arm of chromosome 15, and encodes a 1367 amino acid polypeptide, the IGF-1R pre-proreceptor. The N-terminal signal peptide of the pre-proreceptor is cleaved co-translationally to generate a 220kDa proreceptor containing the alpha and beta

subunits. This proreceptor is then post-translationally glycosylated and dimerized in the endoplasmic reticulum (Adams et al 2000), followed by cleavage in the Golgi apparatus into the alpha (~135kDa) and beta (~96kDa) subunits, to form the mature heterotetrameric $\alpha_2\beta_2$ receptor (Adams et al 2000). The receptor is transported through the trans-Golgi network, and inserted into the cell membrane, with the extracellular alpha subunits containing the ligand binding domain of the receptor, and the beta subunits containing extracellular and trans-membrane regions, an intracellular tyrosine kinase domain, and a carboxy-terminal tail which may serve an anchorage and regulatory function (Kelly et al 2012, Ullrich et al 1986).

The IGF-1R has approximately 70% homology to the insulin receptor (IR), with 84% homology in the tyrosine kinase domain (Ullrich et al 1986). This homology allows the formation of hybrids between the IGF-1R and IR in tissues expressing or over-expressing both receptors (Pandini et al 2002, Soos et al 1990). The IR has two isoforms, IRA and IRB, generated by alternative splicing of exon 11 of the IR gene, and the IGF-1R can form hybrids with both IR isoforms. IRB is the classical isoform, possessing exon 11, and mediating glucose uptake and metabolism in response to insulin. Hybrids comprising half of the IGF-1R, and half of IRB are reported to behave similarly to the IGF-1R, by responding solely to IGF-1 but not to IGF-2 or insulin (Pandini et al 2002) The IRA isoform lacks exon 11, and can bind IGF-2 or insulin and elicit a proliferative and anti-apoptotic response (Belfiore 2007, Belfiore et al 2009). Hybrids comprising one half of the IGF-1R and one-half of IRA can bind both IGF-1, IGF-2 and insulin, and again, appear to have a similar function to IGF-1R homodimers in terms of eliciting proliferative and migratory responses (Belfiore et al 2009, Pandini et al 2002).

1.2.3 Insulin-like growth factor binding proteins and IGFBP proteases

The IGFBPs are found both in the circulation, where they control the transport and stability of IGFs, and at the tissue level where they influence the availability of the ligands to bind to their receptors, hence regulating receptor activity (Jones et al 1993a, Le Roith 2003). Circulating IGF-1 forms a ternary complex with IGFBP3 and the acid labile subunit (ALS), protecting it from the action of proteases, and regulating its bioavailability (Rajaram et al 1997). Thus the predominant effect of IGFBPs is to inhibit IGF actions, but some BPs promote IGF delivery to the IGF-1R and some are also known to have effects independent of the IGF axis (Jones et al 1993b, McIntosh et al 2010, Monzavi and Cohen 2002, Oh et al 1993, Rajah et al 1997). The exact function of the numerous IGFBPs and their potential role in tumorigenesis, both in relation to the IGF-1R and separately, is still far from clear. There are three recognised classes of proteases that can cleave IGFBPs, the kallikreins, matrix metalloproteinases (MMPs) and cathepsins (Rajah et al 1995). Cleavage of IGFBPs by these proteases can increase the availability of IGFs and hence receptor activation and signalling.

1.3 IGF-1R signalling

Ligand binding to the IGF-1R results in a conformational change in the receptor, and autophosphorylation of tyrosine residues 1131, 1135 and 1136 in the kinase domain, followed by phosphorylation of juxtamembrane tyrosines and carboxy-terminal serines (Adams et al 2000). These phosphorylation events lead to recruitment of adaptor proteins including IR substrates 1 to 4 (IRS-1 to IRS-4), and Src homology and collagen domain protein (Shc), and subsequent signalling via two major pathways, the phosphatidylinositide-3-kinase (PI3K)-Akt pathway and the Ras-

Raf-Mitogen-activated protein kinase (MAPK) pathway (Baserga et al 1997), outlined in figure 1.1.

1.3.1 PI3K-Akt signalling

Class IA PI3Ks are heterodimeric proteins, comprising a regulatory (p85) subunit and catalytic (p110) subunit (Engelman et al 2006). The p85 subunit binds to activated IRS proteins via the Src homology 2 (SH2) domain (Carpenter et al 1993), allowing the p110 catalytic subunit to convert phosphatidylinositol 4,5-biphosphate (PIP2) into phosphatidylinositol 3,4,5-triphosphate (PIP3) at the plasma membrane (Courtney et al 2010). Phosphastase and tensin homologue (PTEN) is a negative regulator of the pathway at this step by dephosphorylating PIP3 to PIP2 (De Luca et al 2012), and inactivating mutations of PTEN are frequently seen in advanced prostate cancer (McMenamin et al 1999). PIP3 recruits Akt to the plasma membrane and into close proximity with phosphoinositide-dependent kinase 1 (PDK1), which phosphorylates Akt at threonine 308 (Courtney et al 2010). The IGF-1R activates the mammalian target of rapamycin complex 2 (mTORC2), by an as yet unknown mechanism, resulting in Akt phosphorylation at serine 473. It has been suggested that mTORC2 facilitates Akt phosphorylation at both ser 473 and Thr 308, and that phosphorylation at both sites is required for full activation of Akt (Bhaskar and Hay 2007, Lang et al 2010, Sarbassov et al 2005). The downstream effects of Akt phosphorylation include survival, cell growth and motility, as described below.

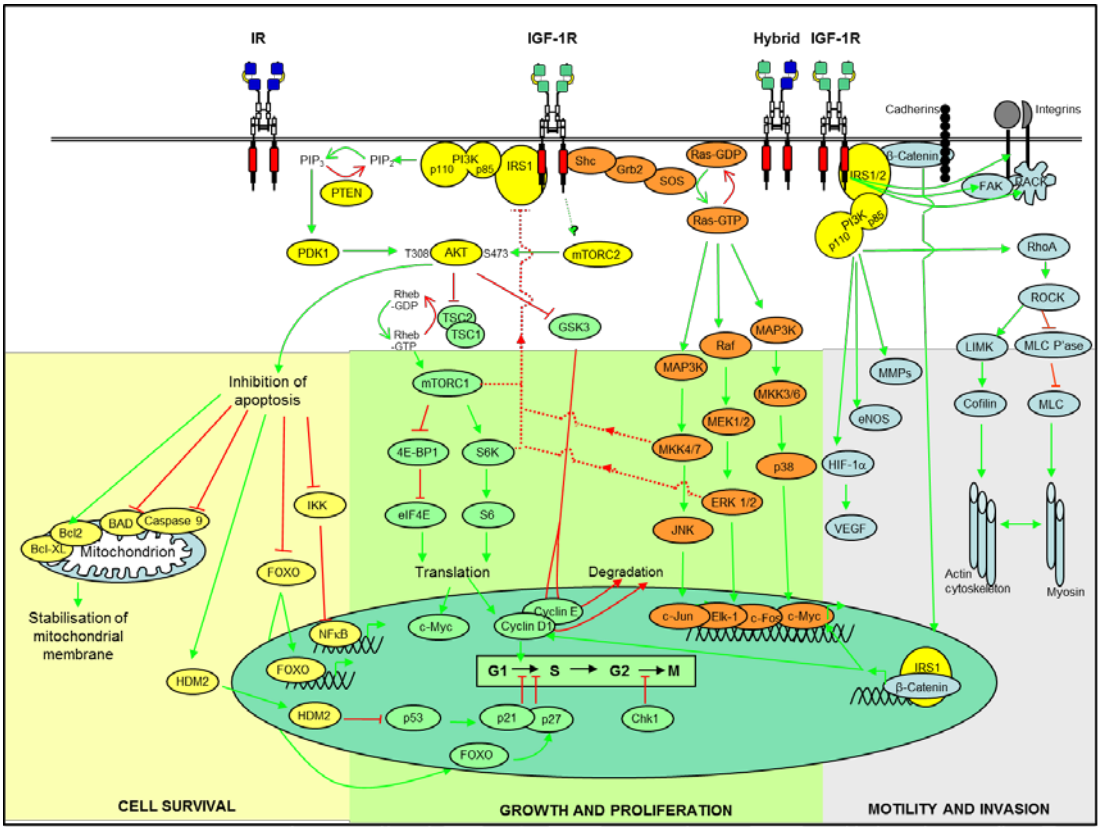

Figure 1.1: Signalling pathways of the IGF-1R
The figure shows the components of the major signalling pathways involving IGF-1R and hybrid IGF-1R-IR receptors. Ligand binding to the IGF-1R leads to activat
ion of two major pathways, the IRS-1-Akt pathway and the Ras-Raf-MAPK pathway. The figure also shows the subsequent downstream effects of IGF-1R activation, which include protection from apoptosis, growth and proliferation, and motility and invasion. The diagram combines information from different studies of IGF-1R signalling, and not all pathways operate in every cell.
Green arrows = activation; red lines/arrows = inhibition; dashed lines represent negative feedback pathways; figure modified from Chitnis *et al*, 2008 (Chitnis et al 2008).

1.3.1.1 Cell survival

PI3K-Akt signalling promotes cell survival by the inhibition of pro-apoptotic proteins, activation of anti-apoptotic proteins, and transcription of pro-survival genes (see figure 1.1). Inhibitory phosphorylation of the pro-apoptotic protein B cell leukemia 2 antagonist of cell death (Bad) and the cysteine-aspartic protease 9 (caspase 9) results in suppression of apoptosis (Cardone et al 1998, Datta et al 1997). Forkhead homolog (rhabdomyosarcoma) like 1 (FKHRL1 also known as FOXO3a) translocates to the nucleus and induces expression of pro-apoptotic genes including Fas ligand. Phosphorylation of FKHRL1 by Akt results in its cytoplasmic retention via association with 14-3-3 proteins, thus repressing expression of pro-apoptotic genes (Brunet et al 1999). Transcription factors FOXO 1 and FOXO4 are also targets of Akt signalling (Manning and Cantley 2007). A further survival mechanism involves suppression of p53 mediated apoptosis. Human double minute 2 (Hdm2) binds to the transcriptional domain of p53, thus blocking p53 target gene expression (Haupt et al 1997). Hdm2 then shuttles p53 from the nucleus into the cytoplasm, where it acts as a ubiquitin ligase, targeting p53 for degradation (Honda et al 1997, Roth et al 1998). Akt promotes nuclear translocation of Hdm2, resulting in increased cytoplasmic relocation and degradation of p53 (Mayo and Donner 2001). AKT also activates NF-kB activity and hence expression of anti-apoptotic genes such as TNF receptor-associated factor 1 and 2 (*TRAF1 and TRAF2*) (Kane et al 1999, Ozes et al 1999, Wang et al 1998).

1.3.1.2 Cell growth and proliferation

PI3K-Akt signalling activates the mammalian target of rapamycin complex 1 (mTORC1) to promote cell growth. The mechanism of mTORC1 activation is

illustrated in figure 1.1. Initially, Akt mediated inhibition of tuberous sclerosis 2 (TSC2) disrupts the Ras homologue enriched in brain (Rheb)-GTPase activity of the tuberous sclerosis 1 (TSC1)/TSC2 complex, allowing Rheb to activate the mammalian target of rapamycin complex 1 (mTORC1) (Tee et al 2002). Activated mTORC1 phosphorylates p70 ribosomal protein S6 kinase 1 (S6K) and also eukaryotic translation initiation factor 4E-binding protein 1 (4EBP1), allowing 4EBP1 to dissociate from eukaryotic translation initiation factor 4E (eIF4E), resulting in transcription of growth promoting genes (Fingar et al 2002). Negative feedback loops exist between mTORC1 and S6K and IRS-1, to limit signalling via the IGF axis when mTOR is activated (Carracedo and Pandolfi 2008, O'Reilly et al 2006).

IGF-1R signalling through the PI3K-Akt pathway can also affect cell proliferation by its effect on cell cycle regulatory proteins. Numerous downstream targets of Akt can influence cell cycle progression including phosphorylation of the cyclin dependent kinase (CDK) inhibitors p21 and p27 (Liang et al 2002, Shin et al 2002, Zhou et al 2001). Association of p21 and p27 with 14-3-3 proteins leads to cytosolic segregation, thus attenuating their cell cycle inhibitory effects within the nucleus, and allowing progression through the G1 phase of the cell cycle into S phase (Sekimoto et al 2004). Akt inhibition of the FOXO transcription factors can also reduce the expression of p27 (Medema et al 2000). Similarly Hdm2 mediated p53 inhibition can reduce expression of the p53 target p21 (Mayo and Donner 2001). Glycogen synthase kinase-3 beta (GSK3) is important in cell cycle regulation, phosphorylating cell cycle regulators cyclin D and cyclin E, and the transcription factors c-myc and c-jun, leading to their degradation. Akt induces inhibitory phosphorylation of GSK3, stabilising these proteins, and allowing G1 to S phase progression in the cell cycle (Manning and Cantley 2007). In addition, Akt, acting via mTORC1 and eIF4E,

promotes the translation of mRNAs critical for cell cycle progression, including *cyclin D1* and *c-myc* (Mamane et al 2004).

1.3.1.3 Motility, invasion and angiogenesis

Activated IGF-1R can promote motility and invasion. In colorectal cancer cells, phosphorylation of IRS-1 and β-catenin disrupts β-catenin/E-cadherin complexes at the plasma membrane, interrupting the connection of E-cadherin to the actin cytoskeleton and favouring cellular detachment and increased levels of nuclear β-catenin (Playford et al 2000). It was subsequently shown that β-catenin translocates to the nucleus in complex with IRS-1, promoting increased expression of β-catenin target genes (Chen et al 2005b). Interaction of activated IGF-1R with $\alpha_v\beta_3$ integrin affects the proliferation and invasive potential of cervical cancer cells, and activation of the RhoA-Rho-associated kinase (ROCK)-MLC pathway in breast cancer cells promotes actin filament stability and myosin contractility, both of which enhance cellular migration (Shen et al 2006, Zhang et al 2005). IGF-1R signalling can also assist invasion by the expression of matrix metalloproteinases (Zhang et al 2003). Both physiological and tumour associated angiogenesis can be stimulated by Akt via activation of endothelial nitric oxide synthase (eNOS) (Dimmeler et al 1999). Similarly, IGF-1R activation can lead to the increased expression of hypoxia inducible factor-1α (HIF1α) and expression of HIF1α gene targets such as VEGF which promote angiogenesis (Fukuda et al 2002, Gordan and Simon 2007).

1.3.2 Ras-Raf-MAPK signalling pathway

In addition to signalling via PI3K-Akt, IGFs are also capable in some cell types of activating ERK signalling. This is initiated by recruitment of adapter proteins Shc and growth factor receptor-bound protein 2 (GRB2) to activated IGF-1R. GRB2

recruits the guanine-nucleotide exchange factor son of sevenless (SOS) to the plasma membrane, leading to activation of the Ras proteins, namely K-Ras, N-Ras and H-Ras (Katz et al 2007). This leads to the sequential activation of the MAPK kinase kinases (MAP3K), MAPK kinases (MAP2K) and MAPKs. The best characterised pathway of activation is the Raf (B-Raf, A-Raf and c-Raf), MAP kinase/ERK kinase (MEK) 1 and 2 and extracellular signal–regulated kinases (ERK) 1 and 2 pathway. The chosen pathway of MAPK activation is cell and context dependent, mediating growth and proliferation via transcription of growth promoting genes (De Luca et al 2012). ERKs can phosphorylate transcriptional targets including erythroblastosis virus E26 oncogene homolog 1-like gene 1 (Elk-1), cAMP response element binding protein (CREB), c-Fos and c-Jun (De Luca et al 2012, Pearson et al 2001). In addition, ERKs can affect cell cycle progression through G1 by promoting degradation of the CDK inhibitor p27 and inducing transcription of cyclin D1 (Kawada et al 1997, Lavoie et al 1996).

In addition to ERKs, there are two other sub-families of MAPKs namely the c-Jun NH2-terminal kinases (JNK 1, JNK 2, and JNK 3) and p38 (Johnson and Lapadat 2002), and these are independently activated by specific MAP2Ks (Derijard et al 1995). JNK and p38 are activated predominantly by stress related stimuli, including UV irradiation, DNA damage and inflammatory cytokines, but responses can also be elicited via receptor tyrosine kinase activation (Katz et al 2007). Downstream targets of JNK include c-Jun, part of the AP-1 transcription complex, and JNK can also regulate apoptosis in response to specific stimuli (Galvan et al 2003, Tournier et al 2000). The p38 kinases are responsible for the transcription of inflammatory cytokines, hence are important in immune regulation (Lewis and Spandau 2008).

Cross-talk exists at several levels between the IRS-1-Akt pathways and the Ras-Raf MAPK pathway. For example, PDK1 can activate MAPKs by phosphorylation of MEK 1 at Ser^{222} and MEK2 at Ser^{226}, phosphorylation sites crucial for full activation (Sato et al 2004). Ras is known to interact with PI3K via the p110 catalytic subunit, an interaction that is important in Ras driven transformation of cells (Castellano and Downward 2011). ERK can activate mTORC1 via inhibitory phosphorylation of the TSC2 protein (Ma et al 2005a, Roux et al 2004). Also, inhibition of mTORC1, for example by rapamycin, can lead to activation of signalling via MAPK or PI3K-Akt (Carracedo et al 2008, O'Reilly et al 2006). These findings highlight the ability of cell signalling to compensate for inhibition of a single target, and emphasize the potential importance of inhibition of multiple pathways for effective anti-tumour therapy.

1.4 IGF-1R signalling and tumorigenesis

1.4.1 Role of the IGF axis in the risk of developing cancer

Numerous epidemiological studies have shown a relationship between high circulating levels of IGF-1 and the development of common cancers including breast, prostate and bladder (Chan et al 1998, Hankinson et al 1998, Pollak et al 2004, Zhao et al 2003). These associations were confirmed in a meta-analysis where high concentrations of IGF-1 were associated with an increased risk of prostate cancer (odds ratio comparing 75th with 25th percentile 1.49, 95% CI 1.14-1.95) and premenopausal breast cancer (1.65, 1.26-2.08). Overall, however, the associations were more modest than individual reports had suggested. Some studies have reported an association between high or low levels of IGFBP3 and cancer risk, particularly in

breast cancer, although any association now seems unclear (Renehan et al 2004, Renehan et al 2006, Roddam et al 2008)

1.4.2 Aberrant expression of IGF axis components in cancer

A well-established body of evidence, both direct and indirect, links IGF-1R signalling and cancer. There are numerous levels at which the IGF-1R axis can be aberrantly activated:

1.4.2.1 IGF-1R overexpression

Overexpression of IGF-1R can result in increased IGF-1R signalling, either directly through the IGF-1R or via formation of IGF-1R:IR hybrid receptors (Belfiore 2007, Seely et al 1995). IGF-1R over-expression can be secondary to loss of tumour suppressor genes which normally suppress IGF-1R transcription, including breast cancer type 1 susceptibility protein (BRCA1), p53 and, in a report from our group, Von Hippel Lindau (VHL) (Maor et al 2000, Werner et al 1996, Yuen et al 2007). Conversely, IGF-1R expression can be promoted by activation of oncogenes including mutant p53 and c-myb (Reiss et al 1991, Werner et al 1996). Thus, IGF-1R overexpression, while common in cancers, is usually secondary to an initiating mutation in another gene, and is rarely itself the driver event. IGF-1R mutations are generally inactivating, causing growth retardation (Pfaffle et al 2011), and activating mutations have not been described. However, some tumours do show *IGF1R* gene amplification, which is an increase in copy number of a restricted region on a chromosome, associated with overexpression of the amplified gene(s). *IGF1R* gene amplification is present with variable frequency (between 2-6%) in a variety of tumours including small-cell lung carcinoma, thymomas and breast cancer (Badzio et al 2010, Mimae et al 2012, Spears et al 2009).

A large variety of tumours overexpress the IGF-1R, and it is now known that in many tumours including renal, ovarian, gastric, oesophageal, pancreatic, colorectal and non-small cell lung cancer, overexpression confers a negative prognosis (Donohoe et al 2012, Kim et al 2013, Matsubara et al 2008, Parker et al 2002, Spentzos et al 2007, Takahari et al 2009, Valsecchi et al 2012, Yamamoto et al 2012).

1.4.2.2 Activation of components of the IGF axis

There are many levels at which IGF axis activation could occur. Cancers frequently express IGF ligands, often IGF-2, as a consequence of *IGF-2* gene amplification, which can be seen in colorectal carcinomas (Cancer-Genome-Atlas-Network 2012). Loss of maternal imprinting of the *IGF2* gene in tumours, or inactivation of the anti-mitogenic IGF-2R, which binds to and degrades IGF-2, can increase the bioavailability of IGF-2 (Cui 2007, Hebert 2006). This can then activate mitogenic signalling via the IGF-1R, hybrid receptors and the IRA. Tumours can also secrete IGFs in an autocrine fashion, or can respond to IGF-1 produced by paracrine secretion from adjacent stromal cells, resulting in receptor activation (Arnaldez and Helman 2012, Tazzari et al 2007, Vitale et al 2009).

The bioavailability of IGFs at the receptor is determined by the ability of IGFBPs to bind to the ligands and prolong their half-life in the circulation. The relationship between IGFBPs and IGF-1R activation is more complex however, IGFBPs having both agonist and antagonist effects on receptor activation, which are thought to be context dependent (Wetterau et al 1999).

Tumours can secrete IGFBP proteases which can cleave IGFBPs and increase the concentration of free ligand available for receptor activation. Prostate specific antigen (PSA or kallikrein-3), in addition to its normal physiological role, was one of the first identified IGFBP proteases (Cohen et al 1992). PSA is overexpressed in prostate

cancer and has been implicated in releasing bio-active IGF in prostate cancer bone metastases by its cleavage of IGFBP5 (Maeda et al 2009, Rajah et al 1995). Cathepsin D, another IGF-BP protease is also overexpressed in prostate cancer (Stamey et al 1987).

Finally, activating mutations in the IGF-1R signalling cascade such as loss of PTEN or activation of Ras or Raf can result in loss of negative feedback loops or constitutive activation of post-receptor signalling (Mulholland et al 2012, Wang et al 2012).

1.4.2.3 Role of the IGF axis in established cancers

Early evidence on the importance of the IGF-1R axis in maintaining the malignant phenotype was provided by Renato Baserga's group, who showed that IGF-1R null mouse fibroblasts (R- cells) are resistant to transformation and anchorage independent growth induced by known viral and cellular oncogenes (Sell et al 1993, Sell et al 1994). Re-introduction of the IGF-1R into these cells reverses the phenotype, allowing transformation (Sell et al 1994). Down-regulation of the IGF-1R was shown to result in massive apoptosis in tumour cells in anchorage independent growth conditions *in vitro*, and in tumours grown in mice *in vivo* (Resnicoff et al 1998). Consistent with these data, overexpression of the IGF-1R results in tumorigenesis and metastasis in transgenic mouse models of pancreatic and breast cancer (Jones et al 2007, Lopez and Hanahan 2002). These data suggest that the IGF signalling axis has an important role in tumour biology, and also highlights the potential therapeutic impact of IGF-1R inhibition. It is increasingly obvious that a detailed understanding of the pathway is essential to be able to achieve maximal therapeutic impact using IGF-1R inhibitors in the clinical setting, as will be discussed later.

1.5 The IGF-1R in urological cancer

Work from our group and others has shown that the IGF-1R is over-expressed in prostate carcinomas, and is detectable in bone metastases at levels equivalent to those in the primary tumours (Hellawell et al 2002, Ma et al 2012, Metalli et al 2010). Our group has also shown that IGF-1R expression in prostate carcinoma is upregulated or remains high throughout the course of progression to metastatic and/or androgen-resistant disease (Turney et al 2010). In advanced disease this is consistent with the reported ability of androgen receptor (AR) signalling to regulate *IGF-1R* gene expression (Pandini et al 2005). IGF-1R is also up-regulated in bladder cancers, with significant increase in expression in muscle invasive tumours compared with benign bladder epithelium (Rochester et al 2007). Furthermore, IGF-1R has been shown to promote motility and invasion of bladder cancer cells (Metalli et al 2010).

In clear cell renal carcinoma (ccRCC), IGF-1R is reportedly detectable in tumours by IHC in 50% of cases and is associated with poor survival (Parker et al 2003, Parker et al 2004). Work from our lab has shown that *IGF1R* expression is regulated at the RNA level by the VHL tumour suppressor, and IGF-1R over expression in ccRCC is secondary to loss of functional VHL (Yuen et al 2007). This work highlighted a discrepancy between the proportion of ccRCC tumours expressing *IGF-1R* at the mRNA level (100%) and the reported 50% of tumours expressing IGF-1R protein as detected by IHC (Parker et al 2003, Parker et al 2002, Parker et al 2004). This discrepancy warrants further investigation into the expression of the IGF-1R in ccRCC, and the clinical implications of this expression.

In further work from our group, it has also been shown that ccRCC cells expressing mutant VHL and higher IGF-1R are more chemoresistant than cells expressing functional VHL (Yuen et al 2009). Depletion of the IGF-1R sensitises cells

to 5-fluorouracil and etoposide, effects that are significantly greater in ccRCC cells expressing mutant VHL. These data support the hypothesis that IGF-1R up-regulation makes a significant contribution to chemoresistance in ccRCC tumours harbouring VHL mutations (Yuen et al 2009). These findings support the rationale for IGF-1R therapeutic targeting, and validate the IGF-1R as a target in urological cancers.

1.6 IGF-1R Therapeutic Targeting

IGF-1R targeting was first shown to inhibit tumour growth over 20 years ago, in a study demonstrating that IGF-1R antibody inhibits the growth of breast cancer xenografts (Arteaga et al 1989). Subsequent research has focused on the validation of IGF-1R as a therapeutic target by assessing the effects of inhibiting expression or function of the receptor. A wide variety of *in vitro* and *in vivo* models have shown a reduction in tumour growth and/or metastasis following blockade of IGF-1R signalling (Pollak et al 2004, Yuen and Macaulay 2008). Strategies used in these preclinical models have included downregulation of the IGF-1R using antisense or small interfering RNA, or dominant negative IGF-1Rs, approaches that do not have clinical potential (Dunn et al 1998, Resnicoff et al 1994, Rochester et al 2005, Sachdev et al 2004, Yeh et al 2006). Clinical testing of IGF-1R inhibitors has been relatively recent, and has been spurred on by the success of trastuzumab (Herceptin, Roche) an antibody directed to the HER2 receptor in breast cancer (Hudis 2007, Rodon et al 2008).

1.6.1 Classes of IGF-1R inhibitor drugs

Three approaches to IGF-1R inhibition are currently in clinical evaluation, the two main approaches being anti-IGF-1R antibodies and small molecule tyrosine kinase inhibitors (TKIs). Neutralising antibodies against IGF-1 and IGF-2 have also commenced phase II evaluation (Gao et al 2011, Haluska et al 2011). Anti- IGF-1R antibodies are selective for the IGF-1R receptor and IGF-1R-IR hybrid receptors, but do not bind to the IR (Pandini et al 2007). Antibody binding to the IGF-1R results in signaling inhibition, followed by internalization and degradation of the receptor (Sachdev et al 2003). Although these antibodies are selective for IGF-1R and hybrid receptors, it is postulated that the IR can also be internalized and degraded along with the IGF-1R on lipid rafts (Sachdev et al 2006), thus impacting on glucose homeostasis. The class of antibody can also have therapeutic implications. Antibodies of the IgG_1 or IgG_3 isotype can induce immunological responses including antibody dependent cell-mediated cytotoxicity (ADCC), which can enhance the therapeutic effect of the antibody (Liu et al 2008). ADCC may also result in bystander toxicity to normal tissues, and this could be an important consideration when targeting the IGF-1R, which is ubiquitously expressed in normal tissues (Moschos and Mantzoros 2002).

Considerable effort has also been made in the development of small molecule inhibitors against the IGF-1R. The majority of these are TKIs targeting the tyrosine kinase domain of the IGF-1R in different ways. There are ATP binding competitors such as OSI-906 (OSI pharamceuticals) (Mulvihill et al 2009), or non-ATP competitive inhibitors of tyrosine phosphorylation in the activation loop, such as AXL-1717 (Axelar AB) and BMS-754807 (Bristol Myers Squibb) (Carboni et al 2009, Vasilcanu et al 2004). ATP binding competitors are the least selective for IGF-

1R over the IR, and inhibit the IR to varying degrees. This is the result of the significant homology between the IR and IGF-1R, with 84% homology in the tyrosine kinase domain and 100% conservation of the ATP binding cleft (Ullrich et al 1986). Other potential small molecule inhibitors of the IGF-1R are substrate-competitive inhibitors, which are more selective for the IGF-1R due to the lower conservation of the substrate binding domains of the IR and IGF-1R. However, this class of inhibitors is more challenging to design due to the open structure of the domains, and hence there are fewer drugs of this class in development, although a Src kinase inhibitor targeting the peptide substrate binding site has recently entered clinical trials (Han et al 2012, Levitzki and Mishani 2006, Naing et al 2013).

TKIs have the advantage over antibodies of being administered orally. Being small, they have the potential to penetrate the blood-brain barrier (Pan et al 2007). They also exhibit shorter half-lives than antibodies, hours as compared to weeks, hence allowing for much greater flexibility in scheduling of administration, especially in combination regimens with chemotherapeutic agents (Buck and Mulvihill 2011). Initial concerns regarding both therapeutic antibodies and TKIs centered on the potential toxicity to normal tissues as a result of IGF-1R inhibition, and the consequences of inhibition of the IR. These concerns have been somewhat allayed from the results of early trials of IGF-1R blocking agents, which are generally well tolerated. Hyperglycaemia has been mild and easily managed in the majority of cases, settling with drug withdrawal, or in a few cases with oral hypoglycaemic agents or insulin (Haluska et al 2007, Karp et al 2009, Lacy et al 2008, Tolcher et al 2008). In fact, there is support for dual targeting of the IGF-1R and the IR in terms of anti-tumour efficacy, in that the pro-tumorigenic effects of IGF-2 signalling via the IR splice variant IR-A may confer resistance to IGF-1R blockade (Bid et al 2012, Ulanet

et al 2010). Other concerns relate to the frequency of activating mutations downstream of the IGF-1R, such as Ras/Raf mutations or *PTEN* inactivation by deletion or mutation (Croce 2008), which may limit the efficacy of inhibition upstream of the mutation. In some models, pathway activation downstream of the IGF-1R, involving mutations in B-Raf, K-Ras, N-Ras and PTEN, does not appear to induce resistance to IGF-1R inhibition or depletion (Ii et al 2011, Plymate et al 2007, Rochester et al 2005, Yeh et al 2006). However, there are conflicting data; for example, in glioblastoma cells, where IGF-1R knockdown or inhibition is less effective in cells possessing either ligand-independent Akt phosphorylation or PIK3CA mutation, compared with cells in which the PI3K-Akt pathway is IGF-responsive (Hagerstrand et al 2010). Similarly, in a recent study in oesophageal cancer cells, expression of mutant Ras reduced sensitivity to the IGF-1R inhibitor NVP-AEW541 (Bao et al 2012).

1.6.2 Preclinical testing of IGF-1R inhibitors

In vitro and in animal models, IGF-1R inhibitory drugs are capable of blocking cell survival and inhibiting tumorigenesis, although some tumour models have been chosen or designed to be IGF-sensitive (Litzenburger et al 2009). Several groups have shown the ability of IGF signalling to influence chemo and radio-sensitivity in pre-clinical models of lung, breast and colon cancer (Iwasa et al 2009, Perer et al 2000, Turner et al 1997). In head and neck cancer cells and xenografts, the anti-IGF-1R antibody A12 has been shown to enhance radiosensitivity by induction of apoptosis up-to six days post treatment (Riesterer et al 2011). The small molecule TKI PQIP and its derivative OSI-906 have shown enhanced antiproliferative effects in colorectal cancer cell lines and xenografts in combination with chemotherapy

compared with chemotherapy alone. The effects were mediated via cell cycle arrest as opposed to apoptosis induction (Flanigan et al 2010).

1.6.3 Clinical trials of IGF-1R inhibitors

Early trials of IGF-1R antibodies have shown dramatic activity in some uncommon tumours such as Ewing's sarcoma, but very little single agent activity in common solid tumours (Haluska et al 2007, Olmos et al 2010, Tolcher et al 2008). However, the importance of IGF-1R signalling in apoptosis protection provides a strong rationale for combining IGF-1R inhibitors with agents that induce apoptosis, as is the case with many chemotherapeutic agents and ionizing irradiation. IGF-1R blocking antibodies have shown benefit in combination with chemotherapy in Phase II clinical trials. For example, Karp *et al* reported an improvement in the response rate and prolongation of progression free survival (PFS) in non-small cell lung cancer (NSCLC) patients treated with figitumumab (Pfizer) in combination with carboplatin and paclitaxel, compared with chemotherapy alone (Karp et al 2009). The improvement in response was particularly striking in the sub-group of NSCLC patients with squamous histology, although absolute numbers of patients in this group were small. However, a subsequent phase III trial (ADVIGO 1016) of figitumumab in combination with carboplatin and paclitaxel in unselected patients with non-adenocarcinoma NSCLC was prematurely discontinued in late 2009, due to failure of the combination arm to prolong time to progression compared with chemotherapy alone (Jassem J et al 2010). A similar fate was met by the IGF-1R antibody dalotuzumab (Merck) in combination with cetuximab and irinotecan in a phase II/III trial in K-Ras wild-type colorectal carcinoma (Watkins et al 2011). In fact, the patients receiving the highest dose of dalotuzumab in the trial fared worse than those in the placebo group. Similarly, there have been negative results from Phase II trials

testing the combination of anti-IGF-1R monoclonal antibodies R1507 (Roche) with erlotinib in unselected NSCLC patients (Ramalingam et al 2011) and ganitumab (Amgen) with hormone therapy in postmenopausal women with breast cancer (Kaufman et al 2010). A Phase II trial in patients with pancreatic cancer indicated that the addition of ganitumab to gemcitabine prolonged the 6-month survival and overall survival (Kindler et al 2012), but a larger Phase III study (GAMMA) based on the same trial design terminated in August 2012 due to failure of the combination to prolong overall survival in an interim analysis. These disappointing Phase II/III trial results have led to some pharmaceutical companies discontinuing their IGF-1R targeting programmes, although others continue to develop and evaluate anti-IGF-1R agents in phase II/III trials, because of the undoubted activity of these agents in a subset of patients (Basu et al 2011, Yee 2012)

The failure of these clinical trials highlights two important issues. Firstly there are currently no validated biomarkers to predict response to IGF-1R inhibition, which would enable the identification of a group of patients likely to benefit from these drugs. Potential bio-markers have been identified, and include tumour histological sub-types, circulating IGF-1 levels or tumour IGF-1R expression. Unlike the situation in breast cancer therapy, where HER2 levels predict a response to trastuzumab, there is currently no robust evidence that IGF-1R levels are a predictive biomarker correlating with response to treatment (Gualberto et al 2010). Overexpression of IGF-1R is common in tumours, and as mentioned earlier, can result in the formation of IGF-1R:IR hybrid receptor (Pandini et al 2002). It is possible that the levels of insulin receptors or hybrid IGF-1R:IR receptors may correlate with response or resistance to IGF-1R therapeutics (Bid et al 2012, Ulanet et al 2010). It is also possible that response to IGF-1R antibodies could be influenced by subcellular IGF-1R

localization, and there is some preliminary evidence to support this. Kim *et al* showed that aberrant *N*-linked glycosylation of the IGF-1R resulted in a failure of IGF-1R to localize to the cell membrane, and correlated with figitumumab insensitivity in gastric and hepatocellular carcinoma cell lines (Kim et al 2012). This may suggest that glycosylation may have value as a predictive biomarker, and also highlights the possibility that IGF-1R sub-cellular localization might be a candidate predictive biomarker warranting further investigation.

The second important point highlighted by the failure of large phase III trials combining IGF-1R inhibitors with standard treatments is the need to understand how IGF-1R inhibition influences the response to chemotherapy and radiotherapy. For example, if IGF-1R inhibition results in cell cycle arrest in G1, it would not be advantageous to combine an IGF-1R inhibitor with a chemotherapeutic agent acting in S-phase of the cell cycle, or one dependent on continued cycles of replication for cell killing. Indeed, the sequence of administration of anti-IGF-1R agents in relation to chemotherapy has been shown to influence the degree of sensitisation that results (Khatri et al 2012, Zeng et al 2012). Therefore, there is clearly a need for a better understanding of the IGF-1R receptor pathway and its effects on the response to damage induced by cancer treatments in order to guide the rational design of therapeutic combinations.

1.7 IGF-1R and DNA Damage Repair

DNA double strand breaks (DSBs) are highly cytotoxic lesions that are induced by gamma irradiation and agents such as etoposide. After sensing the DSB, the cell may respond in a number of ways, by inducing cell cycle arrest and DNA repair, cellular senescence or apoptosis (Burma et al 2006, Shibata et al 2010). The protein Ataxia

Telangiectasia Mutated (ATM) has a central role in the complex process of sensing DSBs (figure 1.2) (Bakkenist and Kastan 2003, Bensimon et al 2011, Shiloh 2006, Shiloh and Ziv 2012). ATM phosphorylates histone protein H2AX (γH2AX) at the site of DSBs and initiates a cascade of events required for the activation of cell cycle checkpoints, DSB repair and/or apoptosis induction. The MRN complex, comprising MRE11, Rad50 and Nbs1, is also rapidly recruited to the site of the DSB and, in concert with ATM, initiates the complex process of DSB repair (Lavin 2007, Lee and Paull 2007, Lee et al 2010).

There are two major pathways for the repair of DNA DSBs in mammalian cells, homologous recombination (HR) and non-homologous end-joining (NHEJ), illustrated in figure 1.2. HR is a high fidelity process that requires a DNA template to repair strand breaks, and occurs in late S/G2 phase of the cell cycle when there is a sister chromatid present (Branzei and Foiani 2008, Kass and Jasin 2010). The initial step in HR involves 5'-3' processing to yield a 3'-single-stranded (SS) overhang, involving proteins including the MRN complex, C-Terminal Binding Protein Interacting Protein (CtIP), BRCA1, EXO-1 nuclease and Bloom syndrome protein (BLM) (Chen et al 2008a, Nimonkar et al 2008, Sartori et al 2007). Replication protein A (RPA) binds to the SS 3' overhang, preventing secondary structure formation (figure 1.2A), and this is required for subsequent breast cancer type 2 susceptibility protein (BRCA2) and deleted in split hand/split foot protein 1 (DSS1) assisted loading of Rad51 onto the DNA (Yang et al 2002) (figure 1.2B). The association of BRCA 2 with BRCA 1 via partner and localizer of BRCA2 (PALB2) appears important in this regard, as interference with this interaction results in defective HR (Sy et al 2009, Zhang et al 2009a). Rad51 then mediates SS invasion into homologous duplex DNA, forming a displacement loop (D-loop), following

which the invading 3' strand is extended by a DNA polymerase (Chen et al 2008b, Yuan et al 1999) (figure 1.2C). HR is completed by synthesis dependent strand annealing, or resolution of Holliday junctions, to give crossover or non-crossover products (Klein and Symington 2009) (figure 1.2D) .

The majority of DSBs are repaired in mammalian cells by the more rapid but error-prone NHEJ pathway (Mahaney et al 2009, Mao et al 2008). NHEJ mediated repair initially involves binding of Ku 70/80 heterodimer to DNA ends (figure 1.2E) (Walker et al 2001, Zhang et al 2004). The DNAPK catalytic subunit (DNAPKcs) is autophosphorylated at two major clusters, or by ATM at Thr2609 (Chen et al 2007, Ding et al 2003, Meek et al 2007, Uematsu et al 2007), resulting in recruitment to the Ku proteins to form the DNAPK holoenzyme (Cary et al 1997, Falck et al 2005). Phosphorylation of DNAPKcs results in conformational changes in the DNAPK complex, and allows end-processing enzymes and other repair proteins to access the DNA DSB (Mahaney et al 2009). The complexity of irradiation induced DSBs requires efficient end-processing mechanisms to remove overhangs, fill in gaps and remove blocking end- groups and secondary structures at the DSB (Mahaney et al 2009). The nuclease Artemis has 5'-3' exonuclease activity and can remove both overhangs and 3'-phosphoglycolate groups from DNA ends (Ma et al 2005b, Povirk et al 2007). Similarly, polynucleotide kinase (PNK) may play a role in NHEJ in the removal of blocking end-groups (Chappell et al 2002, Karimi-Busheri et al 2007). Aprataxin and pink like factor (APLF) and Werner's syndrome protein (WRN) are also known to play a role in DSB end-processing during NHEJ (Kusumoto et al 2008, Macrae et al 2008). Gaps resulting from cleavage during end-processing are filled by the polymerases Polμ and Polλ, belonging to the PolX family, and terminal deoxyribonucleotidyltransferase (TdT) (Davis et al 2008, Ma et al 2004, Moon et al

2007) (figure 1.2F). It is the end-processing occuring prior to ligation of the DSB that accounts for the more error-prone nature of NHEJ compared with HR (Mahaney et al 2009) (figure 1.2H). Following completion of end-processing, direct ligation of the breaks is achieved by DNA ligase IV, via an XRCC4-DNA Ligase IV complex, with XLF acting as a catalyst for the reaction (Calsou et al 2003, Gu et al 2007, Riballo et al 2009) (figure 1.2G).

Several studies have shed light on the processes that determine which DNA repair pathway is initiated following a DSB. As cells need to be in late S/G2 in order for HR to occur, HR must be restricted in G1, and this is achieved by cyclin-dependent kinase (CDK) activity throughout the cell cycle (Ira et al 2004). For example, levels of CtIP, required for end-resection in HR, are up-regulated in S/G2 both by inhibition of G1 associated CtIP degradation, and by activating phosphorylations of CtIP in S/G2 (Buis et al 2012, Chen et al 2008a, You and Bailis 2010, Yu and Chen 2004). More recently, BRCA 1 and p53 binding protein (53BP1) are emerging as key regulators in determining the repair fate of a cell, by regulating the initiation of DNA end-processing required for HR (Chapman et al 2012b). 53BP1 is recruited to DSBs throughout the cell cycle, and in G1 can exert an inhibitory effect on end-processing, thus promoting NHEJ (Bothmer et al 2010, Bunting et al 2010, Chapman et al 2013, Nakamura et al 2006). Conversely, BRCA1 expression in S/G2 is likely to remove 53BP1 from the DSB, inhibit 53BP1 function, or prevent enrichment of 53BP1 at the DSB by inhibiting interaction of 53BP1 with chromatin, thus allowing HR to proceed (Bouwman et al 2010, Bunting et al 2010, Chapman et al 2012a, Lukas et al 2011, Mallette et al 2012).

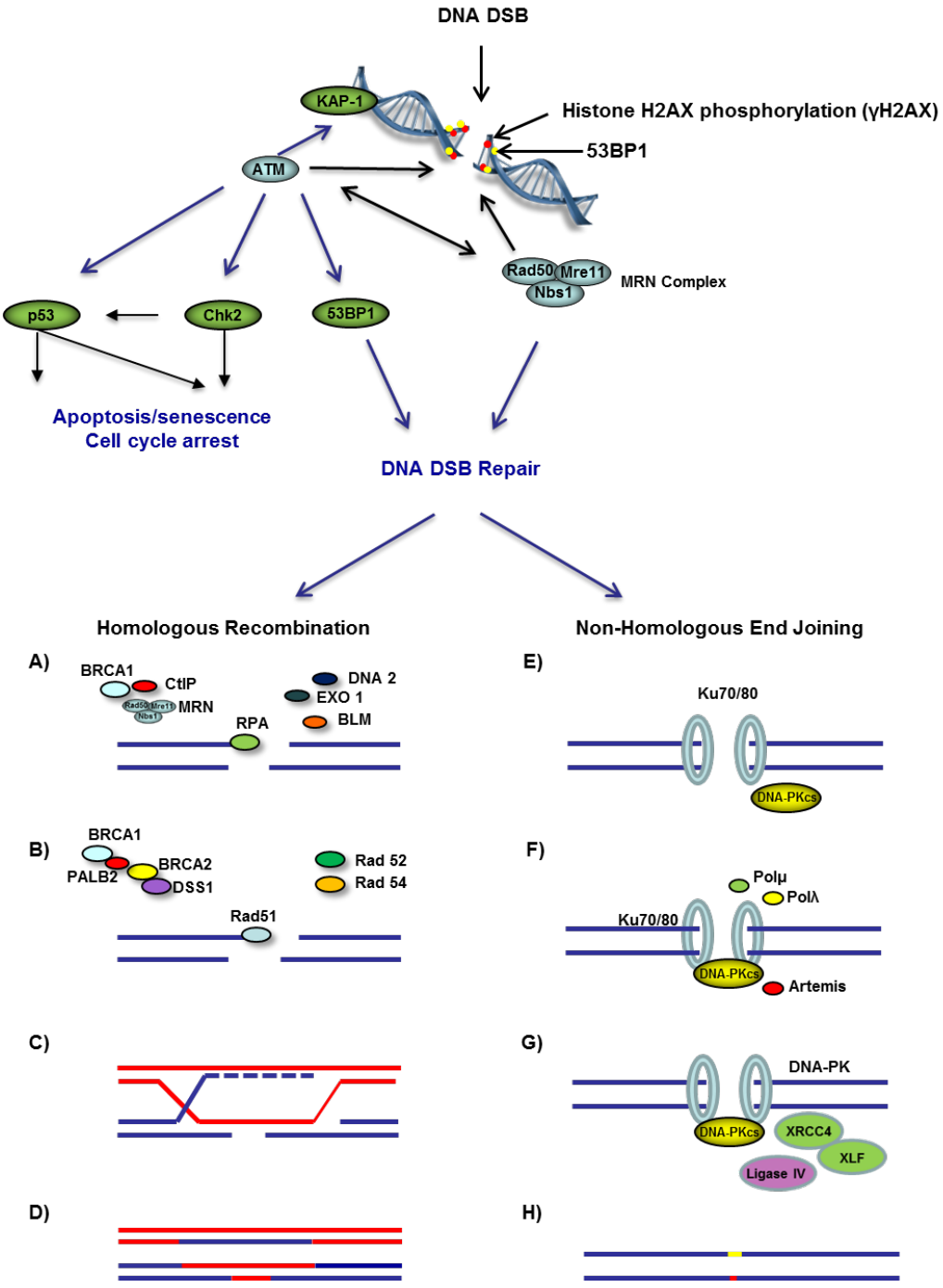

Figure 1.2: The cellular response to DNA double strand breaks
Simplified diagram of the DSB repair response. DSBs or altered chromatin structure are sensed by ATM and result in autophosphorylation of ATM on Ser1981 and dissociation of the ATM oligomers to monomers (Bakkenist and Kastan 2003). ATM phosphorylates both the MRN complex (MRE11, Rad 50, NBS1) and histone protein H2AX (γH2AX) at the site of a DSB. This initiates a cascade of events required for the activation of cell cycle checkpoints, DSB repair and/or apoptosis induction. Phosphorylation of checkpoint kinase 2 (Chk2) and p53 results in cell cycle arrest, apoptosis or senescence (Chen et al 2005a, Lehmann et al 2007, Lobrich and Jeggo 2005). Inactivating phosphorylation of KAP-1 (KRAB-associated protein1) induces relaxation of chromatin structure to facilitate repair in areas of heterochromatin (Goodarzi et al, 2008). DSB repair occurs via two main pathways, homologous recombination (HR) and non-homologous end joining (NHEJ). For a more detailed explanation on steps A) - H) refer to text.

The ability of IGF-1R inhibition to influence chemo- and radio-sensitivity has largely been attributed to apoptosis induction (Baserga 2005, Karasic et al 2010, Luk et al 2011, Pollak et al 2004, Riesterer et al 2011, Rodon et al 2008). However, a role for the IGF-1R is emerging in a more direct effect on DNA DSB repair. In an early report of immunohistochemical analysis in primary breast tumours, high levels of IGF-1R staining correlated strongly with early ipsilateral recurrence within the irradiated site, following breast surgery and radiation therapy (Turner et al 1997). Several other reports, including work from our group, have linked IGF-1R signalling and DNA repair. An initial report in mouse fibroblasts demonstrated that the IGF-1R plays a role in repair of ultraviolet-induced DNA damage, mediated via the p38-MAPK signaling pathway (Heron-Milhavet et al 2001). A functional IGF-1R has also been reported to be required for HR in mouse embryonic fibroblasts, regulating an interaction between IRS-1 and RAD51 (Trojanek et al 2003). IRS-1 reportedly binds to Rad51 in the cytoplasm, and phosphorylation of IRS-1 by IGF-1R results in the release of Rad51, allowing its nuclear translocation and binding to sites of DNA damage (Trojanek et al 2003). This phenomenon was also thought to be responsible for the ability of IGF-1 stimulation to enhance HR in murine mesangial cells following hyperglycaemia-induced DNA damage (Yang et al 2005). A functional IGF-1R was also reported to be required for the proper function of ATM in a murine melanoma model (Macaulay et al 2001), suggesting a potential interaction between the IGF-1R and DNA damage sensing via ATM, either via a direct effect on ATM, or indirectly, via an effect on its numerous downstream effectors (Figure 1.2).

In human cells, a role for IGF-1R signalling in DSB repair was supported by preliminary data suggesting that siRNA depletion of IRS-1 and AKT-2 in MCF7 breast cancer cells led to a reduction in damage-induced CHK2 phosphorylation

(Riedemann and Macaulay unpublished), suggesting that the IGF-1R may influence ATM signalling via the IRS-1-PI3K-AKT pathway. In prostate cancer cells, *IGF-1R* gene silencing enhanced cellular sensitivity to DNA damaging cytotoxic drugs and ionising radiation, but not to cytotoxic drugs that kill without damaging DNA (Rochester et al 2005), suggesting that apoptosis induction alone is an unlikely mechanism for chemosensitization. This is supported by data in VHL mutant ccRCC cells where IGF-1R depletion was shown to induce greater chemosensitization to the topoisomerase II inhibitor etoposide compared with the antimetabolite 5-fluorouracil (Yuen et al 2009). A previous clinical research fellow in our group, Ben Turney, showed that IGF-1R knockdown in prostate cancer cells induced a delay in the resolution of radiation induced γH2AX foci, and also caused a delay in DSB repair measured by pulsed-field gel electrophoresis (PFGE), with 30-40% excess unrepaired breaks at 24 hr (DPhil 2008) and (Turney et al 2012). This effect was associated with a modest reduction in HR, measured using a repair reporter assay (Pierce et al 1999, Turney et al 2012). Given that ATM-deficient or HR-deficient cells show only subtle DSB repair defects (Goodarzi et al 2008, Lundin et al 2005), it seems unlikely that defective HR or ATM could account for the significant difference in DSB repair kinetics seen on PFGE, leading to the hypothesis that the IGF-1R may also influence DNA repair via NHEJ.

A role for IGF-1R in NHEJ was not clearly established at the time of initiation of this project. Assessment of DSB repair in mouse fibroblasts had shown no effect of IGF-1 stimulation on protein levels of Ku70 and Ku80 and no effect on NHEJ mediated plasmid ligation *in vitro* utilising a cell-free NHEJ assay (Trojanek et al 2003). Similarly, IGFs did not influence the NHEJ pathway in response to hyperglycaemia induced DNA damage (Yang et al 2005). Once again protein levels

of Ku70 and Ku80 were unaffected, suggesting that any effect on repair was unlikely to result from a transcriptional response to IGF-1R activation (Yang et al 2005). In contrast, in radioresistant human NSCLC cells, IGF-1R inhibition resulted in a decrease in radiation-mediated binding of Ku 70/86 to a synthetic oligonucleotide substrate, and a reduction in the levels of the Ku 86 (Ku80) protein but not Ku70 (Cosaceanu et al 2007). This effect was mediated via the IGF-1R-p38 pathway and was independent of effects of IGF-1R on PI3K-Akt signaling, although inhibition of both pathways separately resulted in radiosensitization. This study did not directly demonstrate that IGF-1R or p38 signalling influence rejoining by NHEJ in an NHEJ assay, although an effect on Ku proteins is likely to impact on this repair pathway. In contrast, it has been hypothesized that IGF-1R can inhibit NHEJ repair in cervical carcinomas, where overexpression of IGF-1R is associated with increased expression of major vault protein (MVP) (Lloret et al 2008). Both IGF-1R and MVP expression are reported to correlate with reduced levels of Ku70/80 and BAX, and shorter long-term control following radiochemotherapy (Lloret et al 2008, Lloret et al 2009). This apparent association between IGF-1R, MVP upregulation and Ku70/80 downregulation has been hypothesized to suppress NHEJ (Lloret et al 2009), but this has not as yet been demonstrated. It has also been suggested that MVP, by virtue of inhibiting PTEN, may work in concert with IGF-1R in upregulating Bcl-2. Bcl-2 has been shown to interfere with Ku binding to DNA, and inhibits NHEJ (Lloret et al 2009, Wang et al 2008). Although plausible associations, the cellular mechanism of these links has not been shown, nor has a direct effect on NHEJ *per se* been demonstrated.

Thus, IGF-1R appears to play a role in the cellular response to DSBs, but the evidence is conflicting, perhaps due to the different experimental models and methods

that have been used. However, underlying this is a novel and potentially therapeutically important role of the IGF-1R which needs to be clarified.

1.8 Aims of the Project

The introduction has highlighted IGF-1R signalling as an important pathway in the pathogenesis of urological cancers. It has also highlighted the need to better understand the IGF-1R axis in terms of receptor expression and distribution in different cancers, and also its signalling pathways, effectors and functions. This information may reveal new aspects of the role of the IGF-1R axis that may have implications for patient management. Specifically, the aim is to allow novel and rational treatment combinations to be designed, predictive and prognostic biomarkers to be evaluated, and maximal therapeutic impact to be achieved in the clinical setting.

This project has two general aims, related to the distribution and function of the IGF-1R in urological tumours. The first aim relates to the discrepancy observed between data from our group on IGF-1R expression at the mRNA level in ccRCC (Yuen et al 2007), and IGF-1R expression by immunohistochemistry observed by others (Parker et al 2003, Parker et al 2002, Parker et al 2004).

1) To investigate the cellular distribution of the IGF-1R receptor in ccRCC, and assess correlation with clinical parameters.

The second aim was related to previous work carried out in our group in prostate cancer cells, which had used IGF-1R depletion to explore effects on DNA repair:

2) To investigate effects of IGF-1R inhibition on radiosensitivity and DNA repair.

A small molecule inhibitor of the IGF-1R kinase was obtained from AstraZeneca for use in this project, aiming to proceed along the following lines of investigation:

a) To characterize effects of IGF-1R inhibition on receptor phosphorylation, downstream signalling and clonogenic survival in prostate cancer cells.
b) To assess effects of IGF-1R inhibition on radiosensitivity in a panel of prostate cancer cell lines.
c) To determine the extent to which any effects on radiosensitivity are attributable to known properties of IGF-1R in regulating cell cycle progression and cell survival.
d) To investigate the hypothesis that the IGF-1R is involved in DNA repair, assessing effects of IGF-1R inhibition on the cellular response to DSBs, and investigating a putative role in the NHEJ pathway of DSB repair.

The ultimate objective of the project is to gain a better understanding of the role of IGF-1R signalling, aiming to guide the development of early phase clinical studies in patients with urological cancer.

2 Chapter II: Materials and Methods

2.1 Immunohistochemistry of paraffin-embedded tissues

Paraffin embedded whole mount renal tumour sections and renal tumour tissue microarrays (TMAs) were stained for IGF-1Rβ, using a modification of the method described in Turney et al (Turney et al 2010) with further optimisation as described in chapter 3. Human tissue comprised specimens that had been collected between 1983 and 2002, and was used under National Research Ethics study no. 04/Q1606/96, which covered the use of archival tissue.

Slides were dewaxed in Citroclear (TCS Biosciences Ltd., UK) for 5 min followed by rehydration in graded ethanol (100%, 95%, 80%, 70% and 50%) for 2 min intervals and distilled water for 10 min. Antigen retrieval was performed in Tris/EDTA retrieval buffer (50mM Trisma base, 2mM EDTA; adjust pH to 9 with NaOH) using a Decloaking Chamber (DC2002, Biocare Medical, USA) at 125°C for 2 min and 85°C for 10 min. Cooled slides were washed in Tris-buffered saline with 0.05% Tween-20 (TBST) and then blocked with 1.5% peroxide for 30 min. Slides were washed once for 1 min in TBST and blocked for 1 hour in 5% goat serum/1% bovine serum albumin (BSA)/TBST and incubated overnight with primary IGF-1Rβ antibody (#3027, Cell Signaling Technology) at a 1:75 dilution of antibody in 1% BSA/TBST. Slides were then washed four times for 1 min each in TBST and incubated for 1 hr at room temperature with biotinylated secondary antibody at a 1:200 dilution in 1% BSA/TBST. Slides were washed in TBST four times for 1 min each followed by incubation with R.T.U. Vectastain Elite ABC reagent (Vector Laboratories, USA) for 30 min at room temperature. DAB substrate (Envision

Detection System, Dako UK Ltd.) was applied for 5 min followed by counterstaining for 30sec with Mayer's haematoxylin (Vector Laboratories, USA). Slides were washed in tap water and dehydrated in graded ethanol (50%-100%) followed by Citroclear for 5 min, and mounted using DePex mounting medium (VWR International, UK).

Staining controls included pre-incubation of primary antibody with an excess of peptide to which the antibody was raised (Cell Signalling Technology), and slides in which primary antibody was omitted. Optimisation was performed with the help of Helen Turley (Nuffield Department of Clinical Laboratory Sciences). IGF-1R staining was scored in a semi-quantitative manner, incorporating both the intensity and extent of staining (demonstrated in table 2.1). TMA scoring was verified by Dr. Gareth Turner, consultant urological histopathologist.

	Intensity	**Extent**
0	No staining	Negative (0% of cells)
1	Weak but detectable above control	Focal (1-10% of cells)
2	Moderate staining	Moderate (10-50% of cells)
3	Strong staining	Extensive (>50% of cells)

Table 2.1: Scoring of IGF-1R staining:
Criteria for quantification are based on the original analysis by McCarty *et al* (Kinsel et al 1989).

The clinical data for the TMA cases were compiled by Uro-oncology Database manager Neviana Kilbey, and the analyses were carried out by statistician Cheng Han, both of the CRUK Department of Medical Oncology, Oxford Cancer Centre. Contingency tables were analysed using Pearson's χ^2 test to assess relationships between staining of IGF-1R and clinical parameters. Survival curves were estimated

using the Kaplan-Meier method. Prognostic factors were evaluated in multivariate analysis by Cox proportional hazards regression using the STATA package v11.0 (Stata Corporation). Relationships between outcome and clinical or immunohistochemical features were summarized with hazard ratios and 95% CI.

2.2 Cell Lines

The DU145 prostate cancer cell line was originally derived from a metastasis in a patient with prostate cancer (Stone et al 1978). The PC3 cell line originated from a bone metastasis in a 62 year old patient with prostatic adenocarcinoma (Kaighn et al 1979). 22-Rv1 cells originated from the serial propagation in mice of androgen-dependent CWR22 prostate cancer xenografts, following castration induced remission and then relapse (Sramkoski et al 1999). LNCaP-LN3 were generated from the parental LNCaP prostate cancer cell line following serial orthotopic implantation of tumour cells from a lymph node metastasis into the mouse prostate (Pettaway et al 1996). DU145 and PC3 prostate cancer cells were obtained from Cancer Research UK Laboratories, Clare Hall, Hertfordshire, UK. 22Rv1 and LNCaP-LN3 prostate cancer cells were obtained from the laboratory of Sir Walter Bodmer (Weatherall Institute of Molecular Medicine, University of Oxford, UK). Cells lines were authenticated using the DNA fingerprinting service provided by Cancer Research UK Cell Services, utilising STR (short tandem repeat) analysis. IGF-1R–null murine fibroblasts (R− cells) and isogenic R+ cells stably transfected with the CVN-IGF-1R plasmid expressing human IGF-1R cDNA under control of an SV40 promoter were from Renato Baserga (Kimmel Cancer Center, Thomas Jefferson University, Philadelphia, PA) (Rubini et al 1997, Sell et al 1993). M059J and M059K glioblastoma cell lines were obtained from Dr. Anne Kiltie (Gray Institute for

Radiation Oncology and Biology, University of Oxford, UK). All cell lines were regularly tested for mycoplasma infection using the MycoAlert ® detection kit (Lonza, UK). DU145, 22Rv1 and LNCaP-LN3 cell lines were maintained in RPMI-1640 at 37°C in 5% CO_2. PC3 prostate cancer cells were grown in Ham's F12 medium at 37°C in 5% CO_2. R- and R+ cells. were maintained in Dulbecco's Modified Eagle medium (DMEM) at 37°C in 10% CO_2. M059J and M059K cells were grown in 1:1 Ham's F12:DMEM with 1% pyruvate (Gibco/Life Technologies Ltd., UK) and 1% non-essential amino acids (Gibco/Life Technologies Ltd., UK), at 37°C in 10% CO_2. All media were supplemented with 10% fetal bovine serum (FBS), 100 units/ml of penicillin and 0.1mg/ml streptomycin. In addition, the medium for the R- and R+ cells contained 50µg/ml geneticin sulphate (G-418, Gibco/Life Technologies Ltd., UK). HEK-293 cells used in the assays for NHEJ/HR were obtained from the laboratory of Dr. Niedzwiedz (Weatherall Institute of Molecular Medicine, University of Oxford, UK) with permission from Professor Jeremy Stark (Beckman Research Institute of the City of Hope, CA) (Bennardo et al 2008). They were grown in phenol red free DMEM with charcoal stripped 10% FCS, 100 units/ml of penicillin, 0.1mg/ml streptomycin, 1µg/ml puromycin (prepared as 10mg/ml stock in MilliQ water and stored at -20°C) and 5µg/ml blasticidin (prepared as 10mg/ml stock in MilliQ water and stored at -20°C). For routine passage, cells were disaggregated using 3mM EDTA in PBS, washed in complete medium and reseeded.

2.3 Cell Treatments

2.3.1 siRNA knockdown of the *IGF1R*

IGF1R (Hs_IGF1R_1, Qiagen) and All Stars negative control (Qiagen) 20µM siRNA stocks were stored at -20°C and thawed on ice. Cells were seeded at 68 x 10^4 cells/10cm dish and 24 hr post seeding were transfected with 50nM of the appropriate siRNA using Oligofectamine (OF) transfection reagent (Invitrogen/ Life Technologies, UK). Briefly, for cells seeded in 10cm dishes, 6.8µl siRNA was mixed with 1.5ml Opti-MEM® (OM, Invitrogen/ Life Technologies, UK) and incubated for 10 min at room temperature. In addition, 12.3µl OF was separately incubated for 10 min with 409µl of OM. The OF was added to the siRNA mix and incubated together for 25 min at room temperature. Cells were washed twice in PBS, and then 1.9ml of the siRNA complexes in addition to 777µl of OM were added to the cells in a dropwise fashion and incubated at 37°C for 4 hr. Dishes were then topped up to 10mls with media containing FCS, and additional FCS was added to make the final concentration of FCS in the dishes to 10%.

2.3.2 Small Molecule Inhibitors

AZ12253801 is a small molecule inhibitor of the IGF-1R tyrosine kinase that was obtained from AstraZeneca in powder form. This was reconstituted in DMSO to a stock concentration of 10mM and stored in aliquots at -20°C. Aliquots were diluted in media to a working concentration of 1µM. The remaining chemical inhibitors were all commercially available in powder form, and were dissolved in DMSO as follows: the DNAPK small molecule inhibitor NU7441 (#3712, Tocris Bioscience, Missouri, USA) at 5mM; ATM kinase inhibitor (#118500, Calbiochem, UK) at 10mM; PI3-Kinase ATP binding site inhibitor LY294002 (#440202, Calbiochem, UK) to 20mM;

the p38 kinase inhibitor SB203580 (#559389, Calbiochem, UK) to 5mM stock and the MEK 1/2 inhibitor U0126 (#662005, Calbiochem, UK) to 10mM stock. Single use aliquots of all the inhibitors were stored at -20°C for the recommended duration.

2.3.3 Ionising radiation

Cells were either mock-irradiated or irradiated at doses of between 1-10 Gy in an IBL 637 irradiator (CIS Bio International, France) containing four caesium-137 sources of 50 TBq each (located in Biomedical Sciences, John Radcliffe Hospital). The approximate dose rate was 3.26 Gy/min.

2.4 Western Blotting

Monolayer cells were treated with solvent or active agent as the experiment dictated. Cells were washed twice with chilled PBSA and collected by scraping in lysis buffer, either IGF-1R lysis buffer (containing 1%Triton X-100, with protease and phosphatase inhibitors, see appendix), RIPA buffer (containing 0.1% sodium dodecyl sulphate [SDS], with protease and phosphatase inhibitors, see appendix) or SDS lysis buffer (containing 1% SDS, with protease and phosphatase inhibitors, see appendix). Lysates were incubated on ice for 30 min followed by centrifugation at 13,000rpm for 15 min at 4°C to pellet insoluble debris. SDS lysates were sonicated on ice for 10sec continuously at maximum output (Sonopuls GM70 with MS72 microsonotrode, Bandelin, Germany) to shear DNA. Soluble protein was quantified against BSA standards using the Pierce Bicinchoninic Acid (BCA) assay (Thermo Fisher Scientific, UK) or Bio-Rad protein assay (Bio-Rad, Life Technologies Ltd, UK) based on the principles of the Bradford assay (Bradford 1976), and analysed on a plate reader (μQuant Universal Microplate Spectrophotometer, NorthStar Scientific,

UK) at 562 nm and 595nm respectively. Equal amounts of protein were denatured in 3X Laemmli Buffer (70 mM Tris pH 6.8, 5% (v/v) β-mercaptoethanol, 40% (v/v) glycerol, 3% (w/v) SDS, 0.05% (w/v) Bromophenol Blue) at 95°C for 5 min and separated by SDS polyacrylamide gel electrophoresis (SDS-PAGE) on 5% to 15% polyacrylamide gels depending on the size of proteins to be detected. Proteins were transferred to nitrocellulose membrane (Hybond C Extra®, Amersham Biosciences, UK), at 35mA per 10 x 8cm gel, using the semi-dry transfer method (TE 77 PWR Semi-Dry Transfer Unit, Amersham Biosciences UK Ltd.) and blocked for 1 hour at room temperature using 5% non-fat dairy milk or 5% BSA in TBST. Membranes were incubated at 4°C overnight with primary antibody, washed three times in TBST for 5 min on a rocker, and then secondary antibody, either HRP-conjugated goat anti-rabbit or goat anti-mouse (Dako UK Ltd, UK) was applied for one hour at room temperature. Following a further three washes in TBST for 5 min each, protein bound antibodies were detected by enhanced chemiluminescence (ECL+, Amersham Corporation, UK).

2.5 Immunofluorescence

Cells were grown to 80% confluence on sterile coverslips in 6-well plates, treated with solvent or experimental agent for 4 hours followed by irradiation at 3Gy. This dose of irradiation was optimised to allow accurate counting of γH2AX foci and foci formed by other DNA damage repair proteins, namely 53BP1. At specific time points post irradiation cells were fixed for 20 min in 4% paraformaldehyde, 0.1% Triton-X-100 in PBS at room temperature. Cells were permeabilised for 10 mins with 0.5% Triton in PBS, washed in PBS three times, blocked for 60 min in 5% BSA, 5% FCS in PBS at room temperature, and incubated in primary antibody in blocking solution

overnight at 4°C. Negative control cells were incubated in blocking solution with no primary antibody. The following day, cells were washed three times in PBS for 5 min with gentle rocking. Plates were covered in foil and incubated for 1 hr with Alexa Fluor 488-conjugated secondary antibody (Invitrogen Molecular Probes A11029 [mouse] or A11034 [rabbit]) at a 1:2000 dilution. Some dual-staining experiments used Alexa Fluor 594-conjugated secondary antibodies (Invitrogen Molecular Probes A11032 [mouse] or A11037 [rabbit]). Following three further PBS washes, coverslips were mounted with Fluoromount G (Southern Biotech) with DAPI (final concentration 2µg/ml) and allowed to dry at room temperature prior to storage in the dark at 4°C until analysis. Foci were imaged and counted on an Axioskop 2 Zeiss microscope (Carl Zeiss Ltd., UK).

2.6 Clonogenic Survival Assay

2.6.1 Following small molecule inhibitor treatment

Cells were seeded at 1000 cells/ 6 well plate, or 3000 cells /10cm dish. Dishes were seeded in triplicate and the following day were treated with solvent or experimental drugs depending on the particular study undertaken. After 4 hr incubation, dishes were irradiated and cells were incubated at 37°C in either 5% (for DU145, 22Rv1, PC3 and LNCaP-LN3 cells) or 10% CO_2 (for M059J, M059K, R-, R+ cells) for between 9-11 days until discrete colonies of at least 50 cells had developed. Colonies were fixed in methanol:acetic acid 3:1 for 40 min and stained overnight in 0.1% crystal violet (Sigma, UK). Colonies were counted either manually for 6-well plate assays, or using a Colcount automated colony counter (Oxford Optronix, UK) for 10cm dishes.

2.6.2 Following siRNA knockdown

siRNA transfection was carried out as described (section 2.3.1), and 48 hr post transfection cells were disaggregated and seeded at 3000 cells /10cm dish. After 6 hr to allow adherence, cells were irradiated and incubated at 37°C for 9-11 days. Clonogenic survival was measured as above (section 2.6.1)

2.7 Immunoprecipitation (IP)

Monolayer cells were washed twice with chilled PBSA and lysed by scraping into IGF-1R lysis buffer. Lysis was completed on ice for 30 mins followed by centrifugation at 13000rpm for 15 min at 4°C. For Co-IP experiments, typically 1 mg of soluble protein was pre-cleared by adding 20µl of 50% slurry of agarose-conjugated protein A and protein G beads (Sigma) for 20-30 min at 4°C. Beads were collected by centrifugation at 6500 rpm for 30sec at 4°C, and precleared lysates were incubated overnight at 4°C, on a rotating wheel, with antibody at an appropriate concentration as recommended by the manufacturer. IPs were collected with 30µL of 50% slurry of agarose-conjugated protein A or protein G beads, for one hour at 4°C. Following three washes in IGF-1R lysis buffer, samples were boiled for 5 min in 3X Laemmli buffer and separated by SDS PAGE. Proteins were transferred to nitrocellulose membrane and detected by western blotting as described above (section 2.4).

2.8 Chromatin fractionation

Cells were grown to 80% confluence in 15cm dishes. Monolayer cells were treated with either solvent or AZ12253801 for 4 hr followed by irradiation at 3Gy. At chosen

time-points following irradiation cells were washed twice in ice-cold PBS, harvested with a cell scraper and centrifuged at 2000rpm for 3 min at 4 °C. The supernatant was removed and the pellet resuspended in 180µl hypotonic Buffer A (10 mM HEPES pH 7.9, 10 mM KCl, 1.5 mM $MgCl_2$, 340 mM sucrose, 10% glycerol, 1mM dithiothreitol (DTT), 1x EDTA-free Protease Inhibitor Cocktail (Roche)). Triton X-100 was added to a final concentration of 0.1% and samples were vortexed briefly. Cells were incubated on ice for 5 min, centrifuged at 1,300 x g for 5 min, and the supernatant (cytoplasmic components) was separated from the pellet (nuclei). The nuclear pellet was washed in 180µl Buffer A (10mM HEPES pH 7.9, 10mM KCl, 1.5mM MgCl2, 340mM sucrose, 10% glycerol 1mM DTT, protease inhibitor cocktail) and centrifuged at 1,300 x g for 5 min. The pellet was resuspended in 100µl of Buffer B (3mM ethylenediaminetretracetic acid [EDTA], 0.2 mM ethylene-glycol tetraacetic acid [EGTA], 1 mM DTT, Protease inhibitor cocktail), lysed on ice for 30 min and centrifuged at 1,700 x g for 5 min to separate the supernatant (nucleoplasmic proteins) from the pellet (chromatin). The chromatin pellet was washed once with Buffer B and then resuspended in 100µl urea/Tris buffer (UTB: 50 mM Tris-HCl pH 7.5, 8.5 M urea, 150 mM β-mercaptoethanol). Samples were sonicated for 10sec continuously at maximum output prior to carrying out a Bradford assay for protein quantification (section 2.4). Samples were stored at -20°C, and analysed by western blotting.

2.9 Apo-ONE® Homogeneous Caspase-3/7 Assay (Promega)

The Apo-ONE® Homogeneous Caspase-3/7 Assay measures the activities of caspase-3 and 7, which are key effectors of apoptosis in mammalian cells. The substrate for caspase-3/7, rhodamine 110, bis-(N-CBZL-aspartyl-L-glutamyl-L-valyl-L-aspartic acid amide; Z-DEVD-R110), exists as a profluorescent substrate. Caspase

3-like proteases are aspartate-specific cysteine proteases; cleavage occurs at the C-terminal side of the second aspartate residue of the sequence DEVD (Asp-Glu-Val-Asp). Sequential cleavage and removal of the DEVD peptides by caspase-3/7 activity, and excitation at 499nm results in intense fluorescence of the rhodamine 110 leaving group, the intensity of which is in proportion to the amount of caspase-3/7 cleavage activity present in the sample. The emission maximum is at 521nm.

Cells were seeded in black 96-well plates. Each plate included blank, solvent control and assay samples. Wells with medium alone provided values for background fluorescence. Cells were treated with solvent (0.0003% DMSO in complete media) or AZ12253801 and 4 hr later were irradiated (3Gy). Caspase substrate (100x) and Apo-ONE® Caspase-3/7 buffer were thawed and mixed in a 1:100 ratio to make Apo-ONE® Caspase-3/7 Assay Reagent. At specific time points, the reagent was added to wells in a 1:1 (reagent: sample volume) ratio, and gently mixed on a plate shaker at 300-500 rpm for one hour. Fluorescence was measured at an excitation wavelength of 499nm and an emission wavelength of 521nm using a fluorescence plate reader (FLUOstar Optima, BMG LabTech, Germany). Background fluorescence was measured on wells containing cell culture medium minus cells, and this value was subtracted from the other readings. Values of fluorescence were expressed as % increase over solvent treated control values [(treated- solvent)/ solvent x 100].

2.10 Beta galactosidase senescence assay

The assay was carried out using the Senescence Beta Galactosidase Staining Kit (Cell Signalling) using the manufacturers recommendations. Briefly, cells were seeded into 6-well plates and treated with solvent or AZ12253801 for 4 hr, followed by irradiation. At time-points following irradiation, cells were washed once in 2ml

PBS, fixed with 1ml fixative solution (20% formaldehyde, 2% glutaraldehyde in PBS) for 10-15 min at room temperature, washed twice with 2ml PBS, and incubated overnight with 1ml staining solution at 37°C. The staining solution contained (per ml), 930µl Staining solution (400mM citric acid/sodium phosphate pH 6.0, 1.5 M NaCl, 20mM $MgCl_{2)}$, 10µl Staining supplement A (500mM potassium ferrocyanide), 10µl Staining supplement B (500mM potassium ferricyanide), and 50µl 20mg/ml X-gal in dimethylformamide (DMF). Cells were examined under an Axiovert 135 (Zeiss) microscope (10x or 32x magnification) for development of blue colour, indicating expression of β galactosidase. Primary renal cancer cells (provided by Mrs. Olga Perestenko, IGF Group, Weatherall Institute of Molecular Medicine) which were senescent following 4-5 passages in culture, were used as a positive control in the assay.

2.11 Flow cytometric analysis of cell cycle distribution

Monolayer cells grown in 10cm dishes were treated with solvent or AZ12253801, with or without irradiation. At pre-defined timepoints the cell medium was aspirated and cells disaggregated with 3mls of warm PBS/ 3mM EDTA. Cells were collected in a further 7mls of medium and centrifuged in 15ml falcon tubes at 1,500 rpm for 5 min at room temperature (RT) to obtain a cell pellet. Cells were resuspended by flicking the cell pellet and then adding 200µl of PBS and pipetting 8-10 times. Cells were fixed by adding 1ml of ice cold 80% ethanol to the falcon tube whilst on slow vortex to avoid cell clumping. Fixed cells were stored at -20°C until further analysis if not performed immediately. For flow cytometric analysis of cell cycle distribution, cells were re-hydrated in 4mls of PBS containing 1% BSA (PBSB) and centrifuged at 2,000 rpm for 5 min at RT. The pellet was resuspended in 1ml of PBSA containing

0.25% Triton X-100 and placed on ice for 10 min. Then, 5mls of PBSB were added and the cells centrifuged again at 2000rpm for 5 min at RT. The pellet was washed twice with PBSB and resuspended in 200µl PBSA containing 10µg/ml propidium iodide (PI) (from 1mg/ml stock in water) and 100µg/ml RNAse (from 10mg/ml stock in 50mM Tris-HCl, pH 7.4, and 50%glycerol) and transferred to flow tubes. Samples were incubated at RT for 30 min, 300µl PBS was added and then stored at 4°C for up to one hour until analysis. Cells were analysed using the CyAn ADP Analyzer (Beckman-Coulter, UK) with FlowJo 7.6.5 software cell cycle analysis programme (www.flowjo.com).

2.12 RNA Extraction

The RNeasy® kit (Qiagen, UK) was used according to manufacturer's recommendations to extract total RNA. Approximately 10^6-10^7 cells grown in monolayer in 15cm dishes were washed with PBS and lysed in Buffer RLT containing β-mercaptoethanol (Sigma, St. Louis, MO, USA). The resulting highly viscous lysate was homogenised by passage through a 20-gauge needle a minimum of 5 times. Following homogenisation, 1 volume of 70% ethanol was added to the lysate before applying the lysate to a silica-membrane column. After centrifugation for 15s at 13,000rpm, the silica-bound RNA was washed once with Buffer RW1 and an on-column DNA digestion with DNase (RNase-free DNase set, Qiagen, UK) was performed. The column was washed twice with Buffer RPE with added ethanol, following which total cellular RNA was eluted from the column with 30µl of RNase-free water. RNA concentration was assessed by spectrophotometry, by measuring the UV absorbance at 260nm using the ND-1000 spectrophotometer (Nanodrop Technologies, Wilmington, DE, USA) supported with NanoDrop version 3.5.2

software. Spectrophotometric RNA quantification was carried out using a modification of the Beer-Lambert equation,

$$c = (A \times e)/b$$

where c is the nucleic acid concentration in ng/microliter, A is the absorbance in AU, e is the wavelength-dependent extinction coefficient (RNA: 40 ng-cm/µl) and b is the path length in cm. Purity was determined by the ratio of absorbance at 260nm versus 280nm, ideally ~2.0 for RNA. The 260/230 absorbance ratio was used as a secondary measure of RNA purity, with values often higher than the 260/280 ratio, and in the range 1.8-2.2. An appreciably lower 260/280 or 260/230 ratio might indicate the presence of contaminants. RNA was stored at -80°C.

2.13 Gene Expression Microarray analysis

Monolayer cells in 15cm dishes were treated with solvent or 60nM AZ12253801. After 4 hr incubation, half the dishes were irradiated at 5Gy. At 4 hr post irradiation (8 hr post treatment) RNA was extracted from the cells as described above (section 2.12). Microarray analysis was performed at the Cancer Research UK Paterson Institute Microarray Service (Paterson Institute for Cancer Research, University of Manchester, UK), using the Affymetrix GeneChip® Human Exon 1.0 ST Array platform. The analysis required 500ng of total RNA with a minimum concentration of 100ng/µl. The quality of the RNA was checked at the Paterson Institute on an Agilent bioanalyser (Agilent Technologies UK Limited, Cheshire, UK). Expression data were uploaded onto the online microarray database MIAME VICE. Data analysis was performed by Stephen Taylor, (Head of Computational Biology Research Group, Weatherall Institute of Molecular Medicine, Oxford, UK), to generate a list of transcripts regulated by radiation and/or AZ12253801, filtered by

their B-value, the log-odds that a gene is differentially expressed between the conditions. A B-value >3 is equivalent to a >95% chance that the gene is differentially expressed.

2.14 Reverse Transcription (RT)

cDNA was synthesised by reverse transcribing total RNA using the High Capacity cDNA Kit (Applied Biosystems/Life Technologies Ltd., UK) according to the manufacturer's instructions. Briefly, 2µg of total RNA was added to nuclease-free water to a final volume of 10µl in each PCR tube. A reaction mastermix was prepared, comprised of 2µl of 10x RT Buffer, 2µl of 10x Random Primers, 0.8µl of 25x dNTPs, 1.0µl of reverse-transcriptase and 4.2µl of nuclease-free water per reaction, and 10µl of mastermix was added to each PCR tube. A negative control reaction containing RNA but no reverse transcriptase was also set up. Reactions were placed in a DNA Engine Dyad® Peltier Thermal Cyler (MJ Research, Waltham, MA, USA) and incubated at 25°C for 10 min, 37°C for 2 hours, 85°C for 5 min and then 4°C until storage of the cDNA at -20°C prior to further analysis.

2.15 Real time quantitative Polymerase Chain Reaction (qRT-PCR)

2.15.1 Primer design

Primers for qRT-PCR were designed and their specificity checked using the web-based National Centre for Biotechnology Information (NCBI) Primer BLAST (Basic local alignment search tool) programme (www.ncbi.nlm.nih.gov/tools/primer-blast/). NCBI mRNA reference sequence accession numbers (RefSeq) were used for the

generation of primers for each gene of interest. Primers were designed to have a GC content of 50-60%, melting temperature (T_m) of between 50°C and 65°C, and avoidance of long (>4) repeats of single bases and 3' complementarity. Amplicon length was between 75-200 bases. The primers were synthesised by Invitrogen (Life Technologies Ltd., UK) and the sequences (5'→3') were as follows:

Short-chain dehydrogenase/reductase 3 (DHRS3)

RefSeq: NM_004753.4

Forward primer GCGCGCTGGTGATGTTCCCT

Reverse primer: CGACAGGTCCCGCAGCTTGG

Kinesin family member 20A (KIF20A)

RefSeq: NM_005733.2

Forward primer: TGTGCTCTGCGGCTGCGAAA

Reverse primer CAAGCCCGCTGGCGGAGAAA

Primers used to quantify expression of housekeeping genes (HKG) were previously designed and used in the laboratory:

Glyceraldehyde-3-phosphate dehydrogenase (GAPDH)

RefSeq: NM_002046.4

Forward primer: AGCCACATCGCTCAGACAC

Reverse primer: GCCCAATACGACCAAATCC

Tubulin alpha 1c (TUBA 1c)

RefSeq: NM_032704.3

Forward primer: CCCCTTCAAGTTCTAGTCATGC

Reverse primer: ATTGCCAATCTGGACACCA

Hypoxanthine phosphoribosyltransferase 1 (HPRT1)

RefSeq: NM_000194.2

Forward primer: TGACCTTGATTTATTTTGCATACC

Reverse primer: CGAGCAAGACGTTCAGTCCT

2.15.2 qRT-PCR

qRT-PCR was performed on the Rotor Gene 3000® qPCR System (Corbett Research, Sydney, Australia) using the SensiMix™ SYBR kit (Bioline Ltd., UK). The Mastermix was provided as a 2x mix containing SYBR® Green I dye, dNTPs, heat activated DNA polymerase and $MgCl_2$ (6mM). The PCR reaction consisted of 10µl of the Mastermix, 1µl (0.5µM final concentration) each of forward and reverse primers, 2µl (20ng) template cDNA and nuclease free water to a final volume of 20µl. Conditions for the PCR were 2 min at 50°C, 10 min at 95°C and then 40 cycles, each consisting of 15 seconds at 95°C, and 1 min at 60°C. All reactions were carried out in triplicate. A no-template control (NTC) using nuclease-free water instead of cDNA was used as a negative control to exclude cross-contamination of reagents and surfaces. A mock reverse transcription reaction excluding reverse transcriptase enzyme (section 6.13) served as a 'no amplification control' (NAC) to exclude contaminating genomic DNA from RNA preparations.

2.15.3 qRT-PCR Optimisation

The most stable HKG was screened and selected from a panel of 3 commonly used HKGs, GAPDH, TUBA 1c and HPRT1, using Normfinder software, based on analysis previously described (Andersen et al 2004). PCR amplification efficiency was compared for both the HKG and the target gene of interest, by carrying out a PCR reaction with 10-fold serial dilutions of the template cDNA covering a range from 50 to 0.5ng. The C_T values were plotted against the $\log_{10}$ RNA dilution; slopes of the resultant lines were compared by nonlinear regression analysis and a p-value for the difference was generated.

2.15.4 Relative quantification of levels of mRNA of the target genes of interest

Relative quantification was carried out using the $2^{-\Delta\Delta CT}$ method (Livak and Schmittgen 2001) to express a fold-difference in levels of the target nucleic acid in treated samples versus controls. mRNA expression levels of a reference HKG were used as a normalizer to account for differences in loading between samples. Solvent treated samples were used as the calibrator against which fold-changes in expression levels were measured. In brief, first the threshold cycle (C_T) of the target gene was normalised to that of the reference (ref) gene, for both the test sample and the calibrator sample:

$$\Delta C_T \text{ (test)} = C_T \text{ (target, test)} - C_T \text{ (ref, test)}$$

$$\Delta C_T \text{ (calibrator)} = C_T \text{ (target, calibrator)} - C_T \text{ (ref, calibrator)}$$

Then, the ΔC_T of the test sample was normalized to the ΔC_T of the calibrator.

$$\Delta\Delta C_T = \Delta C_T \text{ (test)} - \Delta C_T \text{ (calibrator)}$$

Finally, the expression ratio was calculated as:

$$2^{-\Delta\Delta CT} = \text{Normalized expression ratio}$$

2.16 Reporter assays for NHEJ and HR

2.16.1 Transient transfection reporter assay

The firefly luciferase reporter plasmid pGL2-control (Promega, Madison, WI) was utilised to measure the rejoining of linear DNA, adapted from the method of Bau *et al* (Bau et al 2004). This plasmid contains a luciferase reporter gene and a beta-lactamase (Ampicillin resistance) gene (figure 2.1). For the NHEJ assay, linearization of the plasmid was achieved utilizing two different restriction enzymes. Bam HI cleavage results in 4 base pair long overhangs at the 5' end. pGL2 plasmid digestion with Bam HI results in linearization away from the luciferase reporter which remains intact, and this serves as a control for transfection efficiency within the assay. Hind III cleavage also results in 4 base pair long 5' overhangs, and linearization with Hind III between the luciferase promoter and coding sequence results in interruption of the expression of luciferase. Both forms of linear plasmid were transiently transfected into cells. Rejoining of the promoter and the coding sequence by NHEJ resulted in restoration of luciferase signal, which was detected by luminometry. HR cannot be utilized for repair of the break as there is no sequence homologous to the luciferase reporter plasmid present in the human genome (Bau et al 2004).

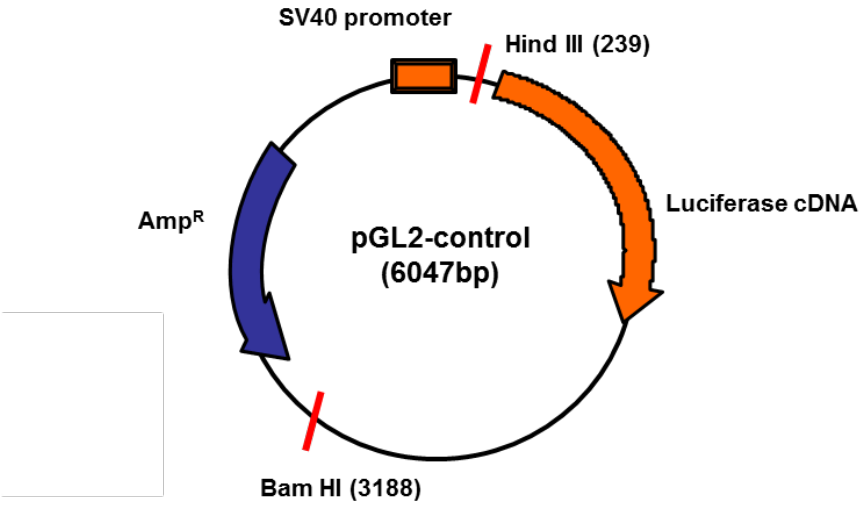

Figure 2.1: pGL2 luciferase reporter plasmid used in the NHEJ assay
Diagrammatic representation of the 6074 base pair pGL2 plasmid showing the unique restriction sites for Bam HI and HindIII, and the ampicillin resistance gene. Other restriction enzyme digestion sites are also present but have been omitted for clarity. Modified from 'pGL2 Luciferase Reporter Vectors' technical manual, Promega.

2.16.1.1 Bacterial Transformation

Bacteria are readily transformed by circular DNA, but extremely inefficiently by linear DNA, which is rapidly degraded by native exonucleases (Biswas et al 1995, El Karoui et al 1999). *E. coli* JM109 competent cells (Promega, Madison, WI) were thawed on ice, and 1ng of pGL2 plasmid DNA was mixed with 200µl competent cells and incubated on ice for 20 min. The cells were heat-shocked at 42°C for 45sec and transferred immediately to ice for 5 min. The mixture was added to 1ml lysogeny broth (LB) and incubated with shaking at 37°C for 60 min, and then 100 µl of the incubation mixture (10% plate) was plated out on LB agar containing 100µg ampicillin. The remaining 900µl was centrifuged at 13,000 rpm for 30sec, the pellet was re-suspended in 200µl LB and spread onto a second agar plate (90% plate). Plates were incubated at 37°C overnight and the following day an individual colony was selected for inoculation of a starter culture for a maxi prep, for plasmid DNA purification.

2.16.1.2 Plasmid DNA purification using Qiagen Plasmid Maxi kit

Plasmid DNA was purified using the Qiagen EndoFree Plasmid maxi Kit. An individual bacterial colony containing the pGL2 plasmid was used to inoculate a starter culture of 10mls of LB containing 60µg/ml of ampicillin, the selective antibiotic. The culture was incubated for approximately 8 hr at 37°C, with vigorous shaking at 300rpm. This culture was diluted 1/1000 into LB medium containing 60µg/ml ampicillin and grown at 37°C for 12-16 hr with vigorous shaking at 300rpm. Bacterial cells were harvested by centrifugation at 6000 x g for 15 min at 4°C, and resuspended in 10ml of buffer P1containing 100µg/ml RNase A. The suspension was resuspended completely by vortexed to ensure no clumps remained. 10ml of buffer P2 was added to the suspension, and the lysate mixed thoroughly by vigorously inverting the tube 4-5 times, followed by incubation at room temperature for 5 min. 10ml of chilled buffer P3 was added to the lysate to precipitate genomic DNA, proteins and cell debris, mixed by vigorously inverting 4-5 times, and then poured into the barrel of a QIAfilter cartridge. The cartridge was incubated at room temperature for 10 min. The cap was removed from the cartridge nozzle and the cell lysate was filtered into a 50ml tube, to which 2.5ml of buffer ER was added, mixed by inverting and incubated on ice for 30 min. The filtered lysate was applied to a equilibrated Qiagen-tip, and allowed to enter the resin by gravity flow. The tip was washed twice with 30ml of buffer QC to remove all contaminants, followed by elution of the resin-bound DNA with 15ml buffer QN. DNA was precipitated by the addition of 10.5ml of room temperature isopropanol, mixed, and centrifuged immediately at ≥15.000 x g for 30 min at 4°C. The supernatant was decanted carefully, the DNA pellet washed with 5ml of endotoxin-free 70% ethanol at room temperature, followed by centrifugation at ≥15.000 x g for 10 min. The supernatant was decanted carefully,

the DNA pellet was air-dried for 5-10 min followed by dissolution in 300µl of endotoxin-free buffer TE. DNA concentration was determined by UV spectrophotometry at 260nm and qualititative analysis on agarose gel.

2.16.1.3 Restriction enzyme digestion for linearization of pGL2 plasmid

For linearization of circular plasmid, the restriction digests contained 50µg of plasmid DNA, 10x buffer appropriate to restriction enzyme (5µl), 100x BSA (for Bam HI only, 0.5µl, final concentration 0.05µg/ml), restriction enzyme (Bam HI or HindIII, 5µl) and distilled water to make up total volume to 50µl. The digest was incubated at 37°C for 6 hr and subsequently 1µl was analysed by agarose gel electrophoresis on a 1% agarose gel to confirm complete digestion. The remainder was aliquoted and stored at -20°C until gel purification.

2.16.1.4 Gel extraction and purification of linearized plasmid

The QIAquick gel extraction kit (Qiagen, UK) was utilized according to the manufacturer's protocol. Briefly, the restriction digest was analysed by electrophoresis on multiple wells of a 1% agarose gel, and linearized DNA fragments were carefully excised with a clean scalpel trimming off any excess agarose. The fragments were weighed in a colourless eppendorf tube up to a maximum of 400mg per extraction column. Three volumes of buffer QG were added to one volume of gel (100mg ~100µl). Tubes were incubated at 50°C for 10 min, vortexing every 2-3 min during the incubation to help dissolve the gel. Once dissolved completely, the colour of the mixture was yellow, indicating a pH of ≤7.5, at which adsorption of DNA to the QIAquick membrane was optimal. One gel volume of isopropanol was added to the mixture, which was applied to a QIAquick spin column in a 2ml collection tube and centrifuged at 13,000 rpm for 1 min. The flow-through was discarded and 0.5ml of

buffer QG was added to the column and centrifuged for 1 min. To wash, 0.75ml of buffer PE was added to the column, allowed to stand for 2-5 min, and centrifuged for 1min at 13,000 rpm. The flow-through was discarded and a further 1 min centrifugation performed. For elution of the DNA, 50µl of buffer EB (10mM Tris-Cl, pH 8.5) was added to the centre of the QIAquick membrane, allowed to stand for 1 min, then centrifuged for 1 min at 13,000 rpm. DNA concentration was determined by UV spectrophotometry (Nanodrop) evaluation and the samples were stored at -20°C. Bacterial transformation was carried out as in section 2.16.1.1 to determine any contamination of linearized plasmid with uncut circular plasmid. Bam HI linearized, Hind III linearized and circular pGL2 plasmid were all plated out on 10% and 90% plates separately. Plates were incubated at 37°C overnight and the following day, colonies were counted and expressed as number of colony forming units (cfu)/µg of DNA.

2.16.1.5 Transfection of linearized plasmid

DU145 cells were seeded in a 6-well plate at 11.25 x 10^4 cells per well. The following day, a 50nM siRNA transfection was carried out into triplicate wells of a 6-well plate as described in section 2.12, with volumes adjusted for a 6-well plate format. A further 48 hr later, linearized plasmid DNA was transfected into cells. Briefly, 4µl of TransIT reagent (Mirus, ratio of DNA:reagent 1:2) was added to 200µl Optimem and incubated for 15 min. Then 2µg of the appropriate linearized plasmid was added and incubated for a further 15 min, followed by 4µl of TransIT boost reagent (ratio of DNA:boost reagent 1:2) and incubated for 15 min. The complexes were added dropwise onto the cells, and luciferase assays were performed 24 hr later.

2.16.1.6 Luciferase assay

The Promega Luciferase Assay System (Promega, Madison, WI) was used as per manufacturer's guidelines. Briefly, medium was aspirated off the cells, which were washed once in 0.5ml PBS. Then 100µl passive lysis buffer was added to each well, and the plates vigorously rocked at room temperature for 45 min. Lysates were pipetted vigorously to break up clumps of cell debris, and 20µl samples of each lysate were transferred to the wells of white opaque 96-well plates (Corning). Following addition of 50µl luciferase assay reagent (LAR), the luminescence was measured on a luminescence plate reader (FLUOstar Optima, BMG LabTech, Germany). A protein assay was performed on each lysate (as in section 2.4) and the luminescence values were corrected for protein content. The results were expressed as:

$$\left[\frac{\text{luminescence of Hind III cut transfectants}}{\text{luminescence of Bam HI cut transfectants}}\right] \text{X } 100$$

The remaining lysates were used for western blot analysis to confirm knockdown of target proteins.

2.16.2 Integrated Reporter assays

NHEJ and HR reporter HEK293 cell lines each contained an integrated GFP reporter: EJ5-GFP for the NHEJ assay or DR-GFP for the HR assay, and stable expression of the TST fusion protein for inducible I-Sce I activation. The reporters had been designed in such a way that repair of I-Sce-I endonuclease induced DSBs by either NHEJ or HR restored GFP expression, which could be detected by flow cytometry. The generation of the plasmids used for these assays and the methodology have been previously described (Bennardo et al 2008) and in figure 2.2, and

permission was obtained from Professor Jeremy Stark (Beckman Research Institute of the City of Hope, CA) for use of these NHEJ and HR reporter HEK293 cell lines.

Cells were grown in 6cm dishes to approximately 60% confluence, and were treated with solvent (control), AZ12253801 or the DNAPKcs inhibitor NU7441 for 4 hours, the latter being used as an inhibitor of NHEJ. The tamoxifen analogue 4-hydroxytamoxifen (4OHT) was added for 24 hours, then removed and replaced with fresh medium containing either AZ12253801 or NU7441, and 72 hours after the addition of 4OHT, cells were collected in 1x trypsin/PBS/EDTA. Cells were pelleted and fixed by re-suspending in 1ml of 4% paraformaldehyde for 10 min at room temperature. Cells were centrifuged at 2,000 rpm for 5 min, re-suspended in 1ml PBSA to wash, centrifuged again, resuspended in 500µl PBSA and transferred to flow tubes. Flow cytometric analysis was carried out on a CyAn ADP Analyzer (Beckman-Coulter) using FlowJo 7.6.5 software (www.flowjo.com).

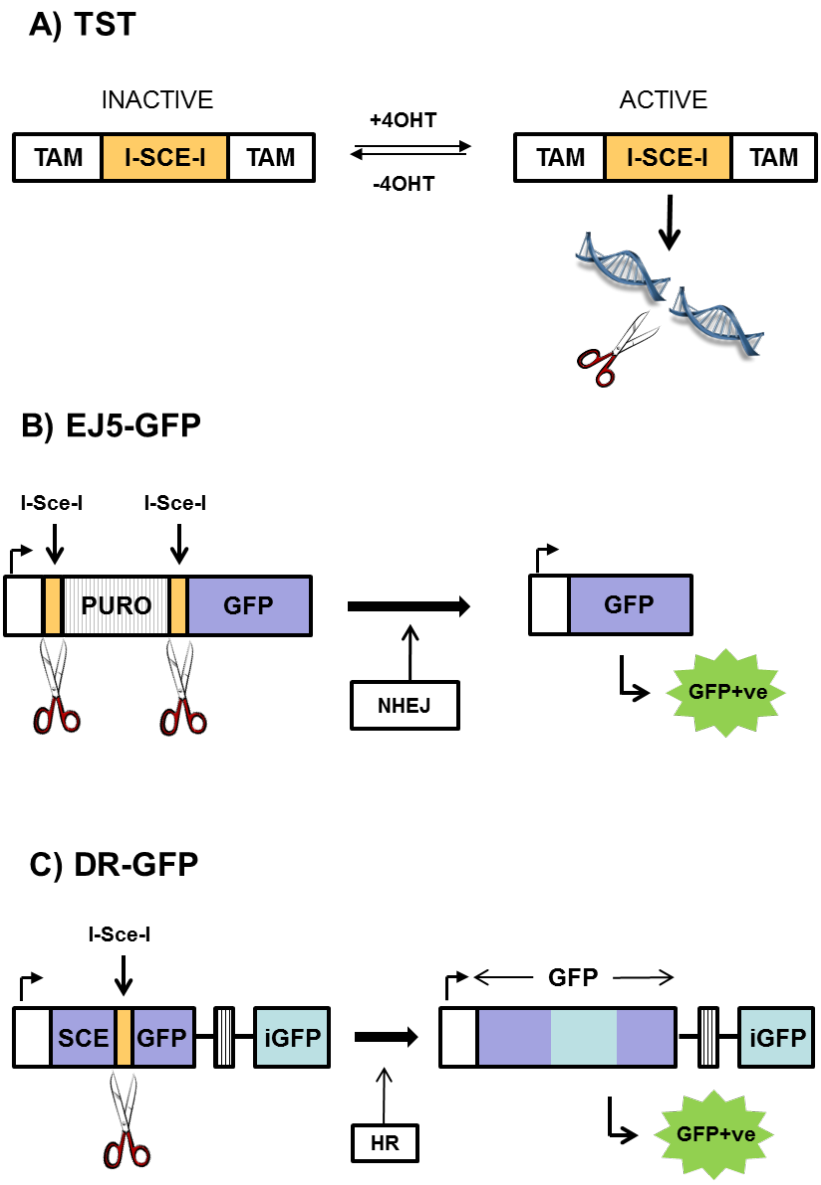

Figure 2.2: Plasmids used in the NHEJ/HR assay for DNA repair
A) The TST expression vector was designed for inducible activation of I-Sce-I. It comprises a mutant form of the oestrogen receptor ligand binding domain (TAM) fused to both ends of I-Sce-I (TAM-I-Sce-I-TAM or TST). In the absence of 4-hydroxytamoxifen (4OHT), I-Sce-I cannot bind and cut DNA, but can in the presence of 4OHT. The TST expression plasmid had been co-transfected with a blasticidin resistance plasmid when generating stable cell lines. B) The total NHEJ reporter plasmid EJ5-GFP contains a promoter and GFP coding sequence separated by a puromycin (puro) resistance gene, which is flanked by two I-Sce-I restriction sites in the same orientation. Induction of I-Sce-I expression leads to excision of the puro gene and repair of the cut ends by NHEJ, joining the promoter to GFP cDNA allowing expression of GFP. C) The HR reporter DR-GFP comprises two differentially mutated GFP genes orientated as direct repeats, and separated by a puro resistance gene. In repeat SceGFP, 11bp of wild type GFP sequence is substituted by a I-Sce-I site. The substituted base pairs are flanked by stop codons to terminate transcription and inactivate the protein. When a DSB is generated in SceGFP, homologous sequence in the downstream repeat iGFP allow repair by HR, restoration of the GFP coding sequence and green fluorescence. Diagrams and descriptions adapted from (Bennardo et al 2008, Pierce et al 1999).

2.17 Statistical analysis

Data were analysed using Office Excel 2003 (Microsoft) and GraphPad Prism 5 (GraphPad Software Inc, USA). Statistical significance was determined using either a t-test for differences between two separate treatment groups, one-way ANOVA for differences between three or more treatment groups, or a two-way ANOVA for trends between treatment curves. A p-value for significance was calculated.

3 Chapter III: Expression and subcellular distribution of the IGF-1R in Clear Cell Renal Cell Carcinomas

3.1 Introduction

The presence and level of expression of the IGF-1R in ccRCC is reported to confer a poor prognosis (Parker et al 2003, Parker et al 2002). A previous study from our group had investigated the effects of VHL on *IGF1R* expression and had found that VHL suppresses *IGF1R* transcription, principally via sequestration of Sp1. In that study, *IGF1R* mRNA was detected in all tested samples of ccRCC, and was present at levels significantly higher than benign kidney (Yuen et al 2007). This was in contrast with previous studies reporting that 40-50% of ccRCCs lack IGF-1R by immunohistochemistry (Parker et al 2003, Parker et al 2002, Parker et al 2004). The study of Yuen *et al* had not examined IGF-1R at the protein level. Therefore it was decided to investigate this apparent inconsistency by assessing a larger panel of ccRCCs than had been previously investigated by Yuen *et al*, for IGF-1R by immunohistochemistry.

3.2 Results

3.2.1 Optimisation of IGF-1R immunostaining:

Conditions for immunostaining were carefully optimised on whole mount ccRCC specimens prior to staining of ccRCC tumour microarrays (TMAs). The initial conditions were based on optimisation performed in our laboratory (Turney et al 2010), with further testing of a range of primary antibody concentrations and

conditions for antigen retrieval. Appropriate controls were included namely omission of primary antibody to exclude non-specific staining attributable to the secondary antibody, utilisation of peptide block to assess quenching of signal from the primary antibody (figure 3.1) and comparison of signal from control or cells with siRNA induced IGF-1R depletion, to determine specificity of staining (figure 3.2).

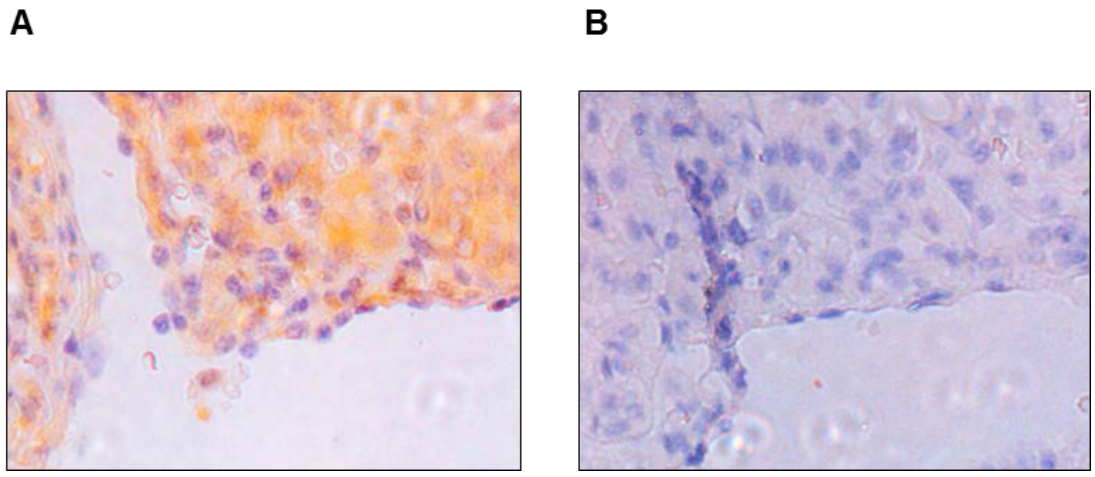

Figure 3.1: IGF-1R immunohistochemistry: signal attenuated by peptide block.
A) Staining of a ccRCC tumour with IGF-1R antibody (Cell Signaling Cat.no. 3027) using the final optimised protocol. B) Staining of an adjacent section of the same ccRCC, following pre-absorption of the IGF-1R antibody by incubation with excess of blocking peptide corresponding to the epitope to which the antibody was raised (obtained from Cell Signalling). (10x objective)

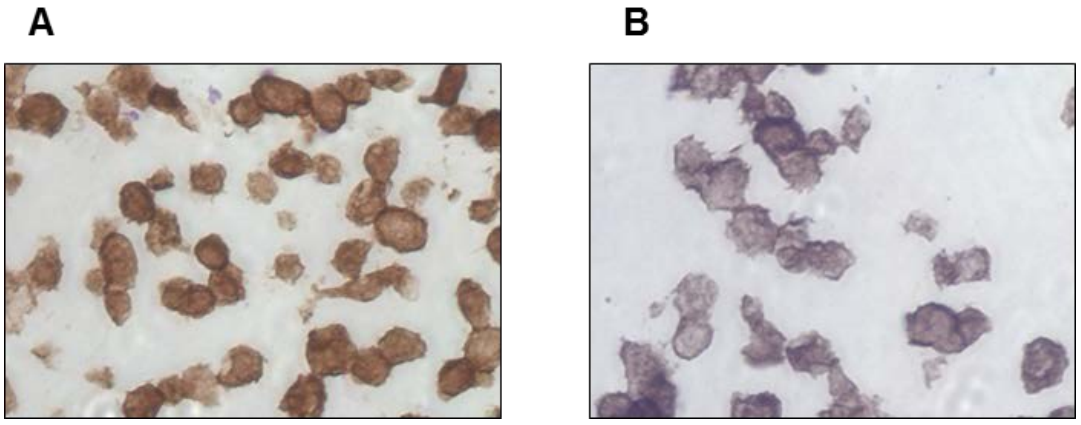

Figure 3.2: IGF-1R immunohistochemistry: staining of MCF7 control cells and cells with siRNA mediated IGF-1R depletion
A) Positive staining of control MCF7 cells stained with IGF-1R antibody (Cell Signaling Cat.no. 3027, concentration 1:75) B) Reduced staining of MCF-7 cells following IGF-1R knockdown using the same antibody. (20x objective)

The optimal conditions for IGF-1R staining were selected with the help of Uropathologist Dr. Gareth Turner. The chosen protocol was capable of discriminating between control and IGF-1R depleted MCF7 cells (figure 3.2). These conditions (section 2.1) were used to stain 198 cases of ccRCC on three TMAs (TA38, TA71 and TA74). In total, 89% of tumours stained positive for IGF-1R, with considerable heterogeneity in the staining pattern between and within individual tumours. The presence of IGF-1Rβ staining in the nucleus was the most striking feature as this was a novel finding not previously reported. Therefore, the subcellular distribution of IGF-1R in ccRCC was investigated, assessing the intensity and extent of staining in the cell membrane, cytoplasm and nucleus as described in Materials and Methods (section 2.1).

3.2.2 Sub-cellular distribution, extent and intensity of IGF-1R staining in a panel of ccRCCs and correlation with survival:

The ccRCCs were scored for IGF-1R positivity in the membrane, cytoplasm and nucleus separately. Representative staining patterns for intensity are shown in Figure 3.3. TMA scoring was verified by Dr. Gareth Turner. It was observed that almost half of all tumours were positive for nuclear IGF-1R staining (figure 3.4A). Of the nuclear IGF-1R positive tumours, just over half had moderate to high intensity of nuclear staining (Figure 3.4B) and the same proportion had an extensive distribution of nuclear IGF-1R within the tumour (Figure 3.4C).

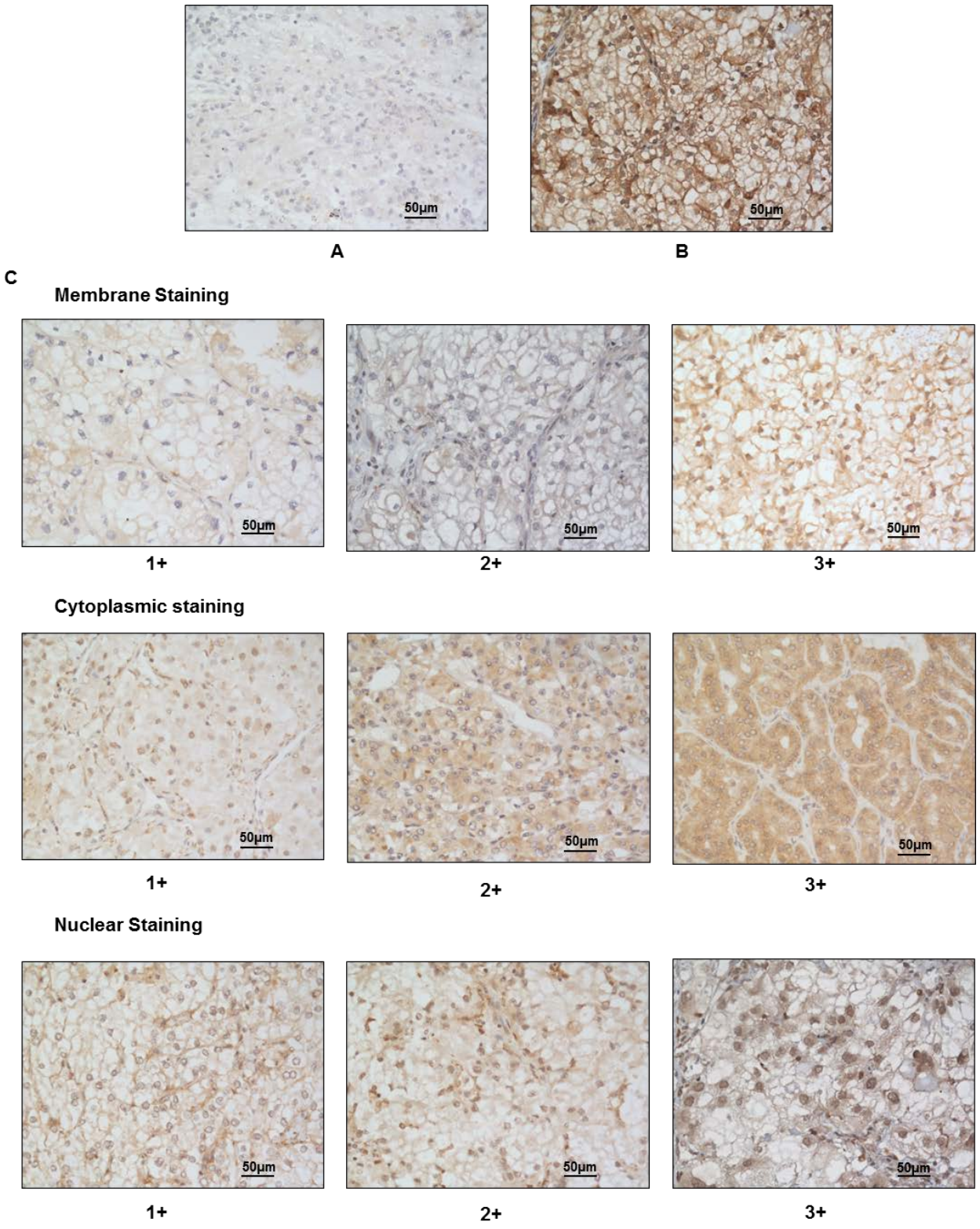

Figure 3.3: IGF-1R immunostaining of ccRCC tumour arrays
Intensity of IGF-1R staining in the membrane, nucleus and cytoplasm. (A) Tumour negative for cytoplasmic, membrane and nuclear staining; (B) Tumour with 3+ positive cytoplasmic, membrane and nuclear staining. C) Panels show tumours with representative IGF-1R staining, intensity quantified as 1+, weak; 2+, moderate; 3+, strong, in the cell membrane, cytoplasm and nucleus. Bar represents 50µm.

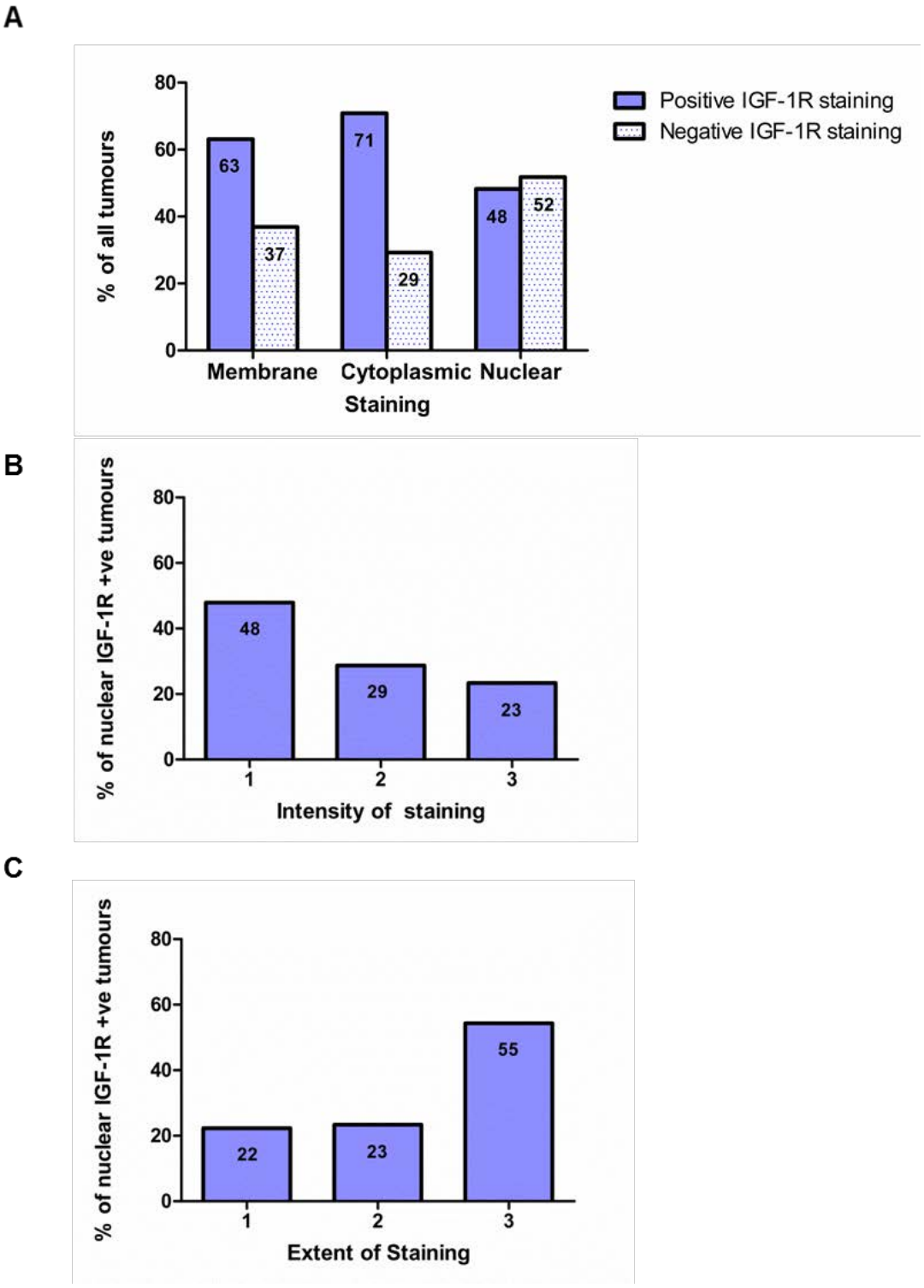

Figure 3.4: Analysis of IGF-1R staining on ccRCC tumour arrays
A) Percentage of tumours showing membrane, cytoplasmic or nuclear staining. B) Variation in intensity of IGF-1R staining in tumours positive for nuclear IGF-1R, quantified as 1, weak; 2, moderate; 3, strong. C) Variation in extent of IGF-1R staining in tumours positive for nuclear IGF-1R, quantified as 1, focal (1-10%); 2, moderate (10-50%) and 3, extensive (>50% of cells). Numbers within columns signify the actual % value.

Clinical data, held on the Urology Database of the Department of Medical Oncology, were available on 195 of the 198 ccRCC cases on the TMAs. Of the 195 cases, 70% were male (n=135) and 30% female (n=60). The mean age of the patients at time of surgery for their ccRCC was 62 years (SD 11, range 27yrs-87yrs). Mean tumour size was 8cm (SD 3.4, range 2-20cm) and pathological grading of tumours showed 10% to be grade 1 (n=20), 51% grade 2 (n=99), 27% grade 3 (n=52) and 12% grade 4 (n=23). Data on tumour necrosis was available in reports from 131 patients of which 42% (n=55) had necrosis as a feature. Staging of tumours showed 24% to be T1 (n=47), 12% T2 (n=23), 62% T3 (n=121) and 2% T4 (n=4). Mean overall survival (defined as time from surgery until death or last follow-up) was 308 weeks (median 260, range 0.5-1138 weeks). IGF-1R IHC scores were correlated with these clinical parameters (tabulated in appendix 7.1), and analysis was performed by statistician Cheng Han and Urology database manager Neviana Kilby (Dept. of Medical Oncology). There was no significant correlation between intensity or extent of cytoplasmic and membranous IGF-1R staining and age, gender, tumour grade, stage or presence of necrosis. Larger tumours appeared to have a lower intensity and extent of membranous IGF-1R staining ($p<0.001$ and <0.003 respectively). Intensity of nuclear IGF-1R was negatively correlated with both tumour grade ($p<0.02$) and pathological stage ($p<0.01$) but the small numbers of ccRCC cases at both the lowest and highest tumour grades and stages may have had some bearing on this result.

Multivariate analysis for survival was performed on clinical parameters including IGF-1R IHC to assess the effect of known or novel prognostic indicators. Tables 3.1 and 3.2 highlight the parameters that showed a statistically significant correlation with survival in the multivariate analysis.

	Hazard ratio	95% Conf. Interval	Better survival	p-value
Age	2.32	1.58 – 3.41	Young	< 0.001
Tumour size	1.76	1.19 – 2.62	Small	0.005
Grade	1.55	1.22 – 1.98	Low	< 0.001
Tumour stage	1.46	1.15 – 1.85	Low	0.002
Nuclear IGF-1R	1.25	1.04 – 1.50	Low	0.005

Table 3.1: Multivariate analysis of factors correlating with survival based on intensity of IGF-1R staining

	Hazard ratio	95% Conf. Interval	Better survival	p-value
Age	2.27	1.57 – 3.27	Young	< 0.001
Grade	1.51	1.19 – 1.91	Low	0.001
Tumour stage	1.48	1.17 – 1.87	Low	0.001
Nuclear IGF-1R	1.23	1.07 – 1.41	Low	0.003

Table 3.2: Multivariate analysis of factors correlating with survival based on extent of IGF-1R staining

Thus, survival was significantly longer in patients with younger age, smaller tumour size, lower tumour grade and lower stage. Small tumours <5cm, lower stage, and lower tumour grade (1 or 2) are established as favourable prognostic factors in ccRCC, and form part of the SSIGN algorithm used to determine survival from ccRCC (Frank et al 2002). Young age has also been linked to improved disease-specific and recurrence free survival (Sanchez-Ortiz et al 2004). Importantly, there was a significant correlation between nuclear IGF-1R and survival, with higher intensity of staining (p=0.005) and more extensive distribution (p=0.003) of staining both associated with a poorer prognosis. There was no correlation between survival and intensity of membrane or cytoplasmic IGF-1Rβ staining (p=0.98 and p=0.75 respectively). The Kaplan-Meier curve for survival by intensity of nuclear IGF-1R is shown in figure 3.5.

3.2.3 Transitional cell carcinomas (TCC) of the renal pelvis

Included in the ccRCC TMAs were six cases of TCC of the renal pelvis. All six tumours demonstrated nuclear and cytoplasmic IGF-1R staining, with intense nuclear staining (3+) in 5 out of the 6 cases (figure 3.6). It would thus be very interesting to look at a panel of TCCs of the bladder and assess the sub-cellular distribution of IGF-1R in those cases.

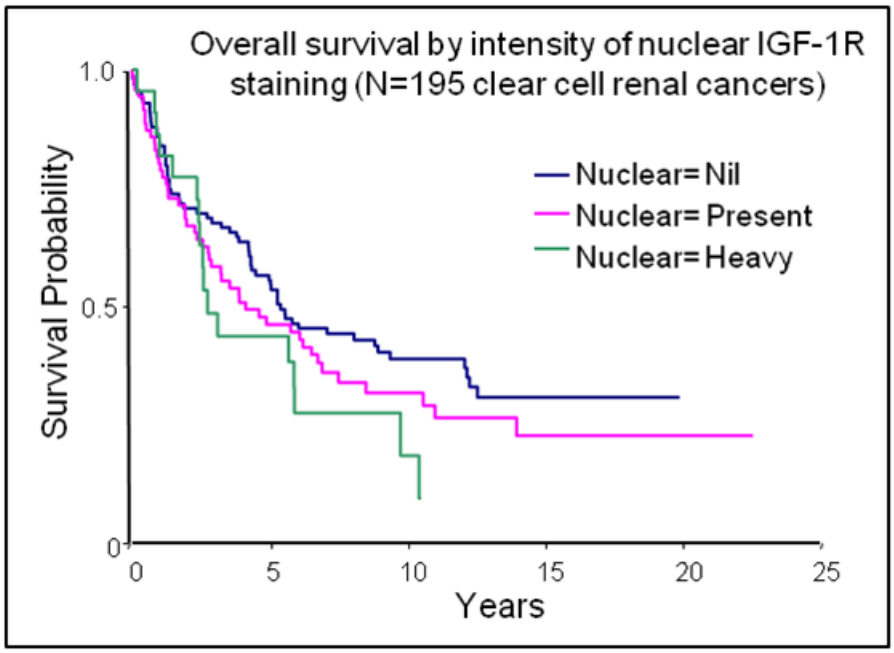

Figure 3.5: Kaplan-Meier Survival Curve for 195 ccRCC patients by intensity of nuclear IGF-1R
Nuclear nil, present and heavy correspond to IHC nuclear intensity scores of 0, 1+2, and 3 respectively. The graph demonstrates worse survival with increasing intensity of nuclear IGF-1R staining (p=0.005).

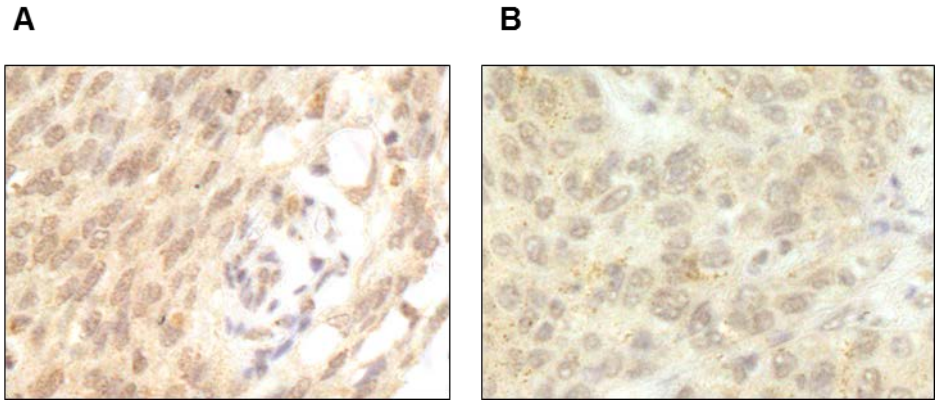

Figure 3.6: Presence of nuclear IGF-1R in transitional cell carcinomas of the renal pelvis.
A) 3+ nuclear staining intensity and 3+ cytoplasmic staining intensity and B) 2+ nuclear staining intensity and 3+ cytoplasmic staining intensity in two separate TCCs of the renal pelvis. (20x objective).

3.3 Discussion

This analysis demonstrated that the majority of ccRCC tumours, almost 90%, were positive for IGF-1R, consistent with the high frequency of IGF-1R expression seen at the RNA level in our previous study (Yuen et al 2007), and in contrast to the work by Parker *et al* (Parker et al 2003, Parker et al 2002, Parker et al 2004). This analysis also demonstrated that approximately 50% of ccRCCs were positive for nuclear IGF-1R, some tumours containing intense and extensive IGF-1R staining. The analysis of ccRCCs carried out by Parker *et al* demonstrated a poor prognosis associated with the presence of IGF-1R in ccRCC, particularly in women (Parker et al 2002), and in early stage, high grade disease (Parker et al 2004). They examined IGF-1R staining as a dichotomous variable, being either present or absent, and also the extent of staining, whether greater than or less than 50% (Parker et al 2002). Membrane positivity was demonstrated, but nuclear IGF-1R staining was not reported. The current study has also suggested that IGF-1R has an adverse prognostic significance in ccRCC, but only the nuclear component showed this association.

It is possible that differences in immunohistochemistry techniques might account for the discrepancy in results seen between Parker *et al* and this work. Differences in the IGF-1R antibody used might contribute to the differential results seen. Parker *et al* used a monoclonal IGF-1R antibody (clone 24-31) (Soos et al 1992) targeting the alpha subunit of the IGF-1R which, in a previous report from our group (Turney et al 2010), was seen to give more prominent membrane staining when compared with the beta subunit antibody (3027) used in this work (Turney et al 2010). However, using the 24-31 antibody with the same antigen retrieval used here, a similar pattern of nuclear IGF-1R was seen in prostate cancer compared with adjacent sections stained with the 3027 polyclonal antibody (Aleksic et al 2010). Differences in antigen

retrieval may also influence staining patterns. Previous work from our group using the same 3027 antibody with a milder antigen retrieval protocol had not shown evidence of nuclear IGF-1R (Turney et al 2010). However, a similar IHC protocol used by Klinakis *et al* did appear to show nuclear positivity, although the authors did not comment on this (Klinakis et al 2009). If either of the above reasons limited the detection of nuclear IGF-1R by Parker *et al*, then a proportion of tumours expressing solely nuclear IGF-1R would not be included in the results. Ongoing work by others in our group has demonstrated nuclear IGF-1R staining in prostate and breast cancers, and results are awaited on correlation with clinical parameters. This study has demonstrated the presence of nuclear IGF-1R in TCCs of the renal pelvis, and in future, it will also be interesting to assess IGF-1R subcellular localisation in other urological tumours, including TCCs of the bladder.

The association of nuclear IGF-1R with an adverse prognosis suggests that this phenomenon may contribute to an aggressive phenotype. Further work to identify the mechanism and role of nuclear IGF-1R translocation has formed the basis of a separate project within our laboratory. This has revealed that cell surface IGF-1R undergoes ligand-dependent translocation to the nucleus following clathrin mediated endocytosis, with a potential role in transcriptional regulation. These data together with the ccRCC TMA analysis were incorporated into a published paper (Aleksic et al 2010). Another group has also reported nuclear IGF-1R import, and suggest that this process is SUMOylation-mediated and associated with a possible transcriptional role (Sehat et al 2010), although the precise function of the IGF-1R in the nucleus is as yet unclear. Very recently there have been two further reports implicating nuclear IGF-1R in regulation of its own expression (Sarfstein et al 2012), and in resistance to the EGFR inhibitor Gefitinib (Bodzin et al 2012). However, the results reported in this

thesis are to date the only data that have tested the association of nuclear IGF-1R with patient survival. In light of its prognostic implications in ccRCC, and its presence in prostate and bladder carcinomas, it is reasonable to speculate that nuclear IGF-1R may contribute to the ability of IGF-1R to mediate aspects of the malignant phenotype. If future research confirms this hypothesis, it is possible that therapeutic strategies that inhibit IGF-1R transport into and function within the nucleus, might be of benefit in the treatment of urological cancers.

4 Chapter IV: Assessment of the effects of IGF-1R inhibition on radiosensitivity and the response to DNA damage

4.1 Introduction

The major focus of this project was to test the hypothesis that IGF-1R inhibition influences radio- and chemo-sensitivity and may be involved in DNA repair. The role of the IGF-1R in protection from apoptosis and cell cycle regulation is well established (Dupont and Holzenberger 2003, Galvan et al 2003, Huang et al 2010, Kooijman 2006, Kurmasheva and Houghton 2006), but a role in the DNA damage response is still unclear. Previous work from our laboratory showed that IGF-1R antisense and siRNA approaches enhanced the sensitivity of tumour cells to DNA damaging cancer treatments. IGF-1R knockdown had suggested a possible role in DNA repair, with a suggestion that IGF-1R depletion could impair the function of ATM in murine cells (Macaulay et al 2001, Rochester et al 2005). Thus the initial focus of this project was to investigate the hypothesis that a small molecule IGF-1R inhibitor may influence the response to DNA damage. These experiments used gamma irradiation, which causes a variety of DNA lesions of which DSBs are the most toxic (Jeggo et al 2011).

An ATP-competitive small molecule inhibitor of the IGF-1R tyrosine kinase domain, AZ12253801, was obtained from AstraZeneca (figure 4.1A). Table 4.1 shows data provided by AstraZeneca on the inhibitory profile of this compound.

AZ12253801	IC_{50} (nM)
Inhibition of IGF-1R Phosphorylation	2
Inhibition of IR Phosphorylation	45
Inhibition of EGFR *	250

Table 4.1: IGF-1R inhibitor AZ12253801 obtained for use in this study
Table shows IC_{50} (the concentration of AZ12253801 required to inhibit 50% of ligand-induced phosphorylation) values for inhibition of IGF-1R and IR phosphorylation. *Data for EGFR inhibition relates to EGF-driven proliferation. AZ12253801 has been tested against a wide range of other relevant kinases, where IC50s are generally >1 μmol/L or the compound has little or no inhibitory activity at 10 μmol/L. In-house data compiled from AstraZeneca product profiling.

4.2 Results

4.2.1 Effects of IGF-1R inhibition on receptor phosphorylation, signalling and cell survival

Initial experiments characterised the effects of the IGF-1R inhibitor AZ12253801 on receptor phosphorylation, signalling and cell survival. The cell line model utilized was the PTEN wild-type DU145 prostate cancer cell line, derived from a metastasis in a patient with prostate cancer (Stone et al 1978). Immunoprecipitation (IP)-western blot analysis showed that AZ12253801 induced dose-dependent inhibition of the IGF-1R, with an $IC_{50,}$ for 50% inhibition of IGF-induced phosphorylation, of 2nM (Figure 4.1B and C). This was in agreement with data from AstraZeneca (Table 4.1 and Dr. Elaine Kilgour personal communication). The next experiment tested the concentration of AZ12253801 required to inhibit signalling downstream of the IGF-1R. While inhibition of IGF-1R phosphorylation was clearly dose dependent, effects on phosphorylation of Akt and MAPK did not vary in a linear fashion with increasing concentrations of AZ12253801 (Figure 4.2A). However, at 30nM, AZ12253801 was effective in inhibiting IGF-induced phosphorylation of IGF-1R and Akt. IGF-1

induced phosphorylation of MAPK was reduced to levels in serum starved, untreated cells, although not completely inhibited. A time-course experiment showed that the inhibitory effect of 30nM AZ12253801 persisted for up to 48 hr (Figure 4.2B). The cells in these initial experiments characterising the effects of AZ12253801 were serum starved in order to detect a strong pIGF-1R signal following stimulation with IGF-1.

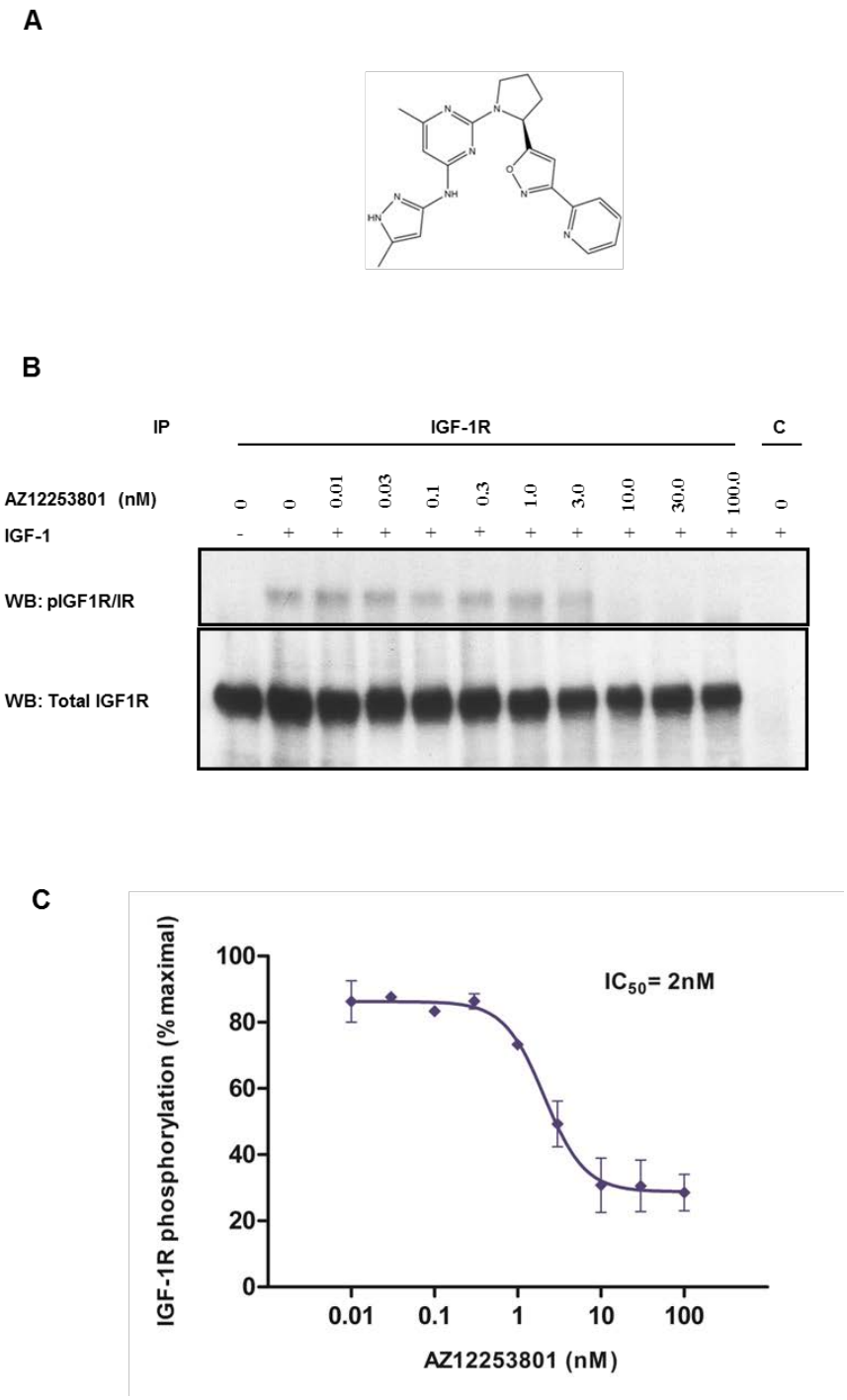

Figure 4.1: AZ12253801 inhibits IGF-1 induced IGF-1R phosphorylation in DU145 cells
A) Structure of AZ12253801. B) IP-western blot showing inhibition of IGF-1R phosphorylation in DU145 cells with increasing concentrations of AZ12253801. DU145 cells were serum starved overnight, treated with either solvent or AZ12253801 for 1 hr and with 50nM IGF-1 for the final 15min. Cell lysates were immunoprecipitated with IGF-1Rβ antibody (CS#3027) or rabbit IgG (C) and IPs were probed using pIGF-1R/IR antibody (CS #3024) and re-probed for total IGF-1R. Images were analysed using ImageJ software. C) Dose-dependent inhibition of IGF-1R phosphorylation by AZ12253801 in DU145 cells. The graph shows IGF-1R phosphorylation corrected for total IGF-1R, and expressed as % of phosphorylation in cells treated with IGF-1 without AZ12253801. Points represent the mean ± SEM for triplicate values from three separate experiments. Using GraphPad Prism, the data were fitted to a curve from which the IC_{50} value for phosphorylation inhibition was extrapolated.

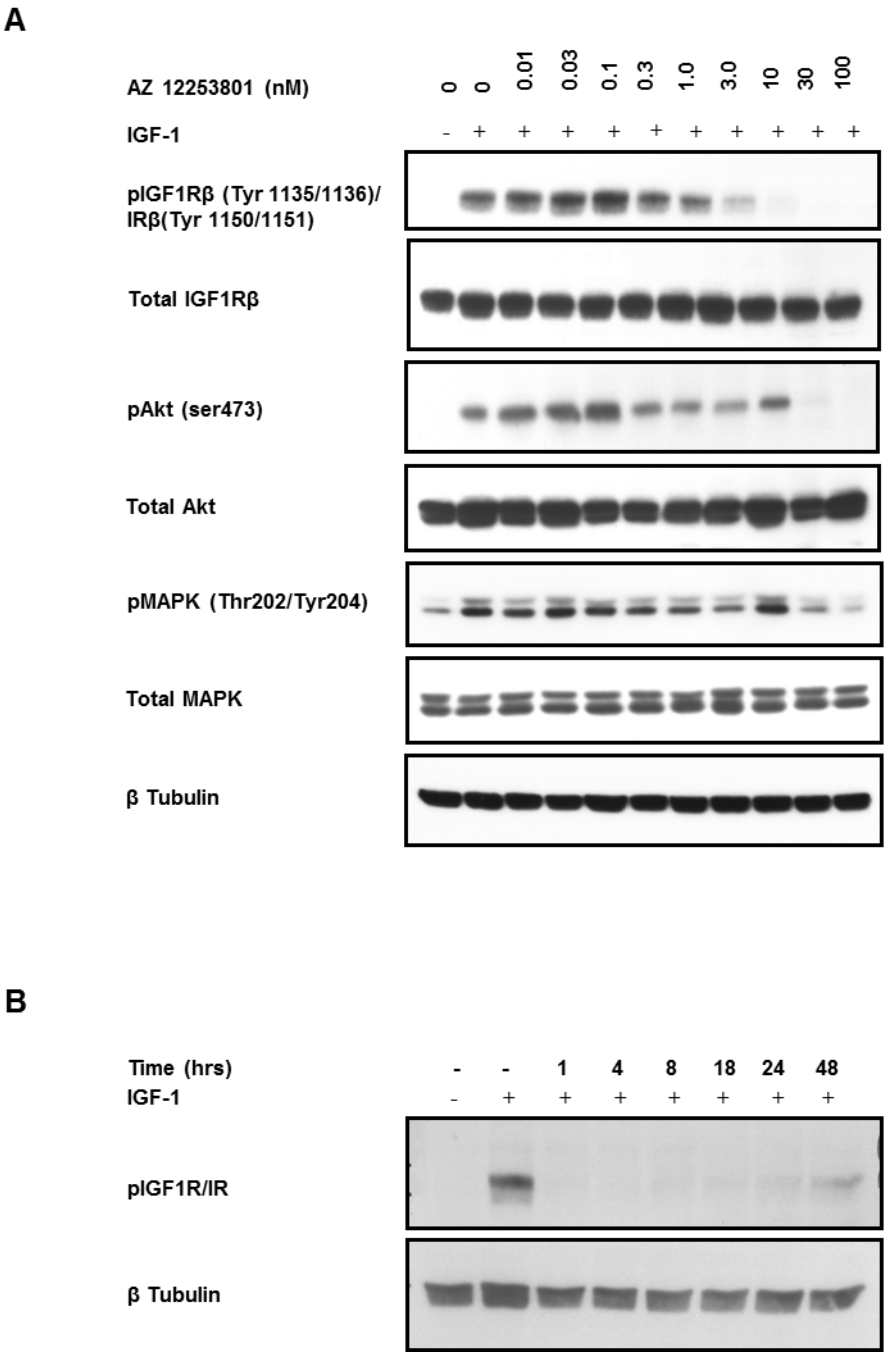

Figure 4.2: AZ12253801 inhibits downstream effectors of IGF-1R signalling in DU145 cells
A) DU145 cells were serum starved overnight and the following day were treated with AZ12253801 for 1 hr and in the final 15 min with 50nM IGF-1. Whole cell lysates were prepared for western blot analysis to measure phosphorylation of Akt and MAPK. Similar results were obtained in a second set of independent lysates. B) DU145 cells were serum starved overnight and the following day treated with 30nM AZ12253801. At predetermined time-points, cells were treated with 50nM IGF-1 for 15 min prior to lysis. Whole cell lysates were prepared for western blot analysis to measure phosphorylation of IGF-1R, with beta tubulin as the loading control.

Clonogenic survival assays were performed to determine the IC_{50} concentration of AZ12253801 that resulted in 50% inhibition of colony survival, and are shown in figure 4.3. The IC_{50} for survival inhibition was found to be 60nM. AZ12253801 at a concentration of 30nM had a more minor effect on cell survival (mean 77± 3% survival of solvent-treated controls; figure 4.3). Subsequent experiments used AZ12253801 either at a concentration of 30nM, or 60nM.

4.2.2 Effect of AZ12253801 on clonogenic survival of R+ and R- cells

In order to assess whether AZ12253801 exerts its effects predominantly via the IGF-1R, IGF-1R–null murine fibroblasts (R− cells) and isogenic cells over-expressing human IGF-1R (R+ cells) were utilised. Western blot analysis confirmed the IGF-1R null status of the R-cells, and that IGF-1R phosphorylation in the R+ cells could be inhibited by AZ12253801 at 30nM and 60nM (figure 4.4A and B).

Clonogenic survival assays using increasing concentrations of AZ12253801 were performed on both R+ and R- cell lines. The R- cells showed little response to AZ1225380, as would be expected in cells that lack IGF-1R, and the IC_{50} concentration for inhibition of 50% colony survival was not achieved. In contrast R+ cells, which overexpress the IGF-1R, demonstrated reduced clonogenic survival in response to AZ12253801 with an IC_{50} of 80nM (Figure 4.5A). The difference between the two survival curves was significant by two-way ANOVA ($P \leq 0.0005$). However, it was observed that even the IGF-1R null R- cells demonstrated a reduction in clonogenic survival at concentrations of AZ12253801 over 100nM. At concentrations above 60nM, the morphology of both the R- and R+ cells changed, with cells becoming larger and flatter (figure 4.5B).

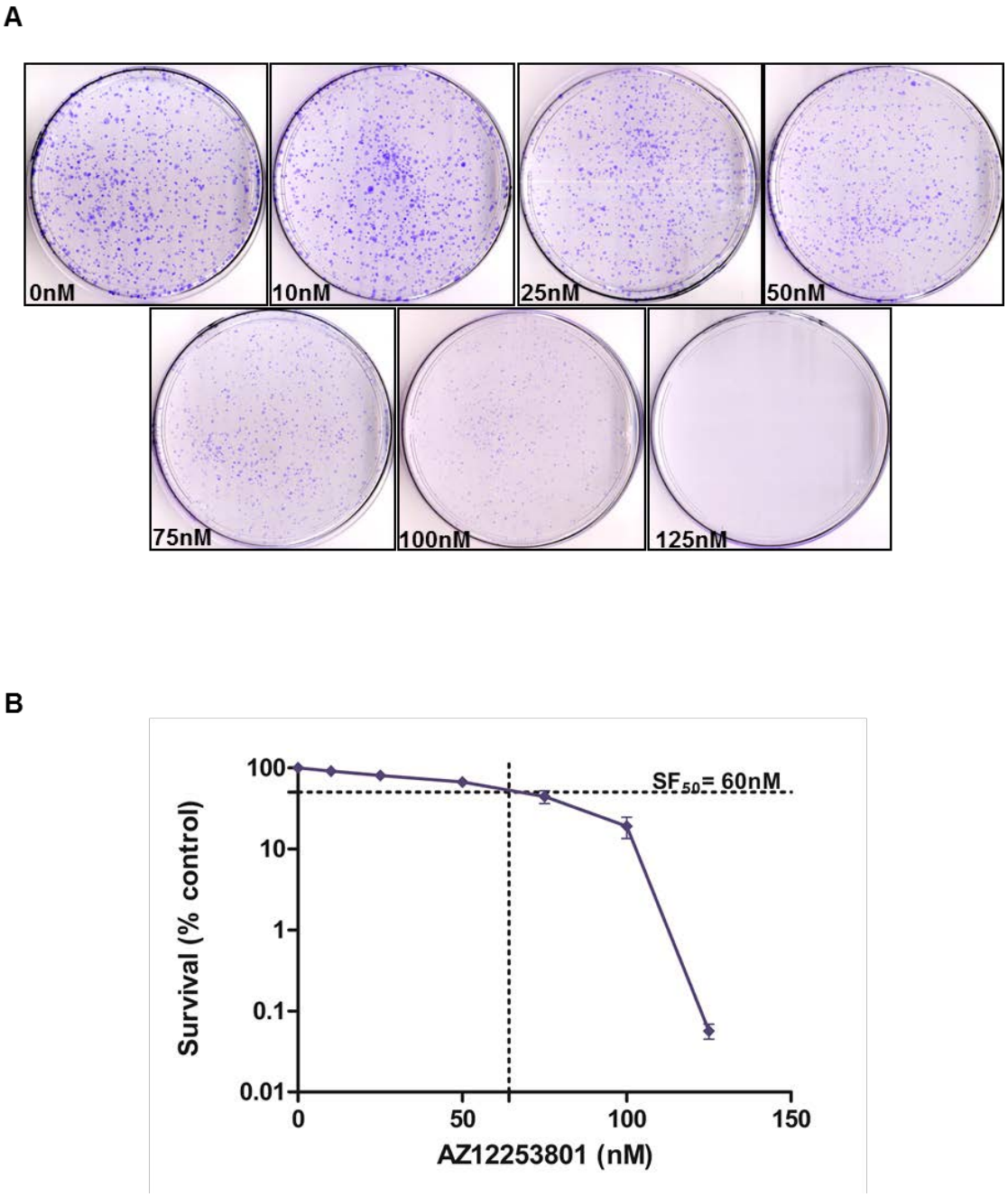

Figure 4.3: AZ12253801 inhibits clonogenic survival of DU145 prostate cancer cells
A) DU145 cells were seeded at 3000 cells/10cm dish and the following day were treated with solvent or AZ12253801. After 11-12 days, colonies were stained and counted. B) Dose dependent reduction in clonogenic survival in DU145 cells. The graph shows colony survival expressed as a percentage of survival in solvent treated controls. Points represent the mean ± SEM for triplicate values in three separate experiments.

Beta-galactosidase staining confirmed that these changes were not a result of senescence induced by IGF-1R blockade (not shown). As both cell lines were correspondingly affected, it is possible that off-target effects of AZ12253801 may be responsible for the morphological changes seen at these higher concentrations in murine fibroblasts. Similar morphological changes were not evident in human DU145 cells over the same concentration range (Figure 4.6), but were evident at 300nM. To minimise confounding effects on targets other than IGF-1R, AZ12253801 concentrations of 30nM - 60nM were used for subsequent experiments in the R+/R- cell lines.

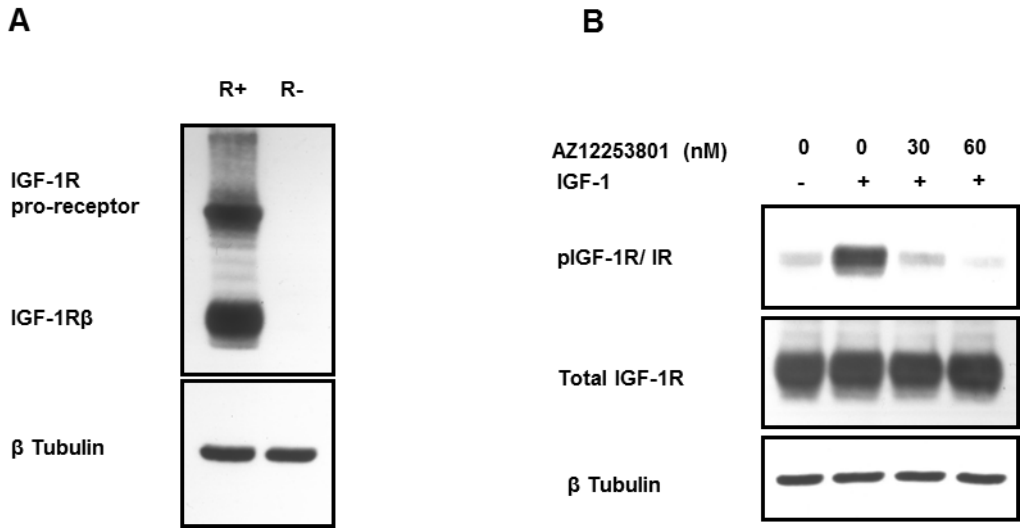

Figure 4.4: AZ12253801 inhibits IGF-1R phosphorylation in IGF-1R overexpressing R+ cells
A) Whole cell lysates were prepared from R+ cells for western blot analysis (using antibody CS #3027) to measure levels of IGF-1R, with beta tubulin as the loading control. B) R+ cells were serum starved overnight. The following day, cells were pre-treated with solvent, 30nM or 60nM of AZ12253801 for 4 hr prior to stimulation with 50nM IGF-1 for the final 15 min. Whole cell lysates were prepared for western blot analysis to measure phosphorylation of IGF-1R with beta tubulin as the loading control.

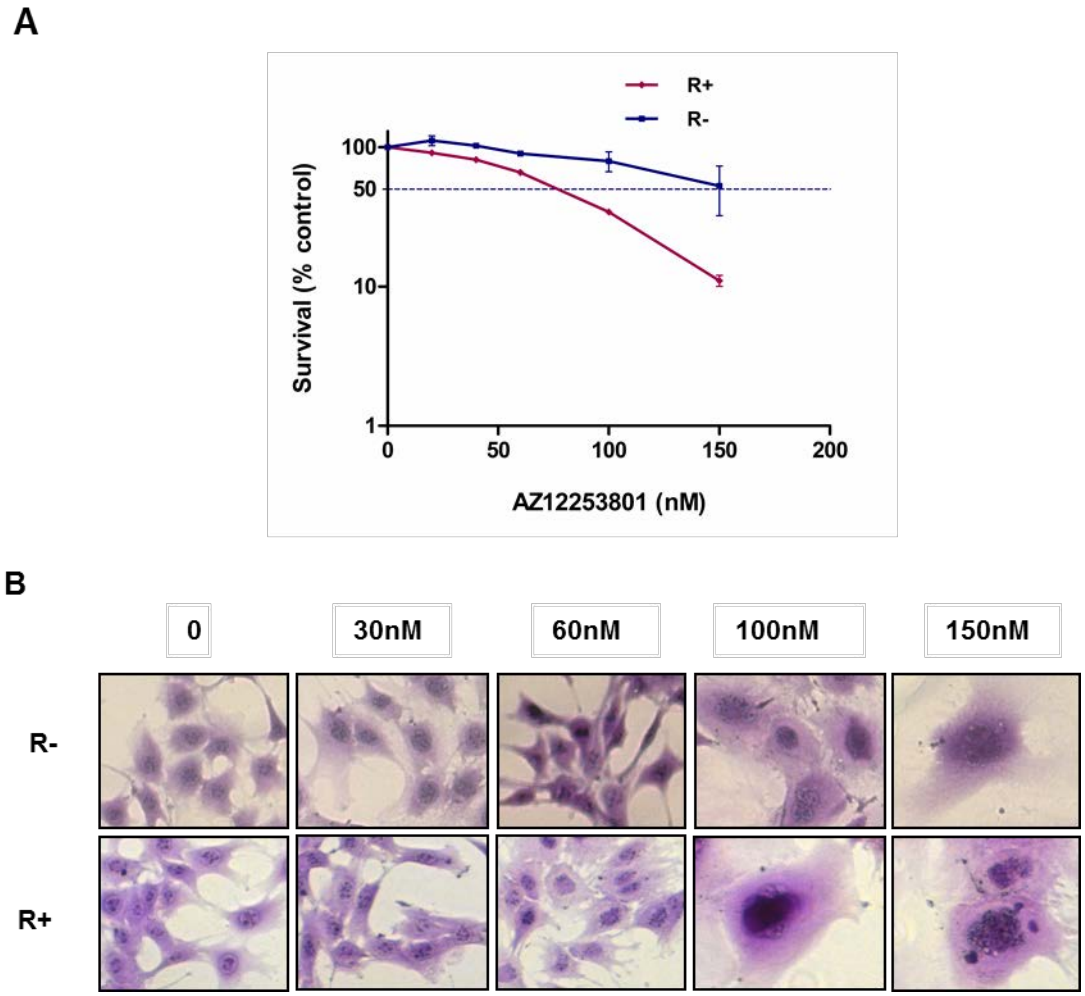

Figure 4.5: Effects of AZ12253801 on clonogenic survival of R+ and R- cells
A) R+ and R- cells were seeded at 3000 cells/10cm dish and the following day were treated with solvent or AZ12253801. After 11-12 days, visible colonies were stained and counted. The graph shows colony survival expressed as a percentage of survival in solvent treated controls. Points represent the mean ± SEM for triplicate values derived from three separate experiments. The curves were significantly different as determined by two-way ANOVA (p=0.0005) B) R- and R+ cells were grown in 10cm dishes as in A, and treated with increasing concentrations of AZ12253801 for 11-12 days, prior to fixing and staining. Images were taken with an Axiovert Zeiss microscope at 10X magnification.

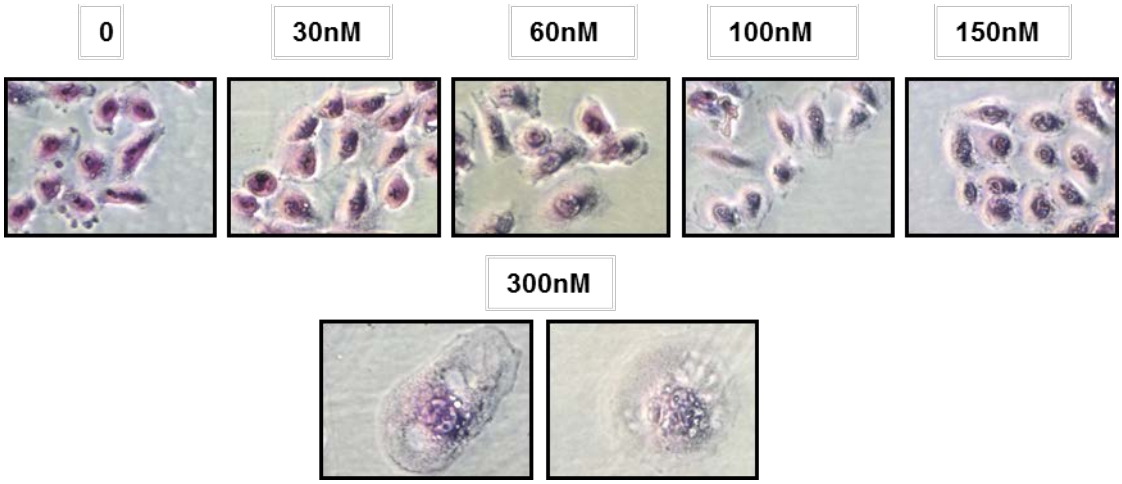

Figure 4.6: Effects of AZ12253801 on morphology of human DU145 prostate cancer cells
DU145 cells were grown in 10cm dishes at 3000 cells/dish and treated with increasing concentrations of AZ12253801 for 11-12 days, prior to fixation and staining. Images were taken with an Axiovert Zeiss microscope at 10X magnification.

4.2.3 Effect of IGF-1R inhibition on the radiosensitivity of DU145 prostate cancer cells

Irradiation is reported to activate the IGF-1R in lung cancer cells (Cosaceanu et al 2007), and so initial experiments tested whether this effect could also be detected in DU145 cells. In figure 4.7, it is seen that gamma irradiation led to very minor phosphorylation of the IGF-1R above the level seen in un-irradiated cells, and not to the extent seen in cells stimulated with IGF-1.

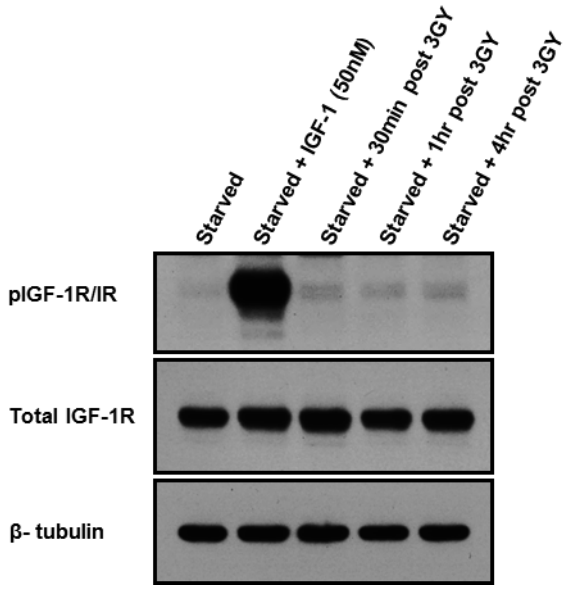

Figure 4.7: Effects of ionising radiation on IGF-1R activation in DU145 cells
DU145 cells were serum starved overnight and the following day were treated with either 50nM IGF-1 for 15 min, or 3Gy irradiation with lysis at 30 min, 1 hr and 4 hr post irradiation. Whole cell lysates were prepared for western blot analysis to measure levels of pIGF-1R/IR and total IGF-1R, with beta tubulin as the loading control.

Assays then compared the radiosensitivity of solvent- or AZ12253801 pre-treated cells, using AZ12253801 either at the concentration of 30nM which had inhibited cell signalling (figure 4.2A) or at the concentration of 60nM which had inhibited 50% of colony survival in clonogenic assays (figure 4.3B). The effect of AZ12253801 was compared with the ATM inhibitor (ATMi) KU 55933 (Hickson et al 2004) as a positive control for radiosensitization. DU145 cells were radiosensitized to 30nM AZ122538013 and 10μM ATMi with sensitivity enhancement ratios (SER; sensitivity enhancement at 10% survival) of 1.4 and 1.9 respectively (figure 4.8A). Subsequent experiments directly compared effects of 30nM and 60nM AZ12253801 (figure 4.8B). It was noted that control (solvent-treated) cells were relatively more sensitive to 10Gy irradiation in these experiments, compared with the previous set of assays (figure 4.8A). This difference in survival in control cells was most likely related to changes in plating from 6-well plates in figure 4.8 A to 10cm dishes in figure 4.8B.

This change was made in order to be able to plate more cells, to have increased confidence in relative survival at higher doses of irradiation. However, the relative effects of 30nM AZ12253801 were very similar between the two assay formats. Data shown in figure 4.8B indicate that AZ12253801 sensitised DU145 cells to radiation, with a SER of 1.4 for 30nM AZ12253801 and 1.8 for 60nM AZ12253801. The detectable effect in cells treated with 30nM AZ12253801 suggested that effects on radiosensitization were at least in part independent of effects on growth and cell survival.

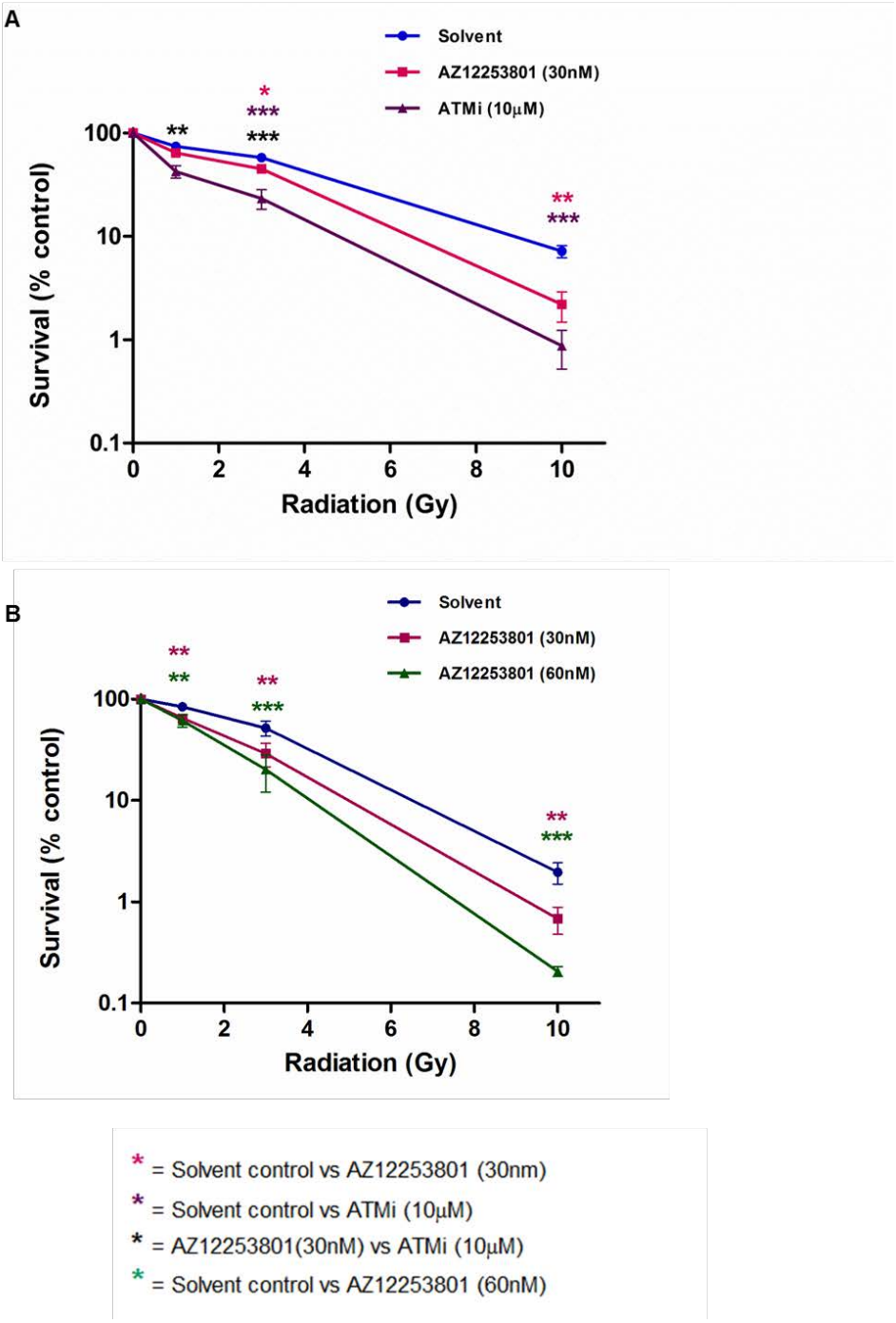

Figure 4.8: IGF-1R inhibition with AZ12253801radiosensitizes DU145 prostate cancer cells
A)-B) DU145 cells were pre-treated with AZ12253801 or ATM inhibitor KU55933 (10μM) in triplicate dishes (6-well plates in A and 10cm dishes in B), for 4 hr prior to irradiation. Parallel dishes were treated with solvent (0.0003% DMSO). Viable colonies were stained and counted on day 11-12. The graph shows colony survival expressed as a percentage of survival in un-irradiated controls. Points represent the mean ± SEM for triplicate values in three separate experiments. The data were analysed by one way ANOVA, to determine statistical significance of survival differences seen between: A) cells treated with 30nM AZ12253801 (red), 10μM ATMi (purple) and solvent control (blue) and B) cells treated with 30nM AZ12253801 (red), 60nM AZ12253801 (green) and solvent control (blue). (*p<0.05; **p<0.01; ***p< 0.001). There was no statistically significant survival difference between cells treated with 30nM AZ12253801 and 60nM AZ12253801 at 1, 3 or 10Gy. Radiosensitisation with both 30nM and 60nM AZ12253801 and ATMi compared with control cells was expressed as the sensitivity enhancement ratio (SER) at 10% survival, which was 1.4, 1.8 and 1.9 respectively.

The next step was to test the extent to which radiosensitization induced by AZ12253801 was as a result of inhibition of the IGF-1R. Firstly, clonogenic survival assays were conducted in DU145 cells following siRNA mediated knockdown of the IGF-1R (figure 4.9A and B). As seen in figure 4.9C, radiosensitization occurred following IGF-1R knockdown, with a similar magnitude to inhibition with AZ12253801. These results using IGF-1R depletion were comparable to previous data from our group, using a different IGF-1R siRNA (Rochester et al 2005).

Secondly, effects of AZ12253801 on radiosensitivity were investigated in IGF-1R null R- and IGF-1R overexpressing R+ cells. These murine fibroblast cell lines proved to be inherently radioresistant, and a previous report has demonstrated a failure of induction of p53 following irradiation, which might partly explain this phenomenon (Nakamura et al 1997). Hence a radiation dose of 15Gy was also used. In R+ cells treated with 60nM AZ12253801 there was modest but significant 1.5-fold radiosensitization at 1Gy ($p<0.01$), and 3Gy ($p<0.001$), with 4-fold sensitisation at 10Gy ($p<0.01$) and 15-fold at 15Gy ($p<0.01$). The isogenic IGF-1R null R- cells were intrinsically more radiosensitive than R+ cells (3-fold at 10Gy, $p< 0.05$ and 25-fold at 15Gy, $p<0.01$), as previously reported (Tezuka et al 2001), but in contrast to the results in R+ cells, no significant radiosensitization was observed following AZ12253801 treatment (figure 4.10). It was noted that IGF-1R inhibition suppressed post-irradiation survival of R+ cells to the level in R- cells, suggesting that the presence of IGF-1R is the major reason for the greater radioresistance of R+ cells compared with R- cells.

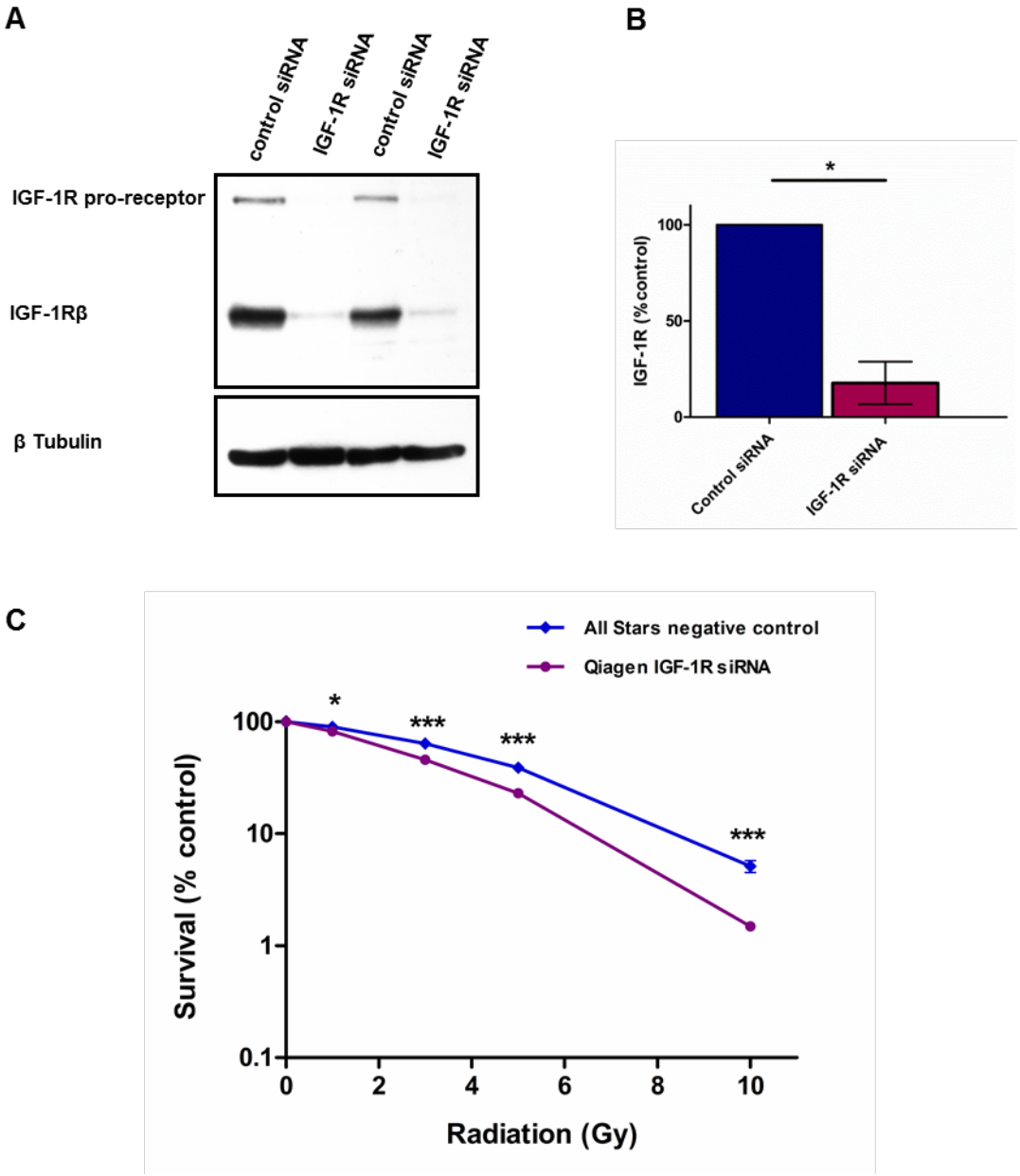

Figure 4.9:IGF-1R depletion radiosensitizes DU145 cells
DU145 cells were seeded in 10cm dishes ($7x10^5$ cells/ dish) and the following day a 50nM transfection was performed with control siRNA or IGF-1R siRNA. A) After 48 hr, whole cell lysates were prepared for western blot analysis to measure levels of IGF-1R, with β-tubulin as the loading control. IGF-1R depletion was confirmed in three sets of independently-prepared lysates. B) IGF-1R levels were quantified in 3 independent sets of lysates, corrected for β-tubulin loading, and expressed as % levels in control-transfected cells. The graph demonstrates IGF-1R depletion following IGF-1R siRNA transfection (*$p<0.05$ by paired t-test). C) Parallel cultures were re-seeded 48 hr after siRNA transfection at 3000 cells/10cm dish, allowed to adhere for 6 hr and then irradiated. After 11-12 days, visible colonies were stained and counted. The graph shows colony survival expressed as a percentage of survival in un-irradiated control cells. Points represent the mean ± SEM of triplicate values in three separate experiments. The data were analysed by t-test, to determine statistical significance of survival differences seen in IGF-1R depleted cells (*$p<0.05$; ***$p< 0.001$).

Both these experiments point to a phenomenon of radiosensitization resulting from inhibition of the IGF-1R by AZ12253801. It was important to assess whether this phenomenon was restricted to DU145 cells, or whether IGF-1R receptor blockade was capable of radiosensitising other prostate cancer cell lines. The next step was to perform clonogenic survival assays following IGF-1R inhibition and irradiation in 22-Rv1, PC3 and LNCaP-LN3 prostate cancer cells.

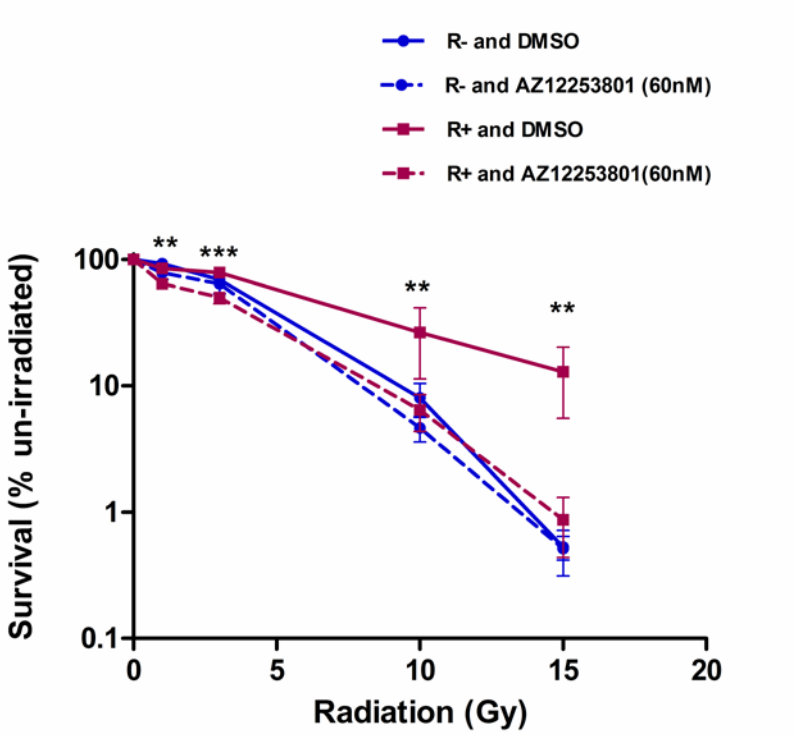

Figure 4.10: AZ12253801 radiosensitizes R+ cells but not isogenic IGF-1R null R- cells
R+ and R- cells were pre-treated with 60nM AZ12253801 for 4 hr prior to irradiation. Parallel dishes were treated with solvent. Viable colonies were stained and counted on day 11-12. The graph shows colony survival expressed as a percentage of survival in unirradiated controls. Points represent the mean ± SEM for triplicate values in three separate experiments. The data were analysed by one way ANOVA, to determine statistical significance of survival differences seen in R+cells treated with AZ12253801 (**p<0.01; ***p< 0.001).

4.2.4 Effect of IGF-1R inhibition on the radiosensitivity of PC3, 22Rv1 and LNCaP-LN3 prostate cancer cells

DU145, PC3, 22Rv1 and LNCaP-LN3 cells differ genotypically and phenotypically, and western blotting confirmed previously noted differences in IGF-1R level, PTEN expression in DU145 and 22Rv1, and androgen receptor expression in LnCaP-LN3 and 22Rv1 cells, (Table 4.2 and figure 4.11A). Assays for intrinsic radiosensitivity (figure 4.11B) showed that DU145 cells were the most radioresistant, 22Rv1 being the most radiosensitive (five-fold reduction in cell survival compared with DU145 at 1Gy), and PC3 and LN-CaP-LN3 cells showing intermediate sensitivity.

Before testing effects of IGF-1R inhibition, the IC_{50} value for inhibition of 50% colony survival for AZ12253801 was individually determined for each cell line (figure 4.11C).

Cell Line	PTEN	p53	Androgen receptor	PSA production	Other
PC3	null	MT	-	-	
DU145	WT	MT	-	-	
22Rv1	WT	WT	+	+	
LNCaP-LN3	MT	WT	+	+	IRS-1 null

Table 4.2: Prostate cancer cell line characteristics
Genotypes obtained from COSMIC (Catalogue of Somatic Mutations in Cancer) database (http://cancer.sanger.ac.uk) and (Festuccia et al 2005, Fraser et al 2012, Lehmann et al 2007, Li et al 1997, Mujoo et al 2005, Reiss et al 2000, Scott et al 2003, Sramkoski et al 1999). WT = wild type; MT= mutated

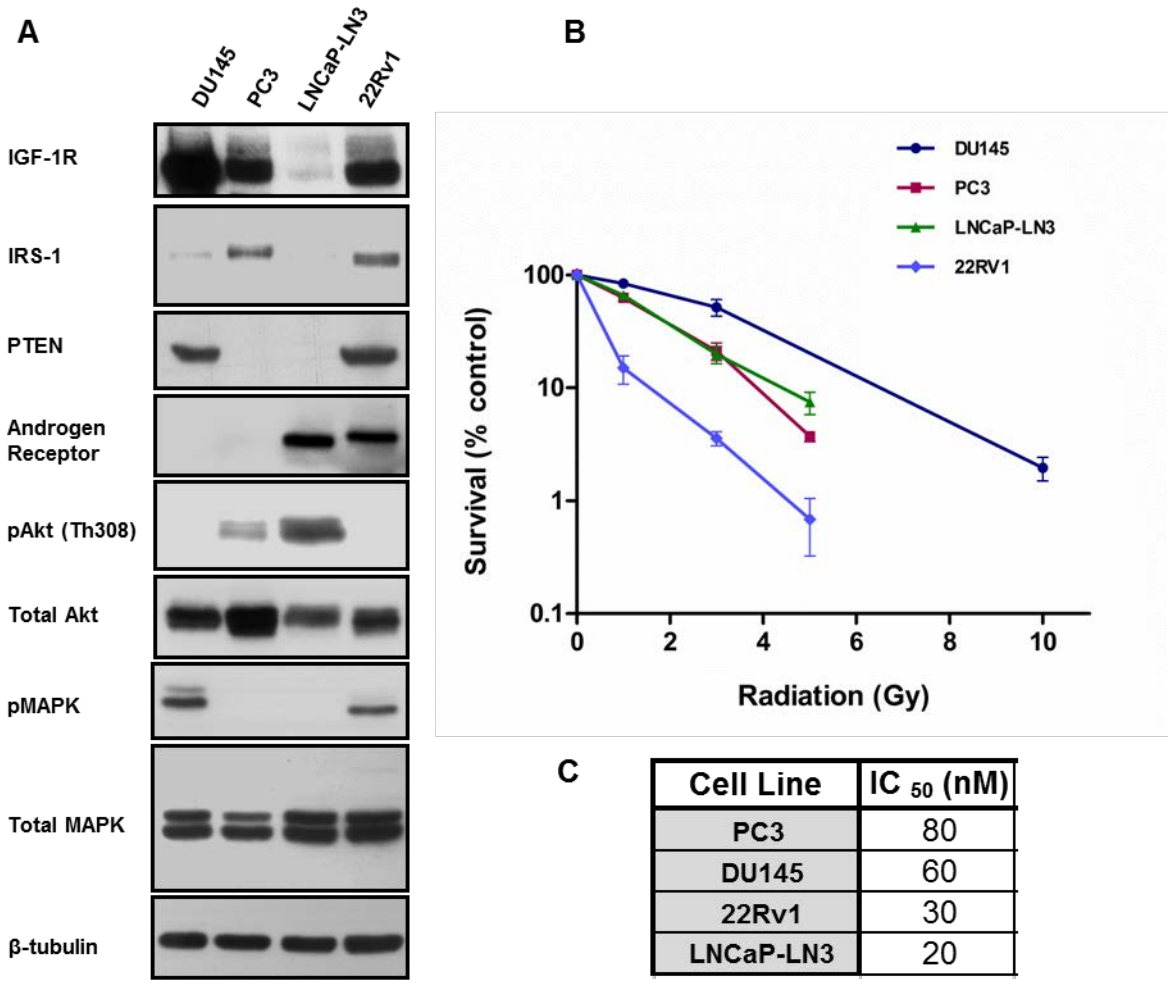

C

Cell Line	IC $_{50}$ (nM)
PC3	80
DU145	60
22Rv1	30
LNCaP-LN3	20

Figure 4.11: Characterisation of prostate cancer cell lines
A) Whole cell lysates were prepared from a panel of prostate cancer cell lines for western blotting, with β-tubulin as the loading control. B) Intrinsic radiosensitivity of a panel of prostate cancer cell lines. Cells were seeded at 3000 cells/10cm dish. The following day, cells were irradiated at 1-10Gy. After 11-12 days, visible colonies were stained and counted. The graph shows colony survival expressed as a percentage of survival in un-irradiated control cells. Points represent the mean ± SEM of triplicate values in three separate experiments. C) Prostate cancer cells were treated with increasing concentrations of AZ12253801 to determine effects on cell survival. Data from three independent experiments were curve-fitted using GraphPad Prism, and IC_{50} values for inhibition of 50% colony survival were extrapolated.

Clonogenic survival assays were performed at or near the IC_{50} concentration of AZ12253801 (for inhibition of 50% colony survival) for each cell line. Results are shown in figure 4.12 A-C. AZ12253801 induced significant radiosensitization of PC3 and 22Rv1 cells, but not LNCaP-LN3 cells.

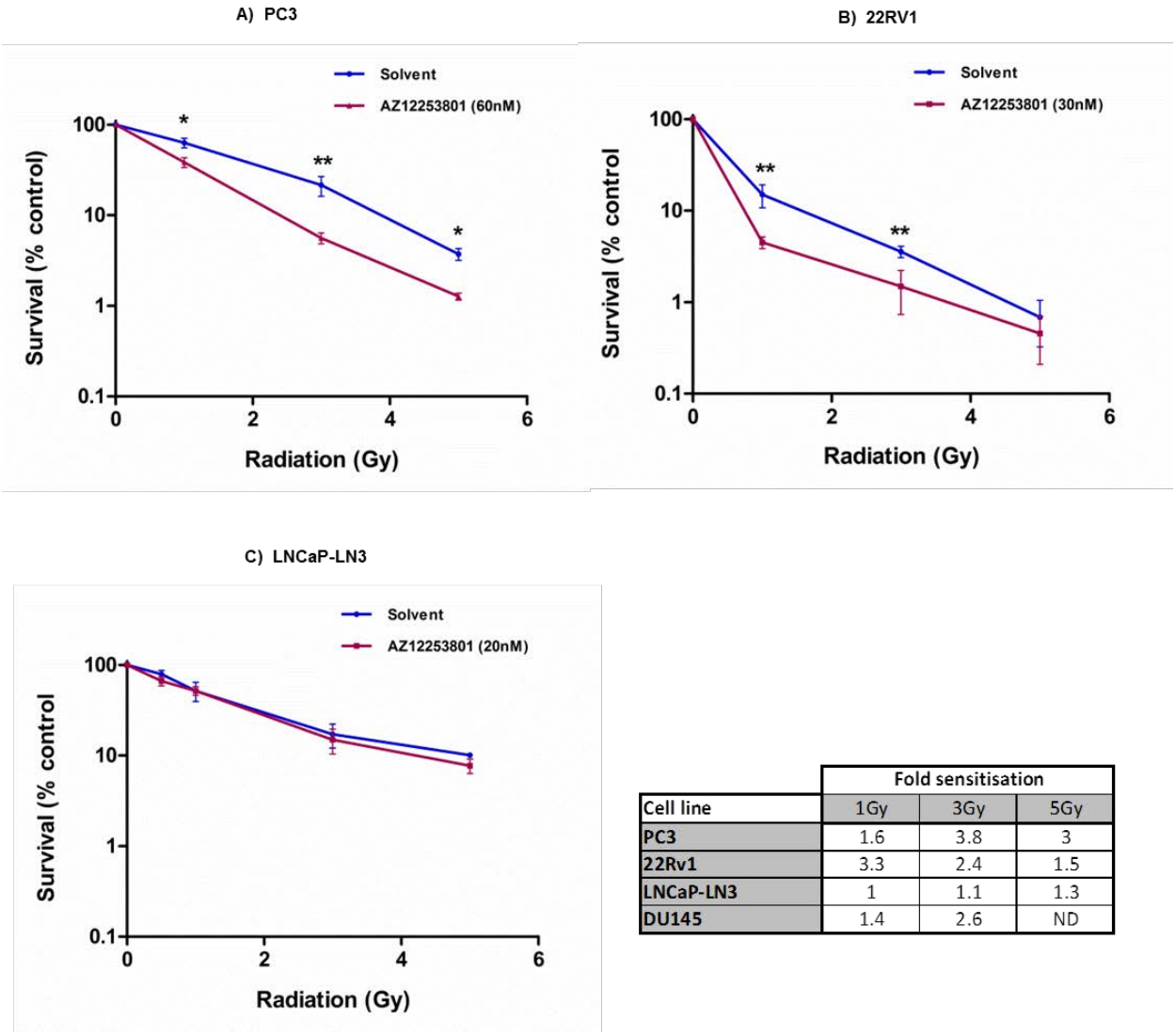

Cell line	Fold sensitisation		
	1Gy	3Gy	5Gy
PC3	1.6	3.8	3
22Rv1	3.3	2.4	1.5
LNCaP-LN3	1	1.1	1.3
DU145	1.4	2.6	ND

Figure 4.12: Effect of IGF-1R inhibition on radiosensitivity of prostate cancer cell lines
A-C) Cells from three different prostate cancer cell lines, PC3, 22Rv1 and LNCaP-LN3, were seeded at 3000 cells/ 10cm dish and the following day were treated with solvent or AZ12253801 at the IC_{50} (for 50% survival inhibition) for each cell line. After 11-12 days, visible colonies were stained and counted. Colony survival was expressed as a percentage of survival in unirradiated controls. Points represent the mean ± SEM for triplicate values in three separate experiments. AZ12253801 enhanced radiosensitivity of PC3 and 22Rv1 cells. (*$p<0.05$, **$p<0.01$). D) Table shows fold sensitisation of IGF-1R inhibited cells compared with controls.

These experiments collectively support a role for IGF-1R inhibition in suppressing cell survival following irradiation induced DNA damage. It is likely that this effect is due, at least in part, to apoptosis induced either directly by IGF-1R inhibition, or indirectly, as a result of DNA damage sustained following irradiation. It is also possible that other properties known to be associated with IGF-1R could contribute to the radiosensitization induced by IGF-1R inhibition. These include regulation of cell cycle distribution and cellular senescence. Thus the next step was to investigate the effects of IGF-1R inhibition on apoptosis, cell cycle profile, and cellular senescence in DU145 cells.

4.2.5 Effects of IGF-1R inhibition on apoptosis in DU145 cells

Apoptosis assays were performed in DU145 cells to clarify the effect of IGF-1R inhibition on apoptosis induction, following IGF-1R inhibition alone or in combination with 3Gy irradiation. The results (figure 4.13A and B) demonstrated that levels of caspase 3/7 activity in cells treated with AZ12253801 at 30nM and 60nM increased progressively above levels in control treated cells for the 48 hr duration of the assay. Irradiation induced a significant increase in apoptosis that was greater than effects of 30nM and 60nM AZ12253801 alone at 24 hr and 48 hr. The combination of 30nM AZ12253801 and 3Gy irradiation did not appear to enhance the apoptotic effect of irradiation alone (figure 4.13A). Pretreatment with 60nM AZ12253801 did not enhance irradiation induced apoptosis at 24 hr; a minor increase at 48 hr did not achieve statistical significance (figure 4.13B). At 48 hr, the combination of 60nM AZ12253801 and irradiation resulted in higher caspase 3/7 activity than 30nM AZ12253801 with irradiation, ($p<0.05$), but there was no difference in apoptosis induction by 30nM or 60nM AZ12253801 in the absence of irradiation ($p>0.05$).

These data suggest that 60nM AZ12253801 may cause minor enhancement of irradiation induced apoptosis, and this may partly account for the radiosensitization seen with 60nM AZ12253801. However, the data also suggest that apoptosis induction alone, especially in cells treated with the lower concentration of 30nM AZ12253801, is unlikely to account entirely for the radiosensitization induced by IGF-1R inhibition. Hence the next experiments explored other processes that could contribute to radiosensitization.

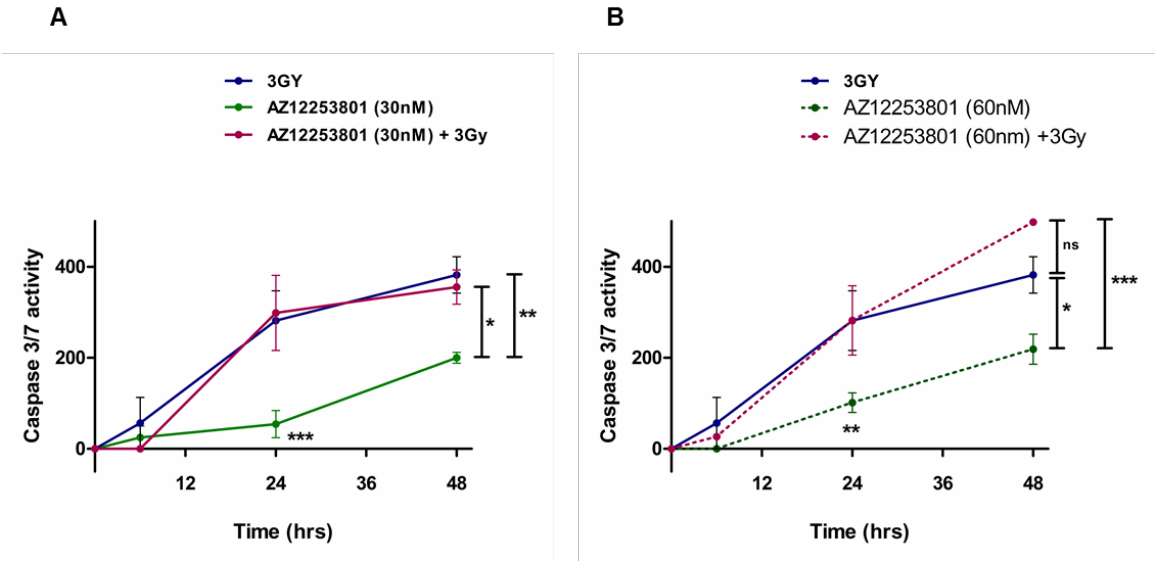

Figure 4.13: Effects of AZ12253801 on irradiation induced apoptosis in DU145 cells
DU145 cells were seeded in 96-well plates and treated with solvent or AZ12253801 for 4 hours prior to 3Gy irradiation. At defined time-points up to 48 hr post irradiation, cells were analysed for apoptosis using the Apo-1 Homogeneous Caspase-3/7 apoptosis assay (Promega). Graph shows fluorescence units expressed as % increase above solvent treated un-irradiated controls. Points represent the mean increase ± SEM in triplicate wells in two independent experiments (*p<0.05, **p<0.01 and ***p<0.001 by one-way ANOVA).

4.2.6 Effect of IGF-1R inhibition on senescence induction in DU145 cells

Senescence is defined as permanent growth arrest of cells which retain viability and biological activity. Senescence is characterised by the accumulation of lysosomal beta-galactosidase at pH 6.0, and is accompanied by morphological changes including flattening, increased cell size and granularity (Chang et al 1999a, Schwarze et al

2005) and see Figure 4.14A. Senescence may take several days to become apparent, unlike apoptosis which is relatively rapid (Ewald et al 2010).

To test whether senescence contributed to reduced clonogenic survival after IGF-1R inhibition, Beta galactosidase senescence assays were conducted on cells that were pre-treated with 30nM or 60nM AZ12253801, and then irradiated at 1-10 Gy. Analysis was performed at 1, 3 and 11 days post irradiation to conform to the time-scale of clonogenic survival assays, which were carried out over a period of 11 days. Visibly senescent cultures of primary RCC cells were used as a positive control, and showed definite beta-galactosidase activity as evidenced by blue staining (figure 4.14A i-ii). However, DU145 cells did not show any induction of senescence either at 24 hours post irradiation (figure 4.14B-E) or after 3 or 11 days (not shown). This makes senescence an unlikely mechanism for the radiosensitization observed in clonogenic survival assays.

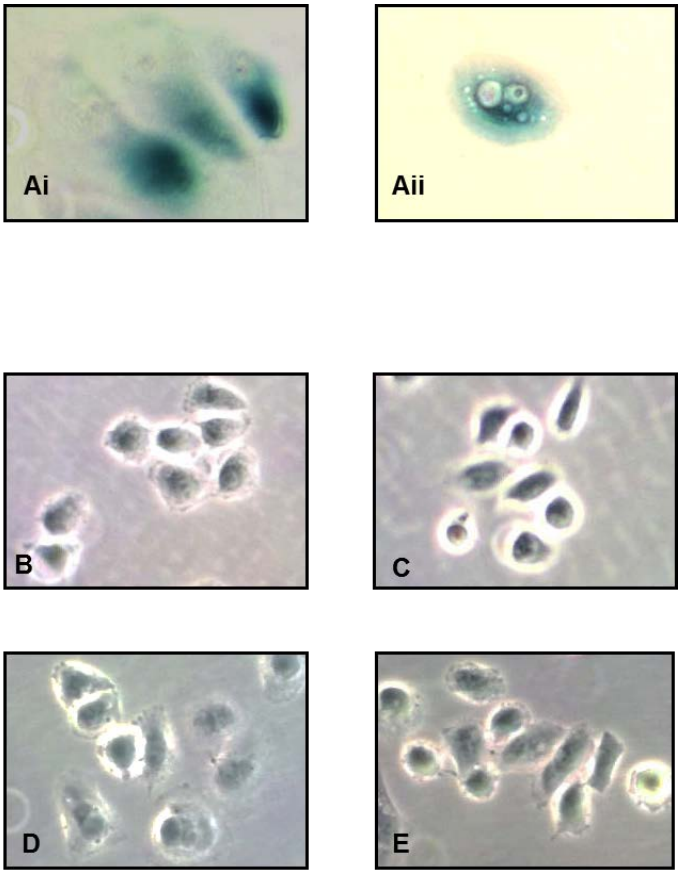

Figure 4.14: IGF-1R inhibition does not induce senescence following irradiation of DU145 cells
Assays for senescence-associated β-galactosidase were performed in Ai-ii) Primary ccRCC cells showing typical senescent morphology, which were used as positive controls. B)-E) DU145 cells were treated with B) solvent, or AZ12253801 at C) 30nM, D) 60nM, E) 120nM, irradiated after 4 hours at 3Gy and after a further 24 hours stained for β-galactosidase, in parallel with staining of primary RCC cells (A). Similar analysis was carried out 3 and 11 days following 3Gy irradiation, and 1, 3 and 11 days following 1Gy and 10Gy irradiation (not shown). Experiments were repeated three times. Aii) 32x magnification; Ai), B-E 10x magnification

4.2.7 Effect of IGF-1R inhibition on cell cycle distribution

Initial experiments assessed the cell cycle profile of DU145 cells following IGF-1R inhibition in the absence of damage. Time course experiments were conducted after treatment with 30nM AZ1225380, and showed no differences in cell cycle distribution compared with solvent treated control cells (figure 4.15). Notably, there was no evidence of G1 arrest in AZ12253801 treated cells. This is consistent with the previous finding that 30nM AZ12253801, while causing detectable (although unlikely total) inhibition of cell signalling, did not significantly affect DU14 cell survival

(figures 4.2A and 4.3). In fact proliferation of DU145 was found by others in our laboratory to be suppressed at higher concentrations of AZ12253801, the concentration inhibiting the growth of 50% of cells (GI_{50}) being 120nM (Aleksic et al 2010).

Next it was determined whether 30nM AZ12253801 would influence the changes in cell cycle distribution induced by irradiation. Control treated cells showed irradiation induced G2-M arrest at 6-8 hr, which had resolved by 18-24 hr (figure 4.16). In the same experiment, pre-treatment with 30nM AZ12253801 appeared to delay the resolution of the G2 arres, which was evident at 18 hr, but this was not consistent, and differences in mean values were not significantly different (figure 4.16).

	Control	AZ12253801
1hr	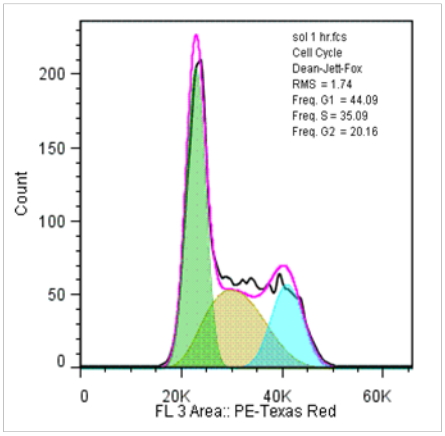	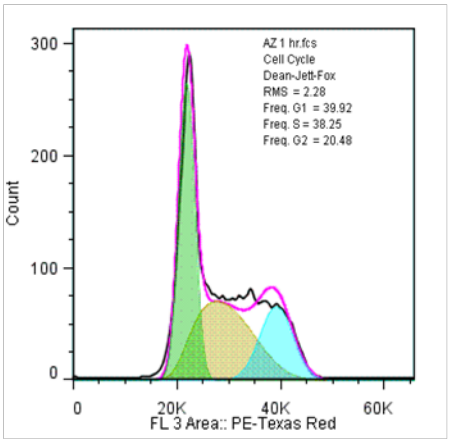
4hr	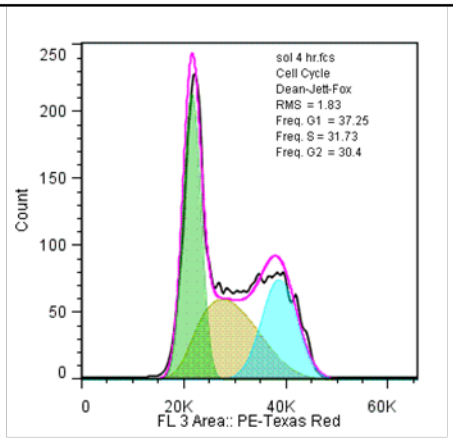	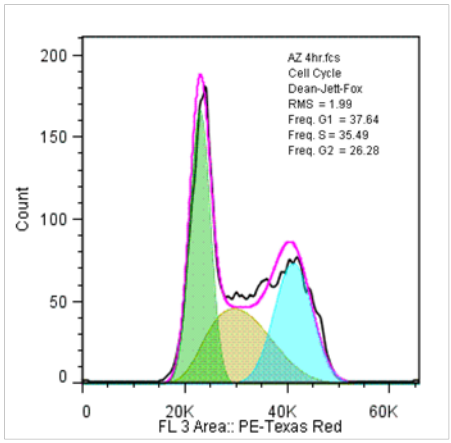
8hr	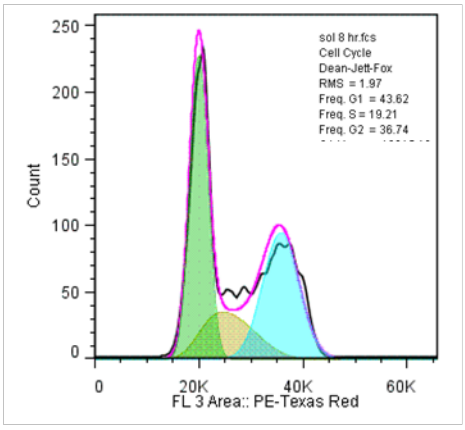	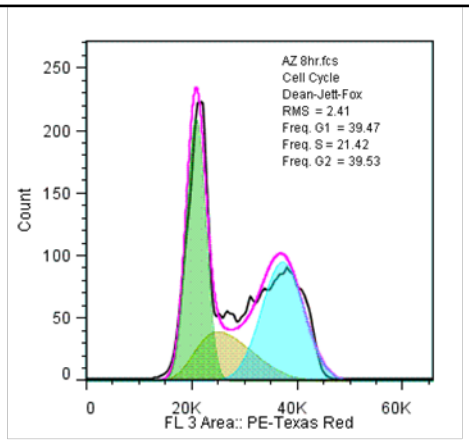
18hr	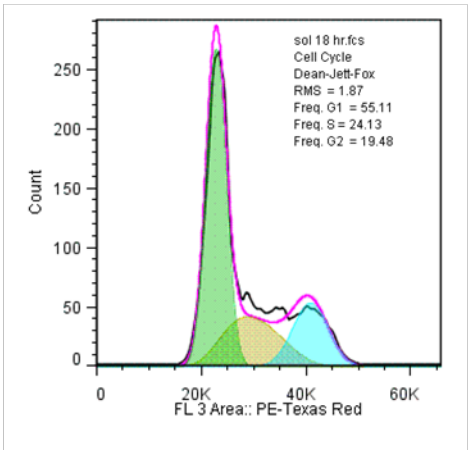	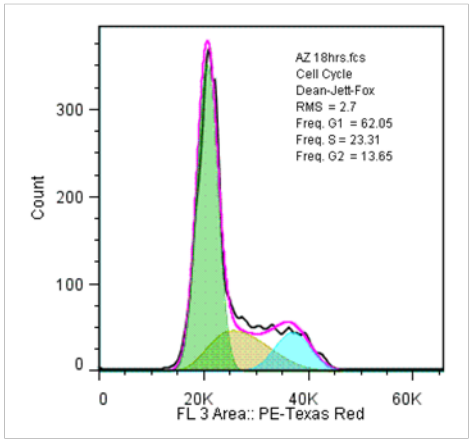

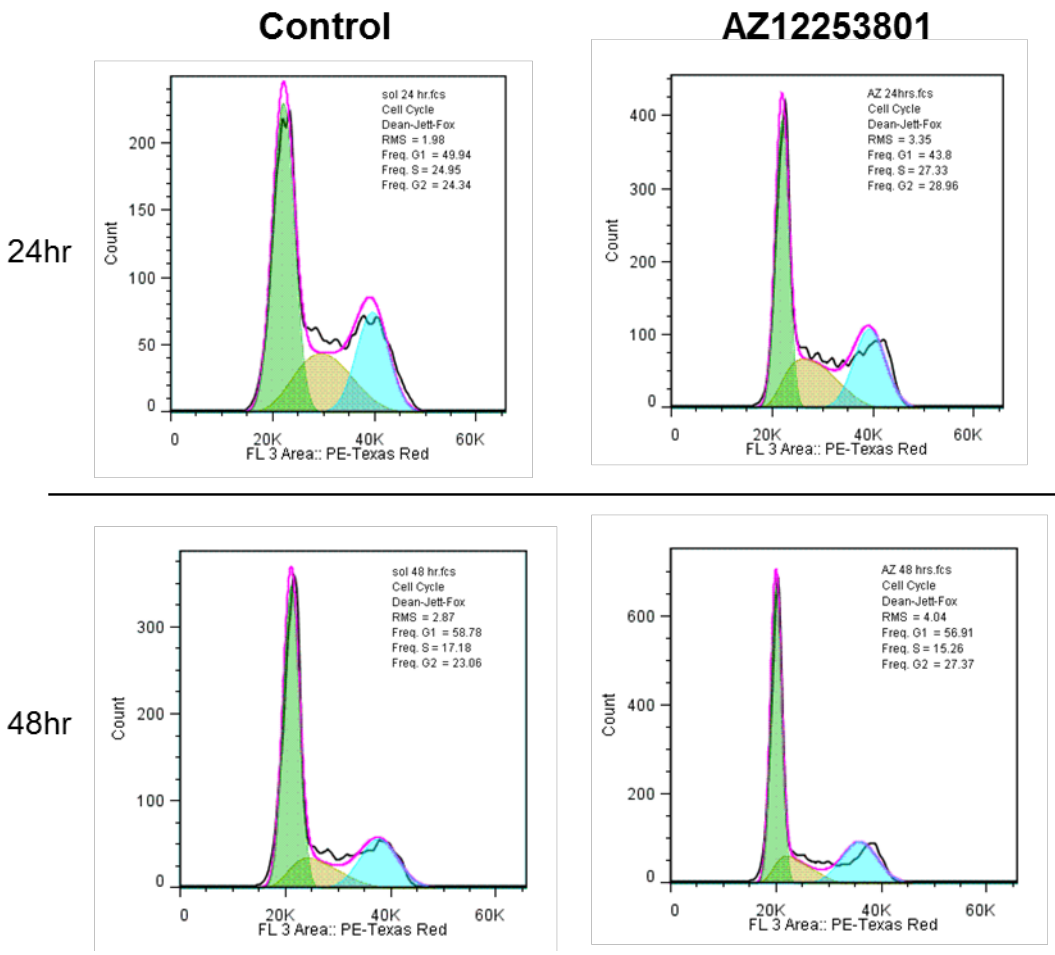

	Solvent (mean ± SEM)			AZ12253801 30nM (mean ± SEM)		
Time (hr)	**G1 (%)**	**S (%)**	**G2/M (%)**	**G1 (%)**	**S (%)**	**G2/M (%)**
1	54.1 ± 5.1	31 ± 4.1	12.5 ± 4	53.2 ± 6.7	31 ± 5	14.3 ± 3.8
4	44.1 ± 5.6	31.7 ± 4	14.5 ± 8	46.6 ± 4.5	33.7 ± 7.8	16.8 ± 7
8	55.2 ± 11.6	18.3 ± 1	25.1 ± 11.7	47.2 ± 7.7	19.8 ± 1.6	26.9 ± 12.6
18	59.3 ± 4.2	21.8 ± 2.3	22.5 ± 3.1	59.8 ± 2.2	20.7 ± 2.7	18.7 ± 5
24	52.1 ± 8	21.7 ± 1.7	13 ± 6.1	55.6 ± 7.3	21 ± 3.7	14.7 ± 7.2
48	42.3 ± 13.1	24.2 ± 11.3	26.1 ± 5	43.3 ± 13.7	22.5 ± 11.3	25.9 ± 5.6

Figure 4.15: IGF-1 inhibition does not alter the cell cycle profile of DU145 cells
DU145 cells were grown to 80% confluence in 10cm dishes, and treated with solvent or 30nM AZ12253801. At specific time points after addition of AZ12253801, cells were harvested in PBS/EDTA, fixed in ice-cold ethanol and prepared for FACS analysis as described in section 6.8.1. Results are from three independent experiments. FlowJo 7.6.5 software, cell cycle analysis programme, was used to assign G1, S and G2/M phases. Percentages of cells in G1, G2 and S phase of the cell cycle were expressed as mean ± SEM of the triplicate values, and differences between control and AZ12253801 treated cells was determined by t-test. There were no significant differences between the mean values for control and 30nM AZ12253801 treated cells.

	Irradiation	AZ12253801 + Irradiation
UI	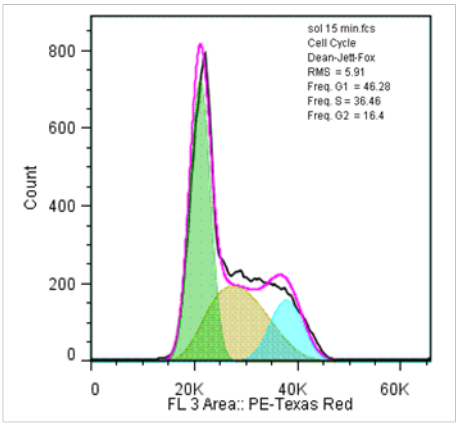	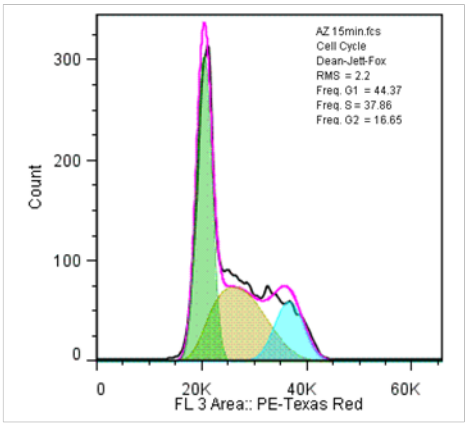
1hr	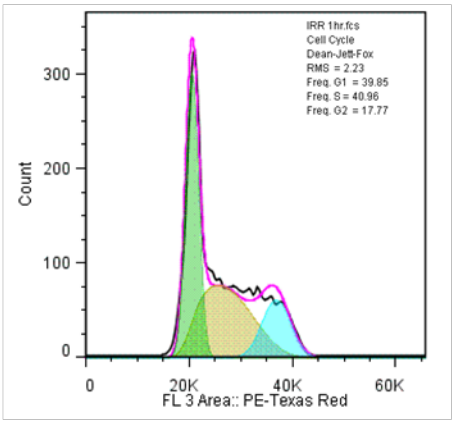	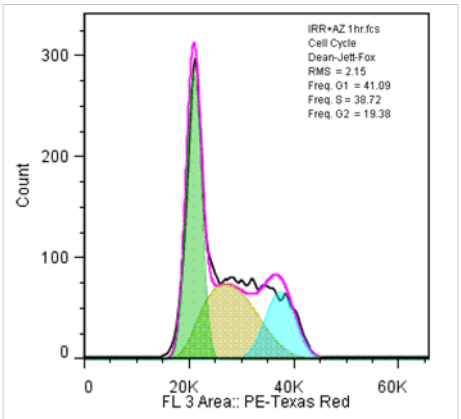
4hr	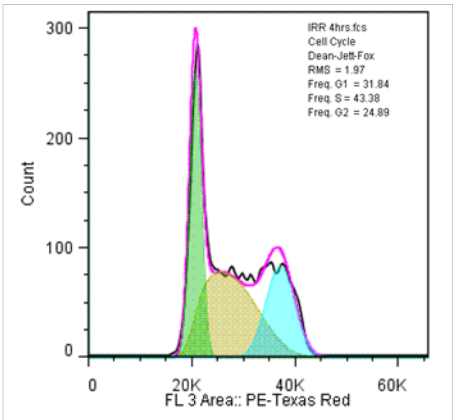	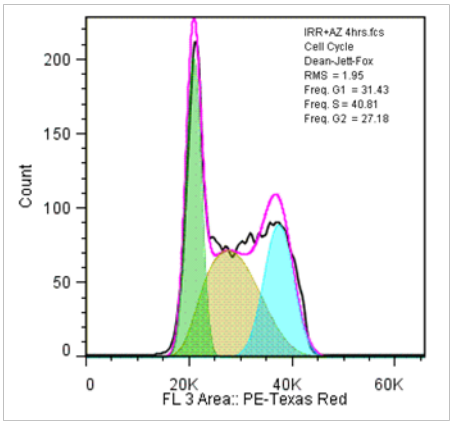
6hr	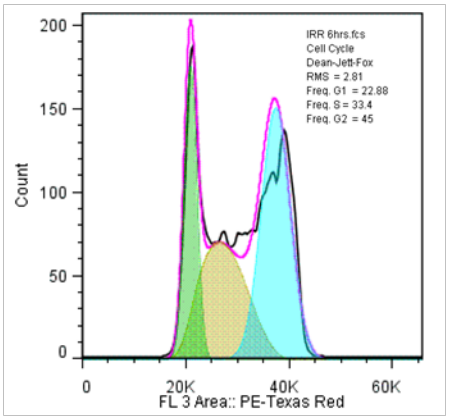	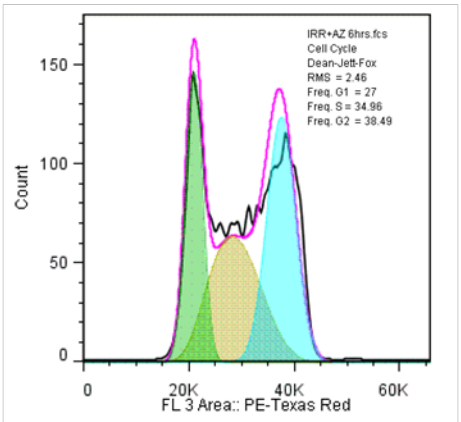

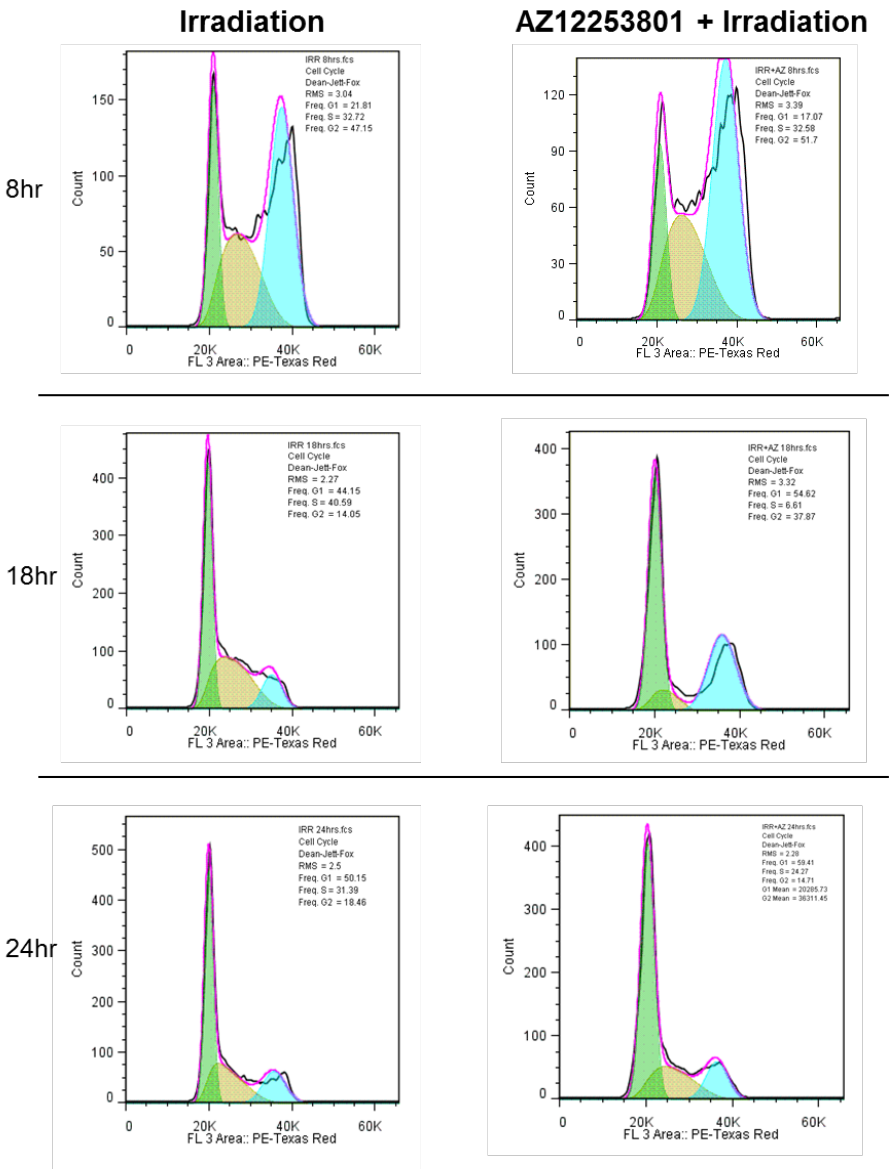

	Control IR (mean +/- SEM)			IR + AZ12253801 30nM (mean +/- SEM)		
Time (hr)	**G1 (%)**	**S (%)**	**G2/M (%)**	**G1 (%)**	**S (%)**	**G2/M (%)**
UI	48.8 ± 1.2	32.7 ± 5.3	17.7 ± 3.9	48 ± 2.4	33.6 ± 1.3	14.4 ± 1.5
1	47.1 ± 3.8	36.9 ± 2.1	13.5 ± 2.2	46.2 ± 3.2	36.9 ± 2.6	15.8 ± 2.3
4	39.5 ± 4	37.9 ± 2.8	21.7 ± 1.8	37.4 ± 3.1	36.3 ± 2.3	23.5 ± 1.9
6	30.9 ± 4.2	35.37 ± 1.9	31.1 ± 7	32.1 ± 2.7	32.9 ± 2.5	31.7 ± 3.9
8	30.3 ± 4.4	34.2 ± 1.3	34.2 ± 6.6	27.5 ± 5.2	33.8 ± 0.6	35.4 ± 8.2
18	54.1 ± 5	27.2 ± 7	15.8 ± 1.2	54.5 ± 0.9	15.8 ± 4.6	25.2 ± 6.4
24	61.4 ± 5.6	22.5 ± 4.7	14.9 ± 2.3	63.2 ± 2.3	20.8 ± 2.8	13.5 ± 1.2

Figure 4.16: IGF-1R inhibition does not alter the cell cycle profile of DU145 cells following irradiation

DU145 cells were grown to 80% confluence in 10cm dishes. Cells were treated with solvent or 30nM AZ12253801. After 4 hr incubation, cells were un-irradiated (UI) or irradiated (IR) at 3Gy, and then at fixed time-points post irradiation, cells were harvested, fixed in ice-cold ethanol and cell cycle distribution was analysed. Results are from three independent experiments. FlowJo 7.6.5 software, cell cycle analysis programme, was used to assign G1, S and G2/M phases. Percentages of cells in G1, G2 and S phase of the cell cycle were expressed as mean ± SEM of triplicate values. Differences between control and AZ12253801 treated cells was determined by t-test, and no significant differences were found.

4.3 Discussion

Data presented here indicate that a small molecule inhibitor of the IGF-1R inhibits the survival of prostate cancer cells following irradiation-induced DNA damage. This is consistent with previous data from our group using *IGF-1R* gene silencing (Rochester et al 2005, Turney et al 2012) and from others using monoclonal antibodies to inhibit the IGF-1R (Iwasa et al 2009). Use of a small molecule inhibitor allowed more precise determination of concentration-dependent effects than is possible using gene silencing. For the experiments in this chapter, concentrations of AZ12253801 were deliberately kept low, to ascertain the extent to which radiosensitization caused by IGF-1R inhibition is related to, or independent of, effects on proliferation and survival. Similarly, the choice of the DU145 cell line, which lacks wild-type p53 and Rb, compromising its ability to undergo G1 arrest, allowed assessment of the effect of IGF-1R inhibition on radiosensitization independent of its effect on proliferation.

Experiments in DU145 cells utilising IGF-1R siRNA knockdown induced a comparable radiosensitization to inhibition with AZ12253801. Further support that AZ12253801 induced radiosensitization was as a result of IGF-1R inhibition was from experiments in R- and R+ murine fibroblasts, where AZ12253801 radiosensitized IGF-1R overexpressing R+ cells, but failed to radiosensitize IGF-1R null R- cells. Moreover, IGF-1R inhibition suppressed post-irradiation survival of R+ cells to the level in R- cells, suggesting that the presence of IGF-1R is the major reason for the greater radioresistance of R+ cells compared with R- cells. Potential off-target effects of AZ12253801 were noted in the R- and R+ cells at concentrations of AZ12253801 above 60nM which might impact on experimental results via IGF-1R independent mechanisms. Indeed, data from AstraZeneca indicate that AZ12253801

is capable of inhibiting Aurora kinases at relatively high concentrations, and that murine cells are particularly susceptible to this (Dr. Elaine Kilgour, AstraZeneca, personal communication). Such an effect would be consistent with the morphological changes seen in R+/R- cells. However, morphological changes in DU145 cells were not evident at the concentrations of 30nM and 60nM used in these experiments, and not until 300nM AZ12253801.

The effect of AZ12253801 on radiosensitization was assessed in PC3, 22Rv1 and LNCaP-LN3 prostate cancer cell lines. LNCaP-LN3 cells were chosen for these assays, because the parental LNCaP cell line grows in semi-adherent clusters rather than in monolayers, hence there was concern that experimental results could be confounded by detachment of cells, for example during transport to the irradiator. Assays for intrinsic radiosensitivity of these cell lines showed DU145 cells to be the most radioresistant, with 22Rv1 being the most radiosensitive. Previous work in our laboratory utilising IGF-1R depleted cells also demonstrated DU145 cells to be the most radioresistant, but LNCaP cells had been found to be more radiosensitive than PC3 cells (Turney et al 2012). The current study found equivalent radiosensitivity in PC3 and LNCaP-LN3 cells, raising the possibility that LNCaP-LN3 cells are intrinsically more resistant than the parental LNCaP cell line, or that the poor adherence of the LNCaP cells in monolayer cultures led to an artificial overestimation of the apparent degree of radiosensitization previously observed. Total levels of IGF-1R as determined by western blotting did not appear to correlate with radiosensitivity in these cell lines. It is likely that the presence of genetic changes such as loss of functional PTEN, IRS-1, and/or p53 mutation (table 4.2) may contribute to the observed pattern of intrinsic radiosensitivity.

The results here demonstrate that small molecule tyrosine kinase inhibition of the IGF-1R resulted in radiosensitization of three out of four prostate cancer cell lines tested. AZ12253801 induced significant radiosensitization of DU145, PC3 and 22Rv1 cells, but not LNCaP-LN3 cells. Previous experiments in our lab have shown a similar result in PC3 cells, with only very modest radiosensitization seen in LNCaP cells (Turney et al 2012). Work by others has suggested that the *PTEN* status of prostate cancer cell lines may influence the ability of IGF-1R inhibition to induce radiosensitization, with *PTEN* null PC3 cells failing to show radiosensitization on treatment with NVP-AEW541, attributed to failure to effectively suppress Akt activity (Isebaert et al 2011). However, studies in R- cells expressing either wild-type IGF-1R or IGF-1R lacking PI3K activation sites suggested that the PI3K pathway is not essential for IGF-1R mediated radioresistance (Dong et al 2002). Consistent with this, studies in our lab have consistently shown radiosensitization of PC3 cells following IGF-1R inhibition or knockdown, suggesting a PTEN independent mechanism determining radiosensitization. The lack of effect in LNCaP-LN3 cells may be related to the lack of IRS-1 in these cells (figure 4.11A) and (Reiss et al 2000). In addition to linking IGF-1R to PI3K, IRS-1 has been shown to form a cytoplasmic complex with Rad51 in mouse fibroblasts, thus sequestering Rad51 in the cytoplasm. Upon IGF-1R receptor activation, IRS-1 is phosphorylated and dissociates from Rad51, allowing Rad51 to enter the nucleus and participate in DNA DSB repair by HR (Trojanek et al 2003). Conversely, inhibition of IGF-1R favours the retention of IRS-1:Rad51 complexes in the cytoplasm, hence suppressing HR related DNA DSB repair (Trojanek et al 2003). The absence of IRS-1 in LNCaP-LN3 might result in the absence of cytoplasmic IRS-1:Rad51 complexes, and hence no alteration in the rate of DSB repair upon either IGF-1R receptor activation or

inhibition. This might explain the failure of AZ12253801 to radiosensitize LNCaP-LN3 cells. However, it is not clear whether IRS-1:Rad51 complexes form in cells other than murine fibroblasts, and certainly work by others in our laboratory has failed to demonstrate such complex formation in DU145 cells (Turney et al 2012). Therefore, the potential contribution of this mechanism to IGF-mediated radioresistance in human prostate cancer cells remains unclear. LNCaP-LN3 cells also have very low levels of IGF-1R (figure 4.11A) and if time had permitted, it would be interesting to test associations between IGF-1R expression levels and degree of radiosensitization induced by AZ12253801 in a larger cell line panel.

The radiosensitivity of mammalian cells varies throughout the cell cycle, with radiosensitivity highest in early G1 and lowest in S phase (Hinz et al 2005, Jackson and Bartek 2009, Shrivastav et al 2008). IGFs are progression factors, predominantly facilitating transition of cells through G1 into S-phase of the cell cycle, by increased synthesis of cyclin D1 and CDK4 (Samani et al 2007), and degradation of p53 (Heron-Milhavet et al 2001, Levine et al 2006). Thus inhibition of the IGF-1R can result in G1 arrest (Flanigan et al 2010). DNA damage can directly cause G1 arrest as a result of p53 induced transcription of p21, and resultant inhibition of cyclin dependent kinases (Dulic et al 1994). DU145 cells harbour mutant p53 and Rb, and the effect of IGF-1R inhibition on cell cycle distribution in DU145 cells may thus be attenuated. This was confirmed in experiments conducted here, where alterations in cell cycle did not appear to be major contributing factors to changes in radiosensitivity in DU145 cells treated with low concentrations of the IGF-1R inhibitor AZ12253801. This was also the reason that this cell line was ideal for subsequent experiments investigating the effects of IGF-1R inhibiton on DNA repair independent of its effects on proliferation and cell cycle. Similarly, there was no clear enhancement of

irradiation-induced, caspase-mediated apoptosis in IGF-1R inhibited DU145 cells. However, this does not exclude the possibility that apoptosis induction may play a role in radiosensitization, particularly in cell lines other than DU145. In a study by Iwasa *et al* looking at CP-751,871 antibody mediated inhibition of the IGF-1R in NSCLC, apoptosis was markedly increased with the combination of IGF-1R inhibition and irradiation at 72 hr compared with either agent alone (Iwasa et al 2009). This was analysed both by measuring the percentage of apoptotic cells, as well as caspase-3 activity in cell lystaes, at 72 hr. The experiments carried out here using AZ12253801 only measured apoptotic activity up to 48 hr post irradiation, and perhaps later time-points should also have been analysed. However, even in the report by Iwasa *et al*, the fraction of apoptotic cells following IGF-1R inhibition was small leading the authors to investigate additional mechansims by which CP-751,871 might contribute to radiosensitization (Iwasa et al 2009). If time had permitted, effects of IGF-1R inhibition on other methods of cell death, including mitotic catastrophe, autophagy and necrosis could also have been investigated.

There was no evidence to support induction of senescence with IGF-1R inhibition in DU145 cells. Replicative senescence is the end result of normal cell division and telomeric shortening. Tumour cell senescence is a protective mechanism by which potentially tumorigenic cells are removed from the cell cycle. It has been linked to the activation of p53, p16, p21 and ARF, and inactivation of these tumour suppressors can lead to impaired senescence (Collado and Serrano 2010). Senescence can be induced by IGF-BP related protein 1, and several other IGF-BPs are upregulated in senescent cells (Ewald et al 2010). Therapy induced senescence (TIS) is increasingly recognized as an alternative pathway to apoptosis in the cellular response to DNA damage induced by irradiation or classical chemotherapeutic agents (Roninson 2003).

Senescence may also be induced by small molecule inhibitors such as the EGFR inhibitor erlotinib, which has been shown to induce cellular senescence following irradiation induced DNA damage (Chan et al 2012, Ota et al 2006, Wang et al 2011). The triggers that select senescence over apoptosis as an outcome to damage are as yet unclear, and the degree of damage sustained may be important (Schwarze et al 2005). IGF-1R inhibition did not induce senescence in DU145 cells. DU145 cells harbour mutant p53 (Carroll et al 1993) which may render them refractory to senescence, given the importance of the p53-p16/p21 pathway in senescence induction (Chang et al 1999a, Collado and Serrano 2010). However, despite the absence of wild-type p53, tumour cells can retain the ability to undergo senescence in response to stress, hence the p53 status of DU145 cells may not always be the determining factor in senescence induction (Chang et al 1999b, Wang et al 2011). To explore this relationship further, senescence could be assessed following IGF-1R inhibition of a prostate cancer cell line that expresses wild-type p53 such as 22Rv1. The absence of functional Rb and p16 in DU145 cells may also be relevant to the lack of senescence induction in these cells (Steiner et al 2000).

Having found no major changes in cell cycle, apoptosis induction, or senescence, the next step was to investigate the effect of IGF-1R inhibition on the induction and repair of radiation-induced DNA DSBs.

5 Chapter V: Effect of IGF-1R inhibition on the induction and repair of DNA double strand breaks

5.1 Introduction

Previous work from our group showed that IGF-1R depletion increased the sensitivity of prostate cancer cells to DNA damaging agents including irradiation and chemotherapeutic agents such as mitoxantrone and etoposide, which cause DNA DSBs, but not to agents such as docetaxel and 5-fluorouracil, which cause cellular damage without inducing direct DNA DSBs (Rochester et al 2005). The work in the previous chapter showed that comparable radiosensitization is induced by IGF-1R inhibition. Previous work from our lab had also shown an enhancement of radiosensitivity and impaired ATM kinase activity following IGF-1R depletion in murine melanoma cells (Macaulay et al 2001). More recent work in MCF7 breast cancer cells implicated the IRS-1/Akt signalling pathway in mediating effects of IGF-1R depletion on ATM (Riedemann, Macaulay unpublished data), and a direct binding interaction between the IGF-1R adaptor IRS-1 and ATM has been demonstrated in MCF7 cells, both in our lab (Akkaya and Macaulay unpublished) and by others (Jeon et al 2008). A relationship between the IGF-1R signalling axis and ATM has not been demonstrated in prostate cancer cells.

A second potential link between receptor tyrosine kinases and DSB repair involves the catalytic subunit of DNA protein kinase (DNAPKcs), a core NHEJ protein known to be phosphorylated by ATM on T2609 (Chen et al 2007). Investigation of the role of the epidermal growth factor receptor (EGFR) has shown that the EGFR can translocate to the nucleus and physically interact with

DNAPKcs and Ku70 (Bandyopadhyay et al 1998, Dittmann et al 2005a, Liccardi et al 2011). Given that we have now shown that IGF-1R undergoes nuclear import (chapter 3) and (Aleksic et al 2010), the possibility was considered that the IGF-1R might directly interact with DNAPKcs and/or ATM. Thus, the next step was to investigate the effect of IGF-1R inhibition on the induction and repair of DNA DSBs following irradiation-induced DNA damage, with a particular focus on ATM as mediating any effects observed.

Although the ratio of SSBs to DSBs induced following irradiation is 20:1, DSBs are by far the most toxic form of DNA damage following irradiation, and induce a complex cellular response involving co-ordinated sensing, signaling and repair of damage (Thompson 2012). One of the initial stages in this process is the phosphorylation of histone protein H2AX, referred to as γH2AX, at the site of the DSB. During S-phase of the cell cycle, SSBs can also induce γH2AX formation at sites of replication fork stalling or collapse, this being one of the caveats to the use of γH2AX as a sensitive marker of DSB repair in unsynchronized cell populations (Lobrich et al 2010). It is also not completely clear whether timing of resolution of a γH2AX focus correlates directly with the repair of the DSB (Kinner et al 2008). Bearing in mind these limitations, γH2AX can still be utilized as a reliable marker of DSB induction and resolution (Ivashkevich et al 2011, Lobrich et al 2010), and hence the next stage utilized γH2AX to investigate the effects of IGF-1R inhibition on DSB formation and repair following irradiation induced DNA damage.

5.2 Results

5.2.1 Effect of IGF-1R inhibition on the repair of DNA damage

5.2.1.1 Effect of IGF-1R inhibition on γH2AX signal resolution by western blotting

DNA DSBs were generated in DU145 cells by ionising radiation, and γH2AX signal was assessed by western blot, as a surrogate marker for DNA damage. In the absence of exogenous damage, cells that had been pre-treated for 4 hr with IGF-1R inhibitor showed detectable γH2AX signal (Figure 5.1A) suggesting endogenous DNA damage. This phenomenon has previously been reported and has been attributed to apoptotic cells with fragmented DNA (Rogakou et al 1999). It could also reflect endogenous damage following replication fork collapse and consequent DNA DSBs (Halazonetis et al 2008). Control cells showed resolution of signal to basal (unirradiated) levels by 24 hr (figure 5.1). Pre-treatment with 30nM AZ12253801 appeared to induce a delay in γH2AX signal resolution. This was apparent at 4 hours ($p<0.01$), with a similar trend, though not statistically significant, at the 24 hr time-point. These results were consistent with the delay in DSB repair measured previously by PFGE after IGF-1R depletion (Ben Turney DPhil 2008). At 48 hours post irradiation, the γH2AX signal in IGF-1R inhibited cells remained elevated, possibly due to apoptosis at this time (figure 5.1B and figure 4.13). It is known that apoptosis can generate γH2AX signal (Solier and Pommier 2009), and western blotting does not allow differentiation between this and DNA damage. Against this, previous results had suggested that 30nM AZ1253801 did not increase the level of apoptosis over that induced by irradiation (figure 4.13). To clarify this, a second

assay, namely immunofluorescence, was used to assess the effect of IGF-1R inhibition on resolution of γH2AX foci.

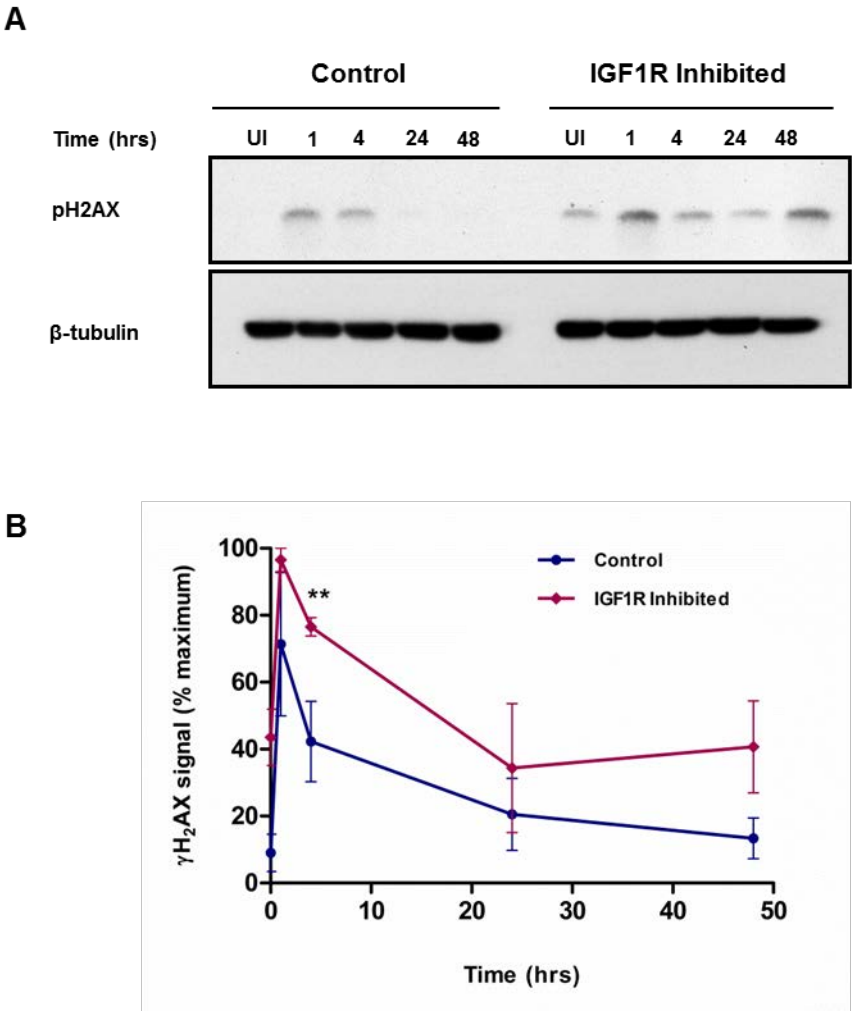

Figure 5.1: AZ12253801 delays the resolution of irradiation-induced γH2AX signal in DU145 cells.
(A) DU145 cells were incubated for 4 hr with 30nM AZ12253801, irradiated at 3Gy and lysed at defined time-points for analysis by western blot for pS139 γH2AX. Images were scanned and analysed using ImageJ software. (B) Graph shows signal intensity of γH2AX with time, expressed as % of maximal signal, corrected for loading. Points represent the mean and SEM of three independent experiments. Statistical significance between control and IGF-1R inhibited cells at each time-point was determined by Student's t-test (**$p<0.01$). There was no statistically significant difference at the 1, 24 and 48 hr time-points.

5.2.1.2 IGF-1R inhibition results in a delay in resolution of γH2AX foci by immunofluorescence

γH2AX signal expands for mega base-pair (bp) lengths on either side of a DNA DSB and hence can be visualized as discrete foci by immunofluorescence (Rogakou et al 1999). Firstly, optimal staining conditions for γH2AX foci were determined over a range of primary antibody (1:1000, 1:2000 and 1:4000) and secondary antibody dilutions (1:2000 and 1:4000). Initial experiments plotted γH2AX focus counts against dose of irradiation to assess the dose range over which linearity was observed (figure 5.2A). From here 3Gy was chosen as the dose at which focus counts were in the linear range, and could be reliably counted both at early and late time-points, with minimal overlap of foci. Another potential confounding factor is that γH2AX foci are reported to occur early during apoptosis, typically with a ring of γH2AX signal around the periphery of the nucleus, progressing to more widespread diffuse signal (Solier and Pommier 2009, Solier and Pommier 2011). Indeed, some DU145 cells analysed by immunofluorescence did show intense γH2AX signal, especially at the 24 and 48 hour time-points, both in control irradiated and AZ12253801 inhibited and irradiated cells (Figure 5.2B). These appearances were consistent with features of apoptotic cells (Solier and Pommier 2009, Solier and Pommier 2011) and so these cells were excluded from subsequent analysis. As a control to ensure that the antibody was detecting γH2AX foci, cells were co-stained for 53BP1 (p53 binding protein 1) foci, which are induced rapidly in an ATM dependent manner at the site of DNA DSBs, and co-localise with γH2AX foci (Wang et al 2002), as was seen in figure 5.2C. A further control included omission of the primary antibody to exclude non-specific staining attributable to the secondary antibody.

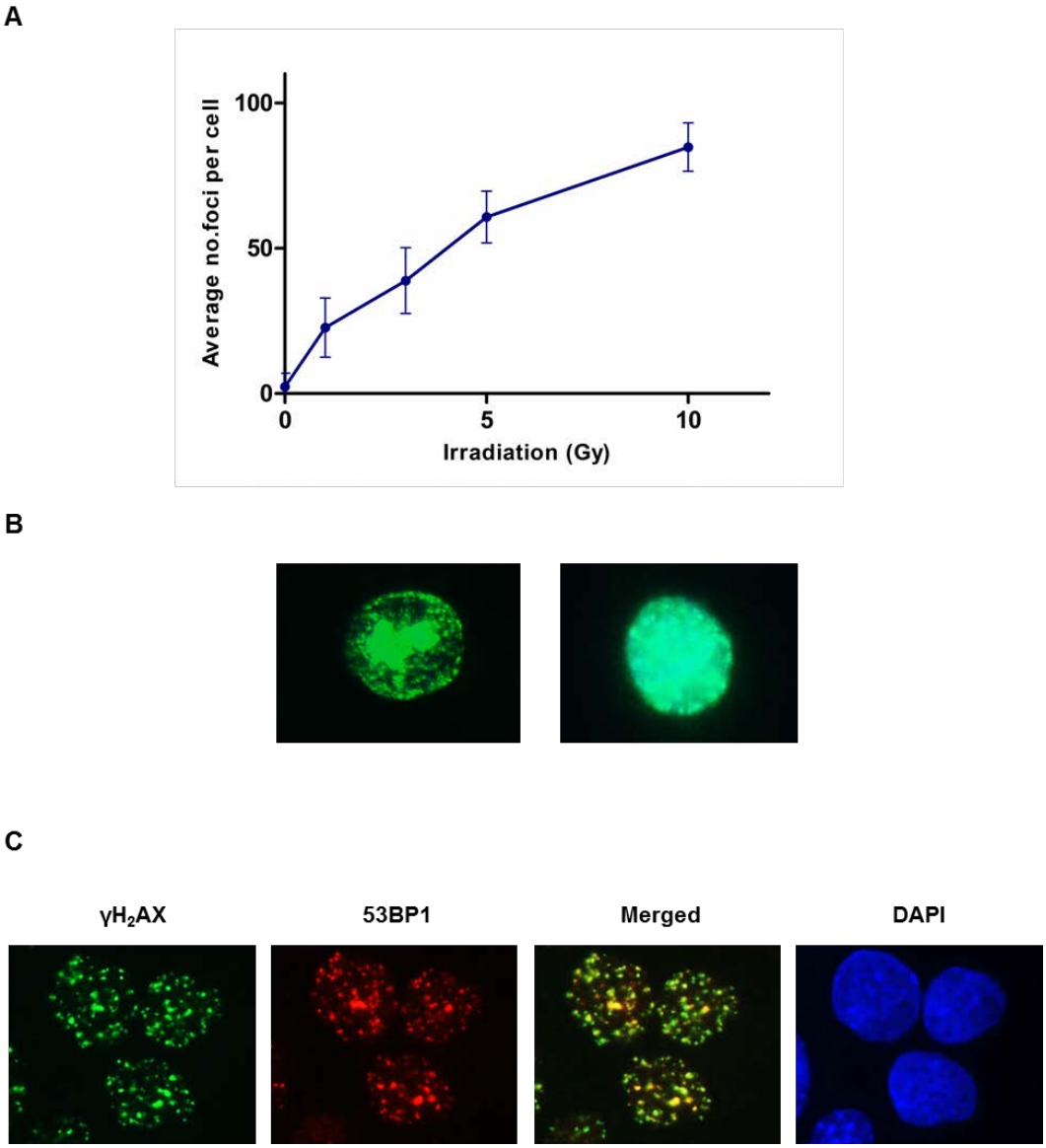

Figure 5.2: Optimisation of γH2AX immunofluorescence to detect irradiation induced DSBs
A) DU145 cells were seeded on coverslips in 6-well plates. The following day cells were either mock irradiated or irradiated at 1Gy, 3Gy, 5Gy and 10Gy, and 1 hr post irradiation cells were fixed and stained for γH2AX. Foci were counted in a minimum of 30 cells for each condition and mean foci/cell ± SEM were plotted against dose of irradiation. B) Examples of nuclei showing: peripheral γH2AX signal (left), and pan-nuclear γH2AX (right) . C) DU145 cells were seeded on coverslips in 6-well plates. The following day, cells were irradiated at 3Gy and 1 hr post irradiation cells were fixed and stained for γH2AX (green), 53BP1 (red), and nuclear DAPI (blue). Merged γH2AX and 53BP1 signal appears as yellow. Images were taken at 40x magnification.

Having established conditions for irradiation and immunofluorescence, the next experiments assessed effects of AZ12253801. Analysis of γH2AX foci showed that unirradiated cells contained a few foci (figure 5.3 and 5.4A) with a significant increase after 3Gy irradiation. In control-treated cells, numbers of γH2AX foci had

resolved to basal levels at 24 hr (figure 5.3 and 5.4A) paralleling results of western blotting (figure 5.1). In IGF-1R inhibited cells, 30nM AZ12253801 induced a significant delay in γH2AX foci resolution that was apparent at 1 hr following irradiation, and persisted for 24 hours (figures 5.3 and 5.4A). In these initial experiments, the significance of the difference at one hour was unclear. It might be expected that the initial degree of damage sustained by both controls and IGF-1R inhibited cells would be equivalent for the same dose of radiation. The difference at 1 hr post irradiation in AZ12253801 treated cells versus controls was apparent both by western blotting and by immunofluorescence (figure 5.1 and 5.4A). This could have been due to maximal damage occurring before one hour, allowing a proportion of DSB repair to have taken place by 1 hr, or to an actual difference between controls and IGF-1R inhibited cells in the degree of damage initially sustained. Therefore, further experiments were carried out to quantify foci at early time points up to 2 hr. It was apparent that in DU145 cells, maximal damage was evident by immunofluorescence analysis at 30 min, with no significant difference between controls and IGF-1R inhibited cells (figure 5.4B). Subsequently a delay in focus resolution and hence in DNA DSB repair became apparent from 1 hr, consistent with the findings of western blotting (figure 5.1) and quantification of γH2AX foci over a longer time-course (figure 5.4A).

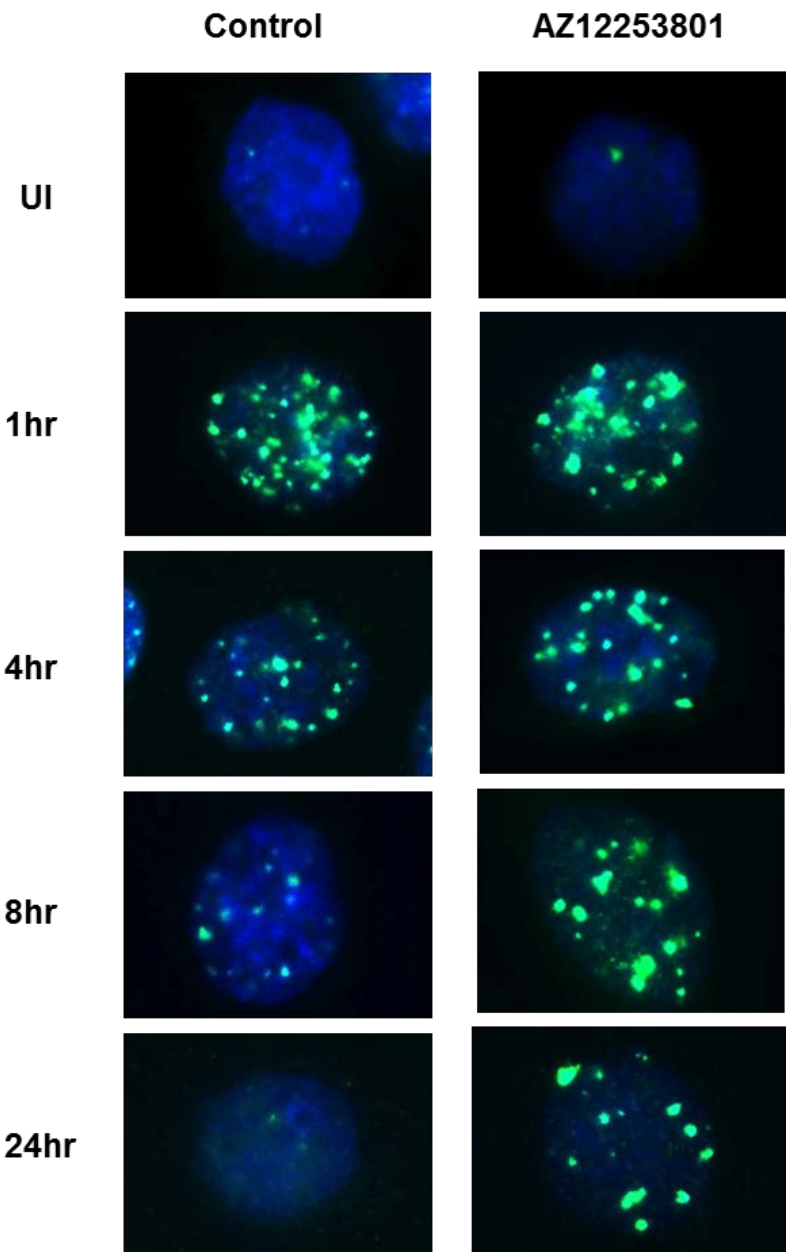

Figure 5.3: IGF-1R inhibition results in a delay in resolution of γH2AX foci in DU145 cells
DU145 cells were treated with 30nM AZ12253801 and after 4 hr irradiated at 3Gy. At time-points up to 48 hr, cells were fixed and stained for S139 γH2AX. Images show merged γH2AX (green) and nuclear DAPI (blue) staining in unirradiated (UI) cells, and cells at 1, 4, 8 and 24 hr post irradiation. Images were taken at 40x magnification

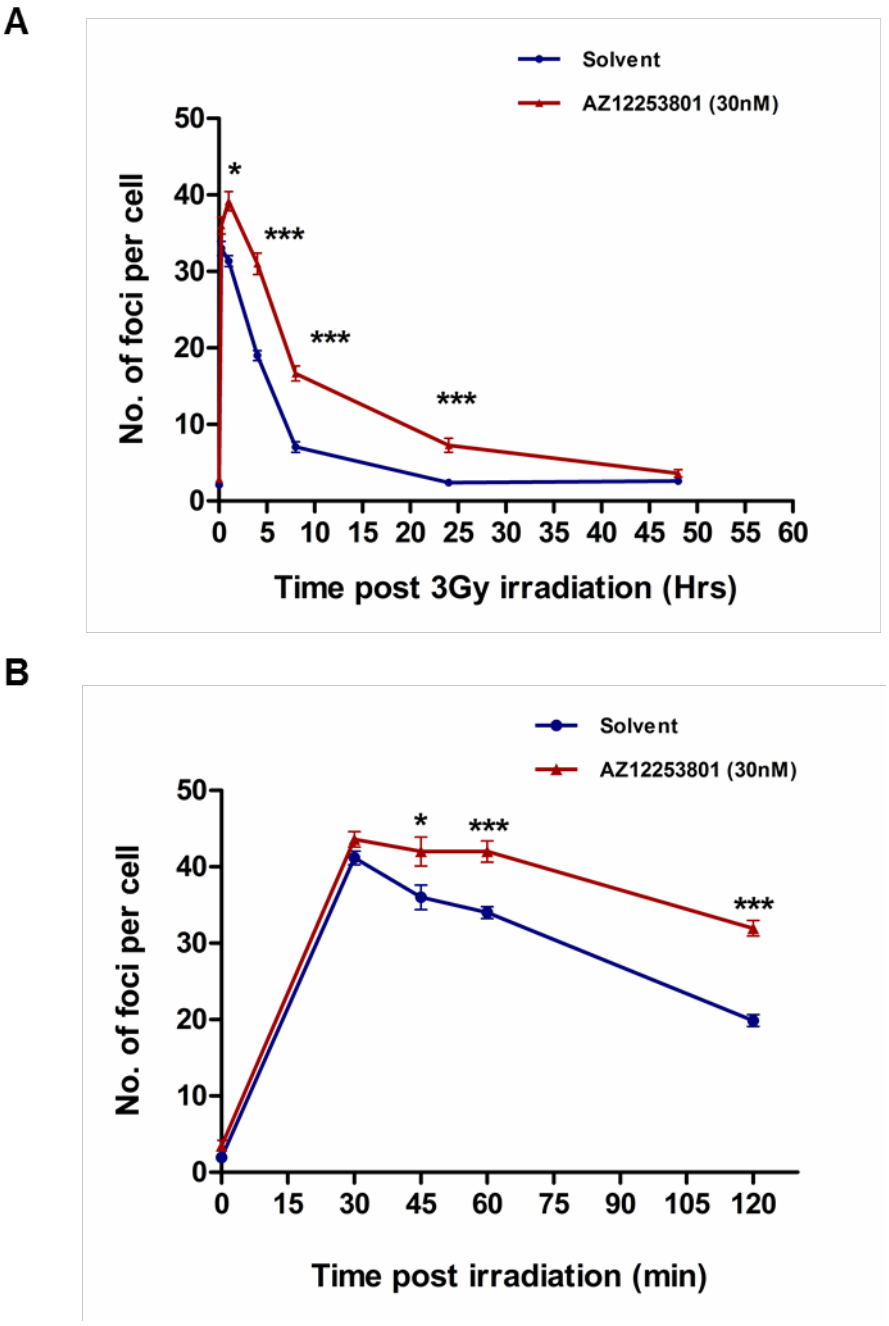

Figure 5.4: Quantification of γH2AX foci following IGF-1R inhibition in DU145 cells
A) DU145 cells were treated with 30nM AZ12253801 and 3Gy irradiation as figure 5.3. Foci were counted manually in 8 separate high powered fields to include at least 60 cells per condition. Graph shows the mean focus count per cell ± SEM for three independent experiments Student's t-test was used to determine the significance of differences between control and AZ12253801 treatment at each time-point (*p<0.05, ***p<0.001). B) The experiment carried out in part A was repeated, counting foci at 0-2 hr (*p<0.05, ***p<0.001). At the 1 hr time-point, control cells contained 80% of foci in IGF-1R inhibited cells in the long-time course A), and 81% in B) suggesting similar kinetics of repair in the two sets of experiments.

Taken together, these data are consistent with a delay in DSB repair following IGF-1R inhibition. The next step was to investigate the mechanism of this effect.

5.2.2 Effect of IGF-1R inhibition on ATM and its downstream mediators

A relationship between the IGF-1R signalling axis and ATM has not been demonstrated in prostate cancer cells, but if present might contribute to the radiosensitization and delayed DSB repair induced by IGF-1R inhibition. The possibility that the IGF-1R or its downstream adaptor protein IRS-1 might directly interact with DNAPKcs and/or ATM was considered. Therefore, the next step was to test for binding associations between the IGF-1R and/or IRS-1, ATM and DNAPKcs.

5.2.2.1 Investigation of the interaction of IGF-1R with ATM and DNAPKcs

Binding between endogenous IGF-1R and ATM or DNAPKcs was explored by reciprocal co-immunoprecipitation (Co-IP). Initial experiments tested for Co-IP in cells that were serum starved or IGF-1 treated, followed by 5Gy irradiation. The aim was to enable detection of any interactions that were promoted by ligand stimulation or DNA damage. IGF-1 induced a mobility shift in IRS-1, consistent with phosphorylation of IRS-1 by activated IGF-1R. However, under these conditions, Co-IP of either ATM, DNAPKcs or IRS-1 with IGF-1R was not demonstrated (figure 5.5A). Similarly, DNAPKcs, ATM or IGF-1R were not detected in IRS-1 IPs (figure 5.5B).

It has been reported that the association of the EGFR with DNAPKcs is maximal at 5 min post irradiation, persists only for 20 min (Dittmann et al 2005a), and is influenced by antibody mediated blockade of EGFR signalling (Dittmann et al 2005b). Therefore these experiments were repeated using shorter time-points (5 or 20 min) post irradiation and including samples treated with IGF-1R inhibitor AZ12253801. Again, no Co-IP was detected (not shown). These results do not support a direct association between IGF-1R or IRS-1 and ATM or DNAPKcs in DU145 prostate cancer cells. .

Even though a direct association between IGF-1R and ATM was not demonstrated, it was possible that IGF-1R signalling could still affect the activity of ATM, which could be manifest as an effect on the numerous downstream mediators of ATM function.

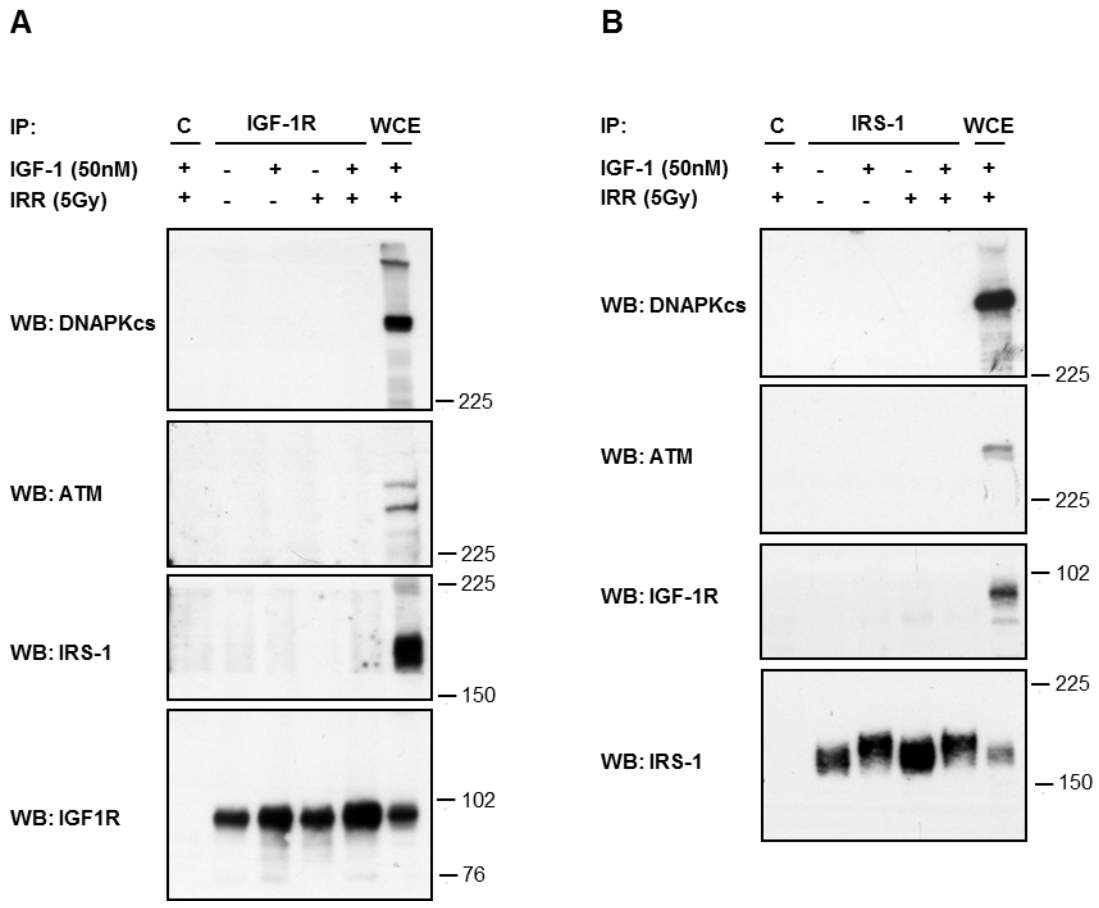

Figure 5.5: ATM and DNAPKcs are not detectable in IGF-1R or IRS-1 IPs in DU145 cells
DU145 cells were grown to 80% confluence in 15cm dishes. Cells were serum starved overnight followed by stimulation with IGF-1 for 15 min prior to lysis, or irradiation at 5Gy and lysis 1 hr post irradiation with IGF-1 stimulation for the last 15 min. Cell lysates were immunoprecipitated with IGF-1Rβ antibody (A), IRS-1 antibody (B) or rabbit IgG (A and B), and IPs were analysed by western blotting for DNAPKcs and ATM. C=rabbit IgG control; WCE = whole cell extract.

5.2.2.2 Effect of IGF-1R inhibition on ATM signalling effectors

ATM has numerous effectors including Chk-2, p53 and KAP-1 (figure 1.2), and changes in phosphorylation of these molecules can be used as markers of ATM activity (Lobrich and Jeggo 2005, Noon et al 2010). Analysis was performed at one hour post irradiation, as at this early time-point ATM is likely to be the predominant signalling protein in the activation of the DSB repair process. Other major players such as ATR are likely to play a part at later time points (Jazayeri et al 2006, Myers and Cortez 2006). A putative association between IGF-1R signalling and ATM was investigated by assessing phosphorylation of ATM effectors following treatment with inhibitors of the IGF-1R signalling axis. These included the IGF-1R inhibitor AZ12253801, and also PI3K, p38 and MEK inhibitors. The concentration of PI3K inhibitor LY294002 was chosen as that which blocks PI3K activation, but is reportedly insufficient to block the PI3K-like kinase domains of ATM and DNAPK (Rosenzweig et al 1997, Stiff et al 2004). An inhibitor of ATM (ATMi) KU-55933 (Hickson et al 2004) was included to assess the ATM dependence of the measured radiation induced changes in phosphorylation.

Irradiation of DU145 cells induced phosphorylation of KAP-1, Chk-2, p53, γH2AX and autophosphorylation of ATM on S1981, detected as a doublet in these cells (figure 5.6A). These events were clearly inhibited by the ATMi, but not by any of the other inhibitors. Previous work in our lab suggested that the IGF-1R influences ATM signalling in MCF7 breast cancer cells via the IRS-1-PI3K-AKT signalling pathway, based on reduction in Chk-2 phosphorylation following siRNA depletion of IGF-1R, IRS-1 or AKT-2 (Riedemann and Macaulay unpublished). However, there was no reduction in Chk-2 phosphorylation following inhibition of the IGF-1R at one hour post irradiation (figure 5.6A). If there were an effect of IGF-1R inhibition, one

would expect a dose response relationship between Chk-2 phosphorylation and increasing concentrations of AZ12253801. Figure 5.6B shows that this was not the case. In fact phosphorylation of ATM was apparently increased at 1 hr post irradiation in AZ12253801 treated cells compared with controls (figure 5.6A). This would be consistent with the delay in γH2AX focus resolution apparent at 1 hr post irradiation in AZ12253801 treated cells compared with control cells (figures 5.3 and 5.4). A similar increase in pATM seen on PI3K inhibition with LY294002 allows speculation that the PI3K-Akt pathway might play a role in mediating this effect.

Thus, there was no support for an early effect on inhibition of ATM function following IGF-1R inhibition in prostate cancer cells. Indeed, ATM deficient cells are reported not to show an early defect in DSB repair, but have a late defect due to failure to repair a subset (~10-15%) of DSBs (Beucher et al 2009, Kuhne et al 2004). Previous experiments had shown an altered time course of γH2AX resolution over a longer period (figure 5.1 and 5.4A). Therefore it was of interest to assess whether IGF-1R inhibition might influence the activity of ATM and its effectors over 24 hr. Following IGF-1R inhibition, there was no evidence of reduction in KAP-1 phosphorylation. Rather, KAP-1 phosphorylation appeared marginally stronger at 4 hours and 24 hours when compared with control irradiated cells (figure 5.7). KAP-1 is known to be phosphorylated by ATM at Ser824 after DSB induction, resulting in relaxation of chromatin structure. Given the slight increase in KAP-1 phosphorylation at 4-24 hr, it is possible that IGF-1R inhibition could have an ATM-independent effect on modifying chromatin structure,

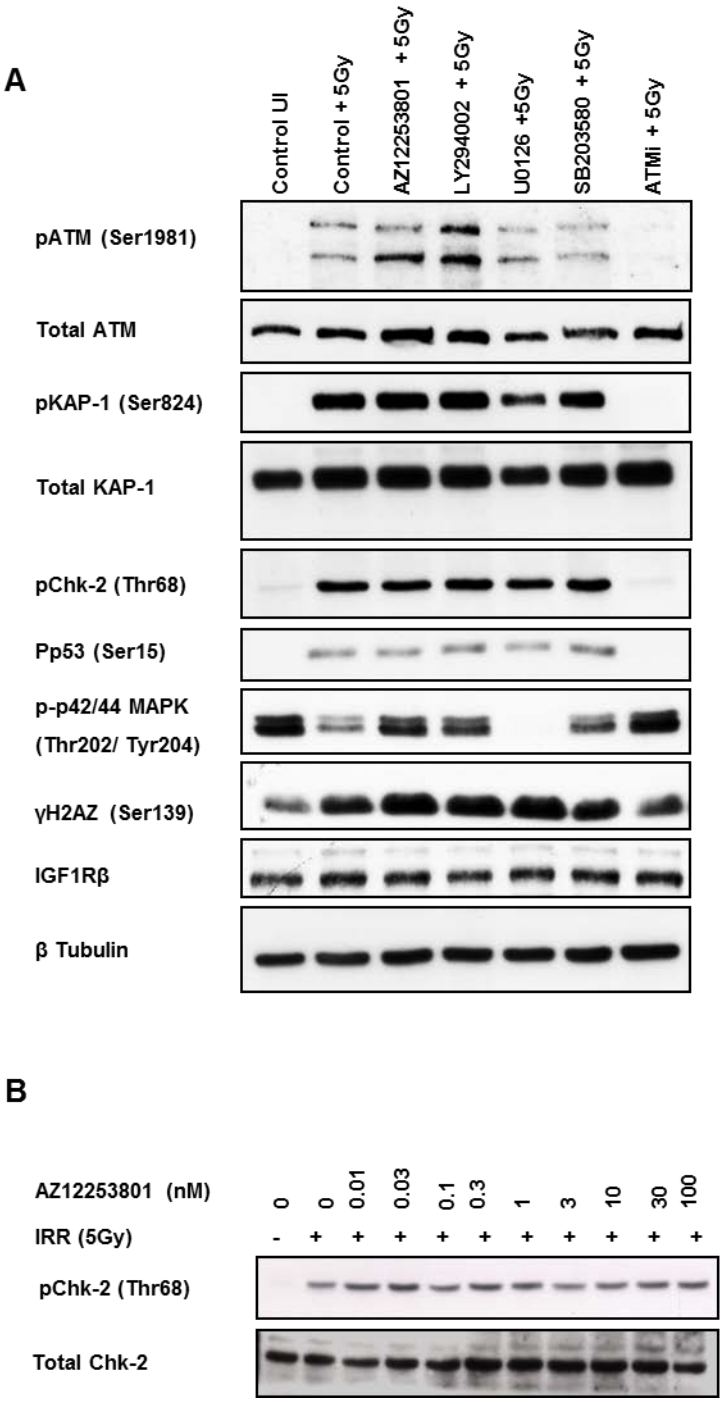

Figure 5.6: Effect of IGF axis inhibition on ATM signalling in DU145 cells
A) DU145 cells were treated for 4 hours with 30nM IGF-1R inhibitor AZ12253801; 20µM PI3K inhibitor LY294002 (Calbiochem); 10µM MEK 1/2 inhibitor U0126 (Calbiochem); 5µM p38 MAPK inhibitor SB203580 (Promega); 10µM ATM inhibitor KU55933 (Calbiochem). Cells were unirradiated (UI) or irradiated at 5Gy and lysed in SDS lysis buffer one hour post irradiation. The results are representative of three independent analyses. B) DU145 cells were treated with solvent (0.0003% DMSO) or increasing concentrations of AZ12253801 for 4 hours, irradiated at 5Gy and lysed one hour post irradiation. Western blot analysis was performed for pChk-2 and total Chk-2.

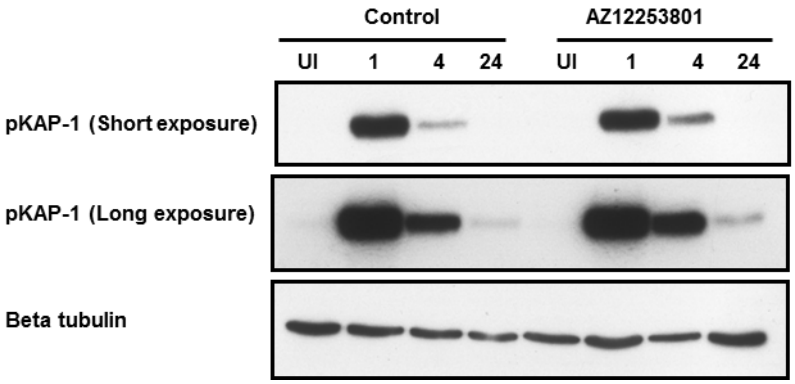

Figure 5.7: Effect of IGF-1R inhibition on KAP-1 phosphorylation in DU145 cells
DU145 cells were treated with 30nM AZ12253801 for 4 hours, irradiated (5Gy) and lysed in SDS lysis buffer at 1, 4 and 24 hr post irradiation. Lysates were prepared for western blot analysis for pKAP-1 (Ser824) with β-tubulin as a loading control.

The concept that IGF-1R might influence chromatin structure was raised in a study of NSCLC cells, induced to be resistant to erlotinib, with cross-resistance to cisplatin. An unbiased screen for resistance mediators highlighted the role of IGF-1R in regulating a chromatin modifying enzyme, histone demethylase KDM5A, which demethylates K4 of histone H3 (Sharma et al 2010). If IGF-1R signalling does indeed modify chromatin structure, reducing access of repair proteins, any subsequent irradiation-induced DSBs in these regions may take longer to repair. This could account for the delay in DSB repair and persistence of γH2AX foci and KAP-1 signal observed following IGF-1R inhibition. Therefore, IGF-1R inhibited DU145 cells were assessed for levels of KDM5A and di- and tri-methylated histone H3K4. However, no changes were observed at 24 hr (figure 5.8).

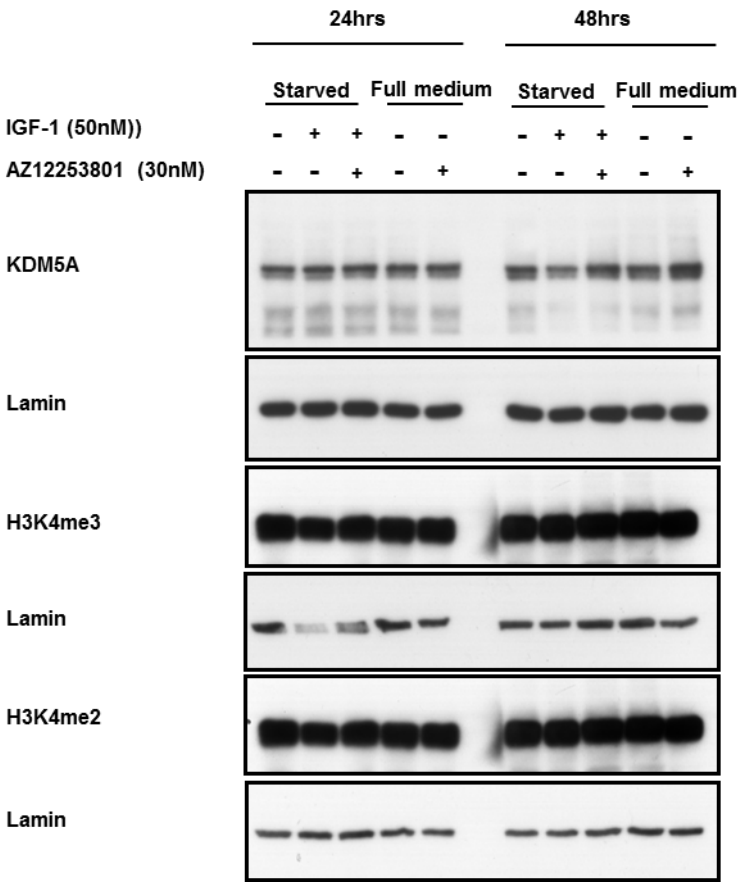

Figure 5.8: IGF-1R inhibition does not influence expression of the histone demethylase KDM5A in DU145 cells
DU145 cells were either serum starved overnight or left in full medium with 10% FCS. Cells were treated with 30nM AZ12253801 for 4 hr and stimulated with IGF-1 in the last 15 min prior to lysis. Cells were lysed in SDS lysis buffer at time-points of 24 and 48 hr post IGF-1R inhibition. Western blot analysis was performed for KDM5A, di- and tri-methylated H3K4, and lamin as a loading control.

At the conclusion of this set of experiments, there was no evidence that IGF-1R inhibition influenced the function of ATM or its effectors in DU145 prostate cancer cells. The next set of experiments tested whether IGF-1R inhibition may have a more direct effect on DNA DSB repair.

5.2.3 Investigating effects of IGF-1R inhibition on DNA DSB Repair

The data generated here using a small molecule IGF-1R inhibitor showed a delay in resolution of γH2AX foci as early as 1 hr after damage (Figure 5.4). Rapid repair of DSBs is mediated by NHEJ, and defects in HR typically cause a repair defect at

later time-points (Mao et al 2008, Shibata et al 2011) . In order to investigate whether IGF-1R inhibition influences the NHEJ pathway of DSB repair, the DNAPKcs deficient cell line M059J and DNAPKcs proficient M059K cells were utilised.

5.2.3.1 Effect of IGF-1R inhibition in combination with DNAPKcs deficiency and DNAPK inhibition

M059J and M059K are human glioblastoma cell lines established from the same tumour biopsy (Allalunis-Turner et al 1993, Allalunis-Turner et al 1995). M059J cells are DNAPKcs deficient compared with DNAPKcs proficient M059K cells, and this was confirmed by western blotting (Allalunis-Turner et al 1995) (figure 5.9A). Levels of other core NHEJ proteins were similar in the two cells lines (figure 5.9A), however, it must be noted that, as reported (Ng et al 2010, Tsuchida et al 2002), M059J cells have lower levels of ATM, important in the sensing of DNA DSBs.

M059J cells were noted to be more radiosensitive than the M059K cells in keeping with published data (Allalunis-Turner et al 1993, Allalunis-Turner et al 1995, Ito et al 2012, Ng et al 2010, Yoshida et al 2002) (figure 5.9B). M059K cells were sensitized to 1-5Gy irradiation by treatment with AZ12253801. M059J cells showed AZ12253801-induced sensitization to 1Gy (43% vs 26%, $p<0.01$), but there was no difference at 2-5Gy (figure 5.9B). These data suggest that IGF-1R inhibition may be epistatic with DNAPKcs deficiency in the repair of DSBs by NHEJ. It was noted that the M059J cells had a slightly lower level of IGF-1R (figure 5.9A). This could be related to low ATM expression, since ATM has been reported to regulate IGF-1R expression at the transcriptional level (Peretz et al 2001). It is possible that reduced IGF-1R could contribute to radiosensitivity, although levels of IGF-1R did not appear to correlate with radiosensitivity in the prostate cell line panel (figure 4.11.and 4.12). It is also possible that the lower levels of ATM in the M059J cells influenced the

ability of AZ12253801 to radiosensitize, but this is less likely for two reasons. Firstly, previous experiments indicated that IGF-1R inhibition with AZ12253801 did not appear to inhibit the function of ATM or its downstream signalling mediators (section 5.2.2). Secondly, experiments using ATM inhibitor KU-55933 showed that inhibition of ATM was capable of radiosensitizing both M059K and M059J cells, suggesting that the lower level of ATM in the M059J cells was functional, and did not limit the ability to radiosensitize these cells to any stimulus acting via ATM (figure 5.9C).

The next step was to determine whether there was similar epistasis between inhibition of IGF-1R and DNAPK in DU145 prostate cancer cells. Permission was obtained from AstraZeneca to use AZ12253801 in combination with a small molecule inhibitor of DNAPK, NU7441. Initial assessment of this compound established that a concentration of 1μM NU7441 suppressed damage induced autophosphorylation of DNAPKcs at Ser2056, assessed by western blotting and focus formation (figure 5.10A and B), but did not inhibit the PI3K-like kinase ATM, as judged by inhibition of phosphorylation of KAP-1 and Chk2 (figure 5.10C). NU7441 at the higher concentrations of 3-10μM did partially suppress KAP-1 phosphorylation, and it was important to avoid such confounding effects in order to interpret results of DNAPK inhibition. A concentration of 1μM NU7441 was also the concentration used by other investigators (Shaheen et al 2011, Zhao et al 2006). Having established a concentration of NU7441 to test on DU145 cells, the next experiment assessed its effects in combination with AZ12253801. In these assays, 30nM AZ12253801 enhanced the radiosensitivity of DU145 cells (figure 5.11) with differences in survival (1.4 fold at 1Gy, 2 fold at 3Gy and 10Gy) that were comparable to the effect observed previously in DU145 cells treated with 30nM AZ12253801 (figure 4.8). Cells treated

with the DNAPK inhibitor alone were significantly more radiosensitive than controls, as expected, but aside from differences at 1Gy (27% vs 16%, $p<0.05$) there was no further enhancement of radiosensitization upon addition of AZ12253801 (figure 5.11). These differences suggest that IGF-1R may be on the same pathway as DNAPK with regards to effects on NHEJ, consistent with data in the M059J/K glioblastoma model (figure 5.9).

It thus seems possible that, in addition to the reported effects on HR, IGF-1R may influence DNA DSB repair via the NHEJ pathway. In addition to the results shown here using DNAPK deficient or inhibited cells, other data supporting this hypothesis include the early delay in DSB repair shown in figures 5.3 and 5.4, and the previous demonstration that IGF-1R depleted cells display a repair defect that is too large to be attributed to inhibition of HR alone (Turney et al 2012). Any effect of the IGF axis could be transcriptional, translational, or post-translational affecting levels or function of core DSB repair proteins. In view of the recently-recognised ability of IGF-1R to translocate to the nucleus (Aleksic et al 2010, Sehat et al 2010) and its potential role in transcriptional regulation, it was plausible that IGF-1R might also function as a transcription factor in regulating expression of proteins that accomplish or influence DNA repair. Hence, initial experiments to explore effects of IGF signalling on DSB repair examined levels of the core DSB repair proteins to investigate possible changes in expression following IGF-1R inhibition.

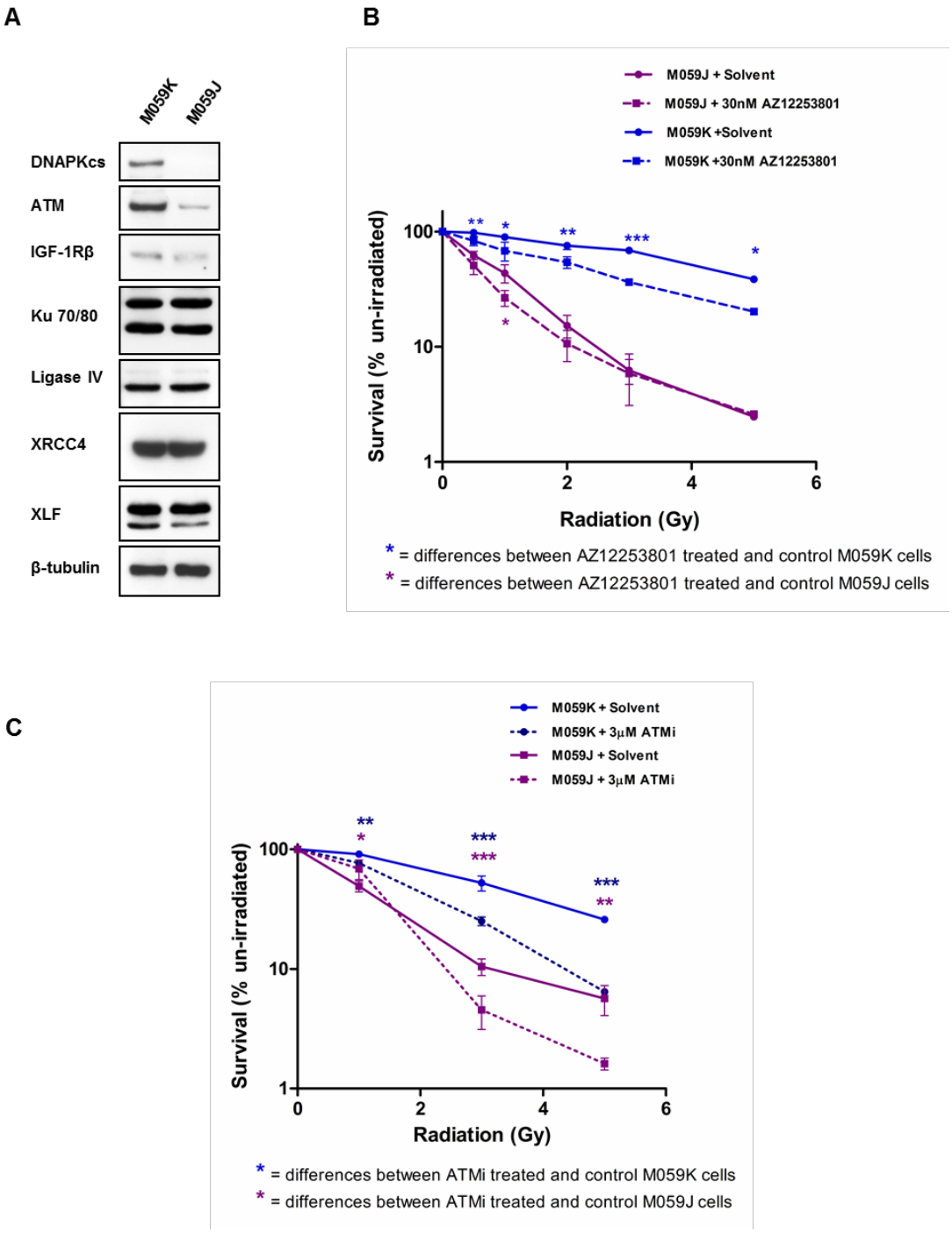

Figure 5.9: IGF-1R inhibition is epistatic with DNAPKcs deficiency in glioblastoma cells
A) M059J and K cells were grown to 80% confluence in 10cm dishes. Cells were lysed in SDS lysis buffer and lysates were subjected to western blot analysis to determine levels of ATM and core NHEJ proteins including DNAPKcs. B) M059J and K cells were seeded at 6000 cells/dish in 10cm dishes. Cells were treated with 30nM AZ12253801 for 4 hr, irradiated, and after 11-12 days, visible colonies were stained and counted. Colony survival was expressed as a percentage of survival in unirradiated controls. Points represent the mean ± SEM for triplicate values in three separate experiments. AZ12253801 enhanced radiosensitivity of M059K cells but not M059J cells (*p<0.05, **p<0.01, ***p<0.001). C) M059J and K cells were seeded at 6000 cells/dish in 10cm dishes, treated with 3μM ATMi for 4 hr, irradiated, and after 11-12 days, visible colonies were stained and counted. Colony survival was expressed as a percentage of survival in unirradiated controls. Points represent the mean ± SEM for triplicate values in three separate experiments. ATMi enhanced radiosensitivity of M059K and M059J cells (*p<0.05, **p<0.01, ***p<0.001).

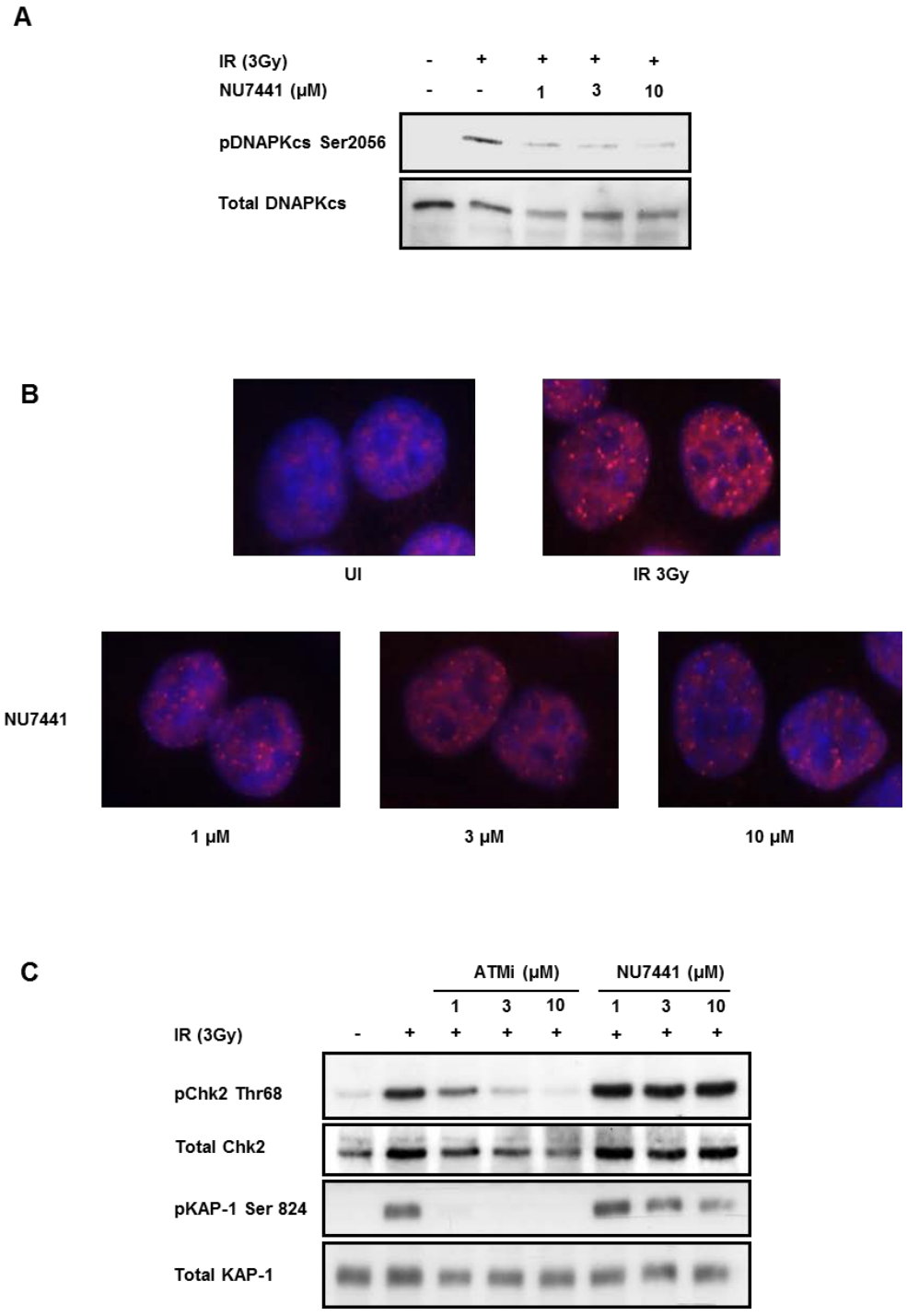

Figure 5.10: NU7441 inhibits DNAPK in DU145 prostate cancer cells
DU145 cells were grown in either 10cm dishes, or on coverslips in 6-well plates. Cells were treated with increasing concentrations of the DNAPK inhibitor NU7441 or ATMi for 4 hr, irradiated at 3Gy and A) lysed at 1 hr post irradiation in SDS lysis buffer and analysed by western blot for autophosphorylation of DNAPKcs at Ser 2056 with total DNAPKcs as a loading control; B) fixed at 1 hr post irradiation and stained for pDNAPKcs Ser2056. Images show typical irradiation induced foci, with merged pDNAPKcs (red) and DAPI (blue) staining in unirradiated cells (UI) and irradiated cells (IR) treated with 1, 3 and 10μM NU7441; C) lysed at 1 hr post irradiation in SDS lysis buffer, with western blot analysis for pChk2 and pKAP-1 with total protein levels as loading controls.

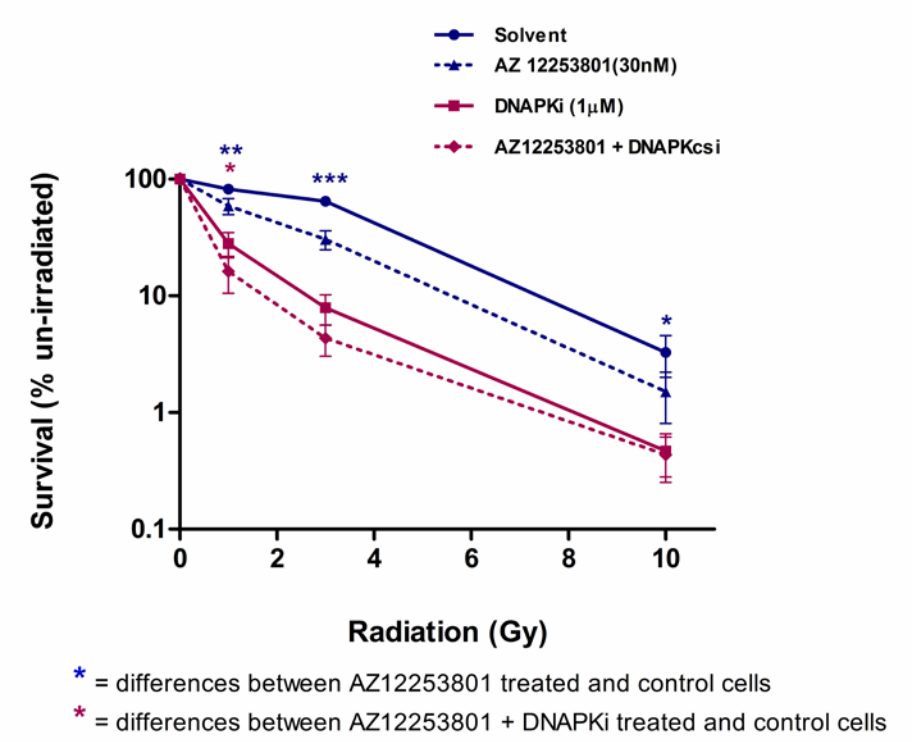

Figure 5.11: IGF-1R inhibition is epistatic with DNAPK inhibition in DU145 cells
DU145 cells were seeded at 3000 cells/25cm^2 flask. Cells were treated with solvent control, 30nM AZ12253801, 1μM NU7441 or a combination of AZ12253801 and NU7441 for 4 hr, irradiated, and after 11-12 days, visible colonies were stained and counted. Colony survival was expressed as a percentage of survival in un-irradiated controls. Points represent the mean ± SEM for triplicate values in three separate experiments. AZ12253801 enhanced radiosensitivity of DU145 cells (*$p<0.05$, **$p<0.01$, ***$p<0.001$). DU145 cells treated with NU7441 were further sensitized by AZ12253801 to 1Gy ($p<0.05$) but not to 3 or 10Gy.

5.2.4 Effect of IGF-1R inhibition on total levels of core DSB repair proteins

An effect of IGF-1R inhibition on the translation of core DSB repair proteins, particularly those involved in NHEJ, might explain the delay in repair observed in IGF-1R inhibited prostate cancer cells. Repair protein levels were initially investigated following treatment with increasing concentrations of AZ12253801. DU145 cells expressed damage sensors ATM, MRE11, Rad50 and NBS1, and core NHEJ and HR proteins (figure 5.12). There were no significant changes observed in any of these proteins following 48 hr of treatment with increasing concentrations of

AZ12253801 (figure 5.12). The assessment was repeated using cells pre-treated for 4 hr with AZ12253801, irradiated and collected 4 hr later for western blot analysis (figure 5.13). As before, there was no significant change in levels of proteins that sense or repair damage. BRCA1 was noted to undergo radiation-induced mobility shift due to phosphorylation, as previously reported (Foray et al 2002, Gatei et al 2001) , but this was not influenced by AZ12253801 (figure 5.13C).

Thus there was no change in the levels of any of the assessed proteins either basally or post-irradiation, in cells pre-treated with AZ12253801. However, it is possible that IGF-1R could regulate expression of other genes such as those that influence repair protein function, access to DNA or chromatin structure. Therefore, further experiments to explore effects of IGF-1R signalling on DSB repair used the approach of performing a microarray analysis, to investigate transcriptional changes following IGF-1R inhibition.

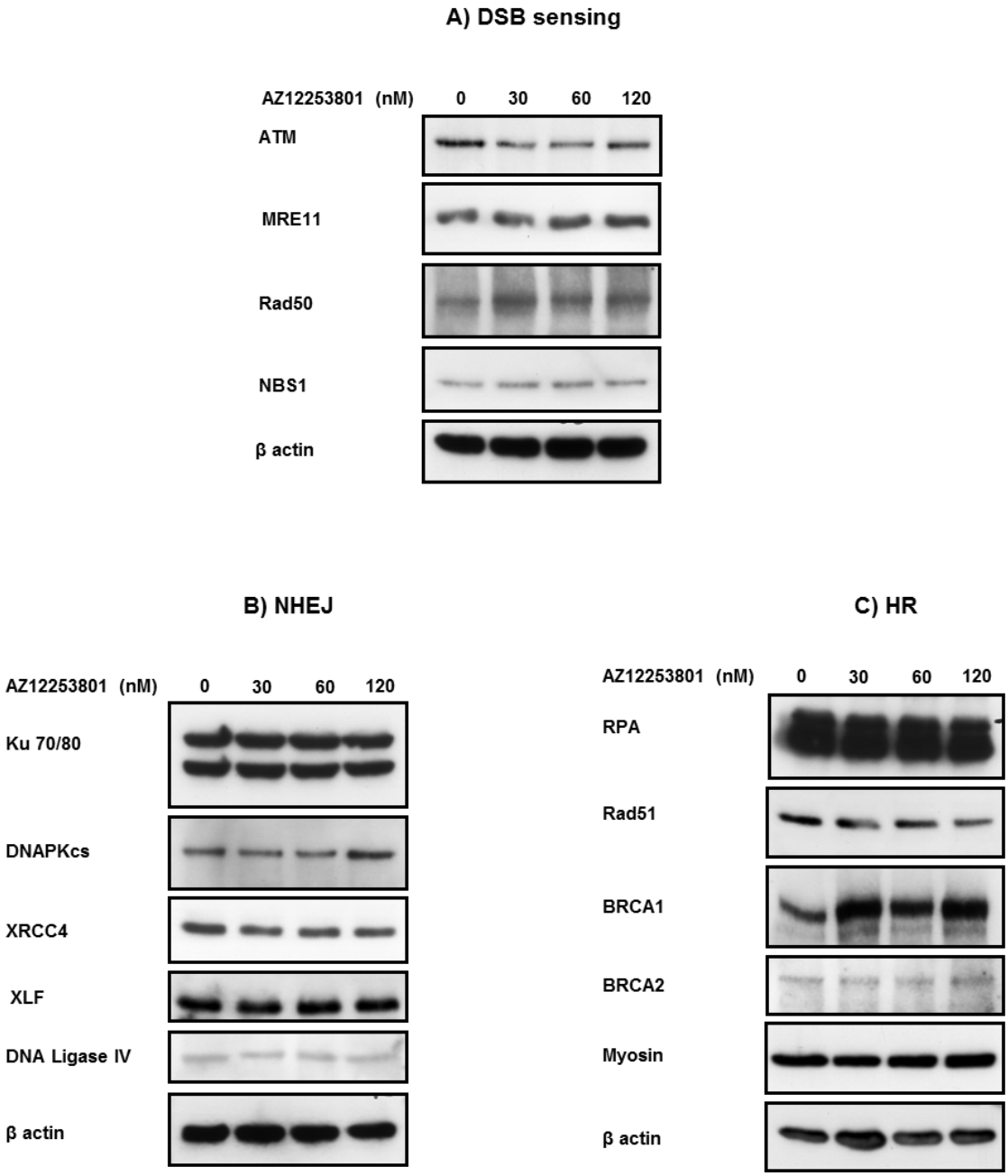

Figure 5.12:IGF-1R inhibition does not influence levels of core DSB repair proteins in undamaged DU145 cells

DU145 cells were treated with 30, 60 or 120nM AZ12253801. Cells were lysed in SDS lysis buffer 48 hr post treatment and western blot analysis was carried out for A) DSB sensing and repair initiation proteins, B) core NHEJ proteins, and C) core HR proteins. For these experiments myosin (200kDa) was used in addition to β actin as a loading control.

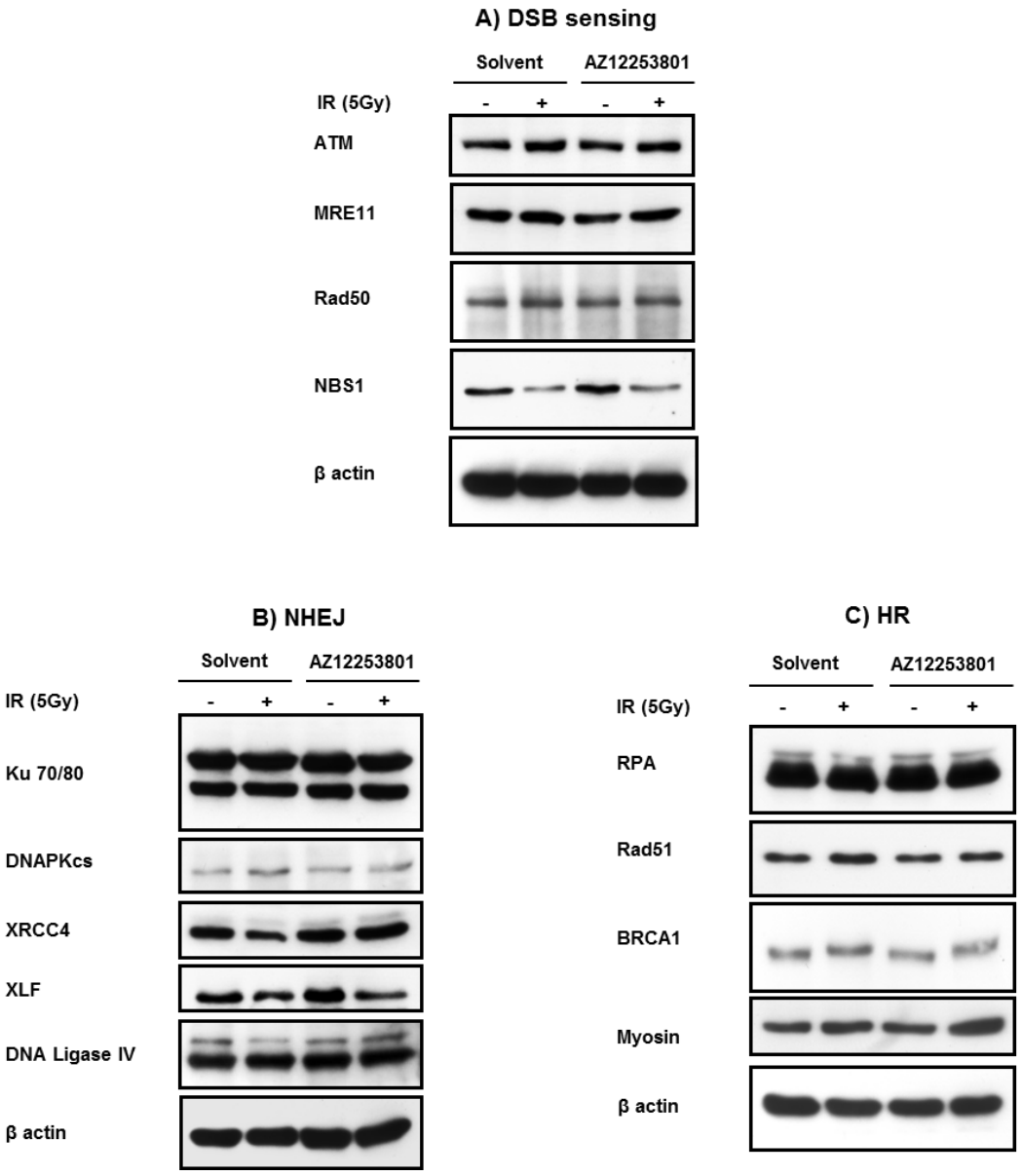

Figure 5.13: IGF-1R inhibition does not influence levels of core DSB repair proteins in irradiated DU145 cells

DU145 cells were treated with 60nM AZ12253801 for 4 hr, irradiated at 5Gy, and then lysed in SDS lysis buffer 4 hr post irradiation. Western blot analysis was carried out for A) DSB sensing and repair initiation proteins, B) core NHEJ proteins, and C) core HR proteins.

5.2.5 Effect of IGF-1R inhibition on the transcription of DNA repair targets at early time-points following DNA damage

The conditions for microarray analysis were carefully chosen in an attempt to obtain useful data on the transcriptional role, if any, of IGF-1R in DNA repair. RNAs were extracted from DU145 cells pre-treated for 4 hr with 60nM AZ12253801, followed by 5Gy irradiation, as these were conditions at which clear radiosensitization had been previously demonstrated (figure 4.8). An early time point of 4 hr post irradiation was chosen for the analysis, because at this early time point there was already a clear difference in γH_2AX resolution (figure 5.4A), and it is also a time-point by which primary changes in transcription could have become established, although could limit the detection of later secondary effects of IGF-1R inhibition. Figure 5.14A summarises the conditions chosen for the analysis, and for each condition, RNAs were extracted from triplicate independent cultures. RNAs were sent to the Cancer Research UK Microarray Facility for microarray analysis, and data analysis was carried out as in section 2.13, by Stephen Taylor, Head of Computational Biology Research Group, Weatherall Institute of Molecular Medicine.

Correlations between the 12 samples (4 conditions, 3 replicates) are visualised on the dendrogram (figure 5.14B), to provide an overall view of relationships between and within groups of replicate samples. It would be expected that the biological replicates would have similar expression profiles and hence correlation values, and so would cluster together closely within groups as sub-trees. Similarly, if expression profiles differ significantly between groups of replicates from different samples, then the sub-trees would be separate from each due to a lower correlation. From figure 5.14B, it was immediately evident that the solvent un-irradiated group (1-3) and AZ12253801 treated, un-irradiated group (4-6) were closely correlated, with no

distinct separation between them, suggesting that the expression profiles conferred by 60nM AZ12253801 did not vary significantly from controls. This was borne out in the results of the analysis, where no statistically significant hits were generated from the comparison between these groups. One sample (solvent irradiated 7) was found not to correlate closely with its biological replicates (8 and 9), and hence this outlier was excluded from the analysis. The separation between the solvent irradiated group (8-9) and AZ12253801 irradiated group (10-12) was more marked than the differences between un-irradiated groups, suggesting some differences in expression profile, but even then the difference was not dramatic. Thus, predictably, few hits were generated from the microarray comparison between solvent irradiated and AZ12253801 irradiated samples, and this might be not be entirely unexpected given that an early time-point of 4 hr had been chosen for the analysis.

Table 5.1 lists the genes showing the greatest change in expression. The magnitude of change in expression is indicated by the M-value (log-transformed ratio), which gives the fold change between conditions, typically calculated as log2 (treatment/control). Hence an M-value of 1 is equivalent to a 2-fold change and an M-value of 1.58 is equivalent to a 3-fold change. The direction of the change is indicated by plus (upregulation) or minus (downregulation). The significance of these changes is indicated by the B-value, the log-odds that a gene is differentially expressed between the conditions. A B-value >3 is equivalent to a >95% chance that the gene is differentially expressed. Two significant hits (table 5.1), with B-values >3.0, were observed in AZ12253801 irradiated compared with solvent irradiated cells, but no core DNA repair protein showed any significant change in expression.

A

Samples for microarray analysis		
Sample (nos.)	vs	**Comparator (nos.)**
AZ12253801 (4-6)	vs	Solvent (1-3)
AZ12253801 + irradiation (10-12)	vs	Solvent + irradiation (7-9)

B

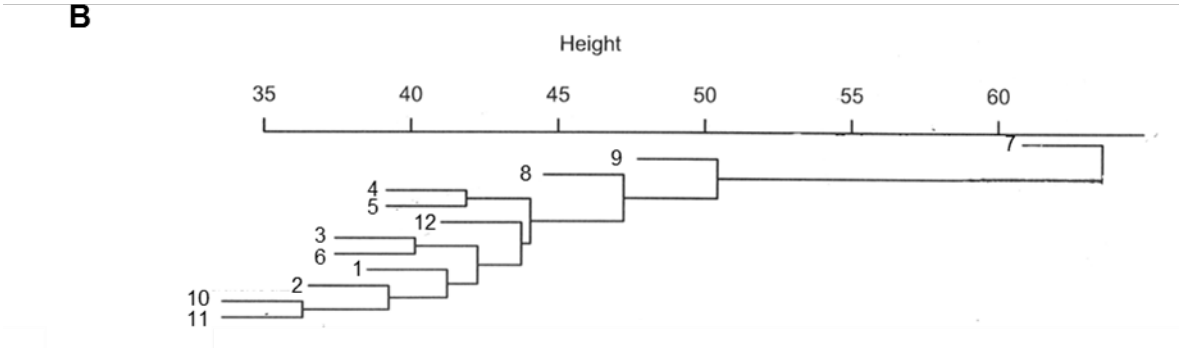

Figure 5.14: Dendrogram showing clustering of similar samples in the microarray analysis
A) Treatment conditions chosen for microarray analysis with corresponding sample numbers of the triplicate repeats. B) Correlations between the 4 biological sample groups in the microarray analysis, each with three biological replicates, were plotted on a dendrogram using correlation statistics (analysis by Stephen Taylor, Head of Computational Biology Research Group, Weatherall Institute of Molecular Medicine).

Affymetrix ID	Symbol	Name	M- value	B-value
7912537	DHRS3	short chain dehydrogenase/reductase member 3	-0.873	4.6
8108301	KIF20A	kinesin family member 20A	-0.432	3.1
7938834	NAV2	neuron navigator 2	-0.448	2.64
7963406	KRT6B	keratin 6B	+0.619	2.57

Table 5.1: Hits generated from the Affymetrix microarray analysis
The table shows the top four hits generated from the microarray analysis for the comparison of AZ12253801 treated irradiated DU145 cells compared with solvent treated irradiated cells. The magnitude of change in expression is indicated by the M-value (log-transformed ratio), which gives the fold change between conditions, typically calculated as log2 (treatment/control). The direction of the change is indicated by plus (upregulation) or minus (downregulation). The significance of these changes is indicated by the B-value, the log-odds that a gene is differentially expressed between the conditions. A B-value >3 is equivalent to a >95% chance that the gene is differentially expressed. The top two hits were considered significant with B-values >3.0.

Short chain dehydrogenase/reductase member 3 (DHRS*3*) is a short chain dehydrogenase/reductase that has numerous functions including the oxidation/ reduction of retinoids and steroids, amongst other substrates. It is an endoplasmic reticulum protein (ER) that plays a part in lipid droplet biogenesis (Deisenroth et al 2011, Haeseleer et al 1998). The kinesin family member 20A (*KIF20A*) gene encoding mitotic kinesin-like protein 2 (Mklp2) is involved in cytokinesis at the end of mitosis, and in retrograde vesicular transport from the Golgi to the ER during interphase (Echard et al 1998, Hill et al 2000). Although the B-values for DHRS3 and KIF20A were significant, the actual fold-changes in expression levels for DHRS3 and KIF20A were small, both down-regulated following AZ12253801 treatment of irradiated cells by 1.8-fold and 1.3-fold respectively. Given that the microarray served as a guide to expression at a particular time-point (here 4 hr post irradiation), it was possible that fold-changes may differ when observed over a time-course following IGF-1R inhibition and irradiation. Furthermore, KIF20A has been reported to be a novel tumour-associated antigen, overexpressed in hepatocellular and pancreatic carcinomas (Gasnereau et al 2012, Imai et al 2011). Down regulation of KIF20A can attenuate the growth of pancreatic carcinoma cells (Taniuchi et al 2005), and hence it was an interesting target to follow-up in its own right. Neuron navigator 2 (NAV2) is involved in cytoskeletal reorganisation and hence proliferation and migration of neuronal as well as other cells (McNeill et al 2011, Schmidt et al 2009), and keratin 6B (KRT6B) encodes a structural keratin protein found in hair, skin and sebaceous glands (Smith et al 1998). None of these genes has any known effect on DNA repair.

Given the apparently significant changes in expression of DHRS3 and KIF20A, it was thus decided to validate these two genes by means of quantitative real-time PCR

(qPCR). DU145 cells were pre-treated for 4 hr with solvent or 60nm AZ12253801, irradiated (5Gy) and RNAs were extracted after 0, 1 hr, 4 hr and 24 hr. After synthesising cDNAs by reverse transcription (as per chapter 2 section 2.12 and 2.14), qPCRs were performed. A negative control reaction containing RNA but no reverse transcriptase was also set up to exclude contamination of the RNA samples with genomic DNA. Three housekeeping genes, TUBA 1c, GAPDH and HPRT 1 were amplified by qPCR utilising cDNAs from both control and IGF-1R inhibited samples at all time-points, and the least variable housekeeping gene amongst the three was determined by utilising Normfinder software (Chapter 2, section 2.15.3) (Andersen et al 2004). This was to ensure stability of housekeeping genes over all experimental conditions tested, which is particularly important when using a semi-quantitative method to determine fold-changes in target genes by means of comparison to known housekeeping genes (Andersen et al 2004). GAPDH was found to be the most stable of the three housekeeping genes tested (figure 5.15A). Primer specificity was determined by melting curve analysis, which should generate a single product peak, as was indeed found for KIF20A (figure 5.15C), DHRS3 (figure 5.15E) and GAPDH (figure 5.15B). This confirmed that only a single product was amplified, and excluded the presence of primer dimers, contaminating DNA and products from mis-annealed primers, which would be detected as separate peaks. Primer efficiency was compared between KIF20A, DHRS3 and GAPDH (figure 5.15D and F) to check whether amplification efficiencies were comparable to allow for semi-quantification. When Ct values were plotted against log RNA dilution, the slopes of the lines were found not to be significantly different (see figure 5.15D and F).

Having established conditions to check expression of the two top microarray hits, qPCRs were performed to amplify KIF20A, DHRS3 and GAPDH for all the

experimental conditions. Data were analysed using the $2^{-\Delta\Delta CT}$ method (Livak and Schmittgen 2001), and the results are shown in Table 5.2. There were very minor changes in expression of each gene over the 24 hr post treatment, with only small changes in levels of either DHRS3 or KIF20A between AZ12253801 treated and solvent treated cells, with or without irradiation, at any time-point. Furthermore, the small changes that were observed indicated upregulation by AZ12253801, whereas both genes appeared to be downregulated by microarray analysis (Table 5.1). A second set of RNAs were extracted from independent samples, and the qPCR analysis was repeated. This confirmed the initial negative results. This was not entirely unexpected, as the original fold-changes seen on the microarray analysis were small. At this point it was decided not to take the analysis any further.

Investigation of possible functional effects of IGF-1R inhibition on recruitment of repair protein(s) to chromatin was the focus of the next set of experiments.

A

Gene name	Stability value
TUBA	0.066
GAPDH	0.060
HPRT	0.175
Most stable	**GAP**

B

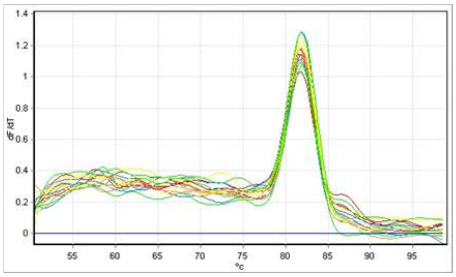

C

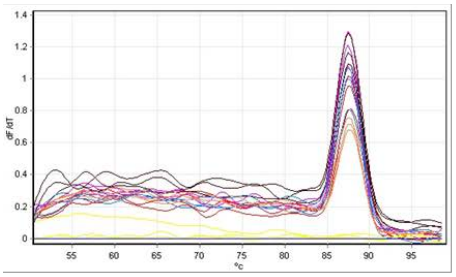

D

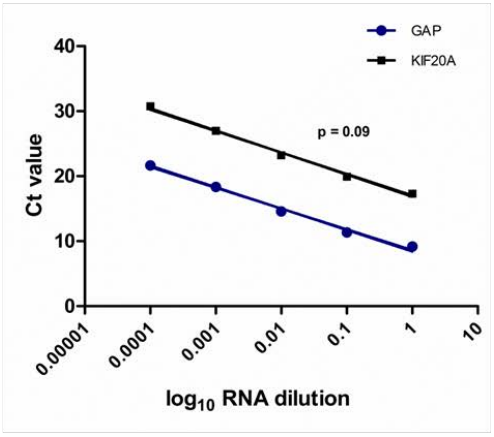

E

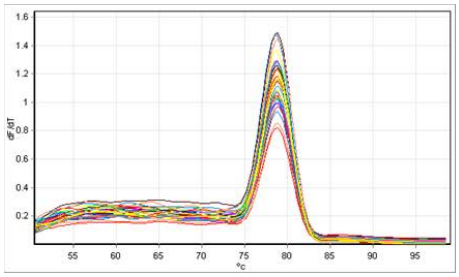

F

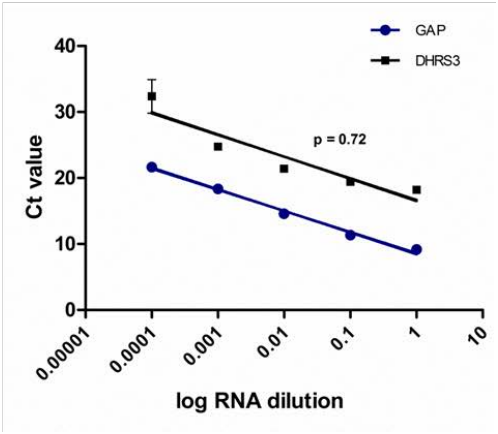

Figure 5.15: Optimisation of primers for qRT-PCR
A) The most stable HKG was selected from a panel of 3 commonly used HKGs: GAPDH, TUBA 1c and HPRT1, using Normfinder software (Andersen et al 2004). B) C) and E) Melting curve analysis for GAPDH, KIF20A and DHRS3 respectively. The rate of change of fluorescence in the reaction (dF/dT) is plotted against temperature. As the temperature is raised, a large change in fluorescence, seen as a peak, accompanies the separation or melting of the double stranded PCR product. This is the melting temperature (Tm). D) and F) PCR amplification efficiency was compared for both the HKG and the target gene of interest, by carrying out a PCR reaction with 10-fold serial dilutions of the template cDNA covering a range from 50 to 0.5ng. The C_T values were plotted against the $\log_{10}$ RNA dilution; slopes of the resultant lines were compared by nonlinear regression analysis and a p-value for the difference was generated, p= 0.09 for KIF20A and p= 0.72 for DHRS3 indicating no difference between the slopes.

Sample	Ct average KIF20A	Ct average GAP	ΔCt (Ct KIF-Ct GAP)	ΔΔCt (ΔCt -ΔCt calibrator)	$2^{-\Delta\Delta Ct}$ (Expression of KIF c/w calibrator)	
					Run one	Run two
UI sol 1hr	19.42	11.09	8.33	0	1.00	1.00
UI AZ 1hr	18.89	10.83	8.06	-0.27	1.21	1.35
UI Sol 4hr	18.64	10.35	8.29	0	1.00	1.00
UI AZ 4hr	18.53	10.42	8.11	-0.18	1.13	1.11
UI Sol 24hr	20.3	11.46	8.84	0	1.00	1.00
UI AZ 24hr	19.19	10.74	8.45	-0.39	1.31	1.40
IRR sol 1hr	18.7	10.57	8.13	0	1.00	1.00
IRR AZ 1hr	18.84	10.87	7.97	-0.16	1.12	1.09
IRR sol 4hr	19.27	10.29	8.98	0	1.00	1.00
IRR AZ 4hr	19.53	10.86	8.67	-0.31	1.24	1.38
IRR sol 24hr	18.64	11.18	7.46	0	1.00	1.00
IRR AZ 24hr	18.24	11.06	7.18	-0.28	1.21	1.91

Sample	Ct average DHRS3	Ct average GAP	ΔCt (Ct DHRS3-Ct GAP)	ΔΔCt (ΔCt -ΔCt calibrator)	$2^{-\Delta\Delta Ct}$ (Expression of DHRS3 c/w calibrator)	
					Run one	Run two
UI sol 1hr	18.55	11.09	7.46	0	1.00	1.00
UI AZ 1hr	18.41	10.83	7.58	0.12	0.92	1.03
UI Sol 4hr	18.17	10.35	7.82	0	1.00	1.00
UI AZ 4hr	18.02	10.42	7.6	-0.22	1.16	0.89
UI Sol 24hr	18.19	11.46	6.73	0	1.00	1.00
UI AZ 24hr	17.81	10.74	7.07	0.34	0.79	1.05
IRR sol 1hr	18.85	10.57	8.28	0	1.00	1.00
IRR AZ 1hr	18.55	10.87	7.68	-0.6	1.52	1.08
IRR sol 4hr	18.91	10.29	8.62	0	1.00	1.00
IRR AZ 4hr	19.3	10.86	8.44	-0.18	1.13	1.39
IRR sol 24hr	18.33	11.18	7.15	0	1.00	1.00
IRR AZ 24hr	18.23	11.06	7.17	0.02	0.99	1.12

Table 5.2: IGF-1R inhibition does not alter the transcription of KIF20A and DHRS3 following irradiation

qRT-PCR was performed on triplicate samples of cDNAs from solvent treated irradiated and AZ12253801 (60nM) inhibited irradiated cells at time points of 0, 1, 4 and 24 hr after irradiation. Relative quantification was carried out using the $2^{-\Delta\Delta CT}$ method (Livak and Schmittgen 2001) to express a fold-difference in levels of the target cDNA in treated samples versus controls. Expression levels of GAPDH were used as a normalizer to account for differences in loading between samples. Solvent treated samples at each time-point were used as the calibrator against which fold-changes in expression levels of target at that time-point were measured. The last column (run 2) shows the fold-change results of the second set of independent samples which were analysed in a similar manner to run 1.

5.2.6 Investigation of the effects of IGF-1R inhibition on the recruitment of repair proteins to chromatin

Repair proteins are recruited to the site of a DSB in a highly regulated sequence, and the timely removal of repair proteins from the site of the DSB is as important in the completion of repair as initial recruitment (Postow 2011). Binding of repair proteins was studied by extracting chromatin from IGF-1R inhibited and irradiated cells as previously described (Chapter 2 section 2.8), and the enrichment of the chromatin fraction was determined by western blot analysis of the chromatin protein histone H3 and cytoplasmic β tubulin (figure 5.16A). This suggested that there was good enrichment of histone H3 in the chromatin fraction, with negligible contamination by cytoplasmic components. Subsequent use of this method on AZ12253801 treated cells showed no difference in levels of core NHEJ repair proteins, ATM, or Rad51 (figure 5.16B). The chromatin fraction was also immunoblotted for one of the subunits of RPA, RPA32, to test whether RPA showed enrichment on chromatin following DNA damage, which is seen after UV or ionising radiation (Rai et al 2006) (Andy Blackford personal communication). The absence of radiation induced RPA enrichment in this experiment might cast doubt as to the purity of the fractionation (Figure 5.16C). If so, subtle changes in recruitment of proteins to the chromatin might be masked. RPA is a heterotrimer composed of 70, 32 and 14kDa subunits, that can be either nucleosolic or chromatin bound (Treuner et al 1999). It is the chromatin associated RPA that contains the phosphorylated form of RPA32 (Oakley and Patrick 2010, Treuner et al 1999), and RPA 32 shows an increase in phosphorylation after DNA damage (Boubnov and Weaver 1995, Fried et al 1996, Liu and Weaver 1993). Indeed, in figure 5.16C, it can be seen that control cells show an RPA32 doublet when blotting for total RPA32, with a subtle increase 1 hr after

irradiation, and resolution of the doublet at 4 hr. In IGF-1R inhibited cells, this doublet is less evident, appearing faintly at 4 and 24 hr (figure 5.16C). .

In the absence of a clear mechanism for the effect of IGF-1R, but with evidence to implicate the involvement of NHEJ (figures 5.9 and 5.11), a functional assay for NHEJ was carried out in an attempt to quantify effects of IGF-1R inhibition.

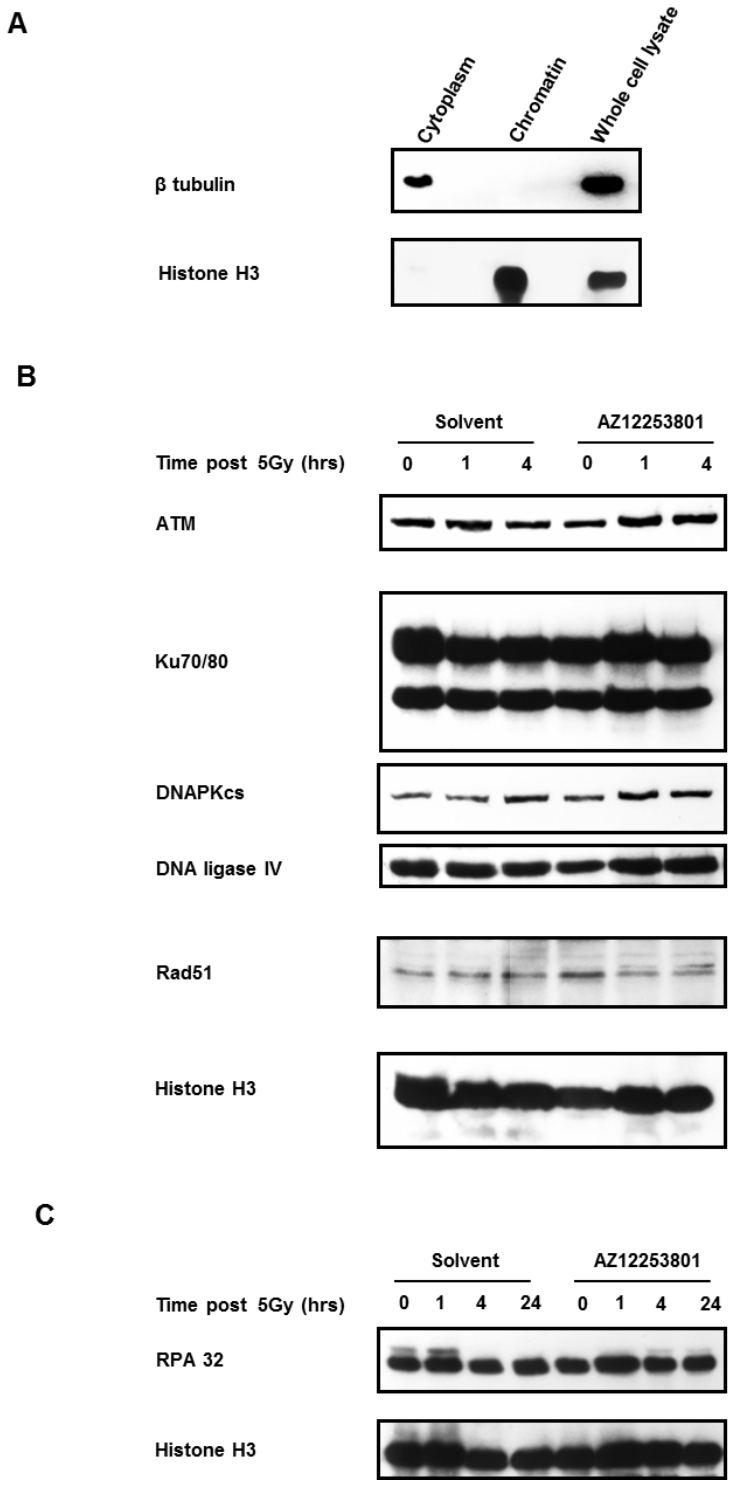

Figure 5.16: Assessing effects of IGF-1R inhibition on recruitment of repair proteins to chromatin in DU145 cells

DU145 cells were treated with solvent or 30nM AZ12253801 for 4 hr followed by irradiation. At time points of 1 - 24 hr post irradiation, chromatin was extracted and used for western blot analysis for A) β tubulin and histone H3 as markers of fractionation, B) core DSB repair proteins with histone H3 as a loading control, and C) RPA with histone H3 as a loading control. Results B and C are representative of two separate experiments.

5.2.7 IGF-1R inhibition inhibits NHEJ

The initial approach to assay for NHEJ in DU145 cells used a cell-based assay to measure re-joining of a transiently transfected, linearised reporter plasmid according to the method described by Bau *et al* (Bau et al 2004) (described in section 2.16.1). Optimisation of this assay was problematic at a number of levels. To prepare the repair substrate, the pGL2 luciferase reporter plasmid was digested with BamHI or HindIII as described in section 2.16.1.3, and completion of digestion was checked by agarose gel electrophoresis (figure 5.17A and B). Linearised plasmid was gel extracted and purified, but yields following gel purification were low, and hence multiple plasmid digests had to be performed in order to obtain sufficient linearised plasmid to carry out the required experiments. Each batch of cut plasmid was tested by bacterial transformation, which is accomplished much more efficiently by uncut circular plasmid, than by linear DNA. Hence, any contaminating circular plasmid would significantly alter luminescence readings if present in linearised plasmid preparations. Despite using consistent procedures, completion of digestion was not always achieved based on the results of bacterial transformation between different batches of plasmid: the number of cfu/µg of DNA varied from 0-8.3 $x10^4$ in the linearised preparations. Because these assays were performed prior to the availability of small molecule IGF-1R and DNAPK inhibitors, siRNA transfection was used to knock down DNA ligase IV as a positive control for NHEJ inhibition, two days prior to plasmid transfection. However, this dual transfection with siRNA and plasmid increased overall cellular toxicity. To conserve linearised plasmid, the assay was originally carried out in a 24-well format, but because of the toxicity of transfection, there was then not enough protein to carry out western blotting to check for knockdown of target proteins. The assay was thus scaled up to a 6-well plate format.

DU145 cells proved refractory to transfection with linearised plasmid using Gene Juice transfection reagent used routinely in the laboratory at the time of these experiments. Optimisation of plasmid transfection into DU145 cells was undertaken with seven different reagents, each used according to manufacturer's recommended guidelines. Trans IT (Mirus bio, Madison, WI) appeared to mediate the most efficient transfection, based on luminescence readings following transfection with BamHI linearised plasmid (figure 5.17C), and this was used for subsequent experiments.

An initial NHEJ assay was performed, using cells transfected with control siRNA, IGF-1R siRNA, or Ligase IV siRNA as a positive control for NHEJ suppression. Two days after siRNA transfection, each culture was transfected with BamHI- or HindIII-linearised pGL2. Luminescence generated by re-joining of Hind III-cut reporter was corrected for total protein, expressed as a % of BamHI luminescence, also corrected for total protein (figure 5.18A), and then these data were expressed as a % of the reporter activity in control siRNA transfectants (figure 5.18B). Initial results suggested that IGF-1R knockdown resulted in a reduction in plasmid re-joining, and hence NHEJ, when compared to control transfected cells (figure 5.18C, Run 1). A similar result was obtained in run 4 (Figure 5.18C), suggesting that IGF-1R knockdown appeared to reduce NHEJ dependent rejoining of linearised luciferase plasmid by 44-53%. However, probably due to the factors outlined above, inter-assay results were very inconsistent, and luminescence values for control samples varied widely between assays. The positive control for NHEJ suppression (ligase IV knockdown), which should have had the lowest luminescence values, showed similar results to the control transfected cells in two assays (figure 5.18C, runs 2 and 3), despite confirmation of ligase IV depletion in western blot (figure 5.18D). This casts doubt on both the adequacy of ligase IV knockdown and/or the purity of linearised

plasmid preparations. Therefore, the reliability of this assay was questioned, and hence an alternative, more reliable, NHEJ assay was sought.

With the availability of small molecule inhibitors of IGF-1R and DNAPK, AZ12253801 and NU7441 respectively, an alternative to siRNA knockdown was available, that potentially avoided the problems associated with toxicity from the siRNA transfection. A cell-based NHEJ assay was identified, based on HEK293 cells that carry a stably integrated reporter plasmid and tamoxifen-inducible I-Sce-I generated DNA DSBs, thus circumventing the need for plasmid purification and transfection (Bennardo et al 2008). Cell sorting was employed to measure GFP positivity in cells capable of using NHEJ to rejoin the reporter plasmid.

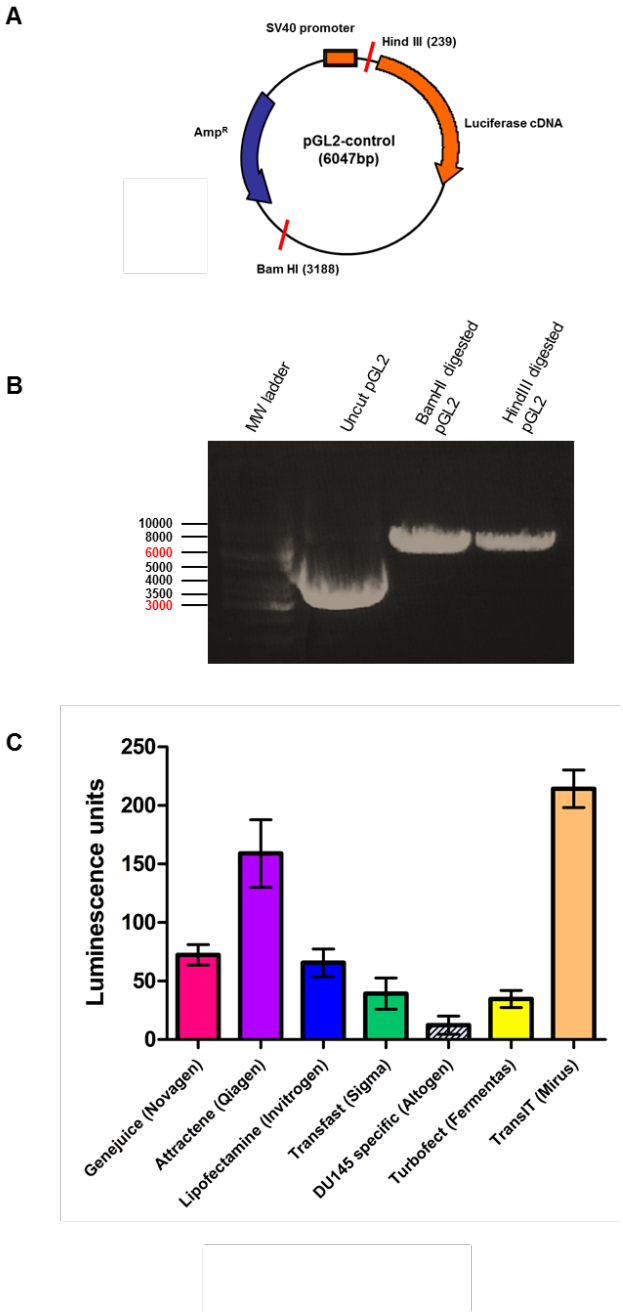

Figure 5.17: Optimisation of reagents for cell based assay, using transient transfection of linearised NHEJ reporter

A) pGL2 luciferase reporter plasmid. Linearization with Hind III between the luciferase promoter and coding sequence results in interruption of expression of luciferase, requiring rejoining by NHEJ to reconstitute reporter activity. Bam HI digestion results in linearization away from the luciferase reporter which remains intact, and this serves as a control for transfection efficiency of linearized plasmid. B) BamHI and HindIII digestion of pGL2 luciferase reporter was carried out over 6 hr. To confirm completion of digestion, 1µg of uncut and each of the linearised products was analysed by agarose gel electrophoresis. Expected product size was 6047bp, with the circular supercoiled plasmid having greater electrophoretic mobility than the linearised plasmid, thus allowing differentiation. C) Optimisation of plasmid transfection in DU145 cells was carried out using 7 different reagents. Cells were seeded in 6-well plates, and 24 hr later were transfected with BamHI linearised plasmid using the indicated transfection reagents, as per manufacturers protocols. Luciferase assays were performed 24 hr post transfection. The graph shows luminescence readings resulting from the different methods of transfection, from a single experiment with triplicate wells for each method.

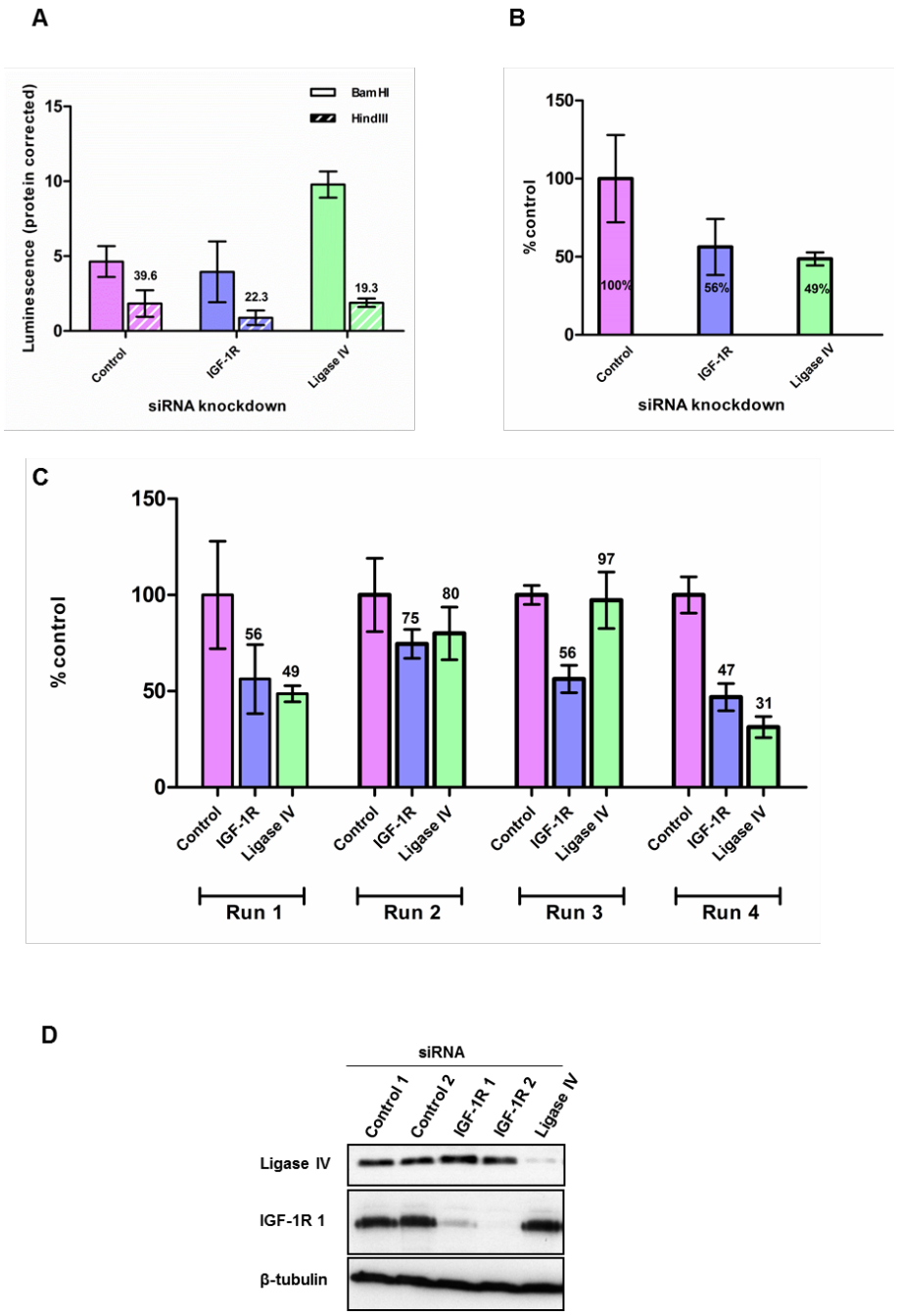

Figure 5.18: Inconsistent results obtained from NHEJ assay utilising transient transfection of linearised reporter in DU145 cells

DU145 cells were seeded in 6-well plates, and the following day were transfected with control, IGF-1R or Ligase IV siRNAs. After 48 hr, linearised plasmid transfection was carried out using BamHI or HindIII linearised pGL2. Luciferase assays were performed 24 hr post plasmid transfection. A) Luminescence readings expressed per µg of protein, in triplicate samples from Run 1. The numbers above the HindIII bar represent the HindIII luminescence value expressed as % of the BamHI value to control for transfection efficiency. B) The luminescence value of HindIII/BamHI obtained from knockdown of IGF-1R and Ligase IV in Run 1 are expressed as % of control transfected samples. C) The graph shows the results of four separate experiments. The HindIII/BamHI luminescence of triplicate repeats (run1) or 4 repeats (runs2-4) for each siRNA knockdown was expressed as % of the control transfected value for each individual experiment. The numbers above the individual bars reflect the actual % value. D) Western blot confirming siRNA knockdown of the target proteins. Similar results were obtained on analysis of cell lysates from one well per siRNA knockdown from each NHEJ assay. Repair assays shown in A-C utilised control siRNA 2 and IGF-1R siRNA 2.

5.2.7.1 IGF-1R inhibition results in a reduction of repair via NHEJ

The principles of this cell-based NHEJ assay are outlined in section 2.16.2 (Bennardo et al 2008). The assay is based on constitutive expression of the restriction endonuclease I-Sce-I flanked by a mutant form of the oestrogen receptor ligand binding domain (TAM), that allows I-Sce-I access to chromatin only in the presence of 4-hydroxytamoxifen (4OHT). HEK 293 cells were characterised for the presence of the IGF-1R and the ability of 30nM AZ12253801 to inhibit IGF-1R and Akt in these cells (figure 5.19). EJ5-GFP-TST-HEK293 cells were seeded in triplicate for treatment with AZ12253801, DNAPK inhibitor NU7441 or solvent control. Cells were treated with 4OHT to induce I-Sce-I to create a DSB in the EJ5-GFP reporter plasmid, and rejoining was measured by GFP positivity. Cells were initially gated for live cell and singlet populations. Untreated cells served as a negative control, to gate out the background autofluorescence (figure 5.20A). Cells transiently transfected with pcDNA3-EGFP-C3 (obtained from Professor Ian Hickson, Weatherall Institute of Molecular Medicine, Oxford), encoding enhanced GFP, served as a control to ensure appropriate settings on the cell sorter for detection of GFP positivity (figure 5.20B). Solvent treated cells were used as a positive control for overall levels of NHEJ repair, as GFP positivity should be maximal in these cells where NHEJ is not compromised (figure 5.20C). As a control for NHEJ inhibition, NU7441 was used at a concentration of 1μM, shown previously to inhibit DNAPK, a core NHEJ protein, in DU145 cells (figure 5.10). Indeed, GFP positivity was reduced in NU7441 treated cells compared with controls (compare figures 5.20C and E). Parallel cultures were treated with 30nM AZ12253801 and GFP positivity in these cells was compared with the control and NU7441 inhibited cells, to assess effects on NHEJ activity (figure 5.20D). Overall levels of GFP positivity in 4OHT-treated control cells was quite low

at 0.1%. Given that 100,000 cells were collected, following exclusion of doublet cells, this represents ~ 100 cells. Previous reports using the EJ5-GFP reporter in mouse ES cells with transient transfection of I-SceI have demonstrated 0.2% -2.5% GFP positivity (Bennardo et al 2008, Bennardo and Stark 2010), consistent with data obtained here. Despite the relatively low levels of GFP positivity, the results were consistent between experiments, and figure 5.20F shows that there was a statistically significant reduction in DSB repair by NHEJ in AZ12253801 treated cells compared with control cells. As expected, there was a significant reduction in NHEJ in cells treated with the DNAPK inhibitor, and these results were not significantly different from the inhibitory effect of AZ12253801 (figure 5.20). These results are not dissimilar to the findings on the 1st and 4th runs of the transiently transfected reporter NHEJ assay (figure 5.18C). The small numbers of GFP positive cells, however, is a limitation of this assay, as it might make differences between treatments harder to detect. Nonetheless, the results of this NHEJ assay support the original hypothesis that IGF-1R inhibition induces a defect in DNA repair by the NHEJ pathway.

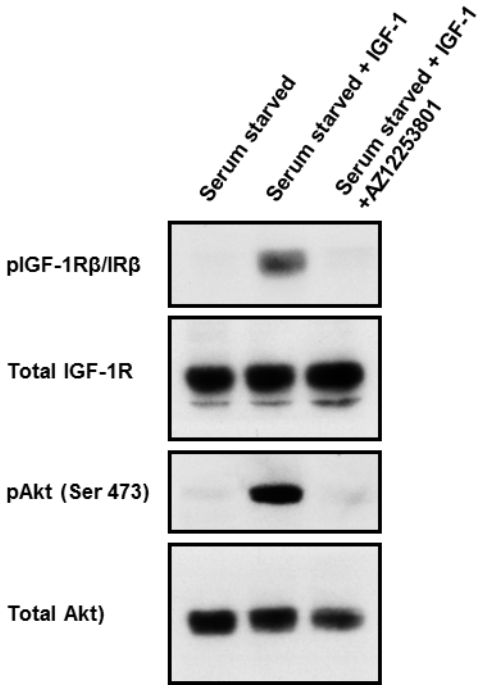

Figure 5.19: Characterisation of EJ5-GFP-TST-HEK 293 cells
HEK293 cells were serum starved overnight and the following day treated with 30nM AZ12253801 for 4 hr, with 50nM IGF-1 stimulation for the last 15 minutes prior to lysis. Lysates were analysed by Western blotting for pIGF-1R, pAkt and total protein levels.

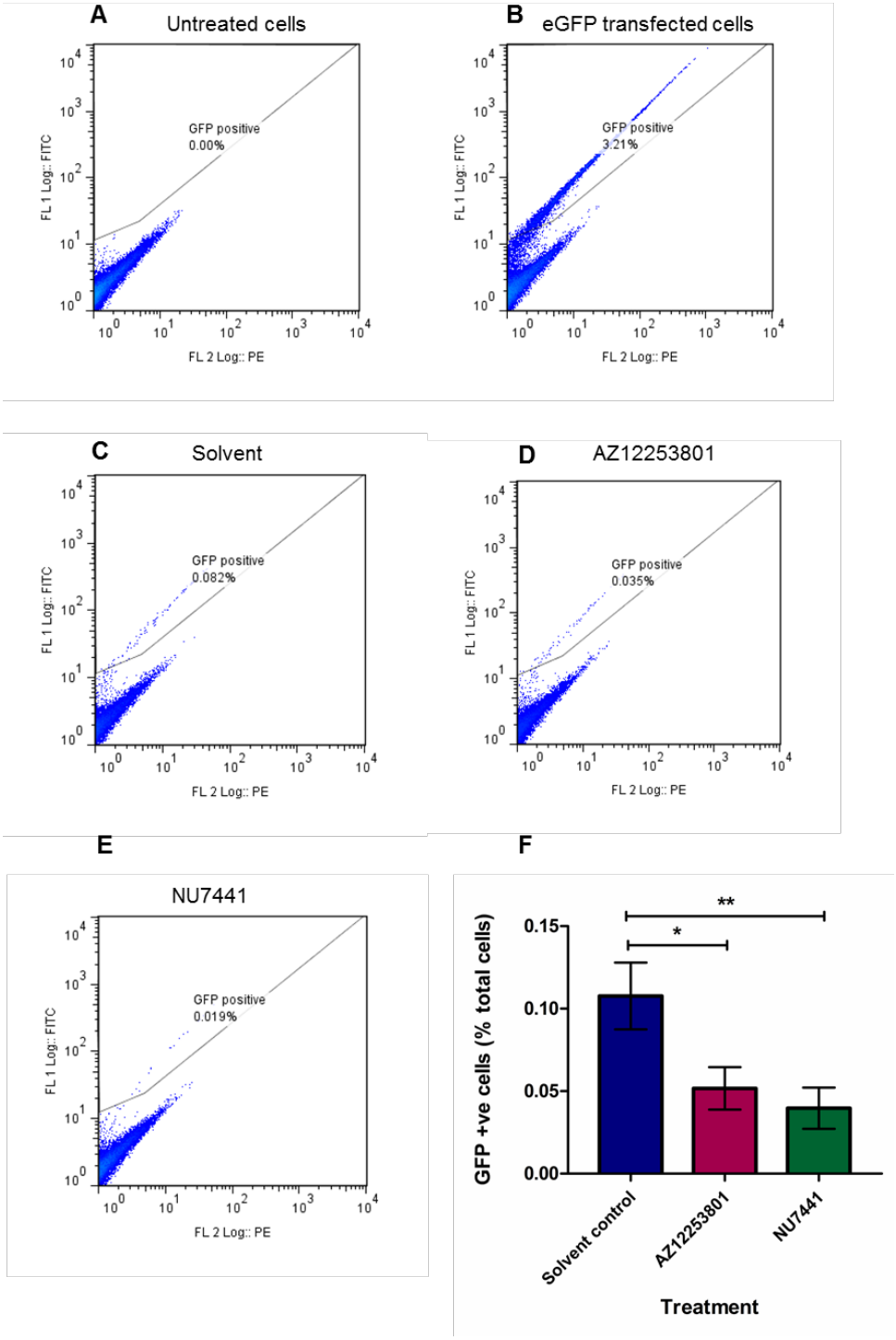

Figure 5.20: IGF-1R inhibition results in a defect in NHEJ in HEK 293 cells
EJ5-GFP-TST HEK 293 cells were seeded in triplicate in 35mm dishes. Cells were treated with solvent, 30nM AZ12253801 or 1µM NU7441, together with 3µM 4OHT. The 4OHT containing medium was removed after 24 hr and replaced with fresh medium containing the respective inhibitors or solvent control. Then, 72 hr after initial treatment with 4OHT, cells were harvested, fixed in 4% PFA, and analysed by cell sorting. A)-E) are representative analyses of A) untreated cells, B) eGFP transfected cells, C) solvent treated cells, D) AZ12253801 treated cells and E) NU7441 treated cells. F) Graph shows the mean ± SEM % GFP positivity in four separate NHEJ assays carried out in triplicate. (*$p<0.05$, **$p<0.01$)

5.3 Discussion

The initial experiments in this chapter, utilising γH2AX foci formation and resolution by immunofluorescence as a marker of DSB, demonstrated a delay in DSB repair evident as early as 1 hr post 3Gy irradiation, and peristing at 24 hrs. The dose of irradiation given determines the number of breaks generated, with each Gy introducing one DSB per 0.2 x 10^9 bp of DNA (de Almodovar 1994). In mammalian cells there are 6 x 10^9 and 12 x 10^9 bp in G1 and G2 of the cell cycle respectively (Rogakou et al 1999). Up to 60% of initial DNA DSBs are transient with rejoining times in minutes, and 40% of breaks are more persistent with rejoining times in the order of hours (Kodym and Horth 1995). Thus, for a dose of 3Gy, one would expect 90-180 DSBs of which 36-72 would be persistent breaks with rejoining half-times in the order of hours. However, there are limitations to the immunofluorescence technique in counting of foci, as increasing amounts of radiation result in larger numbers of foci, and overlap of foci is more likely to occur, compromising accurate counting (Rogakou et al 1999). Also, detection of foci is limited by the resolution capacity of the microscope. Nonetheless, the immunofluorescence results obtained were consistently reproducible between experiments, and the findings were similar to those obtained with γH2AX western blotting.

Previous experiments carried out in our laboratory had demonstrated impaired ATM kinase activity following IGF-1R depletion in murine melanoma cells (Macaulay et al 2001), and a direct binding interaction between the IGF-1R adaptor IRS-1 and ATM has been demonstrated in MCF7 cells, both in our lab (Akkaya and Macaulay unpublished) and by others (Jeon et al 2008). Both the IGF-1R and the EGFR translocate to the nucleus, and the EGFR has been shown to interact directly with DNAPKcs and NHEJ proteins Ku70A (Aleksic et al 2010, Bandyopadhyay et al

1998, Dittmann et al 2005a, Liccardi et al 2011). However, at the conclusion of this set of experiments, a direct interaction between IGF-1R, IRS-1 and ATM or DNAPKcs was not evident in DU145 prostate cancer cells. Despite demonstrating a mobility shift in IRS-1, consistent with its phosphorylation by activated IGF-1R, an IGF-1R:IRS-1 was not detected. This inability to detect IRS-1 in IGF-1R IPs and vice-versa suggests that this system may not have been optimized for detection of protein: protein interactions. Having said that, there are few examples in the literature of clearly documented interactions between endogenous IGF-1R and IRS-1; one of the few examples is the work of Hutcheson and colleagues, where transient IRS-1: IGF-1R Co-IP was reported within a few minutes of IGF-1 stimulation (Knowlden et al 2008).

Following IGF-1R inhibition, there was no evidence that IGF-1R inhibition influenced the function of ATM or its effectors in DU145 prostate cancer cells. This was in contrast to previously documented results in B16 murine melanoma cells (Macaulay et al 2001) and human MCF7 breast cancer cells (Jeon et al 2008) (Riedemann and Macaulay unpublished). It is notable that both B16 and MCF7 cells are p53 wild-type, while DU145 are p53 mutant **(**http://cancer.sanger.ac.uk). It is possible that B16 and MCF7 cells may thus be more likely to respond to suppression of IGF signaling with onset of apoptosis, and apoptosis is reported to induce cleavage of ATM and loss of its kinase activity (Smith et al 1999). Therefore, it is possible that this phenomenon, rather than any direct effect on ATM, could have been responsible for the apparent effects of IGF-1R depletion on ATM in B16 and MCF7 cells.

It was noted that, following IGF-1R inhibition, KAP-1 phosphorylation appeared marginally stronger at 4 hours and 24 hours when compared with control irradiated cells (figure 5.7). KAP-1 is known to be phosphorylated by ATM at Ser824 after

DSB induction, resulting in relaxation of chromatin structure. This allows repair proteins access to the DSB, facilitating repair of DSBs located in regions of heterochromatin (Goodarzi et al 2010, Ziv et al 2006). If IGF-1R depletion or inhibition is causing a delay in DSB repair by suppressing ATM function, one would expect a reduction in KAP-1 phosphorylation even at later time-points, which is not consistent with the observed effect. Hence it is possible that IGF-1R inhibition could have an ATM-independent effect on modifying chromatin structure, and that KAP-1 phosphorylation is simply acting as a marker of persisting DSBs within regions of heterochromatin. If time had permitted it would have been informative to assess effects of IGF-1R signalling on markers of heterochromatin, including the heterochromatin protein HP1 and histone H3K9 di- and tri-methylation, and also on proteins such as 53BP1, known to modulate KAP-1 function (Grewal and Jia 2007, Noon et al 2010). eterochromatin induction is known to occur as a consequence of cellular senescence, which can be regulated by IGF-1R signalling (Kuilman and Peeper 2009), but previous experiments indicated that IGF-1R inhibition does not induce senescence in DU145 cells (figure 4.14).

In a separate experiment, no effect of IGF-1R inhibition was observed on the chromatin modifying histone demethylase KDM5A, in contrast to results in resistant NSCLC cells (Sharma et al 2010). However, the reported IGF-regulated change in KDM5A expression in NSCLC had been seen only in erlotinib/cisplatin resistant cells, and not in parental cells, which may be one explanation for the lack of effect observed here (Sharma et al 2010). Alternatively, there may be a tumour type specific effect on KDM5A, observed in lung cancer cells but not in prostate cancer cells. If time had permitted, it might be informative to perform a more comprehensive screen of the effects of IGF-1R inhibition on histone modification.

A role for IGF signalling in DNA repair by HR was shown by Trojanek *et al* who reported an IGF-regulated interaction between IRS-1 and RAD51, influencing the ability of RAD51 to form damage-induced foci (Trojanek et al 2003). Previous work from our group showed that IGF-1R depletion in DU145 cells induced a significant repair defect (30-40% excess unrepaired DSBs at 24 hr), too large to be attributable in its entirety to the demonstrated modest reduction in repair by HR measured using a reporter assay (Ben Turney DPhil 2008). This led to the hypothesis that IGF-1R may also regulate repair via the NHEJ pathway, and this is supported by the findings of the current study. Firstly, a delay in DSB resolution seen as early as 1 hr after damage . Secondly, it was observed that inhibition of the IGF-1R was epistatic with both DNAPK inhibition in DU145 cells and DNAPKcs deficiency in glioblastoma cells, further supporting an effect of IGF-1R on the NHEJ pathway of DSB repair. Lastly, a cell-based reporter assay in HEK-293 cells confirmed the novel finding that IGF-1R inhibition suppressed DSB repair by NHEJ, helping to explain the radiosensitization seen with IGF-1R inhibition.

An attempt was made to investigate the contribution of IGF-1R inhibition to the HR pathway of DSB repair, utilising the matched HEK-293 cells that carry the HR reporter DR-GFP-TST (Bennardo et al 2008), described in Materials and Methods section 2.16.2. These cells were treated with 30nM AZ12253801 or solvent, together with 3μM 4OHT as in the NHEJ assay and according to the protocol described in (Bennardo et al 2008). Unfortunately, no GFP positive population was detected in this assay, although the cells continued to grow in puromycin and blasticidin selection medium, suggesting the presence of both the DR-GFP and TST plasmids. If time had permitted, further efforts would have been made to optimise this assay, using if

necessary the approach of transiently transfecting the I-SceI plasmid to induce DSBs in the reporter.

In the previous work documenting a modest effect of IGF-1R knockdown on HR, using an integrated HR reporter with transient I-Sce-I transfection (Turney et al 2012), it was unclear whether the observed reduction in HR was attributable, wholly or partly, to the increase in G1 and reduction in G2 populations induced by IGF-1R depletion. It would be informative to assess whether a similar defect is induced by IGF-1R inhibition. The use of a small molecule inhibitor, with careful dose titration, might allow determination of the extent to which the observed reduction in the HR was attributable to altered cell cycle distribution in the IGF-1R inhibited cells.

In contrast, cells are known to be capable of performing NHEJ throughout the cell cycle (Jackson and Bartek 2009). This, together with the finding that relatively low concentrations of AZ12253801 influenced repair but not cell cycle distribution (figure 4.15, 4.16 and 5.20) suggests that effects of IGF-1R inhibition on NHEJ are cell-cycle independent.

In order to elucidate the mechanism for the effect of IGF-1R on DSB repair via NHEJ, a transcriptional effect on DNA repair targets was assessed via microarray analysis. While cells are known to mount a transcriptional response to irradiation (Lu et al 2006, Rashi-Elkeles et al 2011), there was no evidence from this analysis of any differences in gene expression when comparing irradiated cells to un-irradiated cells, at least up-to 4 hr post-irradiation. One could speculate that the p53 mutant status of DU145 cells may have contributed to the lack of response, as p53 has been highlighted to be a central player in the transcriptional response to irradiation (Rashi-Elkeles et al 2011). Thus, this study produced no evidence that the effect of IGF-1R inhibition on the response to radiation in DU145 cells was mediated at a

transcriptional level. Indeed the detection of a repair defect at relatively early time-points after AZ12253801 treatment and irradiation (figures 5.3 and 5.4) would argue against a transcriptional effect.

The potential influence of IGF-1R on NHEJ may be complex, and could involve post-translational modifications to proteins in the repair pathway. Difference in the phosphorylation of chromatin-bound RPA between control and IGF-1R inhibited cells, thought to represent the doublet in figure 5.16C, could be one such example. This could be followed up by checking whether the upper band of the RPA doublet is abolished by phosphatase treatment, and immunoblotting with antibodies directed against specific RPA phospho-epitopes. RPA has a well recognised role in DNA repair pathways including HR, where it coats ssDNA to prevent secondary structure formation prior to RAD51 loading (Oakley and Patrick 2010). RPA was also reported to facilitate repair of DSBs by NHEJ in genomic but not plasmid DNA (Perrault et al 2001, Zhang et al 2009b). It is possible that IGF-1R influences the induction or resolution of other post-translational modifications on repair proteins, and this would fit with the relatively early onset of the delay in DSB resolution after IGF-1R inhibition (figure 5.4).

Thus the mechanism of the effect of IGF-1R inhibition on DNA DSB repair by NHEJ remains unknown.

6 Chapter VI: Conclusion and future directions

The main objective of this work was to gain a better understanding of the role of IGF-1R in urological cancer, focusing on firstly, the potential of IGF-1R as a prognostic biomarker, and secondly, the role of IGF-1R signalling in the DNA damage response. Two novel findings have resulted from this work, and may have implications for future clinical applications of anti-IGF-1R therapy.

Initial work investigated the expression and subcellular distribution of the IGF-1R in ccRCC. IGF-1R was detectable by IHC in the majority of ccRCCs, with expression at the RNA level found in a previous study from our group (Yuen et al 2007). Almost 50% of ccRCCs were found to have nuclear IGF-1R, and this was a novel finding at the time of publication. Of these tumours, approximately 50% had intense and extensive nuclear IGF-1R. Others have now reported the finding of nuclear IGF-1R (Asmane et al 2012, Bodzin et al 2012, Robertson et al 2012, Sarfstein et al 2012, Sehat et al 2010, Wu et al 2012). However, the data presented here represent the only association to date of nuclear IGF-1R with clinical data being correlated with a poor prognosis in terms of survival from ccRCC. These findings raise three important questions. Firstly, does nuclear IGF-1R have the potential to act as a prognostic biomarker and a predictive biomarker of response to anti-IGF-1R therapy? Ongoing work in our laboratory is investigating the association of nuclear IGF-1R with clinical factors in prostate and bladder tumours by IHC staining of tumour arrays and correlation with clinical data. This will determine whether the prognostic significance of nuclear IGF-1R is limited to ccRCC, or whether it is a prognostic biomarker in a wider range of urological cancers. Other tumour types are

also being investigated in a similar manner to assess the potential of nuclear IGF-1R as a prognostic biomarker.

The second question raised is the function of nuclear IGF-1R. Data from our group indicate that nuclear IGF-1R binds to chromatin and co-localises with RNA polymerase II (Aleksic et al 2010). Others have also shown IGF-1R binding to genomic DNA, suggesting a transcriptional role for nuclear IGF-1R, either alone or in association with other proteins as part of a complex (Sehat et al 2010). This is consistent with data from studies of other receptor tyrosine kinases such as the EGFR, HER-2 and fibroblast growth factor receptor-1 (FGFR-1), where transcriptional roles have already been identified (Liao and Carpenter 2007, Lin et al 2001, Stachowiak et al 2003, Wang et al 2004). In corneal epithelial cells, chromatin immunoprecipitation sequencing (ChIP-seq) has shown that nuclear IGF-1R is associated with genes involved in cell proliferation and cell cycle control, apoptosis and cell adhesion (Wu et al 2012). Similar ChIP-seq experiments are in progress in our group using prostate cancer cells. Nuclear IGF-1R has also been shown to regulate its own transcription (Sarfstein et al 2012). It is possible that IGF-1R performs multiple functions within the nucleus, both transcriptional and otherwise, and on-going investigations may reveal other functions of nuclear IGF-1R, as yet unidentified. This might lead to the discovery of novel targets for therapeutic development, or guide the choice of combination treatments to be used in conjunction with IGF-1R inhibitors.

The third question is the potential of nuclear IGF-1R to predict response to anti-IGF-1R therapy. Predictive biomarkers can identify groups of patients likely to respond to a treatment, thus allowing for more individualised treatments. Such biomarkers can be predominantly tumour specific, such as levels of HER-2 predicting response to Herceptin in breast cancer (Slamon et al 2001), or apply across a variety

of tumours, for example K-Ras mutations predicting resistance to EGFR therapy in NSCLC and colorectal carcinomas (Eberhard et al 2005, Khambata-Ford et al 2007). Subcellular localisation of receptors may play a part in predicting response to treatment. Nuclear EGFR has been linked to resistance to both EGFR antibody and small molecule inhibitors, and is being explored as a predictive biomarker (Huang et al 2011, Li et al 2009). The role of nuclear IGF-1R in this regard is far from clear. This current study has not directly addressed the role of nuclear IGF-1R as a predictive biomarker, but a recent report suggests that nuclear IGF-1R may predict response to IGF-1R targeted therapies. Asmane *et al* found that exclusively nuclear IGF-1R staining predicted a favourable response to IGF-1R monoclonal antibody therapy in patients with sarcomas (Asmane et al 2012). This study was done on a small number of tumours (n=16) of which only 4 tumours had exclusively nuclear staining. The mechanism by which an antibody can elicit a response in the absence of binding to membrane receptor is not clear, but if the association holds true on a larger analysis of sarcomas and /or other tumour types, this would warrant further investigation. In contrast, Kim *et al* have shown that defective N-linked glycosylation of the IGF-1R results in cytosolic accumulation of the receptor, and resistance to the anti-IGF-1R monoclonal antibody figitumumab attributable to failure of the receptor to translocate to the cell membrane (Kim et al 2012). It was also suggested that the numbers of hybrid IGF-1R:IR receptors on the cell surface may predict response to figitumumab, as one mechanism of action of the antibody is the disruption of such receptor hybrids (Kim et al 2012). In order to examine further whether nuclear IGF-1R affects the response to IGF-1R inhibitors, experiments could be conducted to express unmodified IGF-1R or IGF-1R modified by addition of a nuclear export signal, and expressed in cells to compare responses to IGF-1R TKIs or antibodies

(Turner et al 2012). Conversely, IGF-1R with an nuclear localisation sequence may accumulate within the nucleus, and could again be compared to cells expressing wild-type IGF-1R with regards response to treatment (Fornerod et al 1997, Mutka et al 2009, Sakakibara et al 2011). Another approach to investigate associations between nuclear IGF-1R and treatment response would be the analysis of tissue samples from patients in clinical trials of IGF-1R inhibitors, quantifying nuclear IGF-1R in responders versus non-responders. As outlined in chapter I, a number of Phase III clinical trials of IGF-1R inhibitors have been halted due to futility, although it is evident that these agents have activity in a subset of patients (Basu et al 2011, Gualberto et al 2011, Karp et al 2009, Yee 2012). This highlights the importance of identifying robust predictive biomarkers of sensitivity to IGF-1R inhibitors.

The second and third chapters of this thesis explored a potential role for the IGF-1R in the response of prostate cancer cells to DNA damage. This followed previous work showing that IGF-1R depletion induced a significant delay in DSB repair, associated with a modest reduction in repair by HR (Ben Turney DPhil 2008). However, it was not clear to what extent the HR defect was a consequence of altered cell cycle distribution in IGF-1R depeleted cells, and furthermore, the DSB defect was too large to be attributed to HR alone (Ben Turney DPhil 2008). This work focused on a prostate cancer cell line, DU145, where the expected induction of G1 arrest on IGF-1R inhibition did not occur, probably because the cells harbour mutations in p53 and Rb proteins (Bookstein et al 1990, Giacinti and Giordano 2006, Lukas et al 1995). The aim was to differentiate any effect of IGF-1R inhibition on proliferation and cell cycle progression from primary effects on DNA repair. A concentration of IGF-1R TKI was identified that inhibited receptor phosphorylation and signalling without significant effects on apoptosis, cell cycle distribution or senescence, and this was

found to induce a delay in DSB repair, suggesting that this effect was independent of cell cycle distribution. A DNA DSB repair defect was demonstrated at early time points following damage, when the NHEJ repair pathway is likely to operate (Mao et al 2008). Epistasis was demonstrated with DNAPKcs in two independent cell models. For the first time, a cell-based assay directly quantifying IGF-1R inhibition on the process of NHEJ has shown an inhibitory effect. This finding helps to explain the radiosensitization demonstrated upon IGF-1R inhibition, and the chemo- and radiosensitization induced by IGF-1R depletion in previous work from our lab (Hellawell et al 2003, Rochester et al 2005, Yuen et al 2009). It may also explain the relatively large defect in DSB repair observed on PFGE following IGF-1R depletion, that was unlikely to be attributable to HR alone.

It did not prove possible to elucidate a mechanism for the effect of IGF-1R inhibition on the NHEJ pathway of DNA repair. Previous work had implicated IGF-1R in regulating the expression and function of the KU proteins (Cosaceanu et al 2007). The work presented here did not demonstrate an effect on KU70/80 expression, in keeping with the findings of others (Trojanek et al 2003), or any of the core proteins involved in NHEJ. Furthermore, microarray analysis of IGF-1R inhibited cells did not reveal any transcriptional targets involved in DNA repair, but due to financial considerations, the analysis was only carried out at one time-point, 4 hr. If it were possible, then later time-points could also have been investigated. Indeed, the finding of a repair defect within a few hours of IGF-1R inhibition argues against a transcriptional effect, and suggests a functional effect. Chromatin extraction experiments did not appear to show a difference in recruitment of core NHEJ proteins to chromatin following IGF-1R inhibition in damaged cells. It is possible that IGF-1R

could induce post-translational modifications of repair proteins, or indeed of chromatin, that could influence the recruitment and function of repair proteins.

It would have been invaluable to be able to carry out HR assays in the HEK293 cell system that was developed by Stark and colleagues in parallel with the NHEJ reporter (Bennardo et al 2008) This might have answered the question of whether IGF-1R signalling genuinely affects both NHEJ and HR, which might suggest an effect on a protein/complex common to both repair pathways, such as the MRN complex. The concentration of AZ12253801 used in these experiments (30nM) is unlikely to have blocked nuclear IGF-1R import (Macaulay unpublished) and hence inhibited any processes attributable to nuclear IGF-1R. Thus, at present, the mechanism of the effect of IGF-1R inhibition on NHEJ remains unknown. This could be investigated by performing a proteomic screen, using mass spectrometry to identify IGF-1R inhibitor-induced changes in the recruitment to chromatin or post-translational modification of repair proteins. In order to determine which signalling molecules mediate effects of IGF-1R on DSB repair, assays for γH2AX focus resolution (Chapter 5, figures 5.3 and 5.4) and NHEJ (Chapter 5, figure 5.20) could be repeated using cells in which specific signalling proteins are depleted or inhibited (for example as in Chapter 5, figure 5.6).

An effect of IGF-1R inhibition on DSB repair via NHEJ has implications for therapeutic combinations with chemo- and radio-therapy. This work has demonstrated radiosensitization with the use of a small molecule inhibitor of IGF-1R. Chemosensitization might also result from combining IGF-1R inhibitors with drugs that cause DNA DSBs directly, for example topoisomerase II inhibitors, or indirectly, such as gemcitabine. However, in view of the epistasis seen with DNAPK deficient

cells, and with DNAPK small molecule inhibition, combinations of IGF-1R inhibitors with inhibitors of NHEJ are unlikely to be of clinical benefit.

Scheduling of the IGF-1R inhibitor in combination regimes would also need to be considered, as the effects of IGF-1R on cell cycle progression and survival might impact on the sequence of administration of the IGF-1R inhibitor in relation to the chemotherapeutic agent (Khatri et al 2012, Zeng et al 2012). The short half-life of TKIs in comparison with therapeutic antibodies might make the task of scheduling much easier with TKIs in clinical trials (Yee 2012).

The NHEJ repair defect demonstrated in prostate cancer cells could be investigated in other urological cancers. In the clinical setting, radiotherapy is often used early in the course of treatment, either with curative intent or for locally advanced disease, with or without combination chemotherapy (chemoradiation). In the palliative setting, radiotherapy is often used to obtain disease control. In light of the role of the IGF-1R in DSB repair, *in vivo* studies of an IGF-1R inhibitor in combination with radiotherapy would be a logical step. However, an effect of IGF-1R inhibition on NHEJ might have implications for toxicity to normal tissues when combined with radiotherapy. A large proportion of normal, slowly cycling cells will be in G1, hence responsive to NHEJ, compared with tumour cells where a large proportion are in G2/S phase and hence responsive to NHEJ and HR (Bristow et al 2007). Thus, the clinical implications of targeting NHEJ and potentially lowering the therapeutic ratio have to be borne in mind. Non-invasive, whole body imaging of DNA damage utilising γH_2AX immunoconjugates is being developed, and would allow assessment of the impact of IGF-1R inhibitors on delaying DSB *in vivo* (Cornelissen et al 2011, Ivashkevich et al 2011).

In conclusion, nuclear IGF-1R has been shown to be associated with prognosis in ccRCC. Further studies should clarify its role as a prognostic biomarker in urological cancers. IGF-1R signalling inhibition delays DNA DSB repair via the NHEJ pathway, paving the way for further research into the mechanism of this effect, and the use of IGF-1R inhibitors in combination with DNA damaging agents.

7 Appendices

7.1 Relationship between Intensity and Extent of IGF-1R staining and clinical parameters

7.1.1 Clinical features of 195 cases of ccRCC showing correlation of intensity of IGF-1R IHC staining with clinical parameters.

A) nuclear, B) cytoplasmic and C) membrane staining by IHC

A: Intensity of nuclear IGF-1R

	0	**1**	**2**	**3**	**P-value**
Total patients	101	45	27	22	
Age:					
< 65	55	22	12	12	0.78
≥ 65	46	23	15	10	
Size:					
< 7.5	39	25	16	12	0.11
≥ 7.5	56	19	10	8	
Sex:					
Female	29	19	6	6	0.26
Male	72	26	21	16	
Grade:					
I	9	7	2	2	0.02
II	43	26	18	12	-ve
III	37	7	6	2	
IV	11	5	1	6	
Necrosis:					
No	40	14	10	12	0.27
Yes	36	4	6	9	
T:					
1	18	14	7	8	0.01
2	9	6	8	0	-ve
3	72	24	11	14	
4	2	1	1	0	

B: Intensity of cytoplasmic IGF-1R

	0	1	2	3	P-value
Total patients	57	50	51	37	
Age:					
< 65	27	26	29	19	0.81
≥ 65	30	24	22	18	
Size:					
< 7.5	26	21	27	18	0.79
≥ 7.5	29	25	22	17	
Sex:					
Female	12	13	18	17	0.06
Male	45	37	33	20	
Grade:					
I	8	5	2	5	0.23
II	31	20	29	19	
III	13	14	16	9	
IV	5	11	3	4	
Necrosis:					
No	17	19	22	18	0.20
Yes	19	15	8	13	
T:					
1	14	7	15	11	0.40
2	8	7	7	1	
3	34	35	28	24	
4	1	1	1	1	

C: Intensity of membrane IGF-1R

	0	1	2	3	P-value
Total patients	72	60	39	24	
Age:					
< 65	39	32	19	11	0.87
≥ 65	33	28	20	13	
Size:					
< 7.5	24	27	23	18	0.001
≥ 7.5	44	30	15	4	-ve
Sex:					
Female	21	16	17	6	0.27
Male	51	44	22	18	
Grade:					
I	5	8	4	3	0.94
II	36	28	21	14	
III	20	16	10	6	
IV	10	8	4	1	
Necrosis:					
No	28	18	15	15	0.47
Yes	19	15	15	6	
T:					
1	11	12	13	11	0.11
2	12	6	3	2	
3	47	40	23	11	
4	2	2	0	0	

7.1.2 Clinical features of 195 cases of ccRCC showing correlation of extent of IGF-1R IHC staining with clinical parameters.

D) nuclear, E) cytoplasmic and F) membrane staining by IHC

.

D: Extent of nuclear IGF-1R

	0	1	2	3	P-valu
Total patients	101	21	22	51	
Age:					
< 65	55	11	12	23	0.74
≥ 65	46	10	10	28	
Size:					
< 7.5	39	11	15	27	0.07
≥ 7.5	56	10	7	20	
Sex:					
Female	29	8	8	15	0.78
Male	72	13	14	36	
Grade:					
I	9	3	5	3	0.005
II	43	12	11	33	-ve
III	37	2	6	7	
IV	11	4	0	8	
Necrosis:					
No	40	5	14	17	0.27
Yes	36	4	4	11	
T:					
1	18	6	10	13	0.06
2	9	3	2	9	
3	72	11	9	29	
4	2	1	1	0	

E: Extent of cytoplasmic IGF-1R

	0	1	2	3	P-valu
Total patients	57	41	25	72	
Age:					
< 65	27	21	13	40	0.84
≥ 65	30	20	12	32	
Size:					
< 7.5	26	24	8	34	0.39
≥ 7.5	29	17	14	33	
Sex:					
Female	12	19	8	21	0.06
Male	45	22	17	51	
Grade:					
I	8	8	1	3	0.20
II	31	21	14	33	
III	13	8	8	23	
IV	5	4	2	12	
Necrosis:					
No	17	17	11	31	0.45
Yes	19	9	8	19	
T:					
1	14	11	3	19	0.87
2	8	5	3	7	
3	34	25	18	44	
4	1	0	1	2	

F: Extent of membranous IGF-1R

	0	1	2	3	P-valu
Total patients	75	40	23	57	
Age:					
< 65	40	21	9	31	0.64
≥ 65	35	19	14	26	
Size:					
< 7.5	26	19	10	37	0.003
≥ 7.5	45	20	12	16	-ve
Sex:					
Female	21	13	10	16	0.52
Male	54	27	13	41	
Grade:					
I	5	5	5	5	0.11
II	39	15	10	35	
III	20	12	8	12	
IV	10	8	0	5	
Necrosis:					
No	30	9	8	29	0.14
Yes	20	15	5	15	
T:					
1	13	8	6	20	0.34
2	12	4	1	6	
3	48	28	15	30	
4	2	0	1	1	

7.2 IGF-1R Lysis Buffer

Component	Stock	To make up 200mls
HEPES 50mM	0.5M	20mls
Sodium chloride 100mM	5M	4mls
EDTA 10mM	0.5M	4mls
Sodium pyrophosphate 4mM	0.1M	8mls
Sodium orthovanadate 2mM	0.2M	2mls
Sodium fluoride 10mM	0.1M	20mls
Triton X-100 1% w/v	10% solution	20mls
Water		122mls

pH to 7.5 with sodium hydroxide and store at 4°C.

Prior to use add:

1.5mM Pefabloc SC Plus (Roche diagnostics)

EDTA-free Protease Inhibitor Cocktail (Roche) one tablet per 25-50ml buffer

Phosphatase Inhibitor Cocktail 1 and 2 (Sigma), 20µl per ml of buffer

7.3 List of antibodies

Antibody	Company	Cat. No.	1° conc.	2° conc.
Akt	Cell Signaling	9272	1:1000	1:5000
Androgen receptor	Cell Signaling	3202	1:1000	1:5000
ATM (D2E2)	Cell Signaling	2873	1:1000	1:5000
beta Actin	abcam	ab8224	1:1000	1:10000
beta Tubulin	Sigma	T 4026	1:5000	1:10000
BRCA1	abcam	ab16780	1:1000	1:5000
BRCA2	calbiochem	CA1033	1:1000	1:2000
Chk2	Cell Signaling	2662	1:1000	1:5000
DNA-PK	Cell Signaling	4602	1:1000	1:5000
H2AX	Cell Signaling	2595	1:1000	1:5000
Histone H3	abcam	ab1791	1:1000	1:5000
Histone H3 dimethyl Lys4	Active Motif	39141	1:5000	1:15000
Histone H3 trimethyl Lys4	Active Motif	39159	1:5000	1:15000
IGF-1Rβ	Cell Signaling	3027	1:1000	1:5000
IRS-1	Cell Signaling	2382	1:1000	1:5000
JARID1A/RBP2 (KDM5A)	Bethyl Lab. Inc.	A300-897A	1:1000	1:5000
KAP-1	Bethyl Lab. Inc.	A300-274A	1:5000	1:10000
Ku (p70) Ab-4 (clone N3H10)	Thermo Scientific	MS-329-P0	1:2000	1:5000
Ku (p80) Ab-2 (clone 111)	Thermo Scientific	MS-285-P0	1:1000	1:5000
Lamin A	abcam	ab8980	1:1000	1:5000
Ligase IV	AbD Serotec	discontinued	1:1000	1:5000
Mre11	Cell Signaling	4895	1:1000	1:5000
Myosin Iib	Cell Signaling	3404	1:2000	1:5000
NBS1	Cell Signaling	3002	1:1000	1:5000
p44/42 MAPK (Erk1/2)	Cell Signaling	4695	1:1000	1:5000
p53 (clone D01)	Thermo Scientific	MA1-2325	1:1000	1:5000
Phosph-KAP1 (Ser824)	Bethyl Lab. Inc.	A300-767A	1:5000	1:10000
Phospho-Akt (Ser473) (587F11)	Cell Signaling	4051	1:1000	1:5000
Phospho-Akt (Thr308)	Cell Signaling	9275	1:1000	1:5000
Phospho-ATM (ser1981)	Cell Signaling	4526	1:1000	1:5000
Phospho-Chk2 (Thr68)	Cell Signaling	2661	1:500	1:5000
Phospho-DNAPKcs (Ser2056)	abcam	ab18192	1:1000	1:5000
Phospho-Histone H2AX (Ser139)	Cell Signaling	2577	1:1000	1:2000
Phospho-IGF-1Rβ (Tyr1135/1136)/ Irβ (Tyr 1150/1151) (19H7)	Cell Signaling	3024	1:500	1:2000
Phospho-p4/42 MAPK (Thr202/Tyr204) (197G2)	Cell Signaling	4377	1:1000	1:5000
Phospho-p53 (ser15)	Cell Signaling	9284	1:1000	1:2000
Phospho-p53 (ser20)	Cell Signaling	9287	1:1000	1:2000
PTEN (26H9)	Cell Signaling	9556	1:1000	1:5000
RAD50 (13B3)	Thermo Scientific	MAI-23269	1:500	1:2000
RAD51 (14B4)	abcam	ab213	1:1000	1:2000
RPA32/RPA2	abcam	ab10359	1:2000	1:5000
XLF	Cell Signaling	2854	1:1000	1:5000
XRCC4	abcam	2857	1:1000	1:5000

8 Bibliography

Adams TE, Epa VC, Garrett TP, Ward CW (2000). Structure and function of the type 1 insulin-like growth factor receptor. *Cellular and molecular life sciences : CMLS* **57:** 1050-1093.

Aleksic T, Chitnis MM, Perestenko OV, Gao S, Thomas PH, Turner GD *et al* (2010). Type 1 insulin-like growth factor receptor translocates to the nucleus of human tumor cells. *Cancer Res* **70:** 6412-6419.

Allalunis-Turner MJ, Barron GM, Day RS, 3rd, Dobler KD, Mirzayans R (1993). Isolation of two cell lines from a human malignant glioma specimen differing in sensitivity to radiation and chemotherapeutic drugs. *Radiat Res* **134:** 349-354.

Allalunis-Turner MJ, Zia PK, Barron GM, Mirzayans R, Day RS, 3rd (1995). Radiation-induced DNA damage and repair in cells of a radiosensitive human malignant glioma cell line. *Radiat Res* **144:** 288-293.

Andersen CL, Jensen JL, Orntoft TF (2004). Normalization of real-time quantitative reverse transcription-PCR data: a model-based variance estimation approach to identify genes suited for normalization, applied to bladder and colon cancer data sets. *Cancer Res* **64:** 5245-5250.

Arnaldez FI, Helman LJ (2012). Targeting the insulin growth factor receptor 1. *Hematology/oncology clinics of North America* **26:** 527-542, vii-viii.

Arteaga CL, Kitten LJ, Coronado EB, Jacobs S, Kull FC, Jr., Allred DC *et al* (1989). Blockade of the type I somatomedin receptor inhibits growth of human breast cancer cells in athymic mice. *J Clin Invest* **84:** 1418-1423.

Asmane I, Watkin E, Alberti L, Duc A, Marec-Berard P, Ray-Coquard I *et al* (2012). Insulin-like growth factor type 1 receptor (IGF-1R) exclusive nuclear staining: a predictive biomarker for IGF-1R monoclonal antibody (Ab) therapy in sarcomas. *Eur J Cancer* **48:** 3027-3035.

Badzio A, Wynes MW, Dziadziuszko R, Merrick DT, Pardo M, Rzyman W *et al* (2010). Increased insulin-like growth factor 1 receptor protein expression and gene copy number in small cell lung cancer. *J Thorac Oncol* **5:** 1905-1911.

Bakkenist CJ, Kastan MB (2003). DNA damage activates ATM through intermolecular autophosphorylation and dimer dissociation. *Nature* **421:** 499-506.

Bandyopadhyay D, Mandal M, Adam L, Mendelsohn J, Kumar R (1998). Physical interaction between epidermal growth factor receptor and DNA-dependent protein kinase in mammalian cells. *J Biol Chem* **273:** 1568-1573.

Bao XH, Takaoka M, Hao HF, Wang ZG, Fukazawa T, Yamatsuji T *et al* (2012). Esophageal cancer exhibits resistance to a novel IGF-1R inhibitor NVP-AEW541 with maintained RAS-MAPK activity. *Anticancer research* **32:** 2827-2834.

Baserga R, Hongo A, Rubini M, Prisco M, Valentinis B (1997). The IGF-I receptor in cell growth, transformation and apoptosis. *Biochim Biophys Acta* **1332:** F105-126.

Baserga R (2005). The insulin-like growth factor-I receptor as a target for cancer therapy. *Expert Opin Ther Targets* **9:** 753-768.

Basu B, Olmos D, de Bono JS (2011). Targeting IGF-1R: throwing out the baby with the bathwater? *Br J Cancer* **104:** 1-3.

Bau DT, Fu YP, Chen ST, Cheng TC, Yu JC, Wu PE *et al* (2004). Breast cancer risk and the DNA double-strand break end-joining capacity of nonhomologous end-joining genes are affected by BRCA1. *Cancer Res* **64:** 5013-5019.

Belfiore A (2007). The role of insulin receptor isoforms and hybrid insulin/IGF-I receptors in human cancer. *Current pharmaceutical design* **13:** 671-686.

Belfiore A, Frasca F, Pandini G, Sciacca L, Vigneri R (2009). Insulin receptor isoforms and insulin receptor/insulin-like growth factor receptor hybrids in physiology and disease. *Endocr Rev* **30:** 586-623.

Bellmunt J, Theodore C, Demkov T, Komyakov B, Sengelov L, Daugaard G *et al* (2009). Phase III trial of vinflunine plus best supportive care compared with best supportive care alone after a platinum-containing regimen in patients with advanced transitional cell carcinoma of the urothelial tract. *J Clin Oncol* **27:** 4454-4461.

Bennardo N, Cheng A, Huang N, Stark JM (2008). Alternative-NHEJ is a mechanistically distinct pathway of mammalian chromosome break repair. *PLoS genetics* **4:** e1000110.

Bennardo N, Stark JM (2010). ATM limits incorrect end utilization during non-homologous end joining of multiple chromosome breaks. *PLoS genetics* **6:** e1001194.

Bensimon A, Aebersold R, Shiloh Y (2011). Beyond ATM: the protein kinase landscape of the DNA damage response. *FEBS Lett* **585:** 1625-1639.

Berthold DR, Pond GR, Soban F, de Wit R, Eisenberger M, Tannock IF (2008). Docetaxel plus prednisone or mitoxantrone plus prednisone for advanced prostate cancer: updated survival in the TAX 327 study. *J Clin Oncol* **26:** 242-245.

Beucher A, Birraux J, Tchouandong L, Barton O, Shibata A, Conrad S *et al* (2009). ATM and Artemis promote homologous recombination of radiation-induced DNA double-strand breaks in G2. *Embo J* **28:** 3413-3427.

Bhaskar PT, Hay N (2007). The two TORCs and Akt. *Developmental cell* **12:** 487-502.

Bid HK, Zhan J, Phelps DA, Kurmasheva RT, Houghton PJ (2012). Potent inhibition of angiogenesis by the IGF-1 receptor-targeting antibody SCH717454 is reversed by IGF-2. *Mol Cancer Ther* **11:** 649-659.

Biswas I, Maguin E, Ehrlich SD, Gruss A (1995). A 7-base-pair sequence protects DNA from exonucleolytic degradation in Lactococcus lactis. *Proc Natl Acad Sci U S A* **92:** 2244-2248.

Bodzin AS, Wei Z, Hurtt R, Gu T, Doria C (2012). Gefitinib resistance in HCC mahlavu cells: upregulation of CD133 expression, activation of IGF-1R signaling pathway, and enhancement of IGF-1R nuclear translocation. *Journal of cellular physiology* **227:** 2947-2952.

Bookstein R, Shew JY, Chen PL, Scully P, Lee WH (1990). Suppression of tumorigenicity of human prostate carcinoma cells by replacing a mutated RB gene. *Science* **247:** 712-715.

Bothmer A, Robbiani DF, Feldhahn N, Gazumyan A, Nussenzweig A, Nussenzweig MC (2010). 53BP1 regulates DNA resection and the choice between classical and alternative end joining during class switch recombination. *The Journal of experimental medicine* **207:** 855-865.

Boubnov NV, Weaver DT (1995). scid cells are deficient in Ku and replication protein A phosphorylation by the DNA-dependent protein kinase. *Mol Cell Biol* **15:** 5700-5706.

Bouwman P, Aly A, Escandell JM, Pieterse M, Bartkova J, van der Gulden H *et al* (2010). 53BP1 loss rescues BRCA1 deficiency and is associated with triple-negative and BRCA-mutated breast cancers. *Nature structural & molecular biology* **17:** 688-695.

Bradford MM (1976). A rapid and sensitive method for the quantitation of microgram quantities of protein utilizing the principle of protein-dye binding. *Analytical biochemistry* **72:** 248-254.

Branzei D, Foiani M (2008). Regulation of DNA repair throughout the cell cycle. *Nat Rev Mol Cell Biol* **9:** 297-308.

Bristow RG, Ozcelik H, Jalali F, Chan N, Vesprini D (2007). Homologous recombination and prostate cancer: a model for novel DNA repair targets and therapies. *Radiother Oncol* **83:** 220-230.

Brunet A, Bonni A, Zigmond MJ, Lin MZ, Juo P, Hu LS *et al* (1999). Akt promotes cell survival by phosphorylating and inhibiting a Forkhead transcription factor. *Cell* **96:** 857-868.

Buck E, Mulvihill M (2011). Small molecule inhibitors of the IGF-1R/IR axis for the treatment of cancer. *Expert opinion on investigational drugs* **20:** 605-621.

Buis J, Stoneham T, Spehalski E, Ferguson DO (2012). Mre11 regulates CtIP-dependent double-strand break repair by interaction with CDK2. *Nature structural & molecular biology* **19:** 246-252.

Bunting SF, Callen E, Wong N, Chen HT, Polato F, Gunn A *et al* (2010). 53BP1 inhibits homologous recombination in Brca1-deficient cells by blocking resection of DNA breaks. *Cell* **141:** 243-254.

Burma S, Chen BP, Chen DJ (2006). Role of non-homologous end joining (NHEJ) in maintaining genomic integrity. *DNA Repair (Amst)* **5:** 1042-1048.

Calsou P, Delteil C, Frit P, Drouet J, Salles B (2003). Coordinated assembly of Ku and p460 subunits of the DNA-dependent protein kinase on DNA ends is necessary for XRCC4-ligase IV recruitment. *Journal of molecular biology* **326:** 93-103.

Cancer-Genome-Atlas-Network (2012). Comprehensive molecular characterization of human colon and rectal cancer
Nature **487:** 330-337.

Carboni JM, Wittman M, Yang Z, Lee F, Greer A, Hurlburt W *et al* (2009). BMS-754807, a small molecule inhibitor of insulin-like growth factor-1R/IR. *Mol Cancer Ther* **8:** 3341-3349.

Cardone MH, Roy N, Stennicke HR, Salvesen GS, Franke TF, Stanbridge E *et al* (1998). Regulation of cell death protease caspase-9 by phosphorylation. *Science* **282:** 1318-1321.

Carpenter CL, Auger KR, Chanudhuri M, Yoakim M, Schaffhausen B, Shoelson S *et al* (1993). Phosphoinositide 3-kinase is activated by phosphopeptides that bind to the SH2 domains of the 85-kDa subunit. *J Biol Chem* **268:** 9478-9483.

Carracedo A, Ma L, Teruya-Feldstein J, Rojo F, Salmena L, Alimonti A *et al* (2008). Inhibition of mTORC1 leads to MAPK pathway activation through a PI3K-dependent feedback loop in human cancer. *J Clin Invest* **118:** 3065-3074.

Carracedo A, Pandolfi PP (2008). The PTEN-PI3K pathway: of feedbacks and cross-talks. *Oncogene* **27:** 5527-5541.

Carroll AG, Voeller HJ, Sugars L, Gelmann EP (1993). p53 oncogene mutations in three human prostate cancer cell lines. *Prostate* **23:** 123-134.

Cary RB, Peterson SR, Wang J, Bear DG, Bradbury EM, Chen DJ (1997). DNA looping by Ku and the DNA-dependent protein kinase. *Proc Natl Acad Sci U S A* **94:** 4267-4272.

Castellano E, Downward J (2011). RAS Interaction with PI3K: More Than Just Another Effector Pathway. *Genes & cancer* **2:** 261-274.

Chan D, Tyner JW, Chng WJ, Bi C, Okamoto R, Said J *et al* (2012). Effect of dasatinib against thyroid cancer cell lines in vitro and a xenograft model in vivo. *Oncology letters* **3:** 807-815.

Chan JM, Stampfer MJ, Giovannucci E, Gann PH, Ma J, Wilkinson P *et al* (1998). Plasma insulin-like growth factor-I and prostate cancer risk: a prospective study. *Science* **279:** 563-566.

Chang BD, Broude EV, Dokmanovic M, Zhu H, Ruth A, Xuan Y *et al* (1999a). A senescence-like phenotype distinguishes tumor cells that undergo terminal proliferation arrest after exposure to anticancer agents. *Cancer Res* **59:** 3761-3767.

Chang BD, Xuan Y, Broude EV, Zhu H, Schott B, Fang J *et al* (1999b). Role of p53 and p21waf1/cip1 in senescence-like terminal proliferation arrest induced in human tumor cells by chemotherapeutic drugs. *Oncogene* **18:** 4808-4818.

Chapman JR, Sossick AJ, Boulton SJ, Jackson SP (2012a). BRCA1-associated exclusion of 53BP1 from DNA damage sites underlies temporal control of DNA repair. *Journal of cell science* **125:** 3529-3534.

Chapman JR, Taylor MR, Boulton SJ (2012b). Playing the end game: DNA double-strand break repair pathway choice. *Mol Cell* **47:** 497-510.

Chapman JR, Barral P, Vannier JB, Borel V, Steger M, Tomas-Loba A *et al* (2013). RIF1 Is Essential for 53BP1-Dependent Nonhomologous End Joining and Suppression of DNA Double-Strand Break Resection. *Mol Cell*.

Chappell C, Hanakahi LA, Karimi-Busheri F, Weinfeld M, West SC (2002). Involvement of human polynucleotide kinase in double-strand break repair by non-homologous end joining. *Embo J* **21:** 2827-2832.

Chen BP, Uematsu N, Kobayashi J, Lerenthal Y, Krempler A, Yajima H *et al* (2007). Ataxia telangiectasia mutated (ATM) is essential for DNA-PKcs phosphorylations at the Thr-2609 cluster upon DNA double strand break. *J Biol Chem* **282:** 6582-6587.

Chen CR, Wang W, Rogoff HA, Li X, Mang W, Li CJ (2005a). Dual induction of apoptosis and senescence in cancer cells by Chk2 activation: checkpoint activation as a strategy against cancer. *Cancer Res* **65:** 6017-6021.

Chen J, Wu A, Sun H, Drakas R, Garofalo C, Cascio S *et al* (2005b). Functional significance of type 1 insulin-like growth factor-mediated nuclear translocation of the insulin receptor substrate-1 and beta-catenin. *J Biol Chem* **280:** 29912-29920.

Chen L, Nievera CJ, Lee AY, Wu X (2008a). Cell cycle-dependent complex formation of BRCA1.CtIP.MRN is important for DNA double-strand break repair. *J Biol Chem* **283:** 7713-7720.

Chen Z, Yang H, Pavletich NP (2008b). Mechanism of homologous recombination from the RecA-ssDNA/dsDNA structures. *Nature* **453:** 489-484.

Chitnis MM, Yuen JS, Protheroe AS, Pollak M, Macaulay VM (2008). The type 1 insulin-like growth factor receptor pathway. *Clin Cancer Res* **14:** 6364-6370.

Choueiri TK, Ross RW, Jacobus S, Vaishampayan U, Yu EY, Quinn DI *et al* (2012). Double-blind, randomized trial of docetaxel plus vandetanib versus docetaxel plus placebo in platinum-pretreated metastatic urothelial cancer. *J Clin Oncol* **30:** 507-512.

Cohen P, Graves HC, Peehl DM, Kamarei M, Giudice LC, Rosenfeld RG (1992). Prostate-specific antigen (PSA) is an insulin-like growth factor binding protein-3 protease found in seminal plasma. *The Journal of clinical endocrinology and metabolism* **75:** 1046-1053.

Cohick WS, Clemmons DR (1993). The insulin-like growth factors. *Annual review of physiology* **55:** 131-153.

Collado M, Serrano M (2010). Senescence in tumours: evidence from mice and humans. *Nat Rev Cancer* **10:** 51-57.

Cornelissen B, Kersemans V, Darbar S, Thompson J, Shah K, Sleeth K *et al* (2011). Imaging DNA damage in vivo using gammaH2AX-targeted immunoconjugates. *Cancer Res* **71:** 4539-4549.

Cosaceanu D, Budiu RA, Carapancea M, Castro J, Lewensohn R, Dricu A (2007). Ionizing radiation activates IGF-1R triggering a cytoprotective signaling by interfering with Ku-DNA binding and by modulating Ku86 expression via a p38 kinase-dependent mechanism. *Oncogene* **26:** 2423-2434.

Courtney KD, Corcoran RB, Engelman JA (2010). The PI3K pathway as drug target in human cancer. *J Clin Oncol* **28:** 1075-1083.

Croce CM (2008). Oncogenes and cancer. *N Engl J Med* **358:** 502-511.

Cui H (2007). Loss of imprinting of IGF2 as an epigenetic marker for the risk of human cancer. *Disease markers* **23:** 105-112.

Datta SR, Dudek H, Tao X, Masters S, Fu H, Gotoh Y *et al* (1997). Akt phosphorylation of BAD couples survival signals to the cell-intrinsic death machinery. *Cell* **91:** 231-241.

Davis BJ, Havener JM, Ramsden DA (2008). End-bridging is required for pol mu to efficiently promote repair of noncomplementary ends by nonhomologous end joining. *Nucleic Acids Res* **36:** 3085-3094.

de Bono JS, Oudard S, Ozguroglu M, Hansen S, Machiels JP, Kocak I *et al* (2010). Prednisone plus cabazitaxel or mitoxantrone for metastatic castration-resistant prostate cancer progressing after docetaxel treatment: a randomised open-label trial. *Lancet* **376:** 1147-1154.

de Bono JS, Logothetis CJ, Molina A, Fizazi K, North S, Chu L *et al* (2011). Abiraterone and increased survival in metastatic prostate cancer. *N Engl J Med* **364:** 1995-2005.

De Luca A, Maiello MR, D'Alessio A, Pergameno M, Normanno N (2012). The RAS/RAF/MEK/ERK and the PI3K/AKT signalling pathways: role in cancer pathogenesis and implications for therapeutic approaches. *Expert Opin Ther Targets* **16 Suppl 2:** S17-27.

De Meyts P, Wallach B, Christoffersen CT, Urso B, Gronskov K, Latus LJ *et al* (1994). The insulin-like growth factor-I receptor. Structure, ligand-binding mechanism and signal transduction. *Hormone research* **42:** 152-169.

Deisenroth C, Itahana Y, Tollini L, Jin A, Zhang Y (2011). p53-Inducible DHRS3 is an endoplasmic reticulum protein associated with lipid droplet accumulation. *J Biol Chem* **286:** 28343-28356.

Derijard B, Raingeaud J, Barrett T, Wu IH, Han J, Ulevitch RJ *et al* (1995). Independent human MAP-kinase signal transduction pathways defined by MEK and MKK isoforms. *Science* **267:** 682-685.

Dimmeler S, Fleming I, Fisslthaler B, Hermann C, Busse R, Zeiher AM (1999). Activation of nitric oxide synthase in endothelial cells by Akt-dependent phosphorylation. *Nature* **399:** 601-605.

Ding Q, Reddy YV, Wang W, Woods T, Douglas P, Ramsden DA *et al* (2003). Autophosphorylation of the catalytic subunit of the DNA-dependent protein kinase is required for efficient end processing during DNA double-strand break repair. *Mol Cell Biol* **23:** 5836-5848.

Dittmann K, Mayer C, Fehrenbacher B, Schaller M, Raju U, Milas L *et al* (2005a). Radiation-induced epidermal growth factor receptor nuclear import is linked to activation of DNA-dependent protein kinase. *J Biol Chem* **280:** 31182-31189.

Dittmann K, Mayer C, Rodemann HP (2005b). Inhibition of radiation-induced EGFR nuclear import by C225 (Cetuximab) suppresses DNA-PK activity. *Radiother Oncol* **76:** 157-161.

Dong Y, Watanabe H, Shibuya H, Miura M (2002). The phosphatidylinositol-3 kinase pathway is not essential for insulin-like growth factor I receptor-mediated clonogenic radioresistance. *Journal of radiation research* **43:** 325-329.

Donohoe CL, Doyle SL, McGarrigle S, Cathcart MC, Daly E, O'Grady A *et al* (2012). Role of the insulin-like growth factor 1 axis and visceral adiposity in oesophageal adenocarcinoma. *The British journal of surgery* **99:** 387-396.

Dreicer R (2012). The future of drug development in urothelial cancer. *J Clin Oncol* **30:** 473-475.

Dulic V, Kaufmann WK, Wilson SJ, Tlsty TD, Lees E, Harper JW *et al* (1994). p53-dependent inhibition of cyclin-dependent kinase activities in human fibroblasts during radiation-induced G1 arrest. *Cell* **76:** 1013-1023.

Dunn SE, Ehrlich M, Sharp NJ, Reiss K, Solomon G, Hawkins R *et al* (1998). A dominant negative mutant of the insulin-like growth factor-I receptor inhibits the adhesion, invasion, and metastasis of breast cancer. *Cancer Res* **58:** 3353-3361.

Dupont J, Holzenberger M (2003). IGF type 1 receptor: a cell cycle progression factor that regulates aging. *Cell Cycle* **2:** 270-272.

Eberhard DA, Johnson BE, Amler LC, Goddard AD, Heldens SL, Herbst RS *et al* (2005). Mutations in the epidermal growth factor receptor and in KRAS are predictive and prognostic indicators in patients with non-small-cell lung cancer treated with chemotherapy alone and in combination with erlotinib. *J Clin Oncol* **23:** 5900-5909.

Echard A, Jollivet F, Martinez O, Lacapere JJ, Rousselet A, Janoueix-Lerosey I *et al* (1998). Interaction of a Golgi-associated kinesin-like protein with Rab6. *Science* **279:** 580-585.

El Karoui M, Amundsen SK, Dabert P, Gruss A (1999). Gene replacement with linear DNA in electroporated wild-type Escherichia coli. *Nucleic Acids Res* **27:** 1296-1299.

Engelman JA, Luo J, Cantley LC (2006). The evolution of phosphatidylinositol 3-kinases as regulators of growth and metabolism. *Nature reviews Genetics* **7:** 606-619.

Escudier B, Eisen T, Stadler WM, Szczylik C, Oudard S, Staehler M *et al* (2009). Sorafenib for treatment of renal cell carcinoma: Final efficacy and safety results of the phase III treatment approaches in renal cancer global evaluation trial. *J Clin Oncol* **27:** 3312-3318.

Ewald JA, Desotelle JA, Wilding G, Jarrard DF (2010). Therapy-induced senescence in cancer. *J Natl Cancer Inst* **102:** 1536-1546.

Falck J, Coates J, Jackson SP (2005). Conserved modes of recruitment of ATM, ATR and DNA-PKcs to sites of DNA damage. *Nature* **434:** 605-611.

Festuccia C, Muzi P, Millimaggi D, Biordi L, Gravina GL, Speca S *et al* (2005). Molecular aspects of gefitinib antiproliferative and pro-apoptotic effects in PTEN-positive and PTEN-negative prostate cancer cell lines. *Endocr Relat Cancer* **12:** 983-998.

Fingar DC, Salama S, Tsou C, Harlow E, Blenis J (2002). Mammalian cell size is controlled by mTOR and its downstream targets S6K1 and 4EBP1/eIF4E. *Genes Dev* **16:** 1472-1487.

Flanigan SA, Pitts TM, Eckhardt SG, Tentler JJ, Tan AC, Thorburn A *et al* (2010). The insulin-like growth factor I receptor/insulin receptor tyrosine kinase inhibitor PQIP exhibits enhanced antitumor effects in combination with chemotherapy against colorectal cancer models. *Clin Cancer Res* **16:** 5436-5446.

Foray N, Marot D, Randrianarison V, Venezia ND, Picard D, Perricaudet M *et al* (2002). Constitutive association of BRCA1 and c-Abl and its ATM-dependent disruption after irradiation. *Mol Cell Biol* **22:** 4020-4032.

Fornerod M, Ohno M, Yoshida M, Mattaj IW (1997). CRM1 is an export receptor for leucine-rich nuclear export signals. *Cell* **90:** 1051-1060.

Frank I, Blute ML, Cheville JC, Lohse CM, Weaver AL, Zincke H (2002). An outcome prediction model for patients with clear cell renal cell carcinoma treated with radical nephrectomy based on tumor stage, size, grade and necrosis: the SSIGN score. *J Urol* **168:** 2395-2400.

Fraser M, Zhao H, Luoto KR, Lundin C, Coackley C, Chan N *et al* (2012). PTEN deletion in prostate cancer cells does not associate with loss of RAD51 function: implications for radiotherapy and chemotherapy. *Clin Cancer Res* **18:** 1015-1027.

Fried LM, Koumenis C, Peterson SR, Green SL, van Zijl P, Allalunis-Turner J *et al* (1996). The DNA damage response in DNA-dependent protein kinase-deficient SCID mouse cells: replication protein A hyperphosphorylation and p53 induction. *Proc Natl Acad Sci U S A* **93:** 13825-13830.

Fukuda R, Hirota K, Fan F, Jung YD, Ellis LM, Semenza GL (2002). Insulin-like growth factor 1 induces hypoxia-inducible factor 1-mediated vascular endothelial growth factor expression, which is dependent on MAP kinase and phosphatidylinositol 3-kinase signaling in colon cancer cells. *J Biol Chem* **277:** 38205-38211.

Galvan V, Logvinova A, Sperandio S, Ichijo H, Bredesen DE (2003). Type 1 insulin-like growth factor receptor (IGF-IR) signaling inhibits apoptosis signal-regulating kinase 1 (ASK1). *J Biol Chem* **278:** 13325-13332.

Gao J, Chesebrough JW, Cartlidge SA, Ricketts SA, Incognito L, Veldman-Jones M *et al* (2011). Dual IGF-I/II-neutralizing antibody MEDI-573 potently inhibits IGF signaling and tumor growth. *Cancer Res* **71:** 1029-1040.

Gasnereau I, Boissan M, Margall-Ducos G, Couchy G, Wendum D, Bourgain-Guglielmetti F *et al* (2012). KIF20A mRNA and its product MKlp2 are increased during hepatocyte proliferation and hepatocarcinogenesis. *The American journal of pathology* **180:** 131-140.

Gatei M, Zhou BB, Hobson K, Scott S, Young D, Khanna KK (2001). Ataxia telangiectasia mutated (ATM) kinase and ATM and Rad3 related kinase mediate phosphorylation of Brca1 at distinct and overlapping sites. In vivo assessment using phospho-specific antibodies. *J Biol Chem* **276:** 17276-17280.

Giacinti C, Giordano A (2006). RB and cell cycle progression. *Oncogene* **25:** 5220-5227.

Goodarzi AA, Noon AT, Deckbar D, Ziv Y, Shiloh Y, Lobrich M *et al* (2008). ATM signaling facilitates repair of DNA double-strand breaks associated with heterochromatin. *Mol Cell* **31:** 167-177.

Goodarzi AA, Jeggo P, Lobrich M (2010). The influence of heterochromatin on DNA double strand break repair: Getting the strong, silent type to relax. *DNA Repair (Amst)* **9:** 1273-1282.

Gordan JD, Simon MC (2007). Hypoxia-inducible factors: central regulators of the tumor phenotype. *Current opinion in genetics & development* **17:** 71-77.

Grewal SI, Jia S (2007). Heterochromatin revisited. *Nature reviews Genetics* **8:** 35-46.

Gu J, Lu H, Tippin B, Shimazaki N, Goodman MF, Lieber MR (2007). XRCC4:DNA ligase IV can ligate incompatible DNA ends and can ligate across gaps. *Embo J* **26:** 1010-1023.

Gualberto A, Dolled-Filhart M, Gustavson M, Christiansen J, Wang YF, Hixon ML *et al* (2010). Molecular analysis of non-small cell lung cancer identifies subsets with different sensitivity to insulin-like growth factor I receptor inhibition. *Clin Cancer Res* **16:** 4654-4665.

Gualberto A, Hixon ML, Karp DD, Li D, Green S, Dolled-Filhart M *et al* (2011). Pre-treatment levels of circulating free IGF-1 identify NSCLC patients who derive clinical benefit from figitumumab. *Br J Cancer* **104:** 68-74.

Haeseleer F, Huang J, Lebioda L, Saari JC, Palczewski K (1998). Molecular characterization of a novel short-chain dehydrogenase/reductase that reduces all-trans-retinal. *J Biol Chem* **273:** 21790-21799.

Hagerstrand D, Lindh MB, Pena C, Garcia-Echeverria C, Nister M, Hofmann F *et al* (2010). PI3K/PTEN/Akt pathway status affects the sensitivity of high-grade glioma cell cultures to the insulin-like growth factor-1 receptor inhibitor NVP-AEW541. *Neuro-oncology* **12:** 967-975.

Halazonetis TD, Gorgoulis VG, Bartek J (2008). An oncogene-induced DNA damage model for cancer development. *Science* **319:** 1352-1355.

Haluska P, Shaw HM, Batzel GN, Yin D, Molina JR, Molife LR *et al* (2007). Phase I dose escalation study of the anti insulin-like growth factor-I receptor monoclonal antibody CP-751,871 in patients with refractory solid tumors. *Clin Cancer Res* **13:** 5834-5840.

Haluska P, Huang J, Lam B, al. e (2011). MEDI-573 as a novel approach to IGF-1R and IR-A signaling inhibition by blocking IGF ligands: Phase I PK/PD, safety data, and disease linkage studies in breast cancer. *J Clin Oncol* **29:** Abstract 271.

Han KC, Kim SY, Yang EG (2012). Recent advances in designing substrate-competitive protein kinase inhibitors. *Current pharmaceutical design* **18:** 2875-2882.

Hankinson SE, Willett WC, Colditz GA, Hunter DJ, Michaud DS, Deroo B *et al* (1998). Circulating concentrations of insulin-like growth factor-I and risk of breast cancer. *Lancet* **351:** 1393-1396.

Haupt Y, Maya R, Kazaz A, Oren M (1997). Mdm2 promotes the rapid degradation of p53. *Nature* **387:** 296-299.

Hebert E (2006). Mannose-6-phosphate/insulin-like growth factor II receptor expression and tumor development. *Bioscience reports* **26:** 7-17.

Hellawell GO, Turner GD, Davies DR, Poulsom R, Brewster SF, Macaulay VM (2002). Expression of the type 1 insulin-like growth factor receptor is up-regulated in primary prostate cancer and commonly persists in metastatic disease. *Cancer Res* **62:** 2942-2950.

Hellawell GO, Ferguson DJ, Brewster SF, Macaulay VM (2003). Chemosensitization of human prostate cancer using antisense agents targeting the type 1 insulin-like growth factor receptor. *BJU Int* **91:** 271-277.

Heron-Milhavet L, Karas M, Goldsmith CM, Baum BJ, LeRoith D (2001). Insulin-like growth factor-I (IGF-I) receptor activation rescues UV-damaged cells through a p38 signaling pathway. Potential role of the IGF-I receptor in DNA repair. *J Biol Chem* **276:** 18185-18192.

Hickson I, Zhao Y, Richardson CJ, Green SJ, Martin NM, Orr AI *et al* (2004). Identification and characterization of a novel and specific inhibitor of the ataxia-telangiectasia mutated kinase ATM. *Cancer Res* **64:** 9152-9159.

Hill E, Clarke M, Barr FA (2000). The Rab6-binding kinesin, Rab6-KIFL, is required for cytokinesis. *Embo J* **19:** 5711-5719.

Hinz JM, Yamada NA, Salazar EP, Tebbs RS, Thompson LH (2005). Influence of double-strand-break repair pathways on radiosensitivity throughout the cell cycle in CHO cells. *DNA Repair (Amst)* **4:** 782-792.

Honda R, Tanaka H, Yasuda H (1997). Oncoprotein MDM2 is a ubiquitin ligase E3 for tumor suppressor p53. *FEBS Lett* **420:** 25-27.

Huang WC, Chen YJ, Li LY, Wei YL, Hsu SC, Tsai SL *et al* (2011). Nuclear translocation of epidermal growth factor receptor by Akt-dependent phosphorylation enhances breast cancer-resistant protein expression in gefitinib-resistant cells. *J Biol Chem* **286:** 20558-20568.

Huang X, Gao L, Wang S, McManaman JL, Thor AD, Yang X *et al* (2010). Heterotrimerization of the growth factor receptors erbB2, erbB3, and insulin-like growth factor-i receptor in breast cancer cells resistant to herceptin. *Cancer Res* **70:** 1204-1214.

Hudes G, Carducci M, Tomczak P, Dutcher J, Figlin R, Kapoor A *et al* (2007). Temsirolimus, interferon alfa, or both for advanced renal-cell carcinoma. *N Engl J Med* **356:** 2271-2281.

Hudis CA (2007). Trastuzumab--mechanism of action and use in clinical practice. *N Engl J Med* **357:** 39-51.

Ii M, Li H, Adachi Y, Yamamoto H, Ohashi H, Taniguchi H *et al* (2011). The efficacy of IGF-I receptor monoclonal antibody against human gastrointestinal carcinomas is independent of k-ras mutation status. *Clin Cancer Res* **17:** 5048-5059.

Imai K, Hirata S, Irie A, Senju S, Ikuta Y, Yokomine K *et al* (2011). Identification of HLA-A2-restricted CTL epitopes of a novel tumour-associated antigen, KIF20A, overexpressed in pancreatic cancer. *Br J Cancer* **104:** 300-307.

Ira G, Pellicioli A, Balijja A, Wang X, Fiorani S, Carotenuto W *et al* (2004). DNA end resection, homologous recombination and DNA damage checkpoint activation require CDK1. *Nature* **431:** 1011-1017.

Isebaert SF, Swinnen JV, McBride WH, Haustermans KM (2011). Insulin-like growth factor-type 1 receptor inhibitor NVP-AEW541 enhances radiosensitivity of PTEN wild-type but not PTEN-deficient human prostate cancer cells. *International journal of radiation oncology, biology, physics* **81:** 239-247.

Ito Y, Ito T, Karasawa S, Enomoto T, Nashimoto A, Hase Y *et al* (2012). Identification of DNA-Dependent Protein Kinase Catalytic Subunit (DNA-PKcs) as a Novel Target of Bisphenol A. *PloS one* **7:** e50481.

Ivashkevich A, Redon CE, Nakamura AJ, Martin RF, Martin OA (2011). Use of the gamma-H2AX assay to monitor DNA damage and repair in translational cancer research. *Cancer Lett*.

Iwasa T, Okamoto I, Suzuki M, Hatashita E, Yamada Y, Fukuoka M *et al* (2009). Inhibition of insulin-like growth factor 1 receptor by CP-751,871 radiosensitizes non-small cell lung cancer cells. *Clin Cancer Res* **15:** 5117-5125.

Jackson SP, Bartek J (2009). The DNA-damage response in human biology and disease. *Nature* **461:** 1071-1078.

Jassem J, Langer CJ, Karp DD, Mok T, Benner RJ, Green SJ *et al* (2010). Randomized, open label, phase III trial of figitumumab in combination with paclitaxel and carboplatin versus paclitaxel and carboplatin in patients with non-small cell lung cancer (NSCLC). *J Clin Oncol (Meet Abstr)* **28(Suppl 15):** 7500.

Jazayeri A, Falck J, Lukas C, Bartek J, Smith GC, Lukas J *et al* (2006). ATM- and cell cycle-dependent regulation of ATR in response to DNA double-strand breaks. *Nat Cell Biol* **8:** 37-45.

Jeggo PA, Geuting V, Lobrich M (2011). The role of homologous recombination in radiation-induced double-strand break repair. *Radiother Oncol* **101:** 7-12.

Jeon JH, Kim SK, Kim HJ, Chang J, Ahn CM, Chang YS (2008). Insulin-like growth factor-1 attenuates cisplatin-induced gammaH2AX formation and DNA double-strand breaks repair pathway in non-small cell lung cancer. *Cancer Lett* **272:** 232-241.

Johnson GL, Lapadat R (2002). Mitogen-activated protein kinase pathways mediated by ERK, JNK, and p38 protein kinases. *Science* **298:** 1911-1912.

Jones JI, Gockerman A, Busby WH, Jr., Camacho-Hubner C, Clemmons DR (1993a). Extracellular matrix contains insulin-like growth factor binding protein-5: potentiation of the effects of IGF-I. *J Cell Biol* **121:** 679-687.

Jones JI, Gockerman A, Busby WH, Jr., Wright G, Clemmons DR (1993b). Insulin-like growth factor binding protein 1 stimulates cell migration and binds to the alpha 5 beta 1 integrin by means of its Arg-Gly-Asp sequence. *Proc Natl Acad Sci U S A* **90:** 10553-10557.

Jones RA, Campbell CI, Gunther EJ, Chodosh LA, Petrik JJ, Khokha R *et al* (2007). Transgenic overexpression of IGF-IR disrupts mammary ductal morphogenesis and induces tumor formation. *Oncogene* **26:** 1636-1644.

Kaighn ME, Narayan KS, Ohnuki Y, Lechner JF, Jones LW (1979). Establishment and characterization of a human prostatic carcinoma cell line (PC-3). *Investigative urology* **17:** 16-23.

Kane LP, Shapiro VS, Stokoe D, Weiss A (1999). Induction of NF-kappaB by the Akt/PKB kinase. *Current biology : CB* **9:** 601-604.

Karasic TB, Hei TK, Ivanov VN (2010). Disruption of IGF-1R signaling increases TRAIL-induced apoptosis: a new potential therapy for the treatment of melanoma. *Experimental cell research* **316:** 1994-2007.

Karimi-Busheri F, Rasouli-Nia A, Allalunis-Turner J, Weinfeld M (2007). Human polynucleotide kinase participates in repair of DNA double-strand breaks by nonhomologous end joining but not homologous recombination. *Cancer Res* **67:** 6619-6625.

Karp DD, Paz-Ares LG, Novello S, Haluska P, Garland L, Cardenal F *et al* (2009). Phase II study of the anti-insulin-like growth factor type 1 receptor antibody CP-751,871 in combination with paclitaxel and carboplatin in previously untreated, locally advanced, or metastatic non-small-cell lung cancer. *J Clin Oncol* **27:** 2516-2522.

Kass EM, Jasin M (2010). Collaboration and competition between DNA double-strand break repair pathways. *FEBS Lett* **584:** 3703-3708.

Katz M, Amit I, Yarden Y (2007). Regulation of MAPKs by growth factors and receptor tyrosine kinases. *Biochim Biophys Acta* **1773:** 1161-1176.

Kaufman PA, Ferrero JM, Bourgeois H, Kennecke H, De Boer R, Jacot W *et al* (2010). A Randomized, Double-Blind, Placebo-Controlled, Phase 2 Study of AMG 479 With Exemestane (E) or Fulvestrant (F) in Postmenopausal Women With Hormone-Receptor Positive (HR+) Metastatic (M) or Locally Advanced (LA) Breast Cancer (BC) *Cancer Research* **70:** Abstract S1-4.

Kawada M, Yamagoe S, Murakami Y, Suzuki K, Mizuno S, Uehara Y (1997). Induction of p27Kip1 degradation and anchorage independence by Ras through the MAP kinase signaling pathway. *Oncogene* **15:** 629-637.

Kelly GM, Buckley DA, Kiely PA, Adams DR, O'Connor R (2012). Serine phosphorylation of the insulin-like growth factor I (IGF-1) receptor C-terminal tail restrains kinase activity and cell growth. *J Biol Chem* **287:** 28180-28194.

Khambata-Ford S, Garrett CR, Meropol NJ, Basik M, Harbison CT, Wu S *et al* (2007). Expression of epiregulin and amphiregulin and K-ras mutation status predict disease control in metastatic colorectal cancer patients treated with cetuximab. *J Clin Oncol* **25:** 3230-3237.

Khatri A, Brundage RC, Hull JM, Williams BW, Yee D, Kirstein MN (2012). Pharmacodynamic modeling of sequence-dependent antitumor activity of insulin-like growth factor blockade and gemcitabine. *The AAPS journal* **14:** 1-9.

Kim JG, Kang MJ, Yoon YK, Kim HP, Park J, Song SH *et al* (2012). Heterodimerization of glycosylated insulin-like growth factor-1 receptors and insulin receptors in cancer cells sensitive to anti-IGF1R antibody. *PloS one* **7:** e33322.

Kim JJ, Gonzalez-Roibon N, Chaux A, al. E (2013). Overexpression of IGF1R to predict outcome in invasive urothelial carcinoma or urinary bladder. *Journal of Clinical Oncology* **31:** Abstract 280.

Kindler HL, Richards DA, Garbo LE, Garon EB, Stephenson JJ, Jr., Rocha-Lima CM *et al* (2012). A randomized, placebo-controlled phase 2 study of ganitumab (AMG 479) or conatumumab (AMG 655) in combination with gemcitabine in patients with metastatic pancreatic cancer. *Ann Oncol*.

Kinner A, Wu W, Staudt C, Iliakis G (2008). Gamma-H2AX in recognition and signaling of DNA double-strand breaks in the context of chromatin. *Nucleic Acids Res* **36:** 5678-5694.

Kinsel LB, Szabo E, Greene GL, Konrath J, Leight GS, McCarty KS, Jr. (1989). Immunocytochemical analysis of estrogen receptors as a predictor of prognosis in breast cancer patients: comparison with quantitative biochemical methods. *Cancer Res* **49:** 1052-1056.

Klein HL, Symington LS (2009). Breaking up just got easier to do. *Cell* **138:** 20-22.

Klinakis A, Szabolcs M, Chen G, Xuan S, Hibshoosh H, Efstratiadis A (2009). Igf1r as a therapeutic target in a mouse model of basal-like breast cancer. *Proc Natl Acad Sci U S A* **106:** 2359-2364.

Knowlden JM, Jones HE, Barrow D, Gee JM, Nicholson RI, Hutcheson IR (2008). Insulin receptor substrate-1 involvement in epidermal growth factor receptor and insulin-like growth factor receptor signalling: implication for Gefitinib ('Iressa') response and resistance. *Breast cancer research and treatment* **111:** 79-91.

Kodym R, Horth E (1995). Determination of radiation-induced DNA strand breaks in individual cells by non-radioactive labelling of 3' OH ends. *Int J Radiat Biol* **68:** 133-139.

Kooijman R (2006). Regulation of apoptosis by insulin-like growth factor (IGF)-I. *Cytokine & growth factor reviews* **17:** 305-323.

Kuhne M, Riballo E, Rief N, Rothkamm K, Jeggo PA, Lobrich M (2004). A double-strand break repair defect in ATM-deficient cells contributes to radiosensitivity. *Cancer Res* **64:** 500-508.

Kuilman T, Peeper DS (2009). Senescence-messaging secretome: SMS-ing cellular stress. *Nat Rev Cancer* **9:** 81-94.

Kurmasheva RT, Houghton PJ (2006). IGF-I mediated survival pathways in normal and malignant cells. *Biochim Biophys Acta* **1766:** 1-22.

Kusumoto R, Dawut L, Marchetti C, Wan Lee J, Vindigni A, Ramsden D *et al* (2008). Werner protein cooperates with the XRCC4-DNA ligase IV complex in end-processing. *Biochemistry* **47:** 7548-7556.

Lacy MQ, Alsina M, Fonseca R, Paccagnella ML, Melvin CL, Yin D *et al* (2008). Phase I, pharmacokinetic and pharmacodynamic study of the anti-insulinlike growth factor type 1 Receptor monoclonal antibody CP-751,871 in patients with multiple myeloma. *J Clin Oncol* **26:** 3196-3203.

Lane BR, Kattan MW (2005). Predicting outcomes in renal cell carcinoma. *Current opinion in urology* **15:** 289-297.

Lang SA, Hackl C, Moser C, Fichtner-Feigl S, Koehl GE, Schlitt HJ *et al* (2010). Implication of RICTOR in the mTOR inhibitor-mediated induction of insulin-like growth factor-I receptor (IGF-IR) and human epidermal growth factor receptor-2 (Her2) expression in gastrointestinal cancer cells. *Biochim Biophys Acta* **1803:** 435-442.

Lavin MF (2007). ATM and the Mre11 complex combine to recognize and signal DNA double-strand breaks. *Oncogene* **26:** 7749-7758.

Lavoie JN, L'Allemain G, Brunet A, Muller R, Pouyssegur J (1996). Cyclin D1 expression is regulated positively by the p42/p44MAPK and negatively by the p38/HOGMAPK pathway. *J Biol Chem* **271:** 20608-20616.

Le Roith D (2003). The insulin-like growth factor system. *Experimental diabesity research* **4:** 205-212.

Lee JH, Paull TT (2007). Activation and regulation of ATM kinase activity in response to DNA double-strand breaks. *Oncogene* **26:** 7741-7748.

Lee JH, Goodarzi AA, Jeggo PA, Paull TT (2010). 53BP1 promotes ATM activity through direct interactions with the MRN complex. *Embo J* **29:** 574-585.

Lehmann BD, McCubrey JA, Jefferson HS, Paine MS, Chappell WH, Terrian DM (2007). A dominant role for p53-dependent cellular senescence in radiosensitization of human prostate cancer cells. *Cell Cycle* **6:** 595-605.

Levine AJ, Feng Z, Mak TW, You H, Jin S (2006). Coordination and communication between the p53 and IGF-1-AKT-TOR signal transduction pathways. *Genes Dev* **20:** 267-275.

Levitzki A, Mishani E (2006). Tyrphostins and other tyrosine kinase inhibitors. *Annual review of biochemistry* **75:** 93-109.

Lewis DA, Spandau DF (2008). UVB-induced activation of NF-kappaB is regulated by the IGF-1R and dependent on p38 MAPK. *The Journal of investigative dermatology* **128:** 1022-1029.

Li C, Iida M, Dunn EF, Ghia AJ, Wheeler DL (2009). Nuclear EGFR contributes to acquired resistance to cetuximab. *Oncogene* **28:** 3801-3813.

Li J, Yen C, Liaw D, Podsypanina K, Bose S, Wang SI *et al* (1997). PTEN, a putative protein tyrosine phosphatase gene mutated in human brain, breast, and prostate cancer. *Science* **275:** 1943-1947.

Liang J, Zubovitz J, Petrocelli T, Kotchetkov R, Connor MK, Han K *et al* (2002). PKB/Akt phosphorylates p27, impairs nuclear import of p27 and opposes p27-mediated G1 arrest. *Nature medicine* **8:** 1153-1160.

Liao HJ, Carpenter G (2007). Role of the Sec61 translocon in EGF receptor trafficking to the nucleus and gene expression. *Molecular biology of the cell* **18:** 1064-1072.

Liccardi G, Hartley JA, Hochhauser D (2011). EGFR nuclear translocation modulates DNA repair following cisplatin and ionizing radiation treatment. *Cancer Res* **71:** 1103-1114.

Lin SY, Makino K, Xia W, Matin A, Wen Y, Kwong KY *et al* (2001). Nuclear localization of EGF receptor and its potential new role as a transcription factor. *Nat Cell Biol* **3:** 802-808.

Litzenburger BC, Kim HJ, Kuiatse I, Carboni JM, Attar RM, Gottardis MM *et al* (2009). BMS-536924 reverses IGF-IR-induced transformation of mammary epithelial cells and causes growth inhibition and polarization of MCF7 cells. *Clin Cancer Res* **15:** 226-237.

Liu VF, Weaver DT (1993). The ionizing radiation-induced replication protein A phosphorylation response differs between ataxia telangiectasia and normal human cells. *Mol Cell Biol* **13:** 7222-7231.

Liu XY, Pop LM, Vitetta ES (2008). Engineering therapeutic monoclonal antibodies. *Immunological reviews* **222:** 9-27.

Livak KJ, Schmittgen TD (2001). Analysis of relative gene expression data using real-time quantitative PCR and the 2(-Delta Delta C(T)) Method. *Methods* **25:** 402-408.

Lloret M, Lara PC, Bordon E, Rey A, Falcon O, Apolinario RM *et al* (2008). MVP expression is related to IGF1-R in cervical carcinoma patients treated by radiochemotherapy. *Gynecologic oncology* **110:** 304-307.

Lloret M, Lara PC, Bordon E, Fontes F, Rey A, Pinar B *et al* (2009). Major vault protein may affect nonhomologous end-joining repair and apoptosis through Ku70/80 and bax downregulation in cervical carcinoma tumors. *International journal of radiation oncology, biology, physics* **73:** 976-979.

Lobrich M, Jeggo PA (2005). The two edges of the ATM sword: co-operation between repair and checkpoint functions. *Radiother Oncol* **76:** 112-118.

Lobrich M, Shibata A, Beucher A, Fisher A, Ensminger M, Goodarzi AA *et al* (2010). gammaH2AX foci analysis for monitoring DNA double-strand break repair: strengths, limitations and optimization. *Cell Cycle* **9:** 662-669.

Lopez T, Hanahan D (2002). Elevated levels of IGF-1 receptor convey invasive and metastatic capability in a mouse model of pancreatic islet tumorigenesis. *Cancer cell* **1:** 339-353.

Lu X, de la Pena L, Barker C, Camphausen K, Tofilon PJ (2006). Radiation-induced changes in gene expression involve recruitment of existing messenger RNAs to and away from polysomes. *Cancer Res* **66:** 1052-1061.

Luk F, Yu Y, Walsh WR, Yang JL (2011). IGF1R-targeted therapy and its enhancement of doxorubicin chemosensitivity in human osteosarcoma cell lines. *Cancer investigation* **29:** 521-532.

Lukas J, Parry D, Aagaard L, Mann DJ, Bartkova J, Strauss M *et al* (1995). Retinoblastoma-protein-dependent cell-cycle inhibition by the tumour suppressor p16. *Nature* **375:** 503-506.

Lukas J, Lukas C, Bartek J (2011). More than just a focus: The chromatin response to DNA damage and its role in genome integrity maintenance. *Nat Cell Biol* **13:** 1161-1169.

Lundin C, North M, Erixon K, Walters K, Jenssen D, Goldman AS *et al* (2005). Methyl methanesulfonate (MMS) produces heat-labile DNA damage but no detectable in vivo DNA double-strand breaks. *Nucleic Acids Res* **33:** 3799-3811.

Ma L, Chen Z, Erdjument-Bromage H, Tempst P, Pandolfi PP (2005a). Phosphorylation and functional inactivation of TSC2 by Erk implications for tuberous sclerosis and cancer pathogenesis. *Cell* **121:** 179-193.

Ma Y, Lu H, Tippin B, Goodman MF, Shimazaki N, Koiwai O *et al* (2004). A biochemically defined system for mammalian nonhomologous DNA end joining. *Mol Cell* **16:** 701-713.

Ma Y, Schwarz K, Lieber MR (2005b). The Artemis:DNA-PKcs endonuclease cleaves DNA loops, flaps, and gaps. *DNA Repair (Amst)* **4:** 845-851.

Ma Y, Cheng Q, Ren Z, Xu L, Zhao Y, Sun J *et al* (2012). Induction of IGF-1R expression by EGR-1 facilitates the growth of prostate cancer cells. *Cancer Lett* **317:** 150-156.

Macaulay VM, Salisbury AJ, Bohula EA, Playford MP, Smorodinsky NI, Shiloh Y (2001). Downregulation of the type 1 insulin-like growth factor receptor in mouse melanoma cells is associated with enhanced radiosensitivity and impaired activation of Atm kinase. *Oncogene* **20:** 4029-4040.

Macrae CJ, McCulloch RD, Ylanko J, Durocher D, Koch CA (2008). APLF (C2orf13) facilitates nonhomologous end-joining and undergoes ATM-dependent hyperphosphorylation following ionizing radiation. *DNA Repair (Amst)* **7:** 292-302.

Maeda H, Yonou H, Yano K, Ishii G, Saito S, Ochiai A (2009). Prostate-specific antigen enhances bioavailability of insulin-like growth factor by degrading insulin-like growth factor binding protein 5. *Biochem Biophys Res Commun* **381:** 311-316.

Mahaney BL, Meek K, Lees-Miller SP (2009). Repair of ionizing radiation-induced DNA double-strand breaks by non-homologous end-joining. *Biochem J* **417:** 639-650.

Mallette FA, Mattiroli F, Cui G, Young LC, Hendzel MJ, Mer G *et al* (2012). RNF8- and RNF168-dependent degradation of KDM4A/JMJD2A triggers 53BP1 recruitment to DNA damage sites. *Embo J* **31:** 1865-1878.

Mamane Y, Petroulakis E, Rong L, Yoshida K, Ler LW, Sonenberg N (2004). eIF4E--from translation to transformation. *Oncogene* **23:** 3172-3179.

Manning BD, Cantley LC (2007). AKT/PKB signaling: navigating downstream. *Cell* **129:** 1261-1274.

Mao Z, Bozzella M, Seluanov A, Gorbunova V (2008). Comparison of nonhomologous end joining and homologous recombination in human cells. *DNA Repair (Amst)* **7:** 1765-1771.

Maor SB, Abramovitch S, Erdos MR, Brody LC, Werner H (2000). BRCA1 suppresses insulin-like growth factor-I receptor promoter activity: potential interaction between BRCA1 and Sp1. *Molecular genetics and metabolism* **69:** 130-136.

Maranchie JK, Vasselli JR, Riss J, Bonifacino JS, Linehan WM, Klausner RD (2002). The contribution of VHL substrate binding and HIF1-alpha to the phenotype of VHL loss in renal cell carcinoma. *Cancer cell* **1:** 247-255.

Matsubara J, Yamada Y, Nakajima TE, Kato K, Hamaguchi T, Shirao K *et al* (2008). Clinical significance of insulin-like growth factor type 1 receptor and epidermal growth factor receptor in patients with advanced gastric cancer. *Oncology* **74:** 76-83.

Maxwell PH, Wiesener MS, Chang GW, Clifford SC, Vaux EC, Cockman ME *et al* (1999). The tumour suppressor protein VHL targets hypoxia-inducible factors for oxygen-dependent proteolysis. *Nature* **399:** 271-275.

Mayo LD, Donner DB (2001). A phosphatidylinositol 3-kinase/Akt pathway promotes translocation of Mdm2 from the cytoplasm to the nucleus. *Proc Natl Acad Sci U S A* **98:** 11598-11603.

McIntosh J, Dennison G, Holly JM, Jarrett C, Frankow A, Foulstone EJ *et al* (2010). IGFBP-3 can either inhibit or enhance EGF-mediated growth of breast epithelial cells dependent upon the presence of fibronectin. *J Biol Chem* **285:** 38788-38800.

McMenamin ME, Soung P, Perera S, Kaplan I, Loda M, Sellers WR (1999). Loss of PTEN expression in paraffin-embedded primary prostate cancer correlates with high Gleason score and advanced stage. *Cancer Res* **59:** 4291-4296.

McNeill EM, Klockner-Bormann M, Roesler EC, Talton LE, Moechars D, Clagett-Dame M (2011). Nav2 hypomorphic mutant mice are ataxic and exhibit abnormalities in cerebellar development. *Developmental biology* **353:** 331-343.

Medema RH, Kops GJ, Bos JL, Burgering BM (2000). AFX-like Forkhead transcription factors mediate cell-cycle regulation by Ras and PKB through p27kip1. *Nature* **404:** 782-787.

Meek K, Douglas P, Cui X, Ding Q, Lees-Miller SP (2007). trans Autophosphorylation at DNA-dependent protein kinase's two major autophosphorylation site clusters facilitates end processing but not end joining. *Mol Cell Biol* **27:** 3881-3890.

Metalli D, Lovat F, Tripodi F, Genua M, Xu SQ, Spinelli M *et al* (2010). The insulin-like growth factor receptor I promotes motility and invasion of bladder cancer cells through Akt- and mitogen-activated protein kinase-dependent activation of paxillin. *The American journal of pathology* **176:** 2997-3006.

Mimae T, Tsuta K, Kondo T, Nitta H, Grogan TM, Okada M *et al* (2012). Protein expression and gene copy number changes of receptor tyrosine kinase in thymomas and thymic carcinomas. *Ann Oncol* **23:** 3129-3137.

Monzavi R, Cohen P (2002). IGFs and IGFBPs: role in health and disease. *Best practice & research Clinical endocrinology & metabolism* **16:** 433-447.

Moon AF, Garcia-Diaz M, Batra VK, Beard WA, Bebenek K, Kunkel TA *et al* (2007). The X family portrait: structural insights into biological functions of X family polymerases. *DNA Repair (Amst)* **6:** 1709-1725.

Moschos SJ, Mantzoros CS (2002). The role of the IGF system in cancer: from basic to clinical studies and clinical applications. *Oncology* **63:** 317-332.

Motzer RJ, Hutson TE, Tomczak P, Michaelson MD, Bukowski RM, Rixe O *et al* (2007). Sunitinib versus interferon alfa in metastatic renal-cell carcinoma. *N Engl J Med* **356:** 115-124.

Motzer RJ, Escudier B, Oudard S, Hutson TE, Porta C, Bracarda S *et al* (2008). Efficacy of everolimus in advanced renal cell carcinoma: a double-blind, randomised, placebo-controlled phase III trial. *Lancet* **372:** 449-456.

Mujoo K, Watanabe M, Khokhar AR, Siddik ZH (2005). Increased sensitivity of a metastatic model of prostate cancer to a novel tetravalent platinum analog. *Prostate* **62:** 91-100.

Mulholland DJ, Kobayashi N, Ruscetti M, Zhi A, Tran LM, Huang J *et al* (2012). Pten loss and RAS/MAPK activation cooperate to promote EMT and metastasis initiated from prostate cancer stem/progenitor cells. *Cancer Res* **72:** 1878-1889.

Mulvihill MJ, Cooke A, Rosenfeld-Franklin M, Buck E, *al. e* (2009). Discovery of OSI-906: a selective and orally efficacious dual inhibitor of the IGF-1 receptor and insulin receptor. *Future Med Chem* **1 (6):** 1153-1171.

Mutka SC, Yang WQ, Dong SD, Ward SL, Craig DA, Timmermans PB *et al* (2009). Identification of nuclear export inhibitors with potent anticancer activity in vivo. *Cancer Res* **69:** 510-517.

Myers JS, Cortez D (2006). Rapid activation of ATR by ionizing radiation requires ATM and Mre11. *J Biol Chem* **281:** 9346-9350.

Naing A, Cohen R, Dy GK, Hong DS, Dyster L, Hangauer DG *et al* (2013). A phase I trial of KX2-391, a novel non-ATP competitive substrate-pocket- directed SRC inhibitor, in patients with advanced malignancies. *Investigational new drugs*.

Nakamura K, Sakai W, Kawamoto T, Bree RT, Lowndes NF, Takeda S *et al* (2006). Genetic dissection of vertebrate 53BP1: a major role in non-homologous end joining of DNA double strand breaks. *DNA Repair (Amst)* **5:** 741-749.

Nakamura S, Watanabe H, Miura M, Sasaki T (1997). Effect of the insulin-like growth factor I receptor on ionizing radiation-induced cell death in mouse embryo fibroblasts. *Experimental cell research* **235:** 287-294.

Ng WL, Yan D, Zhang X, Mo YY, Wang Y (2010). Over-expression of miR-100 is responsible for the low-expression of ATM in the human glioma cell line: M059J. *DNA Repair (Amst)* **9:** 1170-1175.

Nimonkar AV, Ozsoy AZ, Genschel J, Modrich P, Kowalczykowski SC (2008). Human exonuclease 1 and BLM helicase interact to resect DNA and initiate DNA repair. *Proc Natl Acad Sci U S A* **105:** 16906-16911.

Noon AT, Shibata A, Rief N, Lobrich M, Stewart GS, Jeggo PA *et al* (2010). 53BP1-dependent robust localized KAP-1 phosphorylation is essential for heterochromatic DNA double-strand break repair. *Nat Cell Biol* **12:** 177-184.

O'Reilly KE, Rojo F, She QB, Solit D, Mills GB, Smith D *et al* (2006). mTOR inhibition induces upstream receptor tyrosine kinase signaling and activates Akt. *Cancer Res* **66:** 1500-1508.

Oakley GG, Patrick SM (2010). Replication protein A: directing traffic at the intersection of replication and repair. *Frontiers in bioscience : a journal and virtual library* **15:** 883-900.

Oh Y, Muller HL, Lamson G, Rosenfeld RG (1993). Insulin-like growth factor (IGF)-independent action of IGF-binding protein-3 in Hs578T human breast cancer cells. Cell surface binding and growth inhibition. *J Biol Chem* **268:** 14964-14971.

Olmos D, Postel-Vinay S, Molife LR, Okuno SH, Schuetze SM, Paccagnella ML *et al* (2010). Safety, pharmacokinetics, and preliminary activity of the anti-IGF-1R antibody figitumumab (CP-751,871) in patients with sarcoma and Ewing's sarcoma: a phase 1 expansion cohort study. *The lancet oncology* **11:** 129-135.

Ota H, Tokunaga E, Chang K, Hikasa M, Iijima K, Eto M *et al* (2006). Sirt1 inhibitor, Sirtinol, induces senescence-like growth arrest with attenuated Ras-MAPK signaling in human cancer cells. *Oncogene* **25:** 176-185.

Ozes ON, Mayo LD, Gustin JA, Pfeffer SR, Pfeffer LM, Donner DB (1999). NF-kappaB activation by tumour necrosis factor requires the Akt serine-threonine kinase. *Nature* **401:** 82-85.

Pan M, Santamaria M, Wollman DB (2007). CNS response after erlotinib therapy in a patient with metastatic NSCLC with an EGFR mutation. *Nature clinical practice Oncology* **4:** 603-607.

Pandini G, Frasca F, Mineo R, Sciacca L, Vigneri R, Belfiore A (2002). Insulin/insulin-like growth factor I hybrid receptors have different biological characteristics depending on the insulin receptor isoform involved. *J Biol Chem* **277:** 39684-39695.

Pandini G, Mineo R, Frasca F, Roberts CT, Jr., Marcelli M, Vigneri R *et al* (2005). Androgens up-regulate the insulin-like growth factor-I receptor in prostate cancer cells. *Cancer Res* **65:** 1849-1857.

Pandini G, Wurch T, Akla B, Corvaia N, Belfiore A, Goetsch L (2007). Functional responses and in vivo anti-tumour activity of h7C10: a humanised monoclonal antibody with neutralising activity against the insulin-like growth factor-1 (IGF-1) receptor and insulin/IGF-1 hybrid receptors. *Eur J Cancer* **43:** 1318-1327.

Parker A, Cheville JC, Lohse C, Cerhan JR, Blute ML (2003). Expression of insulin-like growth factor I receptor and survival in patients with clear cell renal cell carcinoma. *J Urol* **170:** 420-424.

Parker AS, Cheville JC, Janney CA, Cerhan JR (2002). High expression levels of insulin-like growth factor-I receptor predict poor survival among women with clear-cell renal cell carcinomas. *Hum Pathol* **33:** 801-805.

Parker AS, Cheville JC, Blute ML, Igel T, Lohse CM, Cerhan JR (2004). Pathologic T1 clear cell renal cell carcinoma: insulin-like growth factor-I receptor expression and disease-specific survival. *Cancer* **100:** 2577-2582.

Parmar H, Edwards L, Phillips RH, Allen L, Lightman SL (1987). Orchiectomy versus long-acting D-Trp-6-LHRH in advanced prostatic cancer. *British journal of urology* **59:** 248-254.

Pearson G, Robinson F, Beers Gibson T, Xu BE, Karandikar M, Berman K *et al* (2001). Mitogen-activated protein (MAP) kinase pathways: regulation and physiological functions. *Endocr Rev* **22:** 153-183.

Perer ES, Madan AK, Shurin A, Zakris E, Romeguera K, Pang Y *et al* (2000). Insulin-like growth factor I receptor antagonism augments response to chemoradiation therapy in colon cancer cells. *J Surg Res* **94:** 1-5.

Peretz S, Jensen R, Baserga R, Glazer PM (2001). ATM-dependent expression of the insulin-like growth factor-I receptor in a pathway regulating radiation response. *Proc Natl Acad Sci U S A* **98:** 1676-1681.

Perrault R, Cheong N, Wang H, Iliakis G (2001). RPA facilitates rejoining of DNA double-strand breaks in an in vitro assay utilizing genomic DNA as substrate. *Int J Radiat Biol* **77:** 593-607.

Petrylak DP, Tangen CM, Hussain MH, Lara PN, Jr., Jones JA, Taplin ME *et al* (2004). Docetaxel and estramustine compared with mitoxantrone and prednisone for advanced refractory prostate cancer. *N Engl J Med* **351:** 1513-1520.

Pettaway CA, Pathak S, Greene G, Ramirez E, Wilson MR, Killion JJ *et al* (1996). Selection of highly metastatic variants of different human prostatic carcinomas using orthotopic implantation in nude mice. *Clin Cancer Res* **2:** 1627-1636.

Pfaffle R, Kies W, Klammt J (2011). From GHRH to IGF-1 and downstream: clinical phenotypes and biological mechanisms. *Pediatric endocrinology reviews : PER* **9 Suppl 1:** 529-534.

Pierce AJ, Johnson RD, Thompson LH, Jasin M (1999). XRCC3 promotes homology-directed repair of DNA damage in mammalian cells. *Genes Dev* **13:** 2633-2638.

Playford MP, Bicknell D, Bodmer WF, Macaulay VM (2000). Insulin-like growth factor 1 regulates the location, stability, and transcriptional activity of beta-catenin. *Proc Natl Acad Sci U S A* **97:** 12103-12108.

Plymate SR, Haugk K, Coleman I, Woodke L, Vessella R, Nelson P *et al* (2007). An antibody targeting the type I insulin-like growth factor receptor enhances the castration-induced response in androgen-dependent prostate cancer. *Clin Cancer Res* **13:** 6429-6439.

Pollak MN, Schernhammer ES, Hankinson SE (2004). Insulin-like growth factors and neoplasia. *Nat Rev Cancer* **4:** 505-518.

Postow L (2011). Destroying the ring: Freeing DNA from Ku with ubiquitin. *FEBS Lett* **585:** 2876-2882.

Povirk LF, Zhou T, Zhou R, Cowan MJ, Yannone SM (2007). Processing of 3'-phosphoglycolate-terminated DNA double strand breaks by Artemis nuclease. *J Biol Chem* **282:** 3547-3558.

Rai R, Dai H, Multani AS, Li K, Chin K, Gray J *et al* (2006). BRIT1 regulates early DNA damage response, chromosomal integrity, and cancer. *Cancer cell* **10:** 145-157.

Rajah R, Katz L, Nunn S, Solberg P, Beers T, Cohen P (1995). Insulin-like growth factor binding protein (IGFBP) proteases: functional regulators of cell growth. *Progress in growth factor research* **6:** 273-284.

Rajah R, Valentinis B, Cohen P (1997). Insulin-like growth factor (IGF)-binding protein-3 induces apoptosis and mediates the effects of transforming growth factor-beta1 on programmed cell death through a p53- and IGF-independent mechanism. *J Biol Chem* **272:** 12181-12188.

Rajaram S, Baylink DJ, Mohan S (1997). Insulin-like growth factor-binding proteins in serum and other biological fluids: regulation and functions. *Endocr Rev* **18:** 801-831.

Ramalingam SS, Spigel DR, Chen D, Steins MB, Engelman JA, Schneider CP *et al* (2011). Randomized phase II study of erlotinib in combination with placebo or R1507, a monoclonal antibody to insulin-like growth factor-1 receptor, for advanced-stage non-small-cell lung cancer. *J Clin Oncol* **29:** 4574-4580.

Rashi-Elkeles S, Elkon R, Shavit S, Lerenthal Y, Linhart C, Kupershtein A *et al* (2011). Transcriptional modulation induced by ionizing radiation: p53 remains a central player. *Molecular oncology* **5:** 336-348.

Ravaud A, Dilhuydy MS (2005). Interferon alpha for the treatment of advanced renal cancer. *Expert opinion on biological therapy* **5:** 749-762.

Reiss K, Ferber A, Travali S, Porcu P, Phillips PD, Baserga R (1991). The protooncogene c-myb increases the expression of insulin-like growth factor 1 and

insulin-like growth factor 1 receptor messenger RNAs by a transcriptional mechanism. *Cancer Res* **51:** 5997-6000.

Reiss K, Wang JY, Romano G, Furnari FB, Cavenee WK, Morrione A *et al* (2000). IGF-I receptor signaling in a prostatic cancer cell line with a PTEN mutation. *Oncogene* **19:** 2687-2694.

Renehan AG, Zwahlen M, Minder C, O'Dwyer ST, Shalet SM, Egger M (2004). Insulin-like growth factor (IGF)-I, IGF binding protein-3, and cancer risk: systematic review and meta-regression analysis. *Lancet* **363:** 1346-1353.

Renehan AG, Harvie M, Howell A (2006). Insulin-like growth factor (IGF)-I, IGF binding protein-3, and breast cancer risk: eight years on. *Endocr Relat Cancer* **13:** 273-278.

Resnicoff M, Coppola D, Sell C, Rubin R, Ferrone S, Baserga R (1994). Growth inhibition of human melanoma cells in nude mice by antisense strategies to the type 1 insulin-like growth factor receptor. *Cancer Res* **54:** 4848-4850.

Resnicoff M, Valentinis B, Herbert D, Abraham D, Friesen PD, Alnemri ES *et al* (1998). The baculovirus anti-apoptotic p35 protein promotes transformation of mouse embryo fibroblasts. *J Biol Chem* **273:** 10376-10380.

Riballo E, Woodbine L, Stiff T, Walker SA, Goodarzi AA, Jeggo PA (2009). XLF-Cernunnos promotes DNA ligase IV-XRCC4 re-adenylation following ligation. *Nucleic Acids Res* **37:** 482-492.

Richter S, Sridhar SS (2012). New directions for biologic targets in urothelial carcinoma. *Mol Cancer Ther* **11:** 1226-1235.

Riesterer O, Yang Q, Raju U, Torres M, Molkentine D, Patel N *et al* (2011). Combination of anti-IGF-1R antibody A12 and ionizing radiation in upper respiratory tract cancers. *International journal of radiation oncology, biology, physics* **79:** 1179-1187.

Rini BI, Escudier B, Tomczak P, Kaprin A, Szczylik C, Hutson TE *et al* (2011). Comparative effectiveness of axitinib versus sorafenib in advanced renal cell carcinoma (AXIS): a randomised phase 3 trial. *Lancet* **378:** 1931-1939.

Robertson DM, Zhu M, Wu YC (2012). Cellular distribution of the IGF-1R in corneal epithelial cells. *Experimental eye research* **94:** 179-186.

Rochester MA, Riedemann J, Hellawell GO, Brewster SF, Macaulay VM (2005). Silencing of the IGF1R gene enhances sensitivity to DNA-damaging agents in both PTEN wild-type and mutant human prostate cancer. *Cancer Gene Ther* **12:** 90-100.

Rochester MA, Patel N, Turney BW, Davies DR, Roberts IS, Crew J *et al* (2007). The type 1 insulin-like growth factor receptor is over-expressed in bladder cancer. *BJU Int* **100:** 1396-1401.

Roddam AW, Allen NE, Appleby P, Key TJ, Ferrucci L, Carter HB *et al* (2008). Insulin-like growth factors, their binding proteins, and prostate cancer risk: analysis of individual patient data from 12 prospective studies. *Annals of internal medicine* **149:** 461-471, W483-468.

Rodon J, DeSantos V, Ferry RJ, Jr., Kurzrock R (2008). Early drug development of inhibitors of the insulin-like growth factor-I receptor pathway: lessons from the first clinical trials. *Mol Cancer Ther* **7:** 2575-2588.

Rogakou EP, Boon C, Redon C, Bonner WM (1999). Megabase chromatin domains involved in DNA double-strand breaks in vivo. *J Cell Biol* **146:** 905-916.

Roninson IB (2003). Tumor cell senescence in cancer treatment. *Cancer Res* **63:** 2705-2715.

Rosenzweig KE, Youmell MB, Palayoor ST, Price BD (1997). Radiosensitization of human tumor cells by the phosphatidylinositol3-kinase inhibitors wortmannin and LY294002 correlates with inhibition of DNA-dependent protein kinase and prolonged G2-M delay. *Clin Cancer Res* **3:** 1149-1156.

Roth J, Dobbelstein M, Freedman DA, Shenk T, Levine AJ (1998). Nucleo-cytoplasmic shuttling of the hdm2 oncoprotein regulates the levels of the p53 protein via a pathway used by the human immunodeficiency virus rev protein. *Embo J* **17:** 554-564.

Roux PP, Ballif BA, Anjum R, Gygi SP, Blenis J (2004). Tumor-promoting phorbol esters and activated Ras inactivate the tuberous sclerosis tumor suppressor complex via p90 ribosomal S6 kinase. *Proc Natl Acad Sci U S A* **101:** 13489-13494.

Rubini M, Hongo A, D'Ambrosio C, Baserga R (1997). The IGF-I receptor in mitogenesis and transformation of mouse embryo cells: role of receptor number. *Experimental cell research* **230:** 284-292.

Sachdev D, Li SL, Hartell JS, Fujita-Yamaguchi Y, Miller JS, Yee D (2003). A chimeric humanized single-chain antibody against the type I insulin-like growth factor (IGF) receptor renders breast cancer cells refractory to the mitogenic effects of IGF-I. *Cancer Res* **63:** 627-635.

Sachdev D, Hartell JS, Lee AV, Zhang X, Yee D (2004). A dominant negative type I insulin-like growth factor receptor inhibits metastasis of human cancer cells. *J Biol Chem* **279:** 5017-5024.

Sachdev D, Singh R, Fujita-Yamaguchi Y, Yee D (2006). Down-regulation of insulin receptor by antibodies against the type I insulin-like growth factor receptor: implications for anti-insulin-like growth factor therapy in breast cancer. *Cancer Res* **66:** 2391-2402.

Sakakibara K, Saito N, Sato T, Suzuki A, Hasegawa Y, Friedman JM *et al* (2011). CBS9106 is a novel reversible oral CRM1 inhibitor with CRM1 degrading activity. *Blood* **118:** 3922-3931.

Samani AA, Yakar S, LeRoith D, Brodt P (2007). The role of the IGF system in cancer growth and metastasis: overview and recent insights. *Endocr Rev* **28:** 20-47.

Sanchez-Ortiz RF, Rosser CJ, Madsen LT, Swanson DA, Wood CG (2004). Young age is an independent prognostic factor for survival of sporadic renal cell carcinoma. *J Urol* **171:** 2160-2165.

Sarbassov DD, Guertin DA, Ali SM, Sabatini DM (2005). Phosphorylation and regulation of Akt/PKB by the rictor-mTOR complex. *Science* **307:** 1098-1101.

Sarfstein R, Pasmanik-Chor M, Yeheskel A, Edry L, Shomron N, Warman N *et al* (2012). Insulin-like growth factor-I receptor (IGF-IR) translocates to nucleus and autoregulates IGF-IR gene expression in breast cancer cells. *J Biol Chem* **287:** 2766-2776.

Sartori AA, Lukas C, Coates J, Mistrik M, Fu S, Bartek J *et al* (2007). Human CtIP promotes DNA end resection. *Nature* **450:** 509-514.

Sato S, Fujita N, Tsuruo T (2004). Involvement of 3-phosphoinositide-dependent protein kinase-1 in the MEK/MAPK signal transduction pathway. *J Biol Chem* **279:** 33759-33767.

Scher HI, Fizazi K, Saad F, Taplin ME, Sternberg CN, Miller K *et al* (2012). Increased survival with enzalutamide in prostate cancer after chemotherapy. *N Engl J Med* **367:** 1187-1197.

Schmidt KL, Marcus-Gueret N, Adeleye A, Webber J, Baillie D, Stringham EG (2009). The cell migration molecule UNC-53/NAV2 is linked to the ARP2/3 complex by ABI-1. *Development* **136:** 563-574.

Schwarze SR, Fu VX, Desotelle JA, Kenowski ML, Jarrard DF (2005). The identification of senescence-specific genes during the induction of senescence in prostate cancer cells. *Neoplasia* **7:** 816-823.

Scott SL, Earle JD, Gumerlock PH (2003). Functional p53 increases prostate cancer cell survival after exposure to fractionated doses of ionizing radiation. *Cancer Res* **63:** 7190-7196.

Sehat B, Tofigh A, Lin Y, Trocme E, Liljedahl U, Lagergren J *et al* (2010). SUMOylation mediates the nuclear translocation and signaling of the IGF-1 receptor. *Sci Signal* **3:** ra10.

Sekimoto T, Fukumoto M, Yoneda Y (2004). 14-3-3 suppresses the nuclear localization of threonine 157-phosphorylated p27(Kip1). *Embo J* **23:** 1934-1942.

Sell C, Rubini M, Rubin R, Liu JP, Efstratiadis A, Baserga R (1993). Simian virus 40 large tumor antigen is unable to transform mouse embryonic fibroblasts lacking type 1 insulin-like growth factor receptor. *Proc Natl Acad Sci U S A* **90:** 11217-11221.

Sell C, Dumenil G, Deveaud C, Miura M, Coppola D, DeAngelis T *et al* (1994). Effect of a null mutation of the insulin-like growth factor I receptor gene on growth and transformation of mouse embryo fibroblasts. *Mol Cell Biol* **14:** 3604-3612.

Sfoungaristos S, Giannitsas K, Perimenis P (2011). Present and future therapeutic options for locally advanced and metastatic renal cell carcinoma. *Expert opinion on pharmacotherapy* **12:** 533-547.

Shaheen FS, Znojek P, Fisher A, Webster M, Plummer R, Gaughan L *et al* (2011). Targeting the DNA double strand break repair machinery in prostate cancer. *PloS one* **6:** e20311.

Sharma SV, Lee DY, Li B, Quinlan MP, Takahashi F, Maheswaran S *et al* (2010). A chromatin-mediated reversible drug-tolerant state in cancer cell subpopulations. *Cell* **141:** 69-80.

Shen C, Kaelin WG, Jr. (2013). The VHL/HIF axis in clear cell renal carcinoma. *Seminars in cancer biology* **23:** 18-25.

Shen MR, Hsu YM, Hsu KF, Chen YF, Tang MJ, Chou CY (2006). Insulin-like growth factor 1 is a potent stimulator of cervical cancer cell invasiveness and proliferation that is modulated by alphavbeta3 integrin signaling. *Carcinogenesis* **27:** 962-971.

Shibata A, Barton O, Noon AT, Dahm K, Deckbar D, Goodarzi AA *et al* (2010). Role of ATM and the damage response mediator proteins 53BP1 and MDC1 in the maintenance of G(2)/M checkpoint arrest. *Mol Cell Biol* **30:** 3371-3383.

Shibata A, Conrad S, Birraux J, Geuting V, Barton O, Ismail A *et al* (2011). Factors determining DNA double-strand break repair pathway choice in G2 phase. *Embo J* **30:** 1079-1092.

Shiloh Y (2006). The ATM-mediated DNA-damage response: taking shape. *Trends in biochemical sciences* **31:** 402-410.

Shiloh Y, Ziv Y (2012). The ATM protein: the importance of being active. *J Cell Biol* **198:** 273-275.

Shin I, Yakes FM, Rojo F, Shin NY, Bakin AV, Baselga J *et al* (2002). PKB/Akt mediates cell-cycle progression by phosphorylation of p27(Kip1) at threonine 157 and modulation of its cellular localization. *Nature medicine* **8:** 1145-1152.

Shrivastav M, De Haro LP, Nickoloff JA (2008). Regulation of DNA double-strand break repair pathway choice. *Cell research* **18:** 134-147.

Slamon DJ, Leyland-Jones B, Shak S, Fuchs H, Paton V, Bajamonde A *et al* (2001). Use of chemotherapy plus a monoclonal antibody against HER2 for metastatic breast cancer that overexpresses HER2. *N Engl J Med* **344:** 783-792.

Smith FJ, Jonkman MF, van Goor H, Coleman CM, Covello SP, Uitto J *et al* (1998). A mutation in human keratin K6b produces a phenocopy of the K17 disorder pachyonychia congenita type 2. *Hum Mol Genet* **7:** 1143-1148.

Smith GC, d'Adda di Fagagna F, Lakin ND, Jackson SP (1999). Cleavage and inactivation of ATM during apoptosis. *Mol Cell Biol* **19:** 6076-6084.

Solier S, Pommier Y (2009). The apoptotic ring: a novel entity with phosphorylated histones H2AX and H2B and activated DNA damage response kinases. *Cell Cycle* **8:** 1853-1859.

Solier S, Pommier Y (2011). MDC1 Cleavage by Caspase-3: A Novel Mechanism for Inactivating the DNA Damage Response during Apoptosis. *Cancer Res* **71:** 906-913.

Soos MA, Whittaker J, Lammers R, Ullrich A, Siddle K (1990). Receptors for insulin and insulin-like growth factor-I can form hybrid dimers. Characterisation of hybrid receptors in transfected cells. *Biochem J* **270:** 383-390.

Soos MA, Field CE, Lammers R, Ullrich A, Zhang B, Roth RA *et al* (1992). A panel of monoclonal antibodies for the type I insulin-like growth factor receptor. Epitope mapping, effects on ligand binding, and biological activity. *J Biol Chem* **267:** 12955-12963.

Spears M, Cunningham C, Thomas J, *al e* (2009). The Expression of Insulin-Like Growth Factor-1 Receptor (IGF-1R) in Early Breast Cancer. *Cancer Research* **69:** Issue 24, supplement 23.

Spentzos D, Cannistra SA, Grall F, Levine DA, Pillay K, Libermann TA *et al* (2007). IGF axis gene expression patterns are prognostic of survival in epithelial ovarian cancer. *Endocr Relat Cancer* **14:** 781-790.

Sramkoski RM, Pretlow TG, 2nd, Giaconia JM, Pretlow TP, Schwartz S, Sy MS *et al* (1999). A new human prostate carcinoma cell line, 22Rv1. *In vitro cellular & developmental biology Animal* **35:** 403-409.

Stachowiak EK, Fang X, Myers J, Dunham S, Stachowiak MK (2003). cAMP-induced differentiation of human neuronal progenitor cells is mediated by nuclear fibroblast growth factor receptor-1 (FGFR1). *Journal of neurochemistry* **84:** 1296-1312.

Stamey TA, Yang N, Hay AR, McNeal JE, Freiha FS, Redwine E (1987). Prostate-specific antigen as a serum marker for adenocarcinoma of the prostate. *N Engl J Med* **317:** 909-916.

Steiner MS, Wang Y, Zhang Y, Zhang X, Lu Y (2000). p16/MTS1/INK4A suppresses prostate cancer by both pRb dependent and independent pathways. *Oncogene* **19:** 1297-1306.

Sternberg CN, Davis ID, Mardiak J, Szczylik C, Lee E, Wagstaff J *et al* (2010). Pazopanib in locally advanced or metastatic renal cell carcinoma: results of a randomized phase III trial. *J Clin Oncol* **28:** 1061-1068.

Stiff T, O'Driscoll M, Rief N, Iwabuchi K, Lobrich M, Jeggo PA (2004). ATM and DNA-PK function redundantly to phosphorylate H2AX after exposure to ionizing radiation. *Cancer Res* **64:** 2390-2396.

Sy SM, Huen MS, Chen J (2009). PALB2 is an integral component of the BRCA complex required for homologous recombination repair. *Proc Natl Acad Sci U S A* **106:** 7155-7160.

Takahari D, Yamada Y, Okita NT, Honda T, Hirashima Y, Matsubara J *et al* (2009). Relationships of insulin-like growth factor-1 receptor and epidermal growth factor receptor expression to clinical outcomes in patients with colorectal cancer. *Oncology* **76:** 42-48.

Taniuchi K, Nakagawa H, Nakamura T, Eguchi H, Ohigashi H, Ishikawa O *et al* (2005). Down-regulation of RAB6KIFL/KIF20A, a kinesin involved with membrane trafficking of discs large homologue 5, can attenuate growth of pancreatic cancer cell. *Cancer Res* **65:** 105-112.

Tannock IF, de Wit R, Berry WR, Horti J, Pluzanska A, Chi KN *et al* (2004). Docetaxel plus prednisone or mitoxantrone plus prednisone for advanced prostate cancer. *N Engl J Med* **351:** 1502-1512.

Tazzari PL, Tabellini G, Bortul R, Papa V, Evangelisti C, Grafone T *et al* (2007). The insulin-like growth factor-I receptor kinase inhibitor NVP-AEW541 induces apoptosis in acute myeloid leukemia cells exhibiting autocrine insulin-like growth factor-I secretion. *Leukemia : official journal of the Leukemia Society of America, Leukemia Research Fund, UK* **21:** 886-896.

Tee AR, Fingar DC, Manning BD, Kwiatkowski DJ, Cantley LC, Blenis J (2002). Tuberous sclerosis complex-1 and -2 gene products function together to inhibit mammalian target of rapamycin (mTOR)-mediated downstream signaling. *Proc Natl Acad Sci U S A* **99:** 13571-13576.

Tezuka M, Watanabe H, Nakamura S, Yu D, Aung W, Sasaki T *et al* (2001). Antiapoptotic activity is dispensable for insulin-like growth factor I receptor-mediated clonogenic radioresistance after gamma-irradiation. *Clin Cancer Res* **7:** 3206-3214.

Thompson LH (2012). Recognition, signaling, and repair of DNA double-strand breaks produced by ionizing radiation in mammalian cells: the molecular choreography. *Mutation research* **751:** 158-246.

Tolcher A, Patnaik A, Till E, *al. e* (2008). A phase I study of AVE-1642, a humanized monoclonal antibody IGF-1R (insulin like growth factor 1 receptor) antagonist, in patients (pts) with advanced solid tumor (T). *J Clin Oncol* **26: (May 20 suppl; abstr 3582).** .

Tournier C, Hess P, Yang DD, Xu J, Turner TK, Nimnual A *et al* (2000). Requirement of JNK for stress-induced activation of the cytochrome c-mediated death pathway. *Science* **288:** 870-874.

Treuner K, Findeisen M, Strausfeld U, Knippers R (1999). Phosphorylation of replication protein A middle subunit (RPA32) leads to a disassembly of the RPA heterotrimer. *J Biol Chem* **274:** 15556-15561.

Trojanek J, Ho T, Del Valle L, Nowicki M, Wang JY, Lassak A *et al* (2003). Role of the insulin-like growth factor I/insulin receptor substrate 1 axis in Rad51 trafficking and DNA repair by homologous recombination. *Mol Cell Biol* **23:** 7510-7524.

Tsuchida R, Yamada T, Takagi M, Shimada A, Ishioka C, Katsuki Y *et al* (2002). Detection of ATM gene mutation in human glioma cell line M059J by a rapid frameshift/stop codon assay in yeast. *Radiat Res* **158:** 195-201.

Turner BC, Haffty BG, Narayanan L, Yuan J, Havre PA, Gumbs AA *et al* (1997). Insulin-like growth factor-I receptor overexpression mediates cellular radioresistance and local breast cancer recurrence after lumpectomy and radiation. *Cancer Res* **57:** 3079-3083.

Turner JG, Dawson J, Sullivan DM (2012). Nuclear export of proteins and drug resistance in cancer. *Biochemical pharmacology* **83:** 1021-1032.

Turney BW, Turner GD, Brewster SF, Macaulay VM (2010). Serial analysis of resected prostate cancer suggests up-regulation of type 1 IGF receptor with disease progression. *BJU Int*.

Turney BW, Kerr M, Chitnis MM, Lodhia K, Wang Y, Riedemann J *et al* (2012). Depletion of the type 1 IGF receptor delays repair of radiation-induced DNA double strand breaks. *Radiother Oncol*.

Uematsu N, Weterings E, Yano K, Morotomi-Yano K, Jakob B, Taucher-Scholz G *et al* (2007). Autophosphorylation of DNA-PKCS regulates its dynamics at DNA double-strand breaks. *J Cell Biol* **177:** 219-229.

Ulanet DB, Ludwig DL, Kahn CR, Hanahan D (2010). Insulin receptor functionally enhances multistage tumor progression and conveys intrinsic resistance to IGF-1R targeted therapy. *Proc Natl Acad Sci U S A* **107:** 10791-10798.

Ullrich A, Gray A, Tam AW, Yang-Feng T, Tsubokawa M, Collins C *et al* (1986). Insulin-like growth factor I receptor primary structure: comparison with insulin receptor suggests structural determinants that define functional specificity. *Embo J* **5:** 2503-2512.

Valsecchi ME, McDonald M, Brody JR, Hyslop T, Freydin B, Yeo CJ *et al* (2012). Epidermal growth factor receptor and insulinlike growth factor 1 receptor expression predict poor survival in pancreatic ductal adenocarcinoma. *Cancer* **118:** 3484-3493.

Vasilcanu D, Girnita A, Girnita L, Vasilcanu R, Axelson M, Larsson O (2004). The cyclolignan PPP induces activation loop-specific inhibition of tyrosine phosphorylation of the insulin-like growth factor-1 receptor. Link to the phosphatidyl inositol-3 kinase/Akt apoptotic pathway. *Oncogene* **23:** 7854-7862.

Vitale G, van Koetsveld PM, de Herder WW, van der Wansem K, Janssen JA, Colao A *et al* (2009). Effects of type I interferons on IGF-mediated autocrine/paracrine growth of human neuroendocrine tumor cells. *American journal of physiology Endocrinology and metabolism* **296:** E559-566.

von der Maase H, Hansen SW, Roberts JT, Dogliotti L, Oliver T, Moore MJ *et al* (2000). Gemcitabine and cisplatin versus methotrexate, vinblastine, doxorubicin, and cisplatin in advanced or metastatic bladder cancer: results of a large, randomized, multinational, multicenter, phase III study. *J Clin Oncol* **18:** 3068-3077.

Walker JR, Corpina RA, Goldberg J (2001). Structure of the Ku heterodimer bound to DNA and its implications for double-strand break repair. *Nature* **412:** 607-614.

Wang B, Matsuoka S, Carpenter PB, Elledge SJ (2002). 53BP1, a mediator of the DNA damage checkpoint. *Science* **298:** 1435-1438.

Wang CY, Mayo MW, Korneluk RG, Goeddel DV, Baldwin AS, Jr. (1998). NF-kappaB antiapoptosis: induction of TRAF1 and TRAF2 and c-IAP1 and c-IAP2 to suppress caspase-8 activation. *Science* **281:** 1680-1683.

Wang J, Kobayashi T, Floc'h N, Kinkade CW, Aytes A, Dankort D *et al* (2012). B-Raf activation cooperates with PTEN loss to drive c-Myc expression in advanced prostate cancer. *Cancer Res* **72:** 4765-4776.

Wang M, Morsbach F, Sander D, Gheorghiu L, Nanda A, Benes C *et al* (2011). EGF receptor inhibition radiosensitizes NSCLC cells by inducing senescence in cells sustaining DNA double-strand breaks. *Cancer Res* **71:** 6261-6269.

Wang Q, Gao F, May WS, Zhang Y, Flagg T, Deng X (2008). Bcl2 negatively regulates DNA double-strand-break repair through a nonhomologous end-joining pathway. *Mol Cell* **29:** 488-498.

Wang SC, Lien HC, Xia W, Chen IF, Lo HW, Wang Z *et al* (2004). Binding at and transactivation of the COX-2 promoter by nuclear tyrosine kinase receptor ErbB-2. *Cancer cell* **6:** 251-261.

Watkins DJ, Tabernero J, Schmoll H, al. e (2011). A randomized phase II/III study of the anti-IGF-1R antibody MK-0646 (dalotuzumab) in combination with cetuximab (Cx) and irinotecan (Ir) in the treatment of chemorefractory metastatic colorectal cancer (mCRC) with wild-type (wt) KRAS status. *J Clin Oncol* **29 suppl:** Abstract 3501.

Werner H, Karnieli E, Rauscher FJ, LeRoith D (1996). Wild-type and mutant p53 differentially regulate transcription of the insulin-like growth factor I receptor gene. *Proc Natl Acad Sci U S A* **93:** 8318-8323.

Wetterau LA, Moore MG, Lee KW, Shim ML, Cohen P (1999). Novel aspects of the insulin-like growth factor binding proteins. *Molecular genetics and metabolism* **68:** 161-181.

Wu YC, Zhu M, Robertson DM (2012). Novel nuclear localization and potential function of insulin-like growth factor-1 receptor/insulin receptor hybrid in corneal epithelial cells. *PloS one* **7:** e42483.

Yamamoto T, Oshima T, Yoshihara K, Nishi T, Arai H, Inui K *et al* (2012). Clinical significance of immunohistochemical expression of insulin-like growth factor-1 receptor and matrix metalloproteinase-7 in resected non-small cell lung cancer. *Experimental and therapeutic medicine* **3:** 797-802.

Yang H, Jeffrey PD, Miller J, Kinnucan E, Sun Y, Thoma NH *et al* (2002). BRCA2 function in DNA binding and recombination from a BRCA2-DSS1-ssDNA structure. *Science* **297:** 1837-1848.

Yang S, Chintapalli J, Sodagum L, Baskin S, Malhotra A, Reiss K *et al* (2005). Activated IGF-1R inhibits hyperglycemia-induced DNA damage and promotes DNA repair by homologous recombination. *American journal of physiology Renal physiology* **289:** F1144-1152.

Yee D (2012). Insulin-like growth factor receptor inhibitors: baby or the bathwater? *J Natl Cancer Inst* **104:** 975-981.

Yeh AH, Bohula EA, Macaulay VM (2006). Human melanoma cells expressing V600E B-RAF are susceptible to IGF1R targeting by small interfering RNAs. *Oncogene* **25:** 6574-6581.

Yoshida M, Hosoi Y, Miyachi H, Ishii N, Matsumoto Y, Enomoto A *et al* (2002). Roles of DNA-dependent protein kinase and ATM in cell-cycle-dependent radiation sensitivity in human cells. *Int J Radiat Biol* **78:** 503-512.

You Z, Bailis JM (2010). DNA damage and decisions: CtIP coordinates DNA repair and cell cycle checkpoints. *Trends in cell biology* **20:** 402-409.

Yu X, Chen J (2004). DNA damage-induced cell cycle checkpoint control requires CtIP, a phosphorylation-dependent binding partner of BRCA1 C-terminal domains. *Mol Cell Biol* **24:** 9478-9486.

Yuan SS, Lee SY, Chen G, Song M, Tomlinson GE, Lee EY (1999). BRCA2 is required for ionizing radiation-induced assembly of Rad51 complex in vivo. *Cancer Res* **59:** 3547-3551.

Yuen JS, Cockman ME, Sullivan M, Protheroe A, Turner GD, Roberts IS *et al* (2007). The VHL tumor suppressor inhibits expression of the IGF1R and its loss induces IGF1R upregulation in human clear cell renal carcinoma. *Oncogene* **26:** 6499-6508.

Yuen JS, Macaulay VM (2008). Targeting the type 1 insulin-like growth factor receptor as a treatment for cancer. *Expert Opin Ther Targets* **12:** 589-603.

Yuen JS, Akkaya E, Wang Y, Takiguchi M, Peak S, Sullivan M *et al* (2009). Validation of the type 1 insulin-like growth factor receptor as a therapeutic target in renal cancer. *Mol Cancer Ther* **8:** 1448-1459.

Zeng X, Zhang H, Oh A, Zhang Y, Yee D (2012). Enhancement of doxorubicin cytotoxicity of human cancer cells by tyrosine kinase inhibition of insulin receptor and type I IGF receptor. *Breast cancer research and treatment* **133:** 117-126.

Zhang D, Samani AA, Brodt P (2003). The role of the IGF-I receptor in the regulation of matrix metalloproteinases, tumor invasion and metastasis. *Horm Metab Res* **35:** 802-808.

Zhang F, Fan Q, Ren K, Andreassen PR (2009a). PALB2 functionally connects the breast cancer susceptibility proteins BRCA1 and BRCA2. *Molecular cancer research : MCR* **7:** 1110-1118.

Zhang X, Lin M, van Golen KL, Yoshioka K, Itoh K, Yee D (2005). Multiple signaling pathways are activated during insulin-like growth factor-I (IGF-I) stimulated breast cancer cell migration. *Breast cancer research and treatment* **93:** 159-168.

Zhang Y, Rohde LH, Wu H (2009b). Involvement of nucleotide excision and mismatch repair mechanisms in double strand break repair. *Current genomics* **10:** 250-258.

Zhang Z, Hu W, Cano L, Lee TD, Chen DJ, Chen Y (2004). Solution structure of the C-terminal domain of Ku80 suggests important sites for protein-protein interactions. *Structure* **12:** 495-502.

Zhao H, Grossman HB, Spitz MR, Lerner SP, Zhang K, Wu X (2003). Plasma levels of insulin-like growth factor-1 and binding protein-3, and their association with bladder cancer risk. *J Urol* **169:** 714-717.

Zhao Y, Thomas HD, Batey MA, Cowell IG, Richardson CJ, Griffin RJ *et al* (2006). Preclinical evaluation of a potent novel DNA-dependent protein kinase inhibitor NU7441. *Cancer Res* **66:** 5354-5362.

Zhou BP, Liao Y, Xia W, Spohn B, Lee MH, Hung MC (2001). Cytoplasmic localization of p21Cip1/WAF1 by Akt-induced phosphorylation in HER-2/neu-overexpressing cells. *Nat Cell Biol* **3:** 245-252.

Ziv Y, Bielopolski D, Galanty Y, Lukas C, Taya Y, Schultz DC *et al* (2006). Chromatin relaxation in response to DNA double-strand breaks is modulated by a novel ATM- and KAP-1 dependent pathway. *Nat Cell Biol* **8:** 870-876.

9 Publications and Presentations

9.1 Publications

Turney BW, Kerr M, **Chitnis MM**, Lodhia K, Wang Y, Riedemann J, Rochester M, Protheroe AS, Brewster SF, Macaulay VM. Depletion of the type 1 IGF receptor delays repair of radiation-induced DNA double strand breaks. *Radiother Oncol.* 2012; 103(3):402-9.

Aleksic T, **Chitnis MM**, Perestenko OV, Gao S, Thomas PH, Turner GD, Protheroe AS, Howarth M, Macaulay VM. Type 1 insulin-like growth factor receptor translocates to the nucleus of human tumor cells.*Cancer Res*. 2010; 70(16):6412-9.

Chitnis MM, Yuen JS, Protheroe AS, Pollak M, Macaulay VM.: The type 1 insulin-like growth factor receptor pathway *Clin Cancer Res.* 2008;14(20):6364-70.

9.2 Presentations

Meenali M. Chitnis, Andrew S. Protheroe, Valentine M. Macaulay. Type 1 insulin-like growth factor receptor (IGF-1R) inhibition and radiosensitisation in human tumour cells: a role for IGF1R in DNA repair. Accepted as poster for the NCRI conference, Liverpool 2012.

Meenali M. Chitnis, Andrew S. Protheroe, Valentine M. Macaulay. Radiosensitisation resulting from Type 1 Insulin like Growth Factor Receptor inhibition in Prostate cancer cells: a role for IGF1R in DNA repair *Proceedings Molecular Radiation Biology/Oncology* Vol 9 PIII.8.

Shan Gao, Ilijrana Bajrami, **Meenali M Chitnis**, Chris J Lord, Alan Ashworth, Valentine M Macaulay: An siRNA screen in human prostate cancer to identify proteins whose depletion shows synthetic lethality with inhibition of the type 1 IGF receptor (IGF-1R). Presented 12th Nov 2010 at Young Prostate Researchers Symposium, Cancer Research UK Cambridge Research Institute.